

Preface

Special Issue dedicated to the 70th Birthday of Professor Imre J. Rudas – Part II

Technology development unfolds in medatransds these decades, transforming individuals and the society alike. The Internet of Things, Cloud Robotics, Industry 4.0, agile Cyber-Physical Systems show the way along which these transformations occur. The fundamental engineering concepts behind are rooted in academic research, often presented at the major scientific conferences of the community. The IEEE International Conference on Intelligent Engineering Systems (INES) is one of those, a prestigious series established by Bánki Donát Polytechnic and Budapest Tech as the predecessors of Óbuda University. The IEEE INES series was started in 1997, and in 2019, reaches its 23rd edition, dedicated to a special occasion, the celebration of Professor Imre J. Rudas' birthday. The conference was held April 25-27, 2019 in Gödöllő, in the magnificent Royal Palace, favorite summer residence of Queen Elizabeth in the 1840s. Over 140 attendees were present from 22 countries, delivering 63 talks and 2 keynote lectures in a variety of related research topics.

The current Acta Polytechnica Hungarica issue is a collection of the newest research results based on the selected presentation at the 23rd IEEE INES. The articles span across a wide range of intelligent engineering, focusing on control and applications. The intelligence relates to the characteristics of how uncertainty, i.e., unmodeled dynamics can be handled, or what kind of solutions can be used in order to operate in an uncertain environment with proper sensing techniques. The presented solutions discuss the autonomous or automatic ways to execute given sequences or tasks without human user interaction (without detailed instructions). Arguably, the next few years will be dominated by the topics of artificial intelligence. The control engineering perspectives of soft computing gave new sights of control engineering (e.g., Tensor-Product-based control), and expanded the range of applicability in different fields: robotics, medical applications, data mining, cybersecurity, computer networks, accounting, agriculture, chemical processes, military applications, etc. Theories leading to applications, feeding into product developments for the benefit of all.

As it was clearly articulated duing the confernece, the whole series and probably this journal could not have lived withour Imre J. Rudas. Every such major project has its “power engine”, distinguished senior who channels the connections, mediates the subfields, and keeps this linked scientific community at a high international standard. Imre J. Rudas, just turned 70 during the IEEE INES 2019.

His wide spectrum of professional interest is reflected in the variety of the conference contributions, and this *Acta Polytechnica Hungarica* special issue is dedicated to him. The current volume is a selection of his most renowned collaborators and friends throughout the world, as a special tribute to his whole academic carrier. 70 years of outstanding achievement truly deserves a reflection.

Imre J. Rudas graduated from Bánki Donát Polytechnic (Budapest) in 1971, received Master Degree in mathematics from Eötvös Lóránd University (Budapest) and received Ph.D. in robotics from the Hungarian Academy of Sciences in 1987. Achieved the Doctor of Science degree from the Hungarian Academy of Sciences in 2004. He received his first Doctor Honoris Causa degree from the Technical University of Košice (Slovakia) (2001), followed by the “Politehnica” University of Timișoara (Romania) in 2005, Óbuda University (2014) and the Slovak University of Technology (Bratislava) in 2016. He is Honorary Professor (2013) and Ambassador (2016) of the Technical University of Wrocław. His research activity is related to robotics, computational cybernetics with special emphasis on robot control, soft computing, computer-aided process planning, and fuzzy control and fuzzy sets. He has published more than 850 scientific publications, 125 journal papers, and authored 4 scientific books. The number of his independent citations is over 5000, with h-index of 32. He served as Rector of Budapest Tech from August 1, 2003 and became the founding Rector of Óbuda University in 2010 until 2014. He founded the University Research and Innovation Center of Óbuda University in 2012 and the *Acta Polytechnica Hungarica* journal in 2004, where he still serves as editor-in-chief.

He has a rich history with IEEE as well, started in 1991. He became IEEE Fellow in 2001, member of the IEEE Board of Directors Section/Chapter Support Committee (1998). He was mainly active in two IEEE Societies: the IEEE Industrial Electronics Society he was Administrative Committee Member and Senior Member (1996) and Vice-President of the Society (2000-2001). However, even bigger devotion presented to the IEEE System, Man and Cybernetics Society, where he was several times member of the Board of Governors (2007-2009, 2012, 2014), Vice-President (2013-2016), and currently he is President-Elect of the Society (2019). He is the founding chair of the Computational Cybernetics Technical Committee and co-chair of the Cyber-Medical Systems Technical Committee of the IEEE SMC Society. In the meantime, Imre J. Rudas served and made his footprint in the IEEE Hungary Section as well, where he was first Treasurer (1994-1998), then Vice Chair (2003-2009), and finally Chair (2009-2013). He was founding chair at IEEE Hungary Section level of the IEEE Chapter of Computational Intelligence Society (2003-2008), IEEE Chapter of System, Man and Cybernetics Society (2003-2008) and IEEE Joint Chapter of Industrial Electronics and Robotics & Automation Societies (1997-2002).

Among the several scientific awards received, he is laureate of the John von Neumann Award (2006), the Dennis Gábor Award (2006), the civil division of the Hungarian Order of Merit (2009), Pro Óbuda Award (2014), International Fuzzy

System Association Fellow (2016) and first awardee of the Rudolf Kalman Professor title given jointly by IEEE Hungary Section and Óbuda University (2017).

In the past decades, thousands of students, hundreds of colleagues and dozens of friends gained inspiration and professional support from Imre J. Rudas. His academic work was groundbreaking in Hungary, and the institutions and organization he established became a prominent part of the nation's engineering heritage. His professional network and outreach cover continents, and people around the globe are building on his results.

The editors are grateful to Imre J. Rudas for all his achievements care and support, and thankful to the authors for their excellent work composing this volume.

Budapest, Hungary
November 2019

Levente Kovács
Tamás Haidegger
Anikó Szakál

Smart Engineering Modeling for Smart Industrial Products

László Horváth

Óbuda University, Doctoral School of Applied Informatics and Applied Mathematics and John von Neumann Faculty of Informatics
Bécsi út 96/b, H-1034 Budapest, Hungary
horvath.laszlo@nik.uni-obuda.hu

Abstract: Automation of industrial and consumer products has reached the level on which systems provide for the capability to supervise decisions on physical actions and execution of these actions. Development of these industrial products proceed during their full lifecycle requiring lifecycle integration of innovation, manufacturing, and application as well as utilization the recently emerged methodology of continuous engineering. Engineering in the above level of industrial technology requires contextually integrated model system which serves all research, development, production, and operational activities during the integrated life cycle of product. Smart product requires smart model system which has the capability to recognize situation and apply it at decision on values of relevant product object parameters in virtual to control physical operation of product. This paper introduces recent contributions in modeling for smart engineering. It starts with a novel general model of integrated smart engineering system. Considering this model, smart engineering specific upgrade of formerly published concept of virtual engineering space (VES) is introduced. VES upgrade concentrates on research as key issue in giving smart characteristics for contexts in VES model system. Following this, contextual driving of object parameters is outlined for integrated smart engineering system. The remaining part of paper introduces concept and plan of virtual research laboratory (VRL) in close connection with modeling for integrated smart engineering system. Plans are outlined for next future implementation of the VRL concept and methodology at the Doctoral School of Applied Informatics and Applied Mathematics, Óbuda University. The laboratory system consists of research eligible configuration of the 3DEXPERIENCE engineering modeling platform. It is accessed in the professional cloud of Dassault Systèmes.

Keywords: system level model of engineering structure; virtual engineering space (VES); contextual driving structure in engineering model; virtual research laboratory (VRL)

1 Introduction

An emerging area in advanced engineering is integrated modeling of engineering structure (ES) for its lifecycle. ES [18] is defined as an industrial or a consumer product, a prototype of a product, or an experimental structure. Lifecycle of ES starts with the first concept and ends with recycling. It covers all ES related engineering activities including conceptualization, research, development, production, marketing, application, user services, and recycling. ES is represented in lifecycle model system [7]. Current leading ES model system is a result of long-time development with emphasis on integration. System level ES uses cooperating systems for control of its operating processes. System level modeling of ES requires a product lifecycle management (PLM) system, which is capable of integrating component models in a contextual model system. In this advanced PLM, purposeful procedures check any component model before it is accommodated in the model system. PLM system which implements the formerly prevailing product data management (PDM) methodology is not suitable for system level ES modeling [8]. When ES is capable of autonomous operation of its physical units using its own decision, we say it is smart. In industrial practice, various other technical and marketing purposed definitions are applied for the relative new term ‘smart’.

Modification of a modeling procedure or an entity in model representation in case of smart ES can be executed only in the knowledge of all its consequences in the model system. This request became critical when models started to apply in decisions driving real time physical actions in autonomous smart cyber physical systems (CPSs). Continuous engineering is being developed as methodology to handle the above problem in smart ES operation [2]. The main purpose of continuous engineering is to prevent physical operation malfunctions as a consequence of software modifications which have direct effect on control of those physical operations. In this way, continuous engineering provides a means to avoid erroneous activities of smart cyber control in operation of the CPS physical units. Methodology of Internet of Things (IoT) is highly involved in Continuous engineering. It is obvious that lifecycle development of model system for ES demands methodology from continuous engineering. In this context, authors of [15] define CPS as an approach that targets integration of computational applications with physical devices, relies upon networked and interacting cyber and physical elements, and controls, as well as, monitors real-world physical infrastructures.

Development in the integration of CPS systems places exceptional emphases on behaviors and contexts. Paper [16] introduces the Function-Behavior-State based methodology for integrated CPS design. This methodology applies functional description in multi-domain simulation modeling to represent behavioral-structural aspects of a system.

Laboratory of Intelligent Engineering Systems, Óbuda University and its predecessor represented three consecutive generations of world level engineering modeling technology during the past two decades. These laboratories applied leading representative engineering modeling systems, which implemented the *resource based integrated product information model*, the *industrial practice driven contextual generic model*, and the *requirements, functional, logical, and physical (RFLP) structured system-based model* [3]. This laboratory was among the first in research and education of the world-famous knowledge ware technology [18]. The experience-based modeling has undergone further development and is currently offered by in the 3DEXPERIENCE platform [19]. Recent, establishment of a fourth laboratory was implemented at the Laboratory of Intelligent Engineering Systems in association with the Doctoral School of Applied Informatics and Applied Mathematics. The *Initiative for Model Systems in Engineering of System Based Structures* was proposed as the scientific concept for the new laboratory. The 3DEXPERIENCE platform [4] by Dassault Systèmes decided to implement as the software system for the new Virtual Research Laboratory (VRL). In this way, conventional organization of modeling capabilities was changed for a platform which offered human role organized apps in cloud. The main activity area of VRL includes modeling of smart systems and realistic simulations, as well as, new areas such as modeling for organic shapes and in bionics.

In this paper, recent research results are introduced as contributions to modeling for smart engineering. Issues in this research include: novel general model of integrated smart engineering system, updated concept of virtual engineering space (VES), contextual driving of objects in smart model system of ES, and concept, plan and implementation of VRL. General model of integrated smart engineering system allows studying requirements against new model structures and representations. Smart engineering specific rethinking of the formerly published concept of virtual engineering space (VES) redefined the utmost objective of model development for ES [5]. Essential requirement against model system for smart ES is an advanced self-adaptive feature combining together the capability for automatic propagation of inside and outside contexts. This is necessary because smart ES is too complex for conventional tracking consequences of frequent modification during its lifecycle.

Concept, methodology, software background, and implementation of a new *virtual execution type* and *experimental model based VRL* are also issues in this paper. Cloud environment and research eligible engineering modeling platforms are considered for the new laboratory system. Contrary to many opinions about this style of work, research using experimental model is not only the application of engineering software to assist formerly proven practice but a new style of systematic creative work in a scientifically upgraded modeling environment. VRL is planned to implement relevant achievements discovered in our new century.

This paper may be difficult to read for those who are not familiar in recent system-based engineering modeling of smart industrial and consumer products. Strong trends towards full contextual integration of innovation, production, and application processes of autonomously operating ES configurations require a changed type of understanding. Huge integrated systems need large amounts of, but integrable contributions. This fact motivated work for contributions in this paper.

2 General Model of Integrated Smart Engineering System

The need for representation of all possible contexts in ES model necessitated the definition of the new comprehensive general model of smart engineering system. In this model smart engineering system is considered that which integrates *outside driving context sources, lifecycle model system of generic ES, production system for ES, and physically operating ES* (Fig. 1).

ES is engineered in an appropriate *virtual engineering space (VES)* which provides structured description and representation for engineering activities during the lifecycle of ES. Recently, research and development in ES related issues were extended to lifecycle of ES highly relying upon methodology of *continuous engineering*. To serve this new demand, redefined VES is realized as *lifecycle model system of generic ES*. VES is developed solely by contributions from *outside driving context sources*. While the model system of ES is autonomous, it is under continuous control by outside driving contexts for its lifecycle. When it is programmed or considered necessary, intervention by an authorized human is still available at any step of the model development processes. At the same time, an increased level of automation in smart engineering processes restricts human intervention to critical problems. In this way, entities in ES model system are solely under the control of dedicated *outside driving contexts*. This solution replaces the *conventional direct human interaction* except for special and often critical cases. The revised VES concept which complies with smart ES and the related smart engineering are discussed in the next section of this paper.

As result of inherent complexity and multidisciplinary nature of systems operated ES *lifecycle model system of generic ES* demands a wide variety of configurable modeling capabilities during its long-time development. Capabilities are available in role accessible apps as service of engineering modeling platforms. This new era of engineering modeling requires new human thinking and engineering practice which is very different from the former modeling. The lifecycle model system of generic ES must include *organized driving background, virtually executable system level model of ES, physical level ES model with realistic simulations, and the capability for smart CPS communication*.

Organized driving background was proposed in papers [6] and [7] among others to establish contextual connections between outside driving context sources and system level model system of ES. This background was organized in driving content structure (DCS) [7]. DCS includes sub-levels in each of its four levels to organize driving contexts for system related aspects. RFLP based ES model [8] is supposed as driven structure. DCS receives, collects, evaluates, and processes contexts from *outside driving context sources* for lifecycle of ES and provides actual drives for relevant RFLP structure objects. DCS is not an issue in this paper. Above cited publications include all necessary information about it.

The next unit in the general model of integrated smart engineering system is real world operating smart CPS ES. An additional unit here may be the manufacturing system for ES which behaves as CPS considering the recent paradigm, which is mainly defined by Industry 4.x. Driving of manufacturing purposed CPS requires multilevel structured manufacturing model within model system of ES. In [8], manufacturing model structure consists of levels for activities, system, and resources in case of a generic ES.

It is obvious that modeling in this paper must consider physically operating ES and production system for ES as smart CPSs. As it is well known, CPS consists of cyber and physical units where cyber units interact directly with physical units. This interaction is allowed by intelligent sensor networks which always provide actual real-world information about parameters of physical processes. Actuators operate physical processes in accordance with decisions in cyber units. Essentially, cyber units in smart CPS receive and process sensor information about physical unit parameters, recognize situation, and make decision on physical control action in smart CPS in accordance with the recognized situation (Fig. 1). Finally, actuators are controlled in accordance with decision to execute physical actions.

Smart CPS technology is result of long-term development in automatic equipment and device control and in active knowledge representation for engineering model and product operation control. Authors of [14] analyze changes caused by increasingly complex engineered systems. They define smart cyber-physical system, which is empowered by cyber-physical computing features and has capabilities for reasoning, learning, adapting, and evolving.

It is obvious that smart CPS is different from classical CPS. However, this difference, which is often cited as smartness is very difficult to define mainly because only few experiences are available in relevant published theoretical works. In [9], smartness is claimed to derive from cooperative behavior, self-awareness, self-adaptation, and self-optimization. Similar key concepts were analyzed in works published as preliminaries of work in this paper and will be discussed below. It is important to recognize that bioinspired engineering methodology is useful to learn from nature. Findings can be well utilized in development of representations for smart engineering [10].

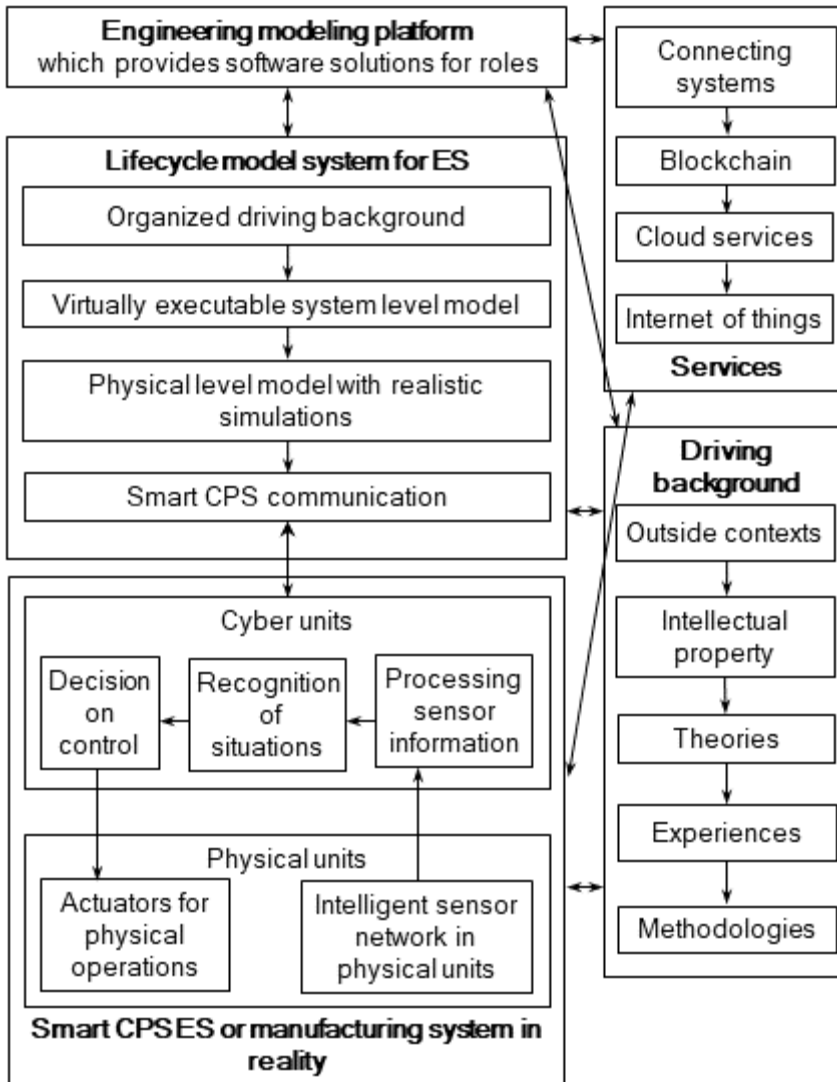


Figure 1

General model of integrated smart engineering system

Importance of *behaviors* is emphasized in [7] because one of the main purposes of DCS is to drive behavior representations in function (F) and logical (L) level ES components in RFLP structured model system. Behavior representations make F and L level models of ES virtually executable. In case of smart ES, cooperative behavior must ensure mutual understanding between cooperating systems as well as between the system and an intervening human. Cooperative behavior is one of the essential issues in smart CPS because physical activity is generally the result

of cooperation between systems or systems and humans. With the advent of smart CPS systems erroneous cooperation has become a main cause of malfunctions. A typical source of malfunction in smart CPS is misunderstanding autonomous system decisions and actions by a human who cannot find the proper intervention. Contradictions between situations recognized by different systems are sometimes attempted to be resolved by authorized but inexperienced humans under time pressure. Very rarely, the above problem leads to serious disturbance or crash even in the most advanced aircraft, cars, and industrial processing equipment.

Self-awareness is the capacity of systems to recognize states using analysis of behavior-related situations. This is basically introspection. The situation is applied in decision on model entities or physical unit action. *Self-adaptation* capability of CPS is also important because inside and outside contexts often change during operation of CPS. As for the ES model system, self-adaption is one of the essential capabilities in leading engineering practice. In this context, *self-optimization* proceeds increasingly in real-time and enhances decisions on adaptive changes. Considering the above criteria of smart CPS, smartness is highly based on methodology from intelligent computing, modeling and simulation.

Driving background includes contexts from outside of the model system and CPS as well as from organized intellectual property (IP). Proven and approved theories, experiences and methodologies improve quality of cyber activities and prevent malfunctions in physical units. More details will be given in the Chapter 4 of this paper.

The last block in Fig. 1 shows *computing services*, which are essential for the operation of smart CPS. In this context, systems are connected, blockchain is managed where it is applied, services often come from cloud, and real time connections between computing and physical devices need availability of advanced IoT services. Computing services are not issues in this paper.

3 Virtual Engineering Space (VES)

Virtual engineering space (VES) was published in 2005 and 2007 [11] as a realistic representation of a physically existing or planned engineering space. Today it is more factual than ever before. VES represents a well-defined segment of our physical world where the remained physical world is replaced by contexts in its mutual affect zone. Trusted source ensures valid and realistic context. Sources are responsible for the content of context. At the same time, any relevant and active context is mandatory to include in VES. VES representation must provide valid self-adaptive reaction for context. VES model system can represent human related aspects such as behavior and physiological process. In this paper, VES is supposed to represent an ES.

Wide availability of cloud-based information technology makes it possible to compose geographically unlimited physical space for a VES. At the same time, recent ES technology demands VES for the representation system based physical space. VES concept was upgraded for systems in [6]. Recently, smart CPS needed new redefinition of VES to better understand this new generation of physical engineering spaces. When implemented, this new VES definition needs engineering modeling platform, which is eligible for the demanded high-level modeling and provides all the capabilities necessary for the representation of VES.

Main structure of smart CPS eligible VES is summarized in Fig. 2. Theoretically, *VES consists of its control contexts, model system which represents it, and services*. Besides the control contexts, *additional VES contexts serve connecting systems and CPS cyber units*. Two-way context allows arbitrary direction for its definition. Consequently, connecting system and CPS not only control VES, but they also can be controlled from VES. Dashed boxes include connected outside units which are not issues in this paper.

VES control contexts include authorized human intervention for the definition of entities in VES representation, decisions and measures from higher-level systems such as governments, authorities, company management, standards organizations and research institutions, and proven and accepted intellectual property (IP) from validated sources. Because VES control contexts are continuously changed during the lifecycle of the represented physical space, VES is under continuous change.

VES concept may be applied far beyond usual ESs. Sometimes, VES represents physical space, which has no predictable lifecycle or its lifecycle is considered as unlimited. The following example is for this case. Central buildings of the Óbuda University were built above ruins of the ancient roman city Aquincum. VES representation of an ancient building needs continuous development as new digging experience, archeological research results and other newly emerged contexts are to be included. This is a fantastic new opportunity to bring these ancient buildings to life again. VES here would establish a limited, but progressively evolving realistic self adaptive model, which reacts to any new context by repeated real time simulation. Although the purpose of VES is model based representation, integration and analysis, recent show and additive manufacturing technologies are suitable to visualize VES represented physical objects to assist scientific analysis or support popular demonstration on a higher level than ever before.

Model system collects, validates and connects models. The purpose characterizes projects in which the model system for VES is involved. Structure connects component models. Component model is developed and executed in its own model space considering relevant contexts between models.

Lifecycle model for ES consists of contextual models, which are defined on seven layers (Fig. 2). *Level driving communication* collects, organizes, validates, and places outside contexts and contexts within the model system. This is followed by

four levels of RFLP structured model of ES using systems engineering (SE) and latest engineering modeling methodologies.

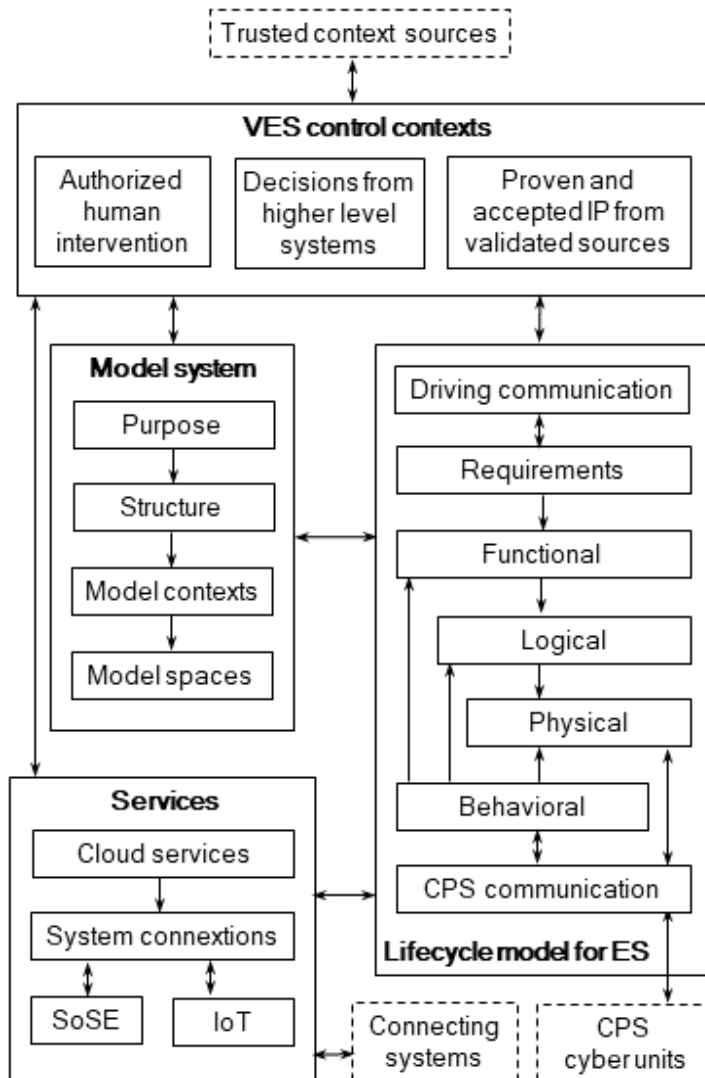


Figure 2
Upgraded VES

The next level is *behaviors* and serves smart CPS characteristics of VES for situation-based decisions on virtual and physical activities. Finally, seventh level serves *bilateral communication* with cyber units of CPS systems. In practice, levelling may be different from the above depending on the task and the modeling platform in which the model system is built and managed.

Services include cloud services, which are essential to provide geographic and time independence of VES definition and application projects, system connections which apply methodology of system of systems engineering (SoSE), and appropriate physical connections using technology from IoT.

4 Contextual Driving Structure

The importance of *self-adaptive generic engineering model systems* was highly increased by wide spreading of industrial and commercial products, which were featured by very complex multidisciplinary structure and smart CPS functions. This main change has brought organized definition of contexts to the foreground. Modern engineering models are capable of high-level and comprehensive representation of contexts between pairs of object parameters in large structures. This achievement makes high-level integration of logical connections, formulas, equations, algorithms, procedures, networks, data arrangements, and stored models possible in model definition. Results from intelligent computing such as Fuzzy, neural networks, evolutionary computing can be integrated in ES model system easily. Theories, methodologies, and experiences are represented in an active model system, which must be driven by consistent system of contexts. Experimental models are developed for well-defined research programs (Fig. 4).

Aspects in contextual driving of model object parameters were published in [6] and [12] including intellectual property (IP) support of model definition and execution. Providing complete and consistent system of contexts is an essential requirement at any time during lifecycle of ES. This is necessary to realize correct context driving of object parameters in the ES model system, which represents smart ES with generic, self-aware, self-adaptation, and self-optimization features.

Current engineering models apply object orientation in an informatically correct manner. Object in a model system is an instance of relevant object class having appropriate parent-children connections in taxonomy. Integration of a new context in a model system supposes that all object parameters connected by the new context are active through appropriate existing contexts.

Essential processing of driving context is introduced in Fig. 3 using a simplified schema to explain the main steps. Context here is supposed as new contribution to context system in an engineering model system. New or modified context must come from well-defined and trusted outside context sources. Parameters which are included in a contextual connection belong to components, elements, features, or other engineering objects represented in ES. Their position in structures and substructures within the model system are defined by special purpose contexts. Owner of any active context takes responsibility during lifecycle of ES. Owner information is included in the model system and available at processing of context.

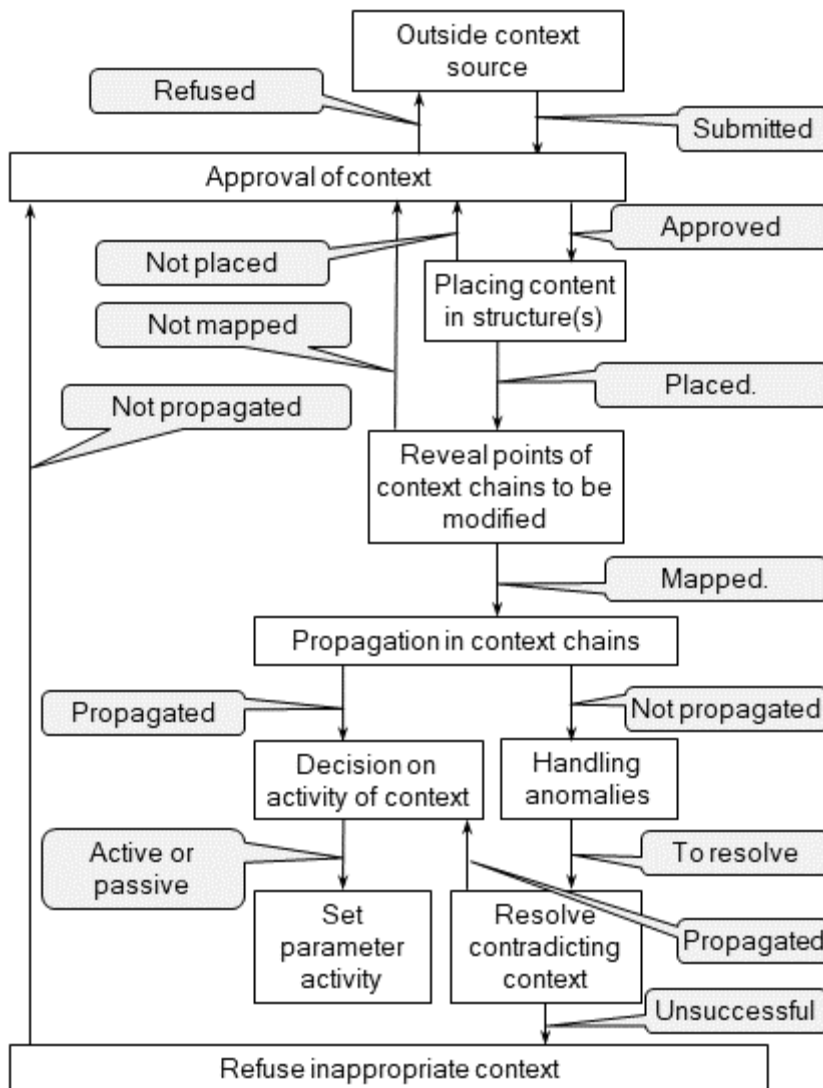


Figure 3
Essential processing of context

Each context has a status parameter, which is changed when a step is completed during its processing. At its submission, context status parameter obtains a *submitted* value. In the course of the basic approval process, status value changes for *approved* or *refused*. Basic approval process decides status considering context parameters such as owner, originality, system relation, discipline, proven principle, method, proven experience, and solution relevance. A former proposal of driving content structure (DCS) included concept for this approval process [7].

When a context has *approved* status, the next step is placing its content in the relevant structure(s). This content will be active in model. It must be suitable for driving the context connected parameter(s) correctly in any situation. Do not forget that the recognized situation, which is applied in decision on real time operation of physical actuators, is critical in correct and safe operation of the relevant smart CPS. Some recently operational problems in advanced smart CPS ESs are often emerged in connection with this issue. Successful placing results *placed* status of context. Otherwise, this status is *unplaced*.

The next step in processing of context having *placed* status is to reveal connecting points in the context chains to be modified. This is an attempt to map the submitted context in relevant content chains of the context system. Successful mapping results *mapped* status of context. Otherwise, the status is *unmapped*.

Propagation in context chains means the attempt to execute driving by the new context in the relevant context chains. This requires experiment to propagate context along chains in the context system. When consequences are acceptable, status of context changes for *propagated*. Otherwise, the new status is *not propagated*.

When the status is *propagated*, activity of the new context is set in accordance with its actual position in the model system. In case of *not propagated* status, attempts for handling anomalies and where necessary resolving context contradiction are done as measures to transform context into valid. When one of these attempts fail, context is refused as inappropriate.

5 Virtual Research Laboratory (VRL)

One of the objectives at the implementation of VES is integration of theory and practice in model system of ES. Industry eligible engineering modeling of smart ES was successfully developed towards capabilities, which made parallel representation of theory and relevant experience possible in model system during the past decade. While definition of model object is still based on the latest theory and methodology, theory driven model object generation procedures use representation of relevant valid experience. In this way, experience representation is applied in validation and correction of theory-based parameter values. A milestone was introduction of the knowledge ware in definition and generation of engineering model system to reuse knowledge representing proven best industrial experience and practice in the first decade of the new century. By now, integration of theory and practice has become one of basic criteria in the development of engineering model system.

It is obvious that integrated research, development, manufacturing planning, marketing, application and recycling during the whole life cycle of ES requires

new ideas and at the same time offers great new possibilities for engineering related research and its laboratory background. In this context, this and the next part of this paper are about concept and implementation of virtual research laboratory (VRL). The term *virtual laboratory* was applied for laboratories with very different visual and virtual reality related purposes during the past three decades [3]. Some virtual laboratories apply *tangible reality* to visualize model space and allow interaction between human and this space. Other known purpose of virtual laboratory is *extended reality* to mix virtual and physical objects to analyze cooperation between them. Additional known purpose of virtual laboratory is to support *collaboration amongst capacities for research and associated activities* in different geographical places. This collaboration includes shared application of facilities, operation of discipline-specific computing, modeling and simulation software, and sharing collective knowledge and expertise. The models are slightly integrated, and documentation and visualization are still in the center of collaboration activities. The VRL concept is different from the above.

The VRL concept places experimental model and its virtual execution in the center of research activities. VRL requires engineering modeling platform, which is in possession of scientific level functionality suitable for this laboratory purpose. Collaboration between participants of research group is done through experimental model using latest collaboration capabilities available in the modeling platform (Fig. 2). Depending on the research program of VRL, platform is demanded to have capabilities for recently emerged areas such as modeling of systems in ES, organic geometry of shapes and bionics. VRL has the potential to gradually replace most of the physical laboratory functions.

The main activity in VRL is conducting virtual experiments in well-defined research projects with participation from various activity areas, organizations, and geographic sites. VRL activities and models are realized in the host engineering modeling platform. Cloud-based platform host platform provides services for platform management, participant management, role management, and workspace management assuring an environment for virtual experiments and related activities (Fig. 4). Platform capabilities for the representation of deep knowledge are essential for researchers who work in VRL. VRL in the cloud assures highly communicative and distributive research environment.

Virtual experiment process (Fig. 4) is controlled by experiment plan. Starting from an active actual experiment plan, experimental model is initially defined then developed during its whole life cycle considering methodology of continuous engineering. In case of a new experiment, units and entities of experimental model can be newly defined or retrieved as stored object configurations. Stored configurations can be used as building blocks of a new experimental model. It is obvious that experimental model is object model in which instances of object classes are defined in contextual structure. Experimental model is created and managed using modeling capabilities available in the platform including user

defined resources. When object class, model entity, parameter, procedure, algorithm, function, process, or other new resource required, user definition and configuration capabilities of the platform are applied.

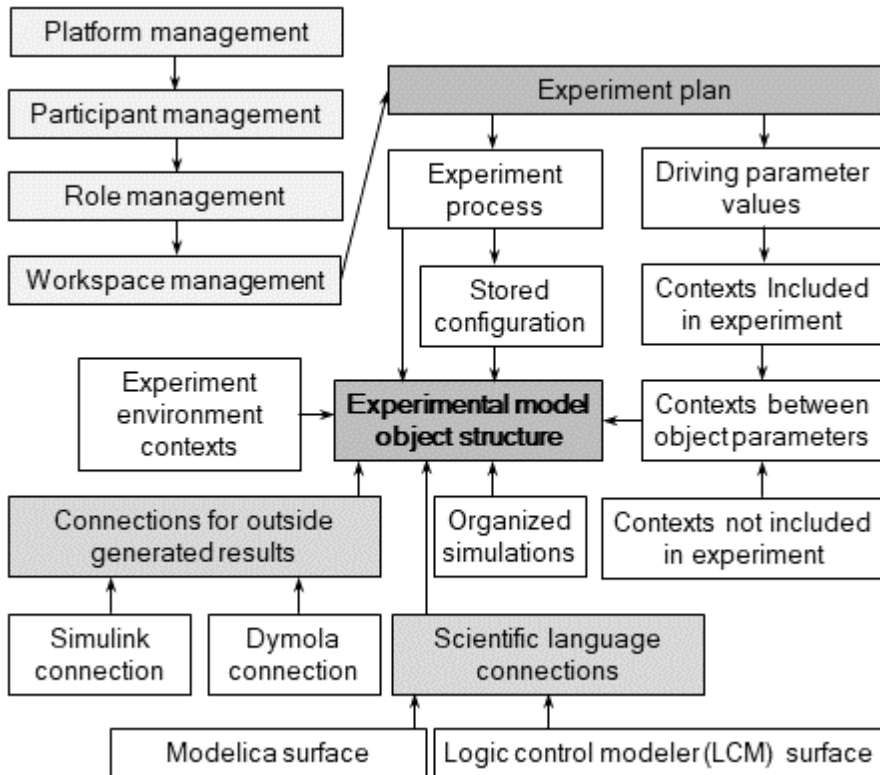


Figure 4
Experiment in VRL

Driving object parameters are analyzed in the course of purposefully defined experiments (Fig. 4). These parameters drive contextually related active objects in the experimental model system. Actual experiments apply relevant experimental model to analyze parameters, their interactions, to find most influential parameters, and to predict parameter values in different situations in accordance with specification in experiment plan. Consistent context system is an essential requirement as in the case of any other model system. All relations of driving parameters and parameters in contextual chains of experimental model must be covered. Using contexts, value sets of driving parameters control execution of experimental model in accordance with actual experiment plan.

Context system of experimental model contains special contexts, *which are subjects of analysis* and are included in experiment. These *contexts carry research*

results, which are to be analyzed and verified in experiments. Objects in experimental model must be suitable to accommodate these contexts. The remaining *contexts which are not included in experiments* are also active in the experimental model and must serve the relevant experiments. Finally, *experiment environment contexts* serve connection of experimental model with affect sources in the outside world. These contexts can be used to widen the scope of experiments. Definition and representation of organized simulations serve execution of experimental model in the context structure.

Research often demands software tools which are outside of platform. To solve this problem, 3DEXPERIENCE platform includes software capabilities (apps) to establish communication between the experimental model and the most important outside modeling and simulation software such as Matlab, Simulink, and Dymola. Availability of capabilities which allow accommodation of model representations prepared in Modelica and Logic control modeler (LCM) languages are also important. These languages are inevitable to represent dynamic and state logic behaviors in the experimental model. Owing to features of platform, experimental model can be configured to be integrator in widespread research program. Platform organizes latest complex virtual engineering technology from leading industries so that VRL offers world level solutions for research program. Theory and experience orientations are inherently integrated in models so that contradiction of them, which is usual in conventional engineering can be avoided using appropriately configured and conducted virtual experiments.

Higher education courses which prepare students for roles which are defined in the industrially oriented platform can be reinforced by industrial and research participation. Establishing dual and other cooperation between universities and industrial companies is easy in VRL environment.

6 VRL in Cloud Organized Platform

The VRL concept was decided to be implemented mainly for PhD research at the Doctoral School of Applied Informatics and Applied Mathematics, Óbuda University. The Laboratory of Intelligent Engineering Systems is being upgraded for this purpose. Comprehensive capabilities of the 3DEXPERIENCE platform are under installation. Server side is configured in cloud operated by Dassult Systèmes as its own system of this VRL. *Platform management* receives and evaluates inquiries from the local VRL managers as cloud service to define new or changed participant roles and to allocate new apps for participant role. The 3DEXPERIENCE provides a complete cloud package which includes comprehensive modeling software with capabilities in apps (SaaS), platform for custom applications (PaaS), and infrastructure (IaaS). Role provides access to a well-defined set of apps. Research specific roles will be defined for participants.

Definition and managing custom apps are awaited in VRL research. The *Design Apps Developer* role is available in the platform for custom definition of apps. This role is important in development of capabilities for representation of reused practice as well as in definition of research program specific methods, procedures, and processes without the need for special programming skill. In this way, research tasks are automated and design assistants are developed. Research will be defined, organized, and conducted in VRL in accordance with its purpose, topic, awaited area, type and publication of results and in coordination with participant institutions, companies and individuals.

Cloud server side of the 3DEXPERIENCE platform of VRL will be accessed by properly installed client workstations. To guarantee the stable operation of the VRL, 3DEXPERIENCE platform certified client workstations will be installed in the next future.

Fig. 5 introduces an example to illustrate that how experiments are planned and conducted. Research for an accredited PhD topic is supposed to be conducted using the 3DEXPERIENCE based VRL environment at the Doctoral School of Applied Informatics and Applied Mathematics, Óbuda University. This PhD research is expected to produce new representations for the application in model of flexible bodies and function driven organic shapes. The modeled physical system is supposed to include both rigid and flexible elements.

Awaited results of research are divided into theoretical and practical groups. Results in the *theoretical group* are new algorithms, procedures, object classes, behaviors, situations, networks, rule sets, mathematical functions which modify relevant parameters and contexts in the actual experimental model. Relevant simulations are defined in the experimental model and are conducted using means available within the platform or using one of connected outside solvers. *Practical group* of research results includes results of execution of the experimental model in the context of appropriate sets of driving parameter values and in accordance with the actual active experiment plan.

The self-adaptive experimental model automatically propagates any modification of contexts then repeats the execution of relevant multiphysics [17] and realistic simulations. Application of continuous engineering methodology is advised to consider in development of experimental models and research results for the full period of a PhD or other actual research. VRL records all important parameters of a research program for the lifecycle of experimental model.

Contexts are revealed and defined for objects inside of the experimental model and for connections of outside objects. Outside affects are handled as contexts defining initial conditions for the experimental program. Among others research task related and higher-level requirements are set here as contexts. Most important outside contexts of the experimental model include value sets for driving input parameters which control experiments and for output of experiments. Practical results are generated by virtual processes. Output parameter values represent performance of results in the theoretical group.

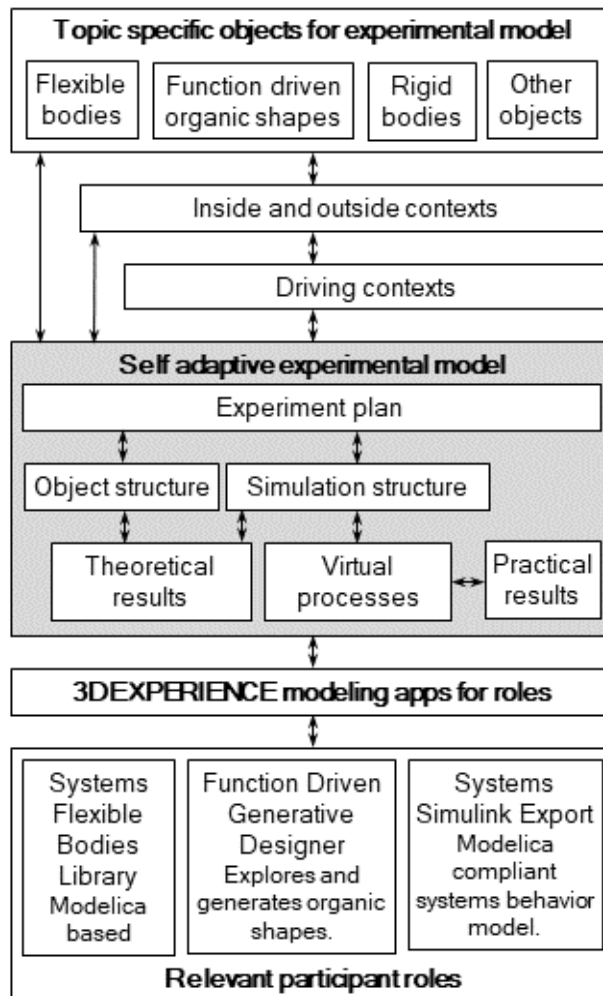


Figure 5
Experiment in VRL

Results of cited research used in a VRL organized research are often available in form which allows their connection to experimental model as context. It is anticipated that this advanced type of citation will gradually replace the conventional passive paper and book citations and at the same time will open the way towards unlimited extension of VRL based research networks in the future. General, cited, and contributed knowledge items are represented as context. General knowledge is available as purchased with the platform. Cited knowledge is owned by other research institutions or individuals. The contributed knowledge is result of research in VRL. The above categories are mandatory to distinguish in all experimental model.

Student who will work on PhD thesis for four years in the VRL will be invited as participants in the 3DEXPERIENCE environment of the laboratory. Specific participant roles will serve this special application of platform. Besides VRL specific roles, research will be served by topic dependent 3DEXPERIENCE roles [13]. In the above example research topic (Fig. 5) three roles are included. The *Systems Flexible Bodies Library* role is based on the Modelica language. The *Function Driven Generative Designer* role explores and generates organic shapes using functional specification. The *Systems Simulink Export* role serves Modelica compliant systems behavior models.

Conclusions

Smart systems operated products, direct connection between model-based virtual decisions and physical actuation, integration of innovation, production and application of ES in a unified cycle and need for reliable lifecycle continuous engineering brought new challenges for physically connected virtual engineering. Above all, smart characteristics of engineering activities will be enforced in the immediate future. Joining in this way of development, this paper introduces some new findings in smart engineering. One of main tasks here is to extend the active context system in generic lifecycle ES model system to outside driving context sources, to production system for ES, and to physically operating ES.

In this paper, contributions to solutions of actual problems of smart engineering include general model of integrated smart engineering system, redefined virtual engineering space (VES) to better understand modeled physical engineering space in case of smart cyber physical system (CPS), an essential processing of new or modified context in consistent context structure, new initiative of engineering model system based virtual research laboratory (VRL), and implementation of VRL concept in cloud organized platform in the Doctoral School of Applied Informatics and Applied Mathematics, Óbuda University.

Acknowledgement

The author gratefully acknowledges the financial support by the Óbuda University and the Doctoral School of Applied Informatics and Applied Mathematics.

References

- [1] J. Stark: Product Lifecycle Management (Volume 1), 21st Century Paradigm for Product Realisation, Springer, 2015
- [2] B. Fitzgerald, K-J. Stol: Continuous software engineering: A roadmap and agenda, Journal of Systems and Software, Vol. 123, 2017, pp. 176-189
- [3] L. Horváth: Virtual Research Laboratory for Smart Engineering in the Cloud, proc. of the IEEE 13th International Symposium on Applied Computational Intelligence and Informatics, Timisoara, Romania, 2019, pp. 179-184

-
- [4] E. Gomez, H. Adli, C. Fernandes, M. Hagege: System Engineering Workbench for Multi-views Systems Methodology with 3DEXPERIENCE Platform. The Aircraft Radar Use Case, Complex Systems Design & Management Asia, 2016, pp. 269-270
- [5] L. Horváth: On the Way Towards Smart Engineering Systems, Proc. of the IEEE 23rd International Conference on Intelligent Engineering Systems, Budapest, Hungary, 2019, pp. 235-240
- [6] L. Horváth, I. J. Rudas: Information Content Driven Model for Virtual Engineering Space, Acta Polytechnica Hungarica, Vol. 15, No. 2, 2018, pp. 7-32
- [7] L. Horváth, Intelligent Content in System Level Model of Industrial Cyber Physical System, Proc. of the 44th Annual Conference of the IEEE Industrial Electronics Society, Washington D.C., USA, 2018, pp. 2914-2919
- [8] S. Kleiner, C. Kramer: Model Based Design with Systems Engineering Based on RFLP Using V6, Smart Product Engineering, Springer, 2013, pp. 93-102
- [9] T. Bures, B. Schmerl, D. Weyns, et. al: Software Engineering for Smart Cyber-Physical Systems: Challenges and Promising Solutions, ACM SIGSOFT Software Engineering Notes, 2017, Vol. 42, No. 2, pp. 19-24
- [10] L. Horváth: Representing Biological Aspects in Engineering Model System, in Proc. of the IEEE International Work Conference on Bioinspired Intelligence, Budapest, Hungary, 2019, pp. 133-138
- [11] L. Horváth: Supporting Lifecycle Management of Product Data by Organized Descriptions and Behavior Definitions of Engineering Objects, Journal of Advanced Computational Intelligence and Intelligent Informatics, Vol. 11, No. 9, 2007, pp. 1107-1113
- [12] L. Horváth, Cyber Physical System in Context with System Level Engineering Model, Proceedings of the 2019 IEEE 28th International Symposium on Industrial Electronics, Vancouver, BC, Canada, 2019, pp. 1627-1631
- [13] Dassault Systèmes (2019, september 6), 3dexperience portfolio-roles, <https://www.3ds.com/products-services/3dexperience/portfolio/>
- [14] J. Tavčar, I. Horváth, A Review of the Principles of Designing Smart Cyber-Physical Systems for Run-Time Adaptation: Learned Lessons and Open Issues, IEEE Transactions on Systems, Man, and Cybernetics: Systems, Vol. 49, No. 1, 2019, pp. 145-158
- [15] P. Leitaoa, A. W. Colomboc, S. Karnouskose, Industrial automation based on cyber-physical systems technologies: Prototype implementations and challenges, Computers in Industry, Vol. 81, 2016, pp. 11-25

- [16] A Canedo, E Schwarzenbach, E. M A Al Faruque, Context-sensitive synthesis of executable functional models of cyber-physical systems, Proc. of the 2013 ACM/IEEE International Conference on Cyber-Physical Systems (ICCPS), Philadelphia, PA, USA, 2013, pp. 99-108
- [17] E. L. Blades, R. S. Miskovich, E. A. Luke, E. M. Collins, A. G. Kurkchubashe, A Multiphysics Simulation Capability using the SIMULIA Co-Simulation Engine, Proc. of the 20th AIAA Computational Fluid Dynamics Conference, Honolulu, Hawaii, 2011, pp. 1-16
- [18] L. Horváth, J. Fodor, I. J. Rudas, Manufacturing Aspect of the IBCA Structure for Active Knowledge Content Representation in Product Model, IFAC-PapersOnLine, Volume 48, Issue 3, 2015, Elsevier, pp. 1616-1621
- [19] Dassault Systèmes (2019, september 6), Product Synthesis Solutions, https://www.3ds.com/products-services/catia/products/v5/portfolio/domain/Product_Synthesis/

Tumor dynamics modeling based on formal reaction kinetics

Dániel András Drexler¹, Tamás Ferenci¹, Anna Lovrics², and Levente Kovács¹

¹Physiological Controls Research Center, Research, Innovation and Service Center of Óbuda University, Óbuda University, Hungary

{drexler.daniel,tamas.ferenci,kovacs.levente}@nik.uni-obuda.hu

²A. Lovrics is with the Membrane Protein Research Group, Institute of Enzymology, Hungarian Academy of Sciences, Hungary

lovrics.anna@ttk.mta.hu

Abstract: Modeling the effect of therapeutic drugs on tumor dynamics is a fundamental step that leads to the optimization of cancer therapy using mathematical tools. We discuss three tumor dynamics models starting from a minimalist model describing the effect of bevacizumab based on experiments where the measurements can be defined with one parameter exponential curves, and finally discussing a more complex model that describes the effect of pegylated liposomal doxorubicin (PLD) based on measurements with richer dynamics. The differential equations are created with the analogy of formal reaction kinetics, enabling universal interpretation of the modeled phenomena. Parametric identification is carried out based on measurements to prove the efficacy of the models. The results of the parametric identification show that the discussed models can sufficiently describe the experimental results. The between-subject variability of the model parameters is given which highlights the parameters that may change the most in a virtual patient set.

Keywords: antiangiogenic therapy; chemotherapy; pegylated liposomal doxorubicin; stochastic approximation expectation maximization

1 Introduction

Model-based optimization and personalization of tumor therapies require tumor growth models which reliably describe the effect of the drug used during the therapy [1]. Creation and validation of tumor models can be carried out using time series measurements in mice experiments involving drugs for cancer treatment [2]. Mathematical models, i.e. differential equations, however, can be hard to interpret by clinical experts, thus we use formal reaction kinetics analogy [3] to create the tumor models, similar to the work of Kuznetsov et al [4].

The most common tumor growth models assume Gompertzian growth function [1, 5], which introduces a nonlinear term in the differential equation. Although,

Gompertzian growth function expresses the fact that the tumor volume (or cell number) has an upper limit, we do not use Gompertzian function in our model. Since our modeling is driven by mice experiments, and during the experiments, the tumor never reaches its upper limit, but operated on the linear dynamics range (i.e., tumor growth is exponential), we use linear dynamics to describe the tumor growth.

The tumor modeling is built up starting from a simple model ending with complex one incorporating nonlinear pharmacokinetics and pharmacodynamics. Section 2 covers the simplest model incorporating the effect of tumor proliferation, drug clearance and drug effects [6], resulting in a planar system with one bilinear term in the differential equations and two linear terms. The solution of the differential equation can be written symbolically if the input is one single injection, which was used for least squares parameter estimation in [6]. This model is also referred to as the minimal model some papers related to tumor control [7–10].

The minimal model is extended with dead tumor volume dynamics, nonlinear pharmacokinetics and pharmacodynamics in Section 3. The model is validated using measurements with angiogenic inhibitor bevacizumab [11]. The extension of the model with dead tumor volume enables more realistic identification, since in the experiment, the sum of the volume of the dead and living tumor volume is measured [12]. The mixed-order pharmacokinetics and nonlinear pharmacodynamics makes the model even more realistic, with the latter incorporating the effective median dose (ED_{50}) parameter, which introduces an input saturation. The qualitative analysis of the extended model is carried in [13].

The extended model is used to model the effect of chemotherapeutic agent pegylated liposomal doxorubicin (PLD) in Section 4, where the dead tumor volume washout is also added to the model. The results show that the model can sufficiently describe the effect of chemotherapeutic agent applied to mice with breast cancer [2], which has been used for therapy optimization in [14] with a modified optimization algorithm of [15].

2 Minimal Tumor Model

The first version of the tumor model based on formal reaction kinetics was published in 2017 [6]. The tumor growth model is given by the planar system

$$\dot{x} = ax - bxy \quad (1)$$

$$\dot{y} = -cy \quad (2)$$

where x is the time function of tumor volume given in mm^3 , y is the time function of the level of drug in the patient given in mg/kg (i.e., mg of inhibitor per body mass kg of the host). The parameters of the model are

- a : the tumor growth rate [$1/\text{day}$];
- b : the drug efficiency rate [$\text{kg}/(\text{mg} \cdot \text{day})$];

- c : the clearance of the drug [1/day].

The drug depletion is defined with linear pharmacokinetics in (2). Thus, the depletion of the drug is governed by a linear differential equation, yielding that the time function of drug level is given by

$$y(t) = y(0)e^{-ct} \quad (3)$$

with $y(0)$ being the initial condition. Suppose, that we give $y(0)$ amount of the drug to the patient at time $t = 0$. If there are no more injections, the level of the drug in the patient is described by (3) if there was no drug present in the patient before the injection.

The parameter c used in (3) is the clearance of the drug. The clearance and half-life of drug are both used in medical practice. The clearance parameter can be acquired from the half-life of the drug denoted by $T_{1/2}$ using

$$c = \frac{\ln 2}{T_{1/2}}. \quad (4)$$

The tumor growth dynamics is described by (1), where the first term on the right-hand side characterizes exponential growth of tumor volume with growth parameter a . This term defines an unstable system if a is positive, i.e., the tumor grows uncontrollably (described by an exponential function with positive exponent), and there is no upper bound for the tumor volume. Tumor growth dynamics is typically described as a Gompertzian growth function [5], i.e., the tumor volume has an upper bound, however, we found that this model without upper bound fits the measurements adequately and we were not able to observe the saturation process of the tumor volume throughout many experiments [12].

The effect of the drug is described by the second term on the right-hand side of (1). This bilinear term is the product of the tumor volume and the drug level, thus if there is no tumor, then there is no therapeutic effect regardless of the amount of drug present in the host. This bilinear term is the most simple term that can describe this phenomenon. The rate of drug efficiency is the constant b , and since the sign of the second term is negative, b is positive if the drug acts against the growth process (thus inhibits tumor growth).

The solution to the differential equation (1) is

$$x(t) = x(0)\exp\left(at - \frac{by_0}{c}(e^{-ct} - 1)\right), \quad (5)$$

with $x(0)$ being the initial tumor volume and $y(0)$ being the amount of drug injected at time 0, provided that there was no drug present in the host before injection and there are no other injections during the therapy.

The minimal model given by (1)-(2) which describes unstable tumor growth, effect of the drug and linear pharmacokinetics can be formulated as a fictive chem-

ical reaction given by the following reaction steps with species X representing the tumor volume and the species Y representing the drug level:

- $X \xrightarrow{a} 2X$ that defines that tumor cells divide with rate a , i.e. species X doubles its volume with a reaction rate coefficient a . Considering mass action kinetics, the corresponding differential equation is $\dot{x} = ax$;
- $Y \xrightarrow{c} O$ that defines that there is an outflow of the species Y with a reaction rate coefficient c , i.e., the drug is cleared from the body of the host, considering mass action kinetics, the corresponding differential equation is $\dot{y} = -cy$;
- $X + Y \xrightarrow{b} Y$ that defines that the species X and Y react and after the reaction the species X disappears with a reaction rate coefficient b , i.e., the drug destroys tumor volume; considering mass action kinetics, the corresponding differential equation is $\dot{x} = -bxy$.

The connection of formal reaction steps and the corresponding differential equations (1)-(2) can be described by the methods that can be found e.g., in [3, 16, 17].

The minimal model can not capture the following phenomena that are physiologically important:

- giving an upper bound for the tumor growth, typically described by Gompertzian functions in the literature [5];
- describing the indirect effect of the inhibitor on tumor growth through modeling the dynamics of the supporting vasculature, if the model is used to describe antiangiogenic therapy;
- modeling the dynamics of dead tumor volume (this will be incorporated into the models in Sections 3 and 4);
- modeling the pharmacodynamics of the drug, i.e., the increase of the drug dose does not yield linear increase in the effect, but the effect has a saturation (this will be incorporated into the models in Sections 3 and 4 as well).

The minimal model has only one equilibrium point specified by (1)-(2), which is the trivial equilibrium, i.e., the equations

$$0 = ax_{\infty} - bx_{\infty}y_{\infty} \quad (6)$$

$$0 = -cy_{\infty} \quad (7)$$

are satisfied only at $x_{\infty} = 0$ and $y_{\infty} = 0$. This equilibrium is unstable, since the Jacobian of the system of differential equations (1)-(2) at the equilibrium point is

$$\begin{aligned} \left(\begin{array}{c} ax - bxy \\ -cy \end{array} \right)' \Big|_{x=0, y=0} &= \left(\begin{array}{cc} a - by & -bx \\ 0 & -c \end{array} \right) \Big|_{x=0, y=0} \\ &= \left(\begin{array}{cc} a & 0 \\ 0 & -c \end{array} \right) \end{aligned} \quad (8)$$

which is a saddle if $a > 0$ (i.e., it implies unstable tumor growth without drug). Thus, if we give only one injection at the beginning of the treatment, the tumor volume will not be stabilized in an equilibrium, but it will grow with growth rate a after the drug is depleted.

However, if we extend the inhibitor dynamics by adding drug inflow rate I (e.g., to model further injections or infusion), i.e., (2) becomes

$$\dot{y} = -cy + I, \quad (9)$$

then the equilibria of the model are the solutions to

$$0 = ax_{\infty} - bx_{\infty}y_{\infty} \quad (10)$$

$$0 = -cy_{\infty} + I_{\infty} \quad (11)$$

that are

$$y_{\infty} = \frac{a}{b} \quad (12)$$

$$I_{\infty} = c \frac{a}{b} \quad (13)$$

with $x_{\infty} \in \mathbb{R}^+$. This implies that if there is an exogenous drug dosage, then the equilibrium is independent of the tumor volume, and only depends on the parameters of the model, thus after we drive the tumor volume in the given state, we give the amount drug described by (12)-(13) to keep the tumor in that state.

Parametric identification of the tumor model based on mice experiments [12] was carried out using mixed-effect model with Stochastic Approximation Expectation-Maximization detailed in [18, 19]. The results of parametric identification fit for each mouse in the experiment is shown in Figure 1. The individual parameter sets show good fit for the measurements.

The identified values of the parameters with 95% confidence intervals and between-subject variability are shown in Table 1. In the identification process, the initial volume appears as an identified parameter. The between-subject variabilities of the parameters are relatively small, the only parameter in the identification with large between-subject variability of the initial tumor volume, which is not a real parameter of the model.

In conclusion, although the model given by (1)-(2) is relatively simple and models only a few physiological phenomena and some critical processes are not modeled, the results in Figure 1 show that the model can describe the measurements. In the next section, the model is extended to incorporate the missing, critical physiological phenomena; the extended model will have similar fit results as the minimal model discussed in this section.

Parameter	Identified value (95%CI)	BSV(CV%)
a	0.206 (0.179, 0.238)	15.4<
b	0.117 (0.00163, 8.47)	23.9>
c	0.0709 (6.35e-005, 79.1)	4.01>
x_{10}	76.4 (47.5, 123)	84.9<

Table 1

Estimated parameters of the non-linear mixed effects model for the tumor model given by the differential equations (1)-(2)., CI: confidence interval, BSV: between-subject variability, CV: coefficient of variation

3 Tumor Model for Antiangiogenic Therapy

The minimal model was extended to incorporate the dynamics of the dead tumor volume, the pharmacodynamics of the drug and mixed-order pharmacokinetics of the drug in [11] and used to explain the effect of the angiogenic inhibitor bevacizumab [12]. The model was also described using formal reaction kinetics analogy as follows: the species X_1 represents the proliferating tumor volume, the species X_2 represents the dead tumor volume and the species X_3 represents the inhibitor serum level. The equations of the model are:

- $X_1 \xrightarrow{a} 2X_1$ that defines that the tumor cells proliferate (divide) with a tumor growth rate a . Using mass-action kinetics, this equation results in the term $\dot{x}_1 = ax_1$;
- $X_1 \xrightarrow{n} X_2$ that defines the necrosis of tumor cells with necrosis rate n . Note that this necrosis is independent of the treatment. Using mass-action kinetics, this equation modifies the dynamics of the proliferating and dead tumor volumes with the terms $\dot{x}_1 = -nx_1$, $\dot{x}_2 = nx_1$;
- $X_3 \xrightarrow{c} O$ that defines that there is an outflow of the drug with a reaction rate coefficient c , i.e. the clearance of the drug. We use Michaelis-Menten kinetics in order to have a mixed-order model for the pharmacokinetics, so this equations results in the term $\dot{x}_3 = -cx_3/(K_B + x_3)$, where the parameter K_B is the Michaelis-Menten constant of the drug;
- $X_1 + X_3 \xrightarrow{b} X_2$ that defines that if the drug meets living tumor cells, the result is dead tumor cells, i.e., the effect of the drug in a general way. This equation is considered with Michaelis-Menten kinetics with Michaelis-Menten constant ED_{50} (called the median effective dose [20]) resulting in the velocity term $x_1x_3/(ED_{50} + x_3)$. The drug effect on the volumes is considered with reaction rate coefficient b . The effect of this equation on the dynamics of the proliferating and dead tumor volumes is expressed by the terms $\dot{x}_1 = -bx_1x_3/(ED_{50} + x_3)$ and $\dot{x}_2 = bx_1x_3/(ED_{50} + x_3)$. Since these terms have the dimension mm^3/day , these terms can not be directly used to modify the dynamics of the drug level, since that has the dimension $\text{mg}/(\text{ml} \cdot \text{day})$. Thus, we use the constant κ with dimension $\text{mg}/(\text{ml} \cdot \text{mm}^3)$ to define the term $\dot{x}_3 = -\kappa bx_1x_3/(ED_{50} + x_3)$. However, for simplicity, in-

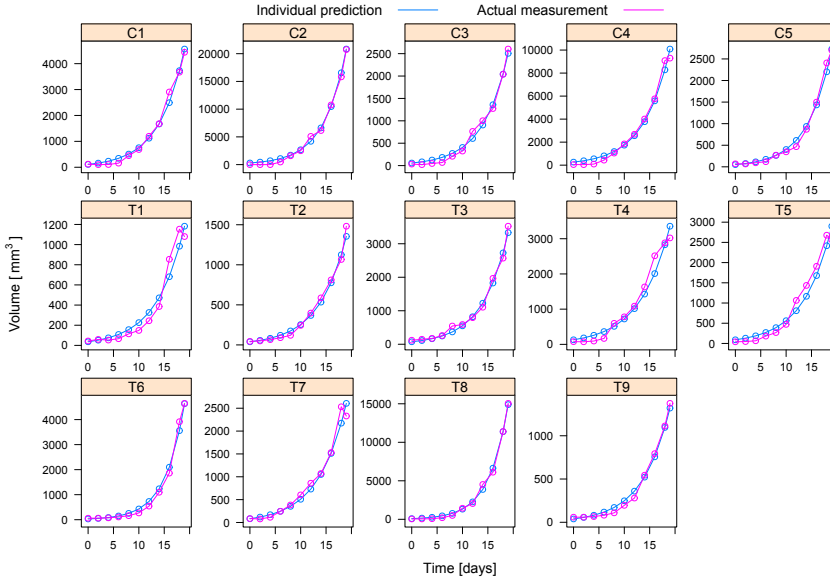


Figure 1

Actual tumor volumes (magenta) from the experiments in [12] and (individual) estimations (blue) from the model described by (1)-(2). The mice got one large dose of bevacizumab at the first day for the cases C1–C5 and one small dose each day for the cases T1–T9.

stead of κ , we introduce the constant $b_\kappa = \kappa b$.

The combination of these terms give the differential equation of the extended tumor growth model:

$$\dot{x}_1 = (a-n)x_1 - b \frac{x_1 x_3}{ED_{50} + x_3} \quad (14)$$

$$\dot{x}_2 = nx_1 + b \frac{x_1 x_3}{ED_{50} + x_3} \quad (15)$$

$$\dot{x}_3 = -c \frac{x_3}{K_B + x_3} - b_\kappa \frac{x_1 x_3}{ED_{50} + x_3} + u, \quad (16)$$

where x_1 is the time function of proliferating tumor volume in mm^3 , x_2 is the time function of the dead tumor volume in mm^3 , x_3 is the time function of drug serum level in mg/ml , u is the input that is the time function of drug injection rate in $\text{mg}/(\text{ml} \cdot \text{day})$.

The output y of the system is the measured tumor volume in mm^3 that is the sum of the proliferating (x_1) and dead (x_2) tumor volumes, i.e.

$$y = x_1 + x_2. \quad (17)$$

The dynamics of the output is described by the differential equation

$$\dot{y} = ax_1 \quad (18)$$

that is the sum of (14) and (15), thus the change of the measured tumor volume depends only on the tumor growth rate constant a and the actual volume of the proliferating tumor volume.

The trivial equilibrium of the model is

$$x_1^* = 0 \quad (19)$$

$$x_3^* = 0 \quad (20)$$

with $x_2^* \in \mathbb{R}^+$. This equilibrium is a stable node if $a - n < 0$, i.e., the tumor is defeated by the host, and a saddle, if $a - n > 0$. In the latter case, the tumor grows without therapy. Qualitative analysis of the model extended with a linear state feedback control law was carried out in [13], and it has been shown that the therapy can be efficient (i.e., there is a positive equilibrium achieved during the therapy) if and only if $a - n - b < 0$. This inequality is also the sufficient and necessary condition to achieve decreasing proliferating tumor volume as it has been shown in [11].

Parametric identification of the tumor model based on mice experiments [12] was carried out using mixed-effect model with Stochastic Approximation Expectation-Maximization detailed in [18, 19]. The identified values of the parameters with 95% confidence intervals and between-subject variability are shown in Table 2. In the identification process, the initial volume appears as an identified parameter, and shows the largest between-subject variability, while the real model parameters have small BSV.

The results of parametric identification fit for each mouse in the experiment is shown in Figure 2. The individual parameter sets show good fit for the measurements, similar to the results in Section 2.

The model described by (14)-(16) has similar modeling power as the model given by (1)-(2) based on the identification using the measurements from [12]. However, the model discussed in this section is more complex, and the equations of the model are physiologically more feasible, the measurements suggest that the complexity of the model is not required. However, in the next section, we modify the model given by (14)-(16) to describe measurements from chemotherapy where the measurement results show much richer dynamics than the simple exponential growth that can be observed on the measurements with bevacizumab [12] in Figures 1 and 2.

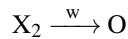
Parameter	Identified value (95%CI)	BSV (CV%)
a	0.373 (0.349, 0.399)	7.56%
b	0.124 (0.116, 0.132)	1.55%
c	0.132 (0.124, 0.14)	4.30%
n	0.176 (0.154, 0.202)	16.2%
b_k	7.25e-7 (6.43e-7, 8.16e-7)	8.01%
$x_1(0)$	46.5 (30, 71.9)	80.6%
K_B	0.591 (0.497, 0.703)	8.80%
ED_{50}	4.63e-005 (2.48e-005, 8.63e-005)	17.1%

Table 2

Estimated parameters of the non-linear mixed effects model for the tumor model for antiangiogenic therapy described by (14)-(16), CI: confidence interval, BSV: between-subject variability, CV: coefficient of variation

4 Tumor Model for Chemotherapy

The model given in [11] was further modified to add the effect of dead tumor cell washout in [18] in order to make it able to describe the dynamics of chemotherapy using PLD [2]. Since the effect of the drug was specified with a general mechanism (i.e., meeting of the proliferating tumor cell and drug results in dead tumor cell), it was unnecessary to modify the corresponding stoichiometric equation to make it more suitable to describe chemotherapy. The dynamics of dead tumor cell washout is given by the stoichiometric equation



which describes the washout of the dead tumor cells with washout rate w . Using mass-action kinetics, this reaction step has the rate $-wx_2$, which modifies the dynamics of the dead tumor cell volume. Thus, the modified differential equations of the model are

$$\dot{x}_1 = (a - n)x_1 - b \frac{x_1 x_3}{ED_{50} + x_3} \quad (21)$$

$$\dot{x}_2 = nx_1 + b \frac{x_1 x_3}{ED_{50} + x_3} - wx_2 \quad (22)$$

$$\dot{x}_3 = -c \frac{x_3}{K_B + x_3} - b_k \frac{x_1 x_3}{ED_{50} + x_3} + u, \quad (23)$$

where x_1 is the time function of proliferating tumor volume in mm^3 , x_2 is the time function of dead tumor volume in mm^3 , x_3 is the time function of drug level in mg/kg and u is the input that is the time function of drug injection rate in $\text{mg}/(\text{kg} \cdot \text{day})$. Since the injection doses were provided in mg/kg [2], the units of x_3 , u , ED_{50} , and K_B differ from the units of the corresponding variables and parameters in the model (14)-(16) where the basic unit was mg/ml .

The output y of the system is the measured tumor volume in mm^3 that is the sum

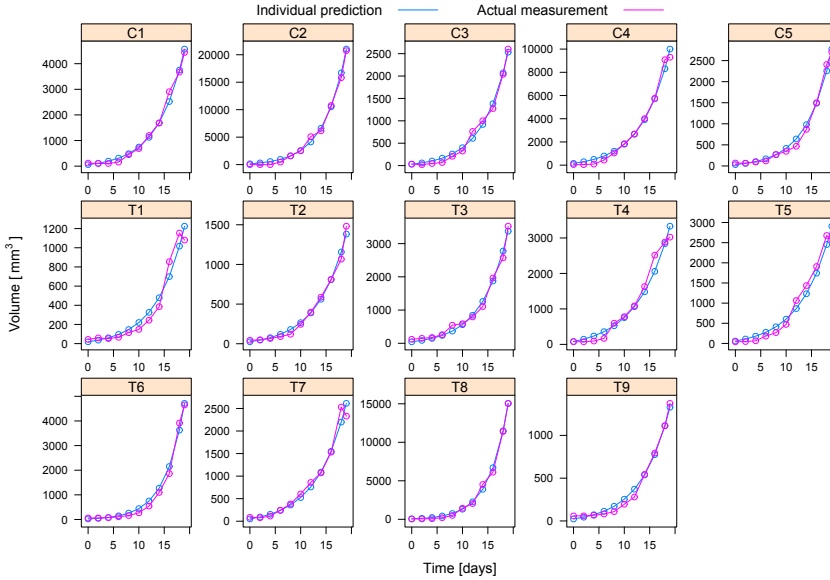


Figure 2

Actual tumor volumes (magenta) from the experiments in [12] and (individual) estimations (blue) from the model described by (14)-(16). The mice got one large dose of bevacizumab at the first day for the cases C1–C5 and one small dose each day for the cases T1–T9.

of the proliferating (x_1) and dead (x_2) tumor volumes, i.e.

$$y = x_1 + x_2. \quad (24)$$

The dynamics of the output is described by the differential equation

$$\dot{y} = ax_1 - wx_2 \quad (25)$$

that is the sum of (21) and (22), thus the change of the measured tumor volume depends directly only on the tumor growth rate constant a , the necrotic washout w and the actual volume of the proliferating tumor volume and the dead tumor volume.

The output dynamics (25) effectively describes a behaviour that seems like the drug has delayed effect on the tumor volume. The delayed effect is produced by the fact that initially the living tumor cells die (and become dead tumor cells), thus the output (the sum of living and dead tumor cell volume) does not change, and the remaining living tumor cells proliferate, resulting in increasing output, and the dead tumor cells start to be cleared during the washout process, which decreases the output. However, as long as the living tumor cells dominate (25), i.e., the ratio of x_1 and x_2 is such that (25) is positive, the output is increasing, and will only start to decrease when the ratio of the dead and living tumor cells

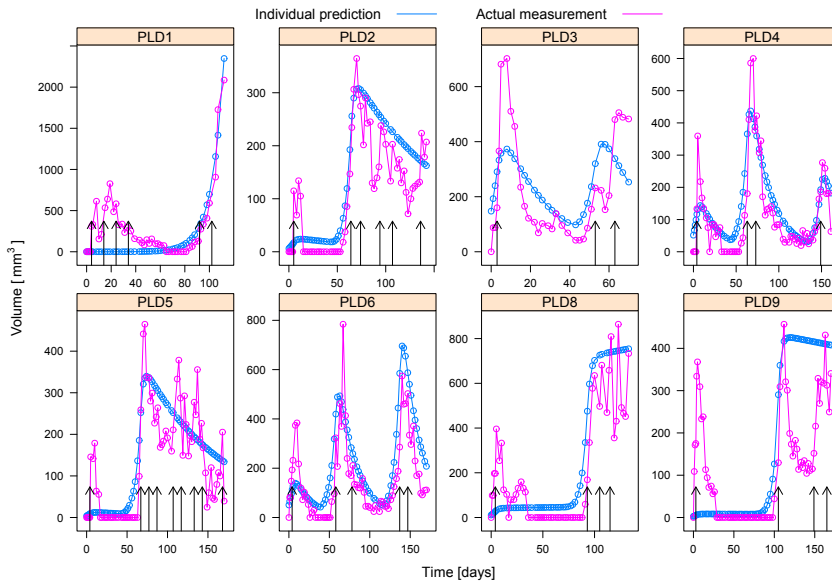


Figure 3

Actual tumor volumes (magenta) from the experiments in [2] and (individual) estimations (blue) from the model described by (21)-(23). The black arrows indicate 8 mg/kg injections of PLD in the experiments.

reach a value when (25) becomes negative. This effect can be observed in the measurements as well in Figure 3, where the measurements are indicated by magenta diamonds, while the injections are indicated as arrows on the horizontal axis. The injections were 8 mg/kg of PLD, a cytotoxic agent injected to mice with breast cancer [2].

Parametric identification of the tumor model based on mice experiments [2] was carried out using mixed-effect model with Stochastic Approximation Expectation-Maximization detailed in [18, 19]. The identified values of the parameters with 95% confidence intervals and between-subject variability are shown in Table 3. In the identification process, the initial volume appears as an identified parameter, and shows the largest between-subject variability, while the real model parameters have small BSV. The only exception is the effective median dose parameter (ED_{50}), which shows large between-subject variability.

The results of parametric identification fit for each mouse in the experiment are shown in Figure 3. The individual parameter sets show good fit for the measurements, except for the cases PLD1, PLD8 and PLD9. The most possible explanation of the bad fit for these cases maybe that the tumor acquired resistance for PLD1, PLD8 and PLD9, and the model is not able to describe this phenomenon.

Parameter	Identified value (95%CI)	BSV (CV%)
a	0.306 (0.265, 0.354)	6.08%
b	0.166 (0.126, 0.219)	18.2%
c	0.257 (0.2, 0.329)	31.9%
n	0.144 (0.127, 0.163)	16.3%
[t!] bk	6.12e-7 (5.57e-7, 6.73e-7)	6.60%
$x_1(0)$	6.94 (1.44, 33.4)	6050%
KB	0.36 (0.253, 0.514)	34.5%
$ED50$	9.71e-5 (2.17e-5, 0.000434)	152%
w	0.34 (0.292, 0.397)	7.43%

Table 3

Estimated parameters of the non-linear mixed effects model for describing the effect of PLD with the equations (21)-(23), CI: confidence interval, BSV: between-subject variability, CV: coefficient of variation.

Conclusions

The tumor models based on formal reaction kinetics analogy demonstrate that the modeling approach can be beneficial for the modeling of physiological systems. The reaction kinetics analogy makes the differential equations interpretable for experts not familiar with the theory of differential equations (e.g., clinical experts), while the different modeling alternatives (e.g., mass-action kinetics or Michaelis-Menten kinetics) can be used to find the optimal choice between model complexity and modeling power.

The simple model, also called the minimal model, has good modeling power in a small "operative" range only, however, if the tumor is controlled, the states of the system can be kept in that range, where the model is realistic. The simplicity of the model is advantageous for model-based controller design, and allows the use of numerous sophisticated control design techniques.

More complex models have the power to describe physiological processes in more detail, however, the complexity makes controller design more difficult. As the results showed with chemotherapy, the complex models can be used to describe the effect of therapy on a larger scale on both time and state space, thus more complex models are more beneficial for designing impulsive therapies.

Acknowledgment

The authors would like to express their thanks to the Membrane Protein Research Group of the Hungarian Academy of Sciences for providing the measurement data. This project has received funding from the European Research Council (ERC) under the European Union's Horizon 2020 research and innovation programme (grant agreement No 679681). Anna Lovrics is supported by the Hungarian National Research, Development and Innovation Office (OTKA PD 124467). The research is partially supported by the Hungarian National Research, Development and Innovation Office (SNN 125739).

References

- [1] J. Shi, O. Alagoz, F. S. Erenay, and Q. Su. A survey of optimization models on cancer chemotherapy treatment planning. *Annals of Operations Research*, 221(1):331–356, October 2014.
- [2] A. Füredi, K. Szebényi, S. Tóth, M. Cserepes, L. Hámori, V. Nagy, E. Karai, P. Vajdovich, T. Imre, P. Szabó, D. Szüts, J. Tóvári, and G. Szakács. Pegylated liposomal formulation of doxorubicin overcomes drug resistance in a genetically engineered mouse model of breast cancer. *Journal of Controlled Release*, 261:287–296, 2017.
- [3] P. Érdi and J. Tóth. *Mathematical Models of Chemical Reactions. Theory and Applications of Deterministic and Stochastic Models*. Princeton University Press, Princeton, New Jersey, 1989.
- [4] V. A. Kuznetsov, I. A. Makalkin, M. A. Taylor, and A. S. Perelson. Non-linear dynamics of immunogenic tumors: Parameter estimation and global bifurcation analysis. *Bulletin of Mathematical Biology*, 56(2):295–321, March 1994.
- [5] P. Hahnfeldt, D. Panigrahy, J. Folkman, and L. Hlatky. Tumor development under angiogenic signaling: A dynamical theory of tumor growth, treatment response, and postvascular dormancy. *Cancer Research*, 59:4770–4775, 1999.
- [6] D. A. Drexler, J. Sápi, and L. Kovács. A minimal model of tumor growth with angiogenic inhibition using bevacizumab. In *Proceedings of the 2017 IEEE 15th International Symposium on Applied Machine Intelligence and Informatics*, pages 185–190, 2017.
- [7] L. Kovács and G. Eigner. A TP-LPV-LMI based control for Tumor Growth Inhibition. *IFAC-PapersOnLine*, 51(26):155–160, 2018.
- [8] G. Eigner and L. Kovacs. Control of tumor growth by modern control methodologies. In *2018 IEEE International Conference on Automation, Quality and Testing, Robotics (AQTR)*, pages 1–6, Cluj-Napoca, May 2018. IEEE.
- [9] D. A. Drexler, J. Sápi, and L. Kovács. Positive control of a minimal model of tumor growth with bevacizumab treatment. In *2017 12th IEEE Conference on Industrial Electronics and Applications (ICIEA)*, pages 2084–2087, June 2017.
- [10] D. A. Drexler, J. Sápi, and L. Kovács. H_∞ control of nonlinear systems with positive input with application to antiangiogenic therapy. *IFAC-PapersOnLine*, 51(25):146–151, 2018.
- [11] D. A. Drexler, J. Sápi, and L. Kovács. Modeling of tumor growth incorporating the effects of necrosis and the effect of bevacizumab. *Complexity*, pages 1–11, 2017.
- [12] J. Sápi, L. Kovács, D. A. Drexler, P. Kocsis, D. Gajári, and Z. Sápi. Tumor volume estimation and quasi-continuous administration for most effective bevacizumab therapy. *PLoS ONE*, 10(11):1–20, 11 2015.
- [13] D. A. Drexler, I. Nagy, V. Romanovski, J. Tóth, and L. Kovács. Qualitative analysis of a closed-loop model of tumor growth control. In *Proceedings of*

- the 18th IEEE International Symposium on Computational Intelligence and Informatics*, pages 329–334, 2018.
- [14] D. A. Drexler, , and L. Kovács. Optimization of impulsive discrete-time tumor chemotherapy. In *Proceedings of the 2019 1st IEEE Conference on Societal Automation*, 2019.
- [15] D. A. Drexler, J. Sápi, and L. Kovács. Optimal discrete time control of antiangiogenic tumor therapy. *IFAC-PapersOnLine*, 50(1):13504 – 13509, 2017. 20th IFAC World Congress.
- [16] D. A. Drexler and J. Tóth. Global controllability of chemical reactions. *Journal of Mathematical Chemistry*, 54:1327–1350, 2016.
- [17] D. A. Drexler, E. Virágh, and J. Tóth. Controllability and reachability of reactions with temperature and inflow control. *Fuel*, 211:906–911, January 2018.
- [18] D. A. Drexler, T. Ferenci, A. Lovrics, and L. Kovács. Modeling of tumor growth incorporating the effect of pegylated liposomal doxorubicin. In *In Proceedings of the IEEE 23rd International Conference on Intelligent Engineering Systems*, pages 369–374, 2019.
- [19] D. A. Drexler, T. Ferenci, A. Lovrics, and L. Kovács. Comparison of michaelis-menten kinetics modeling alternatives in cancer chemotherapy modeling. In *In Proceedings of the IEEE 13th International Symposium on Applied Computational Intelligence and Informatics*, pages 27–32, 2019.
- [20] H.-P. Gerber and N. Ferrara. Pharmacology and pharmacodynamics of bevacizumab as monotherapy or in combination with cytotoxic therapy in pre-clinical studies. *Cancer research*, 65(3):671–680, 2005.

Determining the Position of the Moving Persons in 3D Space by UWB Sensors using Taylor Series Based Localization Method

Dušan Kocur*, Mária Švecová**, Peter Kažimír*

* Department of Electronics and Multimedia Communications

** Department of Mathematics and Theoretical Informatics

Faculty of Electrical Engineering and Informatics

Technical University of Košice

B. Němcovej 32, 042 00 Košice, Slovak Republic

Dusan.Kocur@tuke.sk, Maria.Svecova@tuke.sk, petokazimir@tuke.sk

Abstract: The person localization by ultra-wideband (UWB) sensors is a challenging field attracting researchers worldwide. Whereas the issue of the person localization in 2-dimensional space (2D) has been discussed in many articles, only a few papers have been devoted to the people localization in 3-dimensional space (3D). Combining two 3D localization methods a new approach to the person localization in 3D can be obtained to fill this gap. The new 3D localization method introduced in this paper is referred to as the Taylor series based localization method (TSM). This method combines the 3D-2D method of object localization in 3D with the conventional method of Taylor series. The performance properties of the introduced TSM will be illustrated via the experimental scenario intent on the through-the-wall localization of a moving person by a multistatic UWB radar system.

Keywords: 3D localization; signal processing; target tracking; Taylor series based localization method; UWB radar

1 Introduction

In the last decade, a great effort has been devoted to the study of ultra-wideband (UWB) radar applications for people monitoring [1]. The analyses of performance properties of person monitoring systems based on UWB radar (sensor) have shown that such systems allow localize multiple moving and static persons, as well as persons moving with a change of the character of their motion, not only for line-of-sight (LOS) but also for non-line-of-sight (NLOS) scenarios (e.g. localization of person situated behind of non-metallic obstacle, or localization of person e.g. in rain, snowstorm, dust, smoke, etc. [2]). It is also well-known, due to

fine range resolution based on time-of-arrival (TOA) measurement [3], UWB sensors can provide object localization with high accuracy as well. Moreover, signals transmitted by UWB radars are extremely low-power. As results, they produce only low-level interference of narrowband communication infrastructure and thus they can more easily coexist with such communication systems. These and further unique properties of UWB sensors (comprehensively summarized, e.g. in [1]) have been the impetus in the last years for relatively extensive development of applications of UWB localization systems. Rescue and security operations, critical infrastructures monitoring [1], [4], [5], [6], senior monitoring within their dwellings [7], [8], baby monitoring (e.g. detection of sudden death syndrome), etc. are just a few examples of such applications. Moreover, due to the development of communication and sensor networks, smart-home, smart-cities, Internet of Things and low-cost UWB sensor systems, it is expected the growth of requests for contactless monitoring of people in the near future.

Motivated by these findings we have focused our research on moving people monitoring (e.g. [9], [10], [11], [12], etc.) by means of UWB radars. In this area, great attention has been devoted to the localization of persons through a vertical wall in 2-dimensional (2D) and 3-dimensional space (3D) (e.g. [1], [13]) as well as through-the-floor localization of persons in 3D [10] or to the localization of persons situated behind a corner [14].

While the issue of person localization in 2D has been addressed in many articles, people localization in 3D and localization of persons situated behind a corner has been studied only in a few papers. In order to fill this gap, we prepared this paper focused on person localization through a vertical wall in 3D. The method which will be introduced in this paper is based on the estimation of the length of time interval necessary for electromagnetic waves to travel from transmitting antenna to a target and from the target to the radar receiving antenna. Note that this time interval is commonly referred to as TOA. In addition, our method will be based also on the application of the antenna array (Fig. 1) designed in [15] containing one transmitting antenna and four receiving antennas suitable for localizing objects in 3D.

For the object localization based on TOA measurement for a general antenna array lay-out several iterative and non-iterative algorithms were developed, e.g. in [16], [17], [18]. As an example, a few algorithm such as iterative Taylor series method [19], [20], approximate maximum likelihood methods [21], least-squares algorithms or various localization algorithms based on target bistatic range estimation (e.g. [10], [14], [15], [22]) could be mentioned.

The target localization in 3D by means of UWB radar can be simplified by the application of the antenna array outlined in Fig. 1. Due to the antenna array layout, a geometrical interpretation of the considered localization problem allows finding the target coordinates by a simple computation of 2 intersections of 2 pairs of ellipses as was suggested in [10], [15]. The mentioned ellipses are defined by the

antenna array layout and estimated TOAs corresponding to the target and to particular pairs of transmitting antenna and receiving antenna. This approach to person localization in 3D can be interpreted as the object localization in the x - y plane (i.e. localization in 2D) and in y - z plane (i.e. the second localization in 2D). Then, the final target coordinates can be determined by a fusion of the results of target localization in these two planes [10], [15]. The person localization in 3D based on this idea which has been developed in [10] is known as the 3D-2D method. Its simplified version introduced in [15] is sometimes referred to as approximate 3D-2D method (A-3D-2D).

3D-2D and A-3D-2D method are simple providing quite good accuracy of person localization. However, they do not exploit the full potential of antenna array containing four receiving antennas. One can expect that some improvement in terms of the localization accuracy could be achieved if some optimization principle would be combined with the 3D-2D method or A-3D-2D method. Following this idea originally outlined in [23], the Taylor series based localization method is introduced in this paper. The main novelty of this method consists in the application of the 3D-2D method or the A-3D-2D method in a combination with the well-known Taylor series localization principle. The Taylor series based localization method is here derived for the 3D localization with the respect the antenna array layout according to Fig. 1. The performance properties of the Taylor series based localization method will be examined via the experiment focused on the through-the-wall positioning of a moving person. The comparison of the true and the estimated tracks of the person will show that the Taylor series based localization method can provide better accuracy of the localization in comparison with the localization only by the 3D-2D method.

The paper is organized as follows. The problem statement concerning the localization of a person by a multistatic UWB radar is outlined in the next section. In Section 3, the Taylor series method based on the estimations of TOAs is described. Then, the iterative Taylor series algorithm is introduced. Subsequently, the performance of the Taylor series based localization method will be demonstrated in Section 5. Finally, conclusions are drawn in the last section.

2 System Model

Let us consider the fundamental scenario of a moving target localization by means of a multistatic UWB radar system composed of one transmitting antenna (Tx) and four receiving antennas (Rxs). To locate and track the target denoted as T, Tx emits electromagnetic waves into a monitored area, they are reflected from objects (even from T) and received by Rxs. It is assumed that the antenna configuration and the coordinates of Tx and Rxs are fixed, known, and they are denoted as $Tx = (x_t, y_t, z_t)$ and $Rx_i = (x_i, y_i, z_i)$ for $i = 1, 2, 3, 4$ (Fig. 1). It is also assumed that all

TOA_i belonging to the i th Rx for $i = 1, 2, 3, 4$ have been estimated for a slow-time instant τ as well. The estimated TOA_i for $i = 1, 2, 3, 4$ correspond to the measured round trip propagation times of the electromagnetic wave transmitted by Tx, reflected from T and received by the i th Rx.

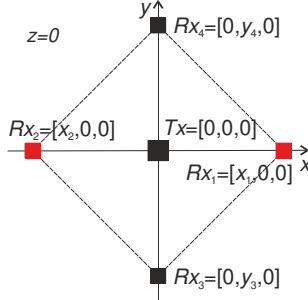


Figure 1

The antenna array layout

The total length of the trajectory along which the electromagnetic wave propagates from Tx to T and then from T to the i th Rx denoted as d_i can be expressed as a set

$$d_i = c \cdot TOA_i, \quad i = 1, 2, 3, 4, \quad (1)$$

where $c = 3 \times 10^8 \text{ ms}^{-1}$ is electromagnetic wave propagation velocity in the air.

Under real conditions, the distances d_i for $i = 1, 2, 3, 4$ are estimated with an error represented by the additive noise components e_i . Let the unknown target coordinates are denoted as $T = (x, y, z)$. Then, the estimated distances d_i can be modeled by the following set of the algebraic equations

$$d_i = \|TxT\| + \|TRx_i\| + e_i = \sqrt{(x-x_i)^2 + (y-y_i)^2 + (z-z_i)^2} + \sqrt{(x-x_i)^2 + (y-y_i)^2 + (z-z_i)^2} + e_i, \quad (2)$$

$i = 1, 2, 3, 4.$

In these equations, $\|TxT\|$ and $\|TRx_i\|$ are the Euclidean distances between the points Tx and T and between the points T and Rx_i , respectively. Note, that e_i for $i=1, 2, 3, 4$ correspond to the estimation errors of the length of the trajectory Tx-T- Rx_i . The problem of the target locating lies in determining the unknown target coordinates (x, y, z) by the solution of the set of the nonlinear equations (2).

It is well known from geometry that the i th equation of (2) is the equation of the spheroid obtained by rotating the ellipse about one of its principal axes. This detailed description and the corresponding mathematical formulas is beyond this paper. Its comprehensive description can be found, e.g. in [10], [24].

The accuracy of distance estimation d_i is affected by several phenomena (e.g., noise, multipath, non-line-of-sight (NLOS) conditions). If the distance estimation error is additive, this results that the spheroids will not intersect at one single point. On the other hand, if the distance estimation error is subtractive, the spheroids may not intersect. So, the goal of the localization algorithm is to estimate the target position as close as the true target position, even in the presence of noisy measurements. It can be done also by the Taylor series method.

3 Taylor Series Method

Finding the location of the target requires the solving of the set of the nonlinear equations (2) based on TOA measurements. The most straightforward method of target position estimation is to solve a set of simultaneous equations (2). Various iterative and non-iterative position estimation algorithms have been developed [18], [22]. Non-iterative algorithms are simple and easy to implement compared to the iterative algorithms, such as spherical interpolation and other least-squares related techniques. The iterative algorithms are more complex and stop only when some pre-defined criterion is satisfied. These include, e.g. the Taylor series method.

The target localization by the nonlinear least-squares method based on a first-order Taylor expansion (i.e. Taylor series method) was originally proposed for target locating issued from one way propagation time measurements [19]. Then, for example in [17], [26], the original Taylor series method was modified for the target localization based on the estimations of TOAs from N receiving antennas. The Taylor series method based on the TOA estimations (TS) applied for the target localization in 3D according to the system model described in Section 2 can be described as follows. Here, the set of the nonlinear equations (2) is linearized by expanding it in a Taylor series around an initial estimate of a point. Only terms below second order are retained. This set of equations is solved to produce a new approximate position of the target, and the process is repeated until the stopping criterion is satisfied.

Let us define new functions of three variables x, y, z

$$f_i(x, y, z) = \sqrt{(x-x_i)^2 + (y-y_i)^2 + (z-z_i)^2} + \sqrt{(x-x_i)^2 + (y-y_i)^2 + (z-z_i)^2}, \quad i = 1, 2, 3, 4. \quad (3)$$

Then, the equations (3) can be rewritten by equations (2) as

$$f_i(x, y, z) = d_i - e_i, \quad i = 1, 2, 3, 4. \quad (4)$$

Here, e_i are the estimation errors of the distances d_i . If x_0 , y_0 , and z_0 are initial estimates of the target coordinates, which can be obtained roughly by other methods, then

$$x = x_0 + \delta_x, \quad y = y_0 + \delta_y, \quad z = z_0 + \delta_z, \quad (5)$$

where δ_x , δ_y , and δ_z are the corresponding location errors to be determined. According to the selected initial coordinates $[x_0 \ y_0 \ z_0]^T$, expanding f_i in a Taylor series and retaining the first two terms we can get

$$f_{i0} + a_{i1}\delta_x + a_{i2}\delta_y + a_{i3}\delta_z \approx d_i - e_i, \quad i = 1, 2, 3, 4, \quad (6)$$

where

$$\begin{aligned} f_{i0} &= f_i(x_0, y_0, z_0), \\ a_{i1} &= \left. \frac{\partial f_i}{\partial x} \right|_{x_0, y_0, z_0} = \frac{x_0 - x_i}{r_{i0}} + \frac{x_0 - x_i}{r_{i0}}, \\ a_{i2} &= \left. \frac{\partial f_i}{\partial y} \right|_{x_0, y_0, z_0} = \frac{y_0 - y_i}{r_{i0}} + \frac{y_0 - y_i}{r_{i0}}, \\ a_{i3} &= \left. \frac{\partial f_i}{\partial z} \right|_{x_0, y_0, z_0} = \frac{z_0 - z_i}{r_{i0}} + \frac{z_0 - z_i}{r_{i0}}, \\ r_{i0} &= \sqrt{(x - x_i)^2 + (y - y_i)^2 + (z - z_i)^2}, \\ r_{i0} &= \sqrt{(x - x_i)^2 + (y - y_i)^2 + (z - z_i)^2}. \end{aligned}$$

Equation (6) can be rewritten in the matrix form as

$$A\delta = D - e, \quad (7)$$

where

$$A = \begin{bmatrix} a_{11} & a_{12} & a_{13} \\ a_{21} & a_{22} & a_{23} \\ a_{31} & a_{32} & a_{33} \\ a_{41} & a_{42} & a_{43} \end{bmatrix}, \quad \delta = \begin{bmatrix} \delta_x \\ \delta_y \\ \delta_z \end{bmatrix}, \quad D = \begin{bmatrix} d_1 - f_{10} \\ d_2 - f_{20} \\ d_3 - f_{30} \\ d_4 - f_{40} \end{bmatrix}, \quad e = \begin{bmatrix} e_1 \\ e_2 \\ e_3 \\ e_4 \end{bmatrix}.$$

From equation (7) by using the least-square algorithm, the least-square solution of δ is

$$\delta = [A^T A]^{-1} A^T D. \quad (8)$$

Given the initial estimations of the target coordinates $[x_0 \ y_0 \ z_0]^T$, the unknown values of location errors δ can be determined by (8). Then the estimations of the target coordinates are updated according to the expression

$$\begin{bmatrix} x_0 & y_0 & z_0 \end{bmatrix}^T = \begin{bmatrix} x_0 + \delta_x & y_0 + \delta_y & z_0 + \delta_z \end{bmatrix}^T. \quad (9)$$

The computation of the target coordinates $[x_0 \ y_0 \ z_0]^T$ according to (9) is repeated until $\|\delta\|$ is sufficiently small, i.e. $\|\delta\| < \varepsilon$, where $\|\delta\| = \sqrt{\delta_x^2 + \delta_y^2 + \delta_z^2}$ denotes Euclidean norm of δ and ε is the small positive number.

4 Taylor Series Algorithm

In the previous section, a basic principle of TS has been described. To reduce the errors of the estimated target positions emergent by the noise measurements of TOAs, TS can be considered as an iterative method of solution of (2). Then, the target localization employing TS can be implemented by using the following iteration algorithm referred to as the Taylor series algorithm:

Step 0:

To solve the equation group (2), Taylor series algorithm requires an initial target position. In this step, a reference estimate of the target coordinates denoted as $T_0 = (x_0, y_0, z_0)$ is obtained by using the 3D-2D method or the A-3D-2D method [15]. Note, that it is not a priori known if TOAs are or are not perfectly estimated.

Step n:

In this step, the n th iteration of the solution of equations (2) is done for $n = 1, 2, \dots, N$.

The unknown coordinates of the person (target) in the n th iteration are estimated from the non-linear equations (2) that are linearized by the Taylor series expansion around the point $T_{n-1} = (x_{n-1}, y_{n-1}, z_{n-1})$. The point $T_{n-1} = (x_{n-1}, y_{n-1}, z_{n-1})$ is the estimate of the person position in the $(n-1)$ th iteration.

The group of the linear equations written in the matrix form (7) is repeatedly solved by the least-squares method at each iteration to refine a new estimate of the target coordinates denoted as $T_n = (x_n, y_n, z_n)$ by equation (8). For the updated estimate of the person position its new coordinates are refined according to $x_n \leftarrow x_{n-1} + \delta_{x,n}$, $y_n \leftarrow y_{n-1} + \delta_{y,n}$, and $z_n \leftarrow z_{n-1} + \delta_{z,n}$.

The parameter $\delta_n = [\delta_{x,n} \ \delta_{y,n} \ \delta_{z,n}]^T$ express a localization error in the n th iteration. It is obtained as the least-squares solution of (7) by (8). Here, it is used to control the iteration process of solution (2) as follows:

- a) If the Euclidean norms fulfill the condition $\|\delta_{n-1}\| \leq \|\delta_n\|$, the iteration process is divergent. The iterative process ends and the final person position in the slow-time instant τ is $T = T_{n-1} = (x_{n-1}, y_{n-1}, z_{n-1})$.

- b) If the Euclidean norms fulfill the conditions $\|\delta_{n-1}\| > \|\delta_n\|$ and $\|\delta_n\| > \varepsilon$, the iterating process is convergent. Note, ε is a small positive number controlling the iteration process. Then, the looking for the solution of (2) will continue by the $(n+1)$ th iteration.
- c) If inequations $\|\delta_{n-1}\| > \|\delta_n\|$ and $\|\delta_n\| \leq \varepsilon$ are fulfilled, the iterating process ends. The final person coordinates in the slow-time instant τ are $T=T_n=(x_n, y_n, z_n)$.
- d) Alternatively to (c), the iteration process ends if $n = N$, where N is the preset maximum allowed number of iteration. Then, the final estimation of person positions in the slow-time instant τ is $T=T_N=(x_N, y_N, z_N)$.

The iteration algorithm of the solution of the system model (2) described herein will be referred to the Taylor series based localization method (TSM).

5 Experimental Results

To illustrate and validate performance properties of TSM, a scenario of the moving person localization in 3D (in the next referred to as the experimental scenario) will be analyzed. This scenario is outlined in Fig. 2. It is focused on the through-the-wall tracking of a person moving behind the brick wall with a thickness of 0.2 m. The person to be localized was walking on the stairs (Fig. 3) at an approximately constant speed from the position P1, through the positions P2, P3, P4, P5, P6, P7, up to the position P8 (Fig. 2).

Table 1
The basic parameters of the UWB radar system

Radar type	M-sequence UWB radar
M-sequence order	12
System clock frequency	7 GHz
Operation bandwidth	DC – 3 GHz
Length of impulse responses	4095 samples spread over 585 ns
Radar range resolution	0.01 m
Unambiguous range	137 m
Transmitted power	1 mW
Radar configuration	One Tx and four Rxs
Antenna spacing	0.39 m
Antenna type	Horn open

The person was monitored by the M-sequence UWB radar system [1] equipped with one Tx and four Rxs depicted in Fig. 4. The parameters of the radar are stated in Table 1. The five double-ridged horn antennas have been placed on the wall

forming a wall-to-air interface. The antenna array layout is shown in Fig. 1. The distance between Tx and Rx's has been 0.39 m, Tx has been located in the middle between four Rx's. For the target positioning in 2D, the antenna array with an appropriate layout of one Tx and two Rx's is sufficient. The antenna array consisting of Tx, Rx₁, and Rx₂ has been located on the x -axis. Such an antenna array should be enough for the localization of a target in the x - y plane (in 2D). Similarly, the antenna array consisting of Tx, Rx₃ and Rx₄ located on the axis y should be enough for the localization of a target in the y plane (in 2D). The antenna array consisting of Tx and four Rx's arranged according to Fig. 1 is proper for 3D localization.

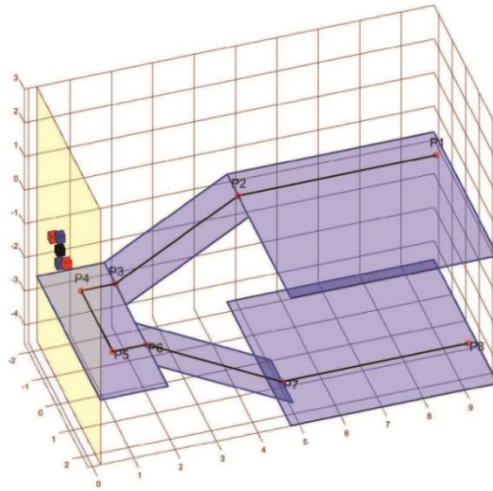


Figure 2

The scheme of measurement with the positions of antennas and the reference positions



Figure 3

The monitored area



Figure 4

The measurement apparatus, M-sequence UWB radar system located behind the wall

To locate and track a moving target, Tx emitted electromagnetic waves into a monitored area, they were reflected from objects (even from the target) and received by Rx's. The raw radar signals retrieved from the radar system can be interpreted as a set of impulse responses of the surrounding through which the electromagnetic waves spread. The set of impulse responses is referred to as radargram [1], [13]. Then, the target positions and its track in the monitored area can be obtained by the sequential processing of particular impulse responses of radargram.

The processing of the radar signals for moving person localization [13], [24], consists of the set of phases responsible for the elimination of stationary clutter (methods of background subtraction), the decision about the target presence or absence (methods of detection), the estimation and association of distances from the same target (methods of TOA estimation), the wall effect compensation (if target detection and tracking by UWB radar is realized through the walls with known thickness and relative permittivity of the wall), the estimation of target positions (methods of localization) and finally the monitoring of target motion over time (methods of tracking). Here, the exponential averaging method [27], CFAR detector [28], [29], trace connection method [11], trace correction of the first kind [30], the 3D-2D method [15], and multiple target tracking system (MTT) [13], [27], [31] have been applied for the background subtraction, target detection, TOA estimation, wall effect compensation, target localization, and target tracking, respectively. The detailed description of the particular phases of radar signal processing together with the corresponding mathematical formulas is beyond this paper. Its comprehensive description can be found, e.g. in [13], [24].

By using the above-mentioned procedure for radar signal processing, the TOAs corresponding the target have been obtained for every slow-time instant τ . Then, the positions of the target in the monitored area have been determined by the 3D-2D method. The obtained results of the localization phase are depicted in Fig. 5. These by the 3D-2D method given target coordinates have been used as the initial estimates for the target positioning by TSM. Finally, the target coordinates have been refined by TSM. By the TSM achieved results are depicted in Fig. 7. The projections of the estimated person coordinates into the x - y plane are illustrated in Fig. 6 and 8.

The last phase of the radar signal processing procedure applied to target positions estimated by the localization method is target tracking. It allows improving the robustness and precision of the target coordinates estimations based on its foregoing positions. Here, the target tracking by MTT has been employed. The person tracks estimated by MTT for the 3D-2D method and TSM are depicted in Fig. 9 and 11, respectively. The projections of the estimated positions of the person into the x - y plane are illustrated in Fig. 10 and 12, respectively.

Since the real width of the person is non-zero and the resolution of the radar used for measurement is approximately 0.01 m, the alternative form of the visualization

of the target position estimation accuracy is shown in Fig. 5-12. In these figures, the yellow cuboids and parallelepipeds, or rectangles in the projection into the x - y plane, are outlined. The part of the monitored area bordered by these shapes, where the true track of the person is located, can be referred to as a region of the true positions of the person. The width of this region is set to 1 m, its height is set to 1.8 m. It corresponds approximately to the effective size of a human body.

The analyses of the results presented in Fig. 9 – 12 show, that the estimated tracks have kept the direction of the target movement very-well. The tracks estimated by TSM and MTT is better than that of the trajectory estimated by MTT coming out of the positions estimated by the 3D-2D method. This improvement is observable especially in these segments of the tracks in which the person was changing the direction of their motion. This performance of TSM over the 3D-2D method is reached at the cost of its higher complexity in comparison with the 3D-2D method.

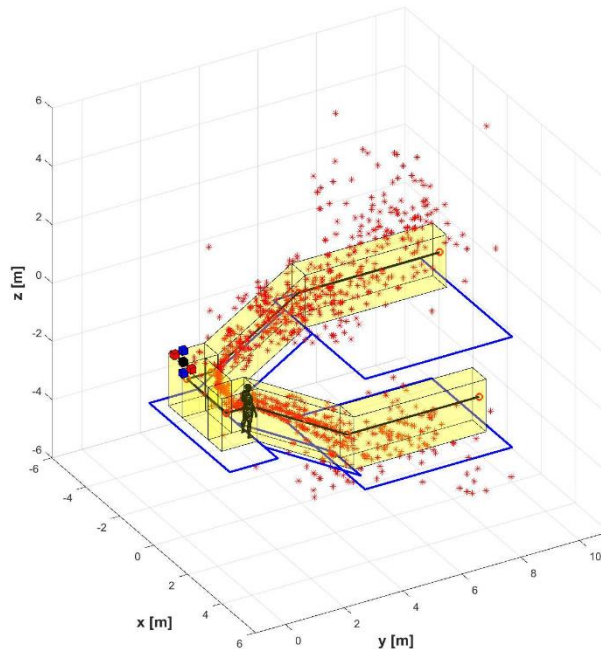


Figure 5

Person positions estimated by the 3D-2D method

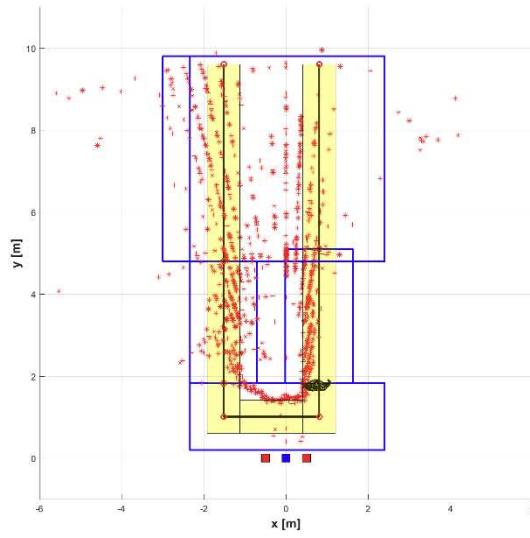


Figure 6

Person positions estimated by the 3D-2D method: the projection into x - y plane

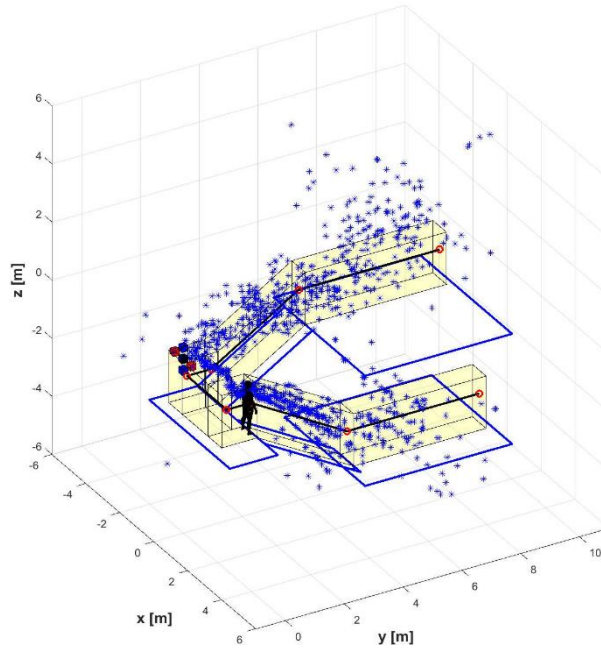


Figure 7

Person positions estimated by TSM

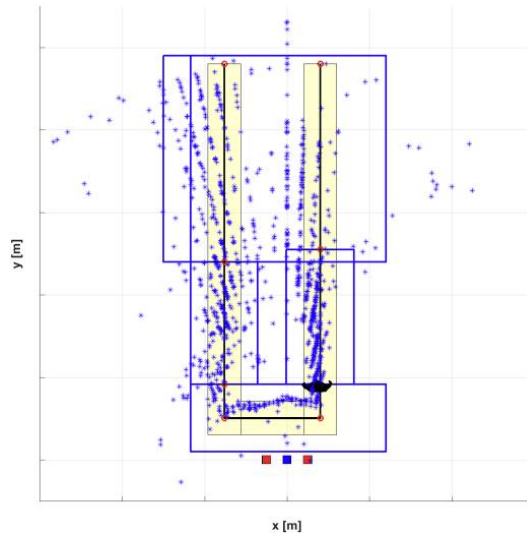


Figure 8

Person positions estimated by TSM: the projection into x - y plane

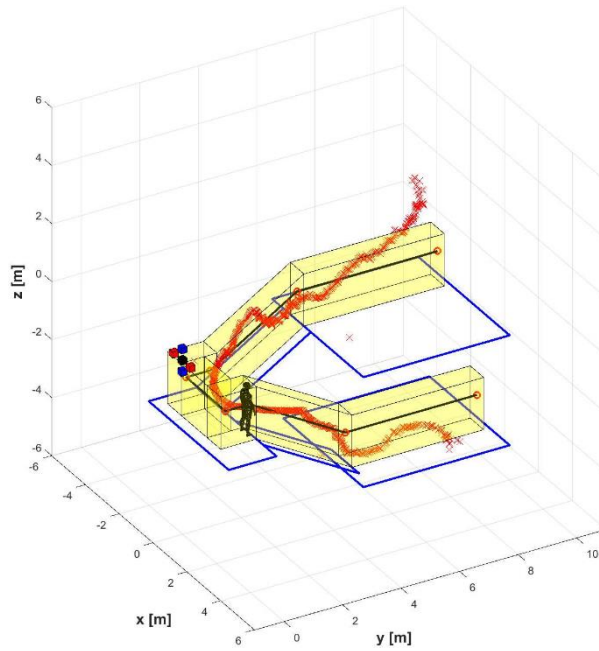


Figure 9

Person track estimated by the 3D-2D method and MTT

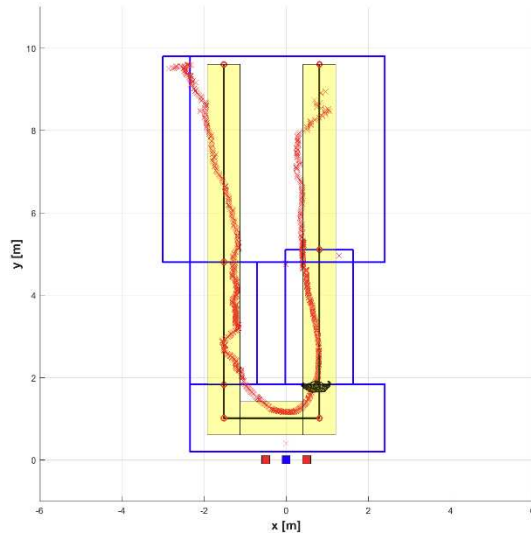


Figure 10

Person track estimated by the 3D-2D method and MTT: the projection into x - y plane

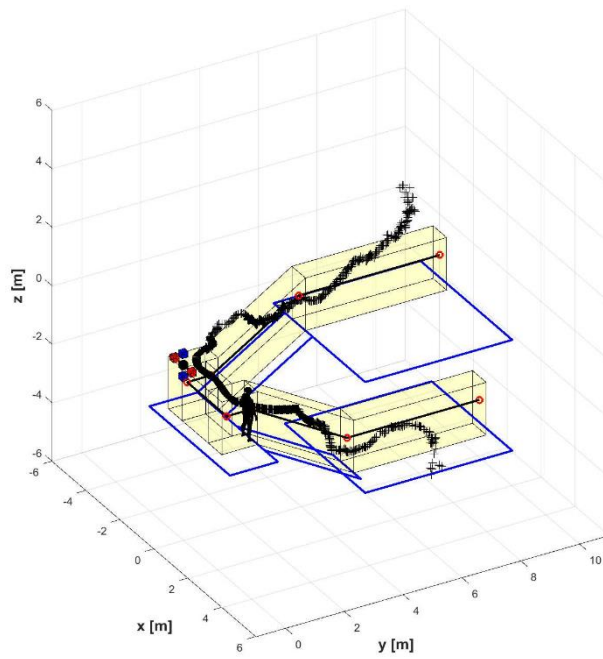


Figure 11

Person track estimated by TSM and MTT

In our opinion, the TS method and TS algorithms represent a universal approach to object localization in 3D based on TOA measurement. Therefore, they can be applied not only for person monitoring but also for localization of other moving objects. The state-of-the-art in the field of localization algorithm exploitation indicates that, e.g. the field of robotics could be considered the very perspective from this point of view. The localization method could be employed, e.g. for monitoring a robot environment (e.g. [32]) or for monitoring robot itself (e.g. [33]). We also believe, the method developed in this paper could be applied, e.g. in the field of robot posing or for the solution of a problem of simultaneous localization and mapping (SLAM), where the robot must simultaneously map the environment and locate itself (e.g. [34], [35], [35], [37]).

Acknowledgement

This work was supported by the Scientific Grant Agency (VEGA) under the contract No. 1/0772/17 and by the Slovak Research and Development Agency under the contract No. APVV-18-0373.

References

- [1] J. Sachs, *Handbook of Ultra-wideband Short-Range Sensing: Theory, Sensors, Applications*, John Wiley & Sons, 2012
- [2] B. Yamauchi, "All-weather perception for man-portable robots using ultra-wideband radar," in *2010 IEEE International Conference on Robotics and Automation*, Anchorage, AK, USA, 2010
- [3] J. Sachs et al., "On the Range Precision of UWB Radar Sensors," in *11-th International Radar Symposium*, Vilnius, Lithuania, 2010
- [4] P. Withington, H. Fluhler, S. Nag, "Enhancing Homeland Security with Advanced UWB Sensors," *IEEE Microwave Magazine*, Vol. 4, No. 3, pp. 51-58, Sept. 2003
- [5] C. Huffman, L. Ericson, "Though-the-Wall Sensors (TTWS) for Law Enforcement: Market Survey," ManTech Advanced Systems International, Inc., 2012
- [6] ReTWis, „Look behind the walls,“ [Online] Available: <http://www.lokalizacni-systemy.cz/en/retwis-en/>
- [7] J. Sachs et al., "Remote vital sign detection for rescue, security, and medical care by ultra-wideband pseudo-noise radar," *Ad Hoc Networks*, Vol. 13, pp. 42-53, Feb 2014
- [8] G. Diraco, A. Leone, P. Siciliano, "A Radar-Based Smart Sensor for Unobtrusive Elderly Monitoring in Ambient Assisted Living Applications," *Biosensors (Basel)*, Vol. 7, No. 4, Nov. 2017

- [9] D. Kocur, M. Švecová, D. Novák, "UWB Radar Based Localization of a Person Changing the Nature of Their Motion State," in *International Conference on Radar (RADAR)*, Brisbane, QLD, Australia, 2018
- [10] M. Švecová et al., "Through-the-floor localization of a static person by a multistatic UWB radar," *Microwave and Optical Technology Letters*, Vol. 61, No. 3, pp. 825-831, 2018
- [11] J. Rovňáková, D. Kocur, "TOA Estimation and Data Association for Through-Wall Tracking of Moving Targets," *EURASIP Journal on Wireless Communications and Networking*, Vol. 2010, No. 1, p. 420767, Aug 2010
- [12] D. Kocur, M. Švecová, R. Zetik, "Basic signal processing principles for monitoring of persons using UWB sensors - An overview," *Acta Electrotechnica et Informatica*, in press
- [13] D. Kocur, J. Rovňáková, M. Švecová, "Through Wall Tracking of Moving Targets by M-Sequence UWB Radar," in *Studies in Computational Intelligence*, Vol. 243, Berlin, Heidelberg, Springer, 2009, pp. 349-364
- [14] G. Shen et al., "Range-Based Localization for UWB Sensor Networks in Realistic Environments," *EURASIP Journal on Wireless Communications and Networking*, Vol. 2010, No. 1, p. 476598, Oct 2009
- [15] P. Kažimír et al., "Localisation of motionless persons in 3D space by UWB radar," in *PIERS Proceedings*, Aug 2014
- [16] K. Yu et al., "UWB location and tracking for wireless embedded networks," *Signal Processing*, Vol. 86, No. 9, pp. 2153-2171, Sept 2006
- [17] M. Svecova, D. Kocur, R. Zetik, "Object localization using round trip propagation time measurements," in *18th International Conference Radioelektronika*, Prague, Czech Republic, April 2008
- [18] A. G. Ferreira et al., "Performance Analysis of ToA-Based Positioning Algorithms for Static and Dynamic Targets with Low Ranging Measurements," *Sensors (Basel)*, Vol. 17, No. 8, p. 1915, 2017
- [19] W. H. Foy, "Position-Location Solutions by Taylor-Series Estimation," *IEEE Transactions on Aerospace and Electronic Systems*, Vols. AES-12, No. 2, pp. 187-194, 1976
- [20] J. Ren, J. Chen, W. Bai, "A New Localization Algorithm Based on Taylor Series Expansion for NLOS Environment," *Cybernetics and Information Technologies*, Vol. 16, No. 5, pp. 127-136, 2016

- [21] Y.-T. Chan, H. Y. C. Hang, P.-C. Ching, "Exact and approximate maximum likelihood localization algorithms," *IEEE Transactions on Vehicular Technology*, Vol. 55, No. 1, pp. 10-16, 2006
- [22] H. Zhang et al., "An improved Taylor series based location algorithm for IEEE 802.15.4a channel," in *Proceedings of 2011 IEEE Pacific Rim Conference on Communications, Computers and Signal Processing*, Victoria, BC, Canada, Aug. 2011
- [23] D. Kocur, M. Švecová, P. Kažimír, "Taylor Series Based Localization Method of Moving Persons in 3D Space by UWB Sensors," in *IEEE 23rd International Conference on Intelligent Engineering Systems*, Gödöllő, Hungary, April 2019
- [24] D. Kocur, M. Švecová, J. Rovňáková, "Through-the-wall localization of a moving target by two independent ultra wideband (UWB) radar systems," *Sensors (Basel, Switzerland)*, Vol. 13, No. 9, pp. 11969-11997, 2013
- [25] X. Zheng et al., "Wireless localization based on the time sum of arrival and Taylor expansion," in *19th IEEE International Conference on Networks (ICON)*, Singapore, Dec 2013
- [26] J. Rovňáková, Complete signal processing for through wall tracking of moving targets, LAP LAMBERT Academic Publishing, 2010
- [27] H. Rohling, "Radar CFAR Thresholding in Clutter and Multiple Target Situations," *IEEE Transactions on Aerospace and Electronic Systems*, Vols. AES-19, No. 4, pp. 608-621, 1983
- [28] G. Minkler, J. Minkler, CFAR: The Principles of Automatic Radar Detection in Clutter, Baltimore: Magellan Book Company, 1990
- [29] J. Rovnakova and D. Kocur, "Compensation of wall effect for through wall tracking of moving targets," *Radioengineering*, Vol. 18, No. 2, pp. 189-195, 2009
- [30] M. S. Grewal, A. P. Andrews, Kalman filtering: theory and practice, Upper Saddle River, NJ, USA: Prentice-Hall, Inc., 1993
- [31] D. Kocur et al., "Short-range UWB radar: Surveillance robot equipment of the future," in *IEEE International Conference on Systems, Man, and Cybernetics (SMC)*, San Diego, CA, USA, Oct 2014
- [32] P. Galajda et al., "Wireless UWB Sensor System for Robot Gripper Monitoring in Non-cooperative Environments," in *Recent Advances in Intelligent Engineering. Topics in Intelligent Engineering and Informatics*, Springer, Cham, March 2019, pp. 177-207

- [33] Á. Takács et al., “Models for Force Control in Telesurgical Robot Systems,” *Acta Polytechnica Hungarica*, Vol. 12, No. 8, pp. 95-114, January 2015
- [34] B. Fernandez-Gauna et al., “Basic Results and Experiments on Robotic Multi-Agent System for Hose Deployment and Transportation,” *International Journal of Artificial Intelligence*, Vol. 6, No. S11, pp. 183-202, March 2011
- [35] B. Sarkar, P. K. Pal, D. Sarkar, “Building maps of indoor environments by merging line segments extracted from registered laser range scans,” *Robotics and Autonomous Systems*, Vol. 62, No. 4, pp. 603-615, 2014
- [36] P. Merriault et al., “Robust robot localization in a complex oil and gas industrial environment,” *Journal of Field Robotics*, Vol. 62, No. 4, pp. 213-230, 2018
- [37] E. Zaikov, J. Sachs, “UWB radar for detection and localization of trapped people,” in *Ultra Wideband*, Rijeka, IntechOpen, 2010

SIT-based Functional Dependency Extraction

Balázs Tusor, János T. Tóth, Annamária R. Várkonyi-Kóczy

Department of Mathematics and Informatics, J. Selye University

Elektrárénská cesta 2, 945 01 Komárno, Szlovákia

E-mail: tusorb@ujs.sk; tothj@ujs.sk; koczya@ujs.sk

Abstract: In the digital age, being able to determine the relationships between attributes in datasets is advantageous for many fields of information technology, such as data mining, machine learning, etc. There are inherent rules, functional dependencies that are derived from the nature of the data, of which many are not trivially obvious to the human data manager. This paper presents a new method to extract such relationships. It uses Sequential Indexing Table structures that can implicitly indicate if the values of an attribute are determined by the combination of the values of the attributes preceding it in the layered architecture, i.e. is functionally dependent on those attributes. A new algorithm is given to use this feature to extract functional dependencies, and the performance is analyzed using real-life datasets.

Keywords: functional dependency extraction; data processing; functional dependencies; data mining; sequential indexing tables

1 Introduction

Data management has been an important part of information technology, gaining more and more prominence in the past few decades. Fields such as big data [1] [2] [3], business intelligence [4] [5] and even machine learning [6] [7] [8] [9] profit tremendously from data analysis that helps discover various hidden relationships between the features of data.

There are many functional dependencies (FDs) that inherently derives from the nature of the data. Although many FDs can be recognized intuitively, (e.g. for a persons database: the name, birth date and place are enough to uniquely identify each person), but many of these relationships are often not trivial for human data managers, thus there is a need for a fast, algorithmic extraction of such relationships.

An extensive research has already been put into FD discovery. The three most widely referenced to, classic approaches are TANE [10], FastFDs [11] and Depminer [12]. While TANE uses an exhaustive breadth-first search on the data using

a containment lattice to find the functional dependencies that hold over them, FastFD takes the difference set of the values of the data samples, applies heuristics and a depth-first search to calculate the minimal covering of the created difference sets. Even though they are efficient at finding FDs, most methods in the literature scale badly with the size of the schema and the number of tuples (data samples), which negatively impacts the time they require for operation [12] [13].

Sequential Indexing Tables and Sequential Fuzzy Indexing Tables (SITs and SFITs [14]) have been proposed in order to implement a classifier that uses the bare minimal steps necessary to classify patterns (i.e. find the known pattern (class) that is the most similar to the input values). They are based on the idea of Lookup Tables ([15] LUTs), which store the precalculated value or class label for all possible input value combinations in suitable arrays [16]. Depending on the problem space, this often results in very large, but sparse arrays (with only a small portion of the stored data being useful). SITs are an attempt to reduce the area of the problem space that is in the focus of the classification, thus only storing areas that hold useful information. This is done sequentially, in a layered structure where each layer restricts the problem space by a given value of an attribute, gradually combining them until the search area is reduced to a single point (SITs) or its fuzzy neighborhood (SFITs) in the problem space. The classification performance of SFITs have been thoroughly investigated by the authors in previous works [17] [18] [19] [20] [21].

SITs and SFITs have an implicit property that they can indicate the presence of functional dependencies in the dataset they have been trained with. If the information that an attribute carries (which is supposed to further restrict the problem space by adding it to the combination of the sequence) is already expressed in the combination of the previous attribute values (i.e. it is functionally dependent on them) then it can be detected in the structure.

In this paper, we describe a new functional dependency extraction approach. It builds upon the idea of using SIT structures to detect and subsequently extract the functional dependencies that hold over the dataset schema considering the available data.

The rest of this paper is as follows. In Section 2 the proposed method is described: in Subsection 2.1 a formal definition of functional dependencies is given, then in Subsection 2.2 the architecture of Sequential Fuzzy Indexing Tables is detailed, while in Subsection 2.3 the new functional dependency extraction method is proposed. In Subsection 3.1 the performance of the proposed method is evaluated, while in Subsection 3.2 complexity analysis is given: Subsection 3.2.1 investigates the time complexity, while 3.2.2. the spatial complexity of the proposed approach. Subsection 3.3 describes possible ways for the expansion of the method in future work. Lastly, the conclusions are drawn.

2 Functional Dependency Detection

2.1 Functional Dependencies

Functional dependencies (FDs) are relationships between attributes of a dataset: such a rule states that the value of an attribute is uniquely determined by the values of other attributes. Formally: over a given relation schema (i.e. the set of attributes) $R, A \in R$ and $X \subseteq R$. $X \rightarrow A$ functional dependency is valid in a given relation r (i.e. the dataset) over $R: \forall u, t \in r, \forall B \in X: \text{if } t[B] = u[B], \text{ then } t[A] = u[A]$. For the rest of the paper, the attributes in the left side of a dependency are regarded as the determinant attributes, and the attribute on the right side is regarded as the dependent attribute.

2.2 Dependency Detection with Sequential Indexing Tables

SITs implement an iterative reduction of the problem space, using the values of the input data directly to restrict the area of focus. In the layered structure of SITs each layer corresponds to an attribute. An index array Λ is used in each layer to store index values that are assigned to each value combination that occurs in the training dataset. The order of the attributes is significant, using two different orderings results in two structures that are different in the sizes of their arrays (though hold basically the same amount of information overall). Each index array has as many columns as the size of the interesting domain of its corresponding attribute (i.e. the range for that attribute in which the training dataset takes values from), and as many rows as the number of index values (so-called *index markers*) that have been assigned in the previous layer (in the first layer, the index array Λ^{L_0} consists of only one row).

Remark #1: Sequential Fuzzy Indexing Tables (SFITs) are the fuzzy extension of SITs, in which an additional fuzzy array is used in each layer in order to handle areas instead of strict integer values (thus adding a certain level of generalization ability to the system, at the price of doubling the size of its structure). However, for classical functional dependency detection and extraction SITs are sufficient as well.

Remark #2: the floating-point values of each tuple are converted into integer format within arbitrary bounds. This is generally done through a suitable linear mapping function:

$$\tilde{X} \cong a \cdot X + b \quad (1)$$

where input value X is scaled with a , and biased with b ($a \in \mathbb{R}, b \in \mathbb{N}$) then rounded.

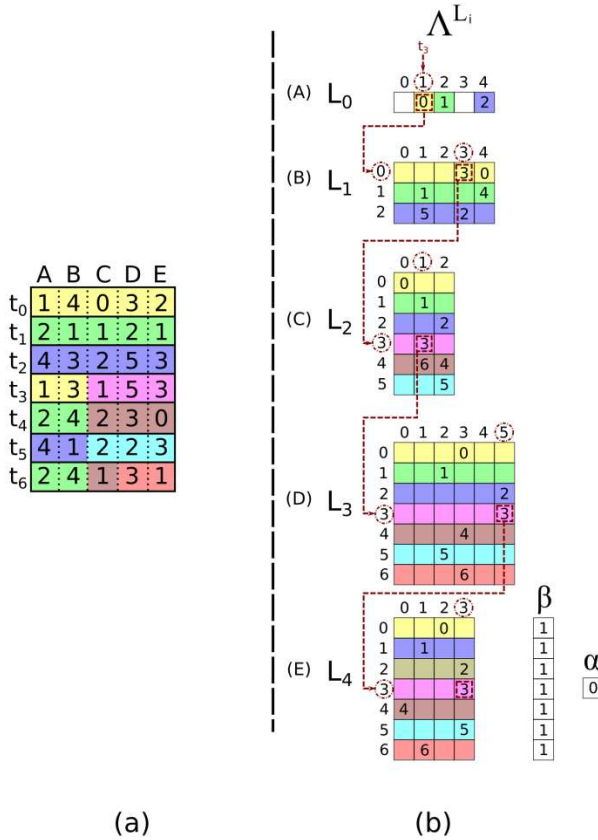


Figure 1

The architecture of Sequential Indexing Tables used for FD detection and extraction

The SIT structure and its usage can be seen in Fig. 1. Let us consider the 7 input tuples $t_0 \dots t_6$ (a), which have been loaded into the SFIT structure (b). In the first iteration, tuple $t_0 = (1,4,0,3,2)$ is inserted. Since there is no marker in $\Lambda_1^{L_0}$, a new one is set: $\Lambda_1^{L_0} = 0$. This also marks that in the next layer the row #0 is considered. In the second layer $\Lambda_{0,4}^{L_1} = 0$ is set, in the third $\Lambda_{0,0}^{L_2} = 0$, etc. Tuples t_1 and t_2 are inserted similarly. However, for the values of $t_3=(1,3,1,5,3)$ there are already markers in place in the first layer, and thus the insertion process follows the route that the markers have marked (which is highlighted with dashed arrows): it only begins inserting new markers in the second layer (L_1). The input data and the rows of the architecture in the figure are colored accordingly in order to help viewing the logic behind the data structure. Each individual stored pattern or tuple realizes a route from L_0 to L_{N-1} .

In the figure, aside from the first layer, every change of color shows that there is a branching in the 'route of restriction' (of the problem space) that the insertion of the data takes throughout the structure.

In each layer, only a specific row is important for a given pattern (given by the marker in the previous layer). Since each marker leads to a given row in the next layer, a row with only one marker in it can be regarded as a straight path, while if there are more than one markers, then it can be regarded as a junction. In the rest of the paper, the former will be regarded as *singular*, while the latter as *non-singular rows*. Out of the two cases, the latter has more importance, as it introduces additional information to the system (distinguishes tuples based on their attribute value). For classification problems, if the index array of a layer L_i only has singular rows, then it does not contribute to the classification process in any meaningful way, therefore it can be ignored and thus save time. This is because the tuples in the structure until layer L_i are already uniquely distinguished by the combination of the layers (or a subset of the layers) that precede it. Which means that for given values of (at least one of) the previous layers, L_i will only take specific values, which is the definition of functional dependencies. Therefore, if there are only singular rows in the index array of a (non-first) layer, then its attribute is the dependent of a functional dependency, and the determinant attributes are among the attributes belonging to the preceding layers.

This can be used to detect functional dependencies: take an ordering of the attributes such that the investigated attribute is in the last place ($N-1$), and build the structure. While filling the arrays, in order to avoid the need to examine the whole of the index matrix of the last layer, the numbers of markers for each row are stored in a column vector β . If any of the elements in is raised above one, a variable α is incremented as well, which indicates if there are any non-singular rows. Thus, after building only α is needed to be checked. If $\alpha=0$, then the attribute is functionally dependent.

2.3 Dependency Extraction with Sequential Indexing Tables

The structure described in Subsection 2.2 can also be used to determine which layers are the determinants of the functional dependencies. The base idea is to create an ordering in which the last layer ($N-1$) corresponds to the attribute that is needed to be examined as the dependent attribute (i). If the index array of the last layer is singular (i.e. all of its rows are singular, $\alpha=0$), then the analysis can commence (otherwise, the attribute is skipped).

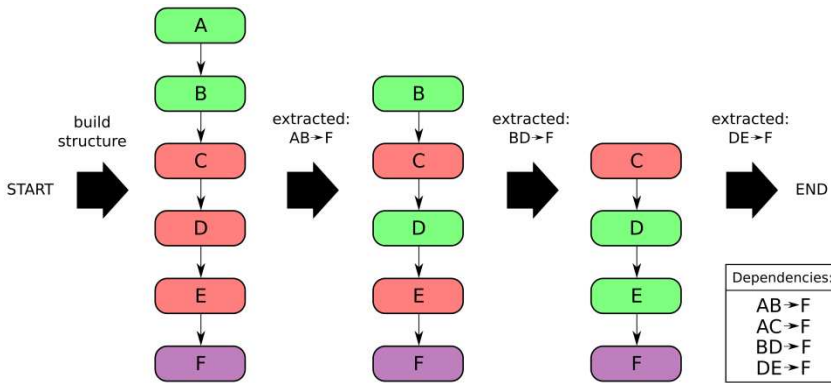


Figure 2

The operation of the FD extractor on a forward order

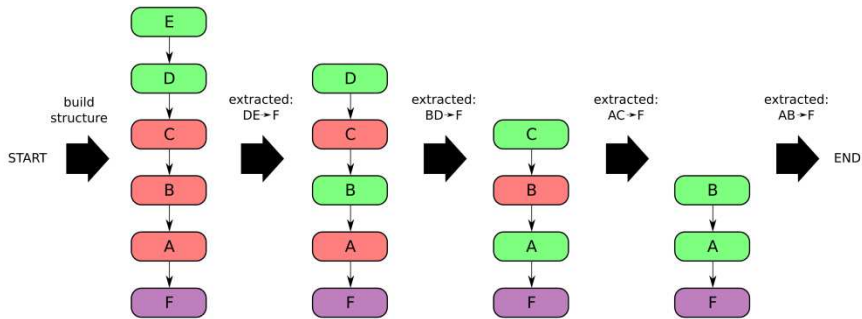


Figure 3

The operation of the FD extractor on a reverse order

The analysis is done in iterations. The structure is built again, but this time without L_{N-2} (the layer that directly precedes the last one). If $\alpha=0$ in the newly rebuilt structure, then attribute of L_{N-2} is not significant in the investigated dependency, it can be ignored in the next steps and move on to the layer before it. If $\alpha>0$, then the preceding layers are no longer sufficient to uniquely identify each stored tuples, information is lost if the layer is skipped. Thus, it is restored and noted as being a part of the determinant. This is done until the first layer is reached and examined.

This algorithm, however, only returns the FD that has an attr. in the highest layer in the topology. This is illustrated in Fig. 2, where a simplified topology stores a dataset, with a schema of $R=(A, B, C, D, E, F)$ where $AB \rightarrow F$, $AC \rightarrow F$, $BD \rightarrow F$ and $DE \rightarrow F$ functional dependencies hold. In the first iteration, E is ignored and proven to be unnecessary, as A and B determines the values of F on their own (and are thus marked with green). D and C are also insignificant in this regard (marked with red). At the end of the analysis, the system returns with $AB \rightarrow F$. In order to

extract the rest of the FDs, the evaluation needs to be restricted: before the next round, attribute A is removed, as it is the highest in the topology among the attributes of the found FD. In the next round, $BC \rightarrow F$ is found, then after B is removed, $DE \rightarrow F$. However, as it can be seen, this method in itself could not find $AC \rightarrow F$, because A was removed prematurely (this is always the case when multiple FDs have the same common attribute, but is high in the topology so it gets removed before all of the FDs are discovered). This can be amended by running the algorithm a second time, but for a *quasi-reversed* order (Fig. 3): reversing the order of the potential determinant attributes but leaving the dependent attribute at the end. The output of the system is the union of the two sets of FDs discovered in each phase (normal and reversed order).

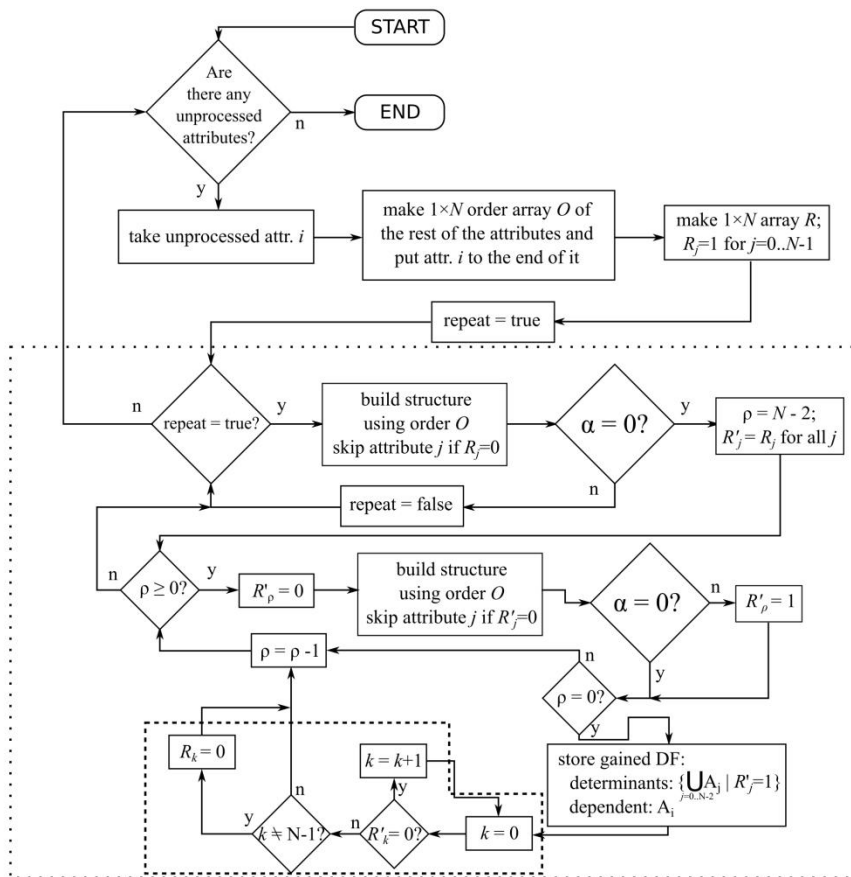


Figure 4
The algorithm of the FD extractor

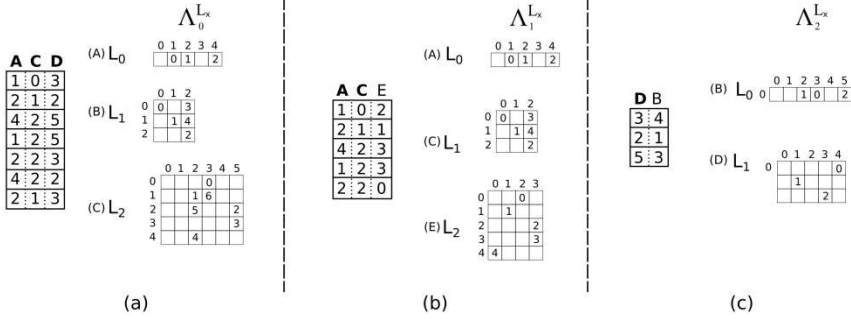


Figure 5

Divided schemas (the key attributes are marked with bold)

Fig. 4 summarizes the algorithm described above, with more details. The ordering of the attributes is stored in $1 \times N$ array O , while the emission of certain attributes or layers is done through $1 \times N$ array R , that stores which attributes are *regarded* in the given iteration. It is used to remove the top attribute of the previously found FD. On the other hand, the temporal removal of layers (from the bottom of the structure) is stored in R' . For each examined attribute, first the auxiliary structures are initialized (O and R), then the FD extraction step (marked by a bounding box with dotted borders). In the extraction step, the SIT structure is built using ordering O regarding the attributes marked by R . If the index array of the last attribute is singular $\alpha > 0$ then there are no more FDs regarding the attr. i , the next attribute is regarded. Otherwise, R is copied into R' , the appropriate layer from the bottom (but above L_i) is marked as disregarded ($R'_p = 0$) and a new SIT structure is built using order O and R' . If $\alpha > 0$, then reinstate the layer ($R'_p = 1$) and go on, until the first layer is reached ($p = 0$), at which point R' marks the attribute of the determinants of the discovered FD. Lastly, the first attribute of the FD is determined (marked by a smaller boxed area in the figure with dashed border), and R is set accordingly.

An interesting (and valuable) consequence of the algorithm is that it always returns the *minimal* FDs, therefore the left side of the relation does not need to be pruned to get the smallest determinant subset that determines the dependent attribute on the right side. The significance of functional dependencies is illustrated in Fig. 6. Examining the same dataset that was used in Fig. 1, the method described above returned the following FDs: $B \rightarrow D$, $D \rightarrow B$, $E \rightarrow C$, $AC \rightarrow E$ and $CD \rightarrow E$. Therefore, the 5-attribute schema in Fig. 1 can be broken up into 3 schemas: (a) ACD, (b) ACE and (c) DB. From a database management viewpoint, this is very valuable as it helps in keeping data consistency, makes modifications easier (e.g. if a value of D changes, then only one element of schema ACD is needed to be changed). Furthermore, if the schemas are stored in SITs, this separation also reduces its size: the structure of ABCDE uses 108 elements, while the 3 combined schemas need only 99 elements (which may not seem like a big reduction, but for larger scales the gap between the numbers is also larger).

3 Performance Evaluation

3.1 Experimental Results

The proposed functional dependency extraction method had been tested on 4 real-life databases from the UCI data repository [23] on using an average PC (Intel® Core™ i5-4590 CPU @ 3.30 GHz, 16 GB RAM).

In the first set of experiments, the Abalone dataset is analyzed with the proposed method, and the effects of the scaling coefficient is examined. The dataset consists of 4177 training samples with 9 attributes. Its original purpose is using the first 8 features (gender, length, diameter, height, whole weight, shucked weight, viscera weight and shell weight) in order to determine the age of the animal (which is measured by the rings of its shell), in hopes that a method can be found that does not necessarily involve the expiration of the abalone (as the counting of the rings requires sawing the shell in half, which has a detrimental effect on the health of the creature.)

Table 1

Number of FDs found for each feature as dependent attribute of the Abalone dataset

Attribute	Scaling Factor		
	200	500	1000
Gender	3	6	7
Length	2	3	5
Diameter	2	4	5
Height	0	3	5
Whole_weight	3	2	4
Shucked_weight	1	5	5
Viscera_weight	3	2	4
Shell_weight	1	4	6
Rings	0	4	7
Number of all FDs found	15	33	48

Table 2

Average time requirements for FD extraction on the Abalone dataset based on the scaling factor

	Scaling Factor		
	200	500	1000
Average time of FD extraction	4.323 s	13.543 s	23.806 s
Average time for building a single SIT structure	0.024 s	0.048 s	0.0545 s

Table 3

Average time requirements for FD extraction on the Abalone, Glass, Wisconsin breast cancer and Iris datasets and the number of extracted FDs

	Number of attributes	Number of tuples	Average time of a full analysis	1 build time	found no. Of FDs	Number of FDs of the last attr.
Abalone ($a=1000$)	9	4177	23.806 s	0.0545 s	48	7
Glass	10	214	1.13 s	0.04 s	70	8
Wisconsin breast cancer	10	683	0.074 s	0.002 s	6	6
Iris	5	150	0.01 s	<0.001 s	2	2

While the gender and the number of the rings are integer numbers, the rest of the features are floating point numbers that are determined to the 3rd or 4th fraction digit. This requires a suitable scaling factor (a_i) that transforms the data into a suitable integer domain. Three different scaling factors are investigated: 200, 500 and 1000. Table 1 shows the results, listing the FDs for each attribute. Interestingly, the larger the scaling factor, the more FDs are discovered that hold on the dataset (15, 33 and 48, respectively). This is due to more details and thus information is lost if the scaling factor is too low. On the other hand, the necessary time is much larger (4.323, 13.543 and 23.806 seconds, respectively), due to the larger sizes of the structure needed to be maintained and the large number of iterations. The average building time of a single SIT structure on the other hand took only 0.024, 0.048 and 0.054 seconds, respectively (Table 2). As for the original purpose of the dataset, the discovered FDs show that the number of rings cannot be directly determined from only the features that does not require the demise of the animal (the closest one features length, diameter, whole weight and shucked weight as the determinants, of which the last one causes the demise of the abalone).

The performance of the FD extractor has been evaluated on 3 other datasets as well: the Iris, the Glass and the Wisconsin breast cancer datasets. The Iris dataset (which is about finding the species of iris plants: Iris Setosa, Iris Versicolor and Iris Virginica) consists of 150 tuples and 5 integer valued attributes. It takes about 10 ms to find the two FDs that holds on the schema. Table 3 summarizes the results. The Wisconsin breast cancer (WBC, determining the nature of mammary tumors) dataset takes slightly more time (74 ms) to process the 683 tuples with 10 integer valued attributes, finding 6 FDs. Finally, in the Glass dataset (determining

the type of glass from its chemical components) has been processed with 214 tuples of 10 floating point features (with suitable scaling factors), finding 70 FDs in 1.13 seconds, of which 8 FDs had the type of glass as the dependent attribute. Interestingly, for the WBC and Iris datasets only the classification target (type of plant and tumor) are determined by the other attributes, but none of the other attributes. The Solar flare data set has also been processed, but no FDs have been found.

3.2 Complexity Analysis

3.2.1 Time Complexity

The computational complexity of FastFDs, TANE ([10][11]) and the SIT-based FD detector and extractor is compared in Table 4. Let R denote the schema (the set of attributes) and r mark the set of values in the dataset, and thus $|R|$ and $|r|$ the number of each set, respectively. If only FD detection is the goal, then the proposed method only requires building a SIT structure (each attribute value is used for one layer only $O(|r| \cdot |R|)$), for each attribute:

$$O(|r| \cdot |R|^2) \quad (2)$$

FD detection is sufficient if the goal is to enhance the speed of a classifier: since the dependent attributes do not contribute additional information into the classification process, skipping them can speed up most classifiers.

If the detected FDs are needed to be extracted as well, then the detection step is needed to be repeated for each attribute, and for each FDs in the dataset:

$$O(\phi \cdot |r| \cdot |R|^3) \quad (3)$$

where ϕ is the number of FDs on a schema considering the given data. The computational complexity of the proposed method is polynomial with respect to the size of the schema ($|R|$), and is linear in the number of tuples ($|r|$), as opposed to the other two methods.

Table 4

Time complexity analysis for Tane, FastFDs and the SIT-based FD detector and extractor

Method	Computational Complexity
TANE	$O(2^{ R } \cdot (r + R ^{2.5}))$
FastFDs	$\sim O(R \cdot r ^2 + R \cdot r ^2 \log(R \cdot r ^2))$
Dependency Detector SIT	$O(r \cdot R ^2)$
Dependency Extractor SIT	$O(\phi \cdot r \cdot R ^3)$

3.2.2 Spatial Complexity

Although the proposed method is less complex computation-wise than the other described methods, it is important to examine its memory requirement as well. The size of the main structure (the index matrices in each layer) of the FD extractor only depends directly on the number of attributes and the size of the domains of each attribute, while it is much less influenced by the number of tuples. On the other hand, the number of tuples can be used as an upper bound to the number of rows (ρ) in the index matrix of each layer:

$$\rho_i = \begin{cases} 1 & , \quad i = 0 \\ \gamma_{i-1} \leq \min(D_{i-1} \cdot \rho_{i-1}, |r|), & i > 0 \end{cases} \quad (4)$$

where ρ_i is the number of rows of the index array in layer i and γ_{i-1} is the number of the index markers in the previous layer. The latter number is typically only known after counting the unique value combinations in the previous layer. Thus, the building of the structure can be done in two ways: going through all of the input data tuples in each layer to get the exact amount of unique value combinations (and thus, γ_i), or construct a structure that is expectedly much larger than necessary using the known upper bounds (from the domain size and number of rows of the previous layer ($D_{i-1} \cdot \rho_{i-1}$), or the number of input tuples ($|r|$)); then go through the input data once, note the γ values for each layer and rebuild the structure with the accurate size. The latter obviously requires less time to do (as the input data is only processed twice), at the cost of temporarily using more memory.

The size of the whole structure is ideally:

$$S = \sum_0^{|R|-1} \rho_i \cdot D_i + \rho_{|R|-1} + 1 \quad (5)$$

Table 5
Spatial complexity analysis for Tane, FastFDs and the SIT-based FD extractor

Method	Spatial Complexity
TANE	$O\left(\frac{(R + r) \cdot 2^{ R }}{\sqrt{ R }}\right)$
FastFDs	$O\left(R \cdot \frac{ r \cdot (r - 1)}{2}\right)$
Dependency Extractor SIT	$O(R \cdot r \cdot D_{max})$

For most cases, it is likely that the lowest layer in the structure has $|r|$ number of rows (unless there is a significant number of redundant tuples), so using $|r|$ as the upper bounds for the row numbers for the worst-case scenario, the size of the structure can be estimated:

$$S = \sum_0^{|R|-1} |r| \cdot D_i + |r| + 1 \quad (6)$$

Thus, the spatial complexity of the SIT-based FD detector in the worst-case scenario:

$$O(|R| \cdot |r| \cdot D_{max}) \quad (7)$$

The spatial complexity of FastFD, TANE ([10] [11]) and the SIT-based FD detector and extractor is compared in Table 5. The complexity of TANE is exponential, though it can be mitigated by keeping parts of the data on the hard drive, which in turn slows the operation as reading and writing from hard drives is significantly slower than memory operations. FastFD uses significantly less memory, though it is still quadratic in the function of $|r|$.

The scaling of the input tuple values during the linear mapping step is also very important, considering the spatial complexity of the system. Although higher scaling factor values increase the chance of finding functional dependencies, they also directly affect the size of the domain of their attributes in question, and subsequently, the size of the SIT structure. Fig. 6 depicts how the size of the structure changes with the scaling factor (a_i) using the Abalone data set. The dataset has 9 attributes, of which 7 have floating point values and 2 have integer type values (thus the latter ones are not scaled). The 7 attributes are scaled using 10 different values (from 100 to 1000), with the same factor in each step (e.g. $a_0=a_2=\dots=a_6=100$).

In the figure, the overall sizes of the main structure (the sum of the sizes of the index matrices, i.e. how many numbers are needed to be stored in them) are compared. As it can be seen, the scaling of the amount of stored data is more or less linear. The smallest examined scaling factor ($a_i=100$) yields a structure with the size of 1940403 elements, while the largest ($a_i=1000$) results in 24523818 elements. To put this into perspective, in order to store the latter amount of array elements using short data type (2 bytes), the structure takes ~46.7 MB to store.

Remark: *short* data type can only be used if the number of indexes in any layer (which in the last layer is the number of unique input tuples) does not exceed the largest number that can be stored in a *short* type variable (65535). For the Abalone data set this is true (since the number of input tuples is 4177), but for larger data sets integer type variables (4 bytes) are needed instead, doubling the memory requirement of the system.

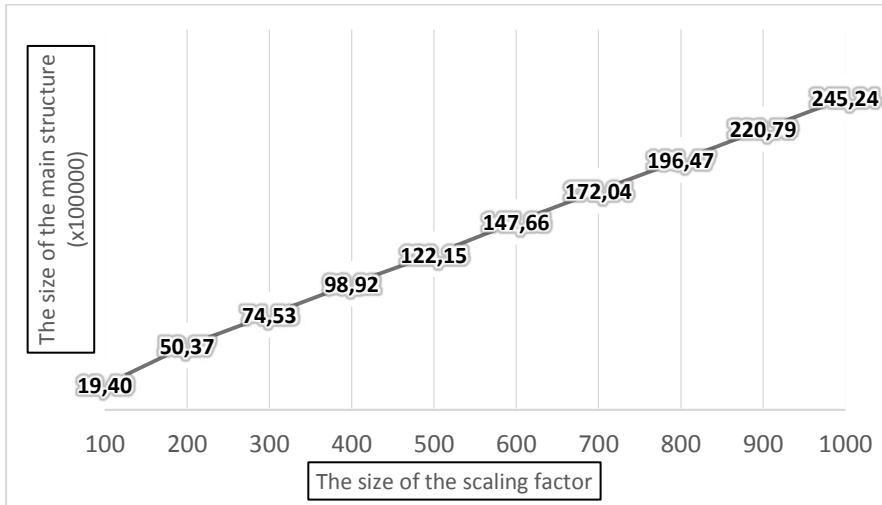


Figure 6

The change of the size of the structure (the amount of array elements stored) in the function of the scaling factor using the Abalone data set

3.3 Future Extensions

Finding clear rules (FDs) in real-life datasets is often hard, if not downright impossible, especially when the amount of the data is very large (raising the possibility of errors, noise or samples that are truly exceptions of the rule). For such cases *Approximate Functional Dependencies* (AFDs) were defined as FDs that hold on a sufficiently large subset of the available tuples. They can be regarded as general rules that have some exceptions to them as well. Being able to extract these rules could also be very advantageous because with them it is still possible to make predictions towards the values of given attributes (e.g. in case of the Solar flare dataset in which no clear FDs can be found, or the Abalone dataset in which the age of the animal could still be predicted from the features that do not require the its destruction). The SIT architecture can already detect the possibility of an attribute being the dependent in an AFD, simply by examining how many of the tuples end in singular and non-singular rows in the index array of the last layer. If their number is sufficient, then ignoring the rest of the tuples (that end in non-singular rows), the proposed method can be used to detect the FDs that hold on them, and thus extract them as AFDs.

The main disadvantage of the proposed method is that its usage is limited in both the number of attributes and the domain in which the attributes can take values from. These directly determine the size of the structure, which can be too large to manage with the average modern computers. The structure, however, can be changed to omit the non-interesting areas (e.g. the empty elements seen in Fig. 1)

and only store the known values. However, this will increase the complexity of the implementation of method and require parallel computing to keep the management of the arrays fast. On the plus side, this can also make it possible to process the tuples in batches, instead of one by one. This upgrade would make it possible for the proposed method to be applied in Big Data applications as well.

Conclusion

In this paper, we describe a new functional dependency extraction approach. It builds upon the idea of using Sequential Indexing Table structures to detect and subsequently extract the functional dependencies that hold over the dataset schema considering the available data.

The proposed method is shown to be able to extract FDs quickly (its computational complexity is a linear function of the number of input tuples), however, at the cost of larger memory usage. The size of the structure is primarily influenced by the number of attributes and the size of the domain they can get values from. The latter can be restricted with suitable scaling factors, although in return of potential loss of information and thus less reliable operation.

In future work, the size problem of the structure will be amended, and the method will be extended to be able to find Approximate Functional Dependencies as well (by disregarding tuples that count as exceptions, if their number is low). Furthermore, parallel programming techniques will be added into the method in order to enhance its speed by processing the input data samples in batches instead of one by one.

Acknowledgement

This publication was created due to support of the Research & Innovation Operational Programme for the Project: "Support of research and development activities of J. Selye University in the field of Digital Slovakia and creative industry", ITMS code: NFP313010T504, co-funded by the European Regional Development Fund.

References

- [1] M. Jocić, E. Pap, A. Szakál, D. Obradović, Z. Konjović, "Managing Big Data Using Fuzzy Sets by Directed Graph Node Similarity," *Acta Polytechnica Hungarica*, Vol. 14, No. 2, 2017, pp. 183-200
- [2] R. Spir, K. Mikula, N. Peyrieras "Parallelization and validation of algorithms for Zebrafish cell lineage tree reconstruction from big 4D image data," *Acta Polytechnica Hungarica*, Vol. 14, No. 5, 2017, pp. 65-84
- [3] A. Vukmirović, Z. Rajnai, M. Radojčić, J. Vukmirović, M. J. Milenković, "Infrastructural Model for the Healthcare System based on Emerging Technologies," *Acta Polytechnica Hun.*, Vol. 15, No. 2, 2018, pp. 33-48

-
- [4] T. Szántai, E. Kovács, A. Egri, "Inventory Control in Sales Periods," *Acta Polytechnica Hungarica*, Vol. 15, No. 1, 2018, pp. 87-104
- [5] V. Farrokhi, L. Pokorádi, S. Bouini, "The Identification of Readiness in Implementing Business Intelligence Projects by Combining Interpretive Structural Modeling with Graph Theory and Matrix Approach," *Acta Polytechnica Hungarica*, Vol. 15, No. 2, 2018
- [6] J. Parra, O. Fuentes, E. Anthony, V. Kreinovich, "Use of Machine Learning to Analyze and – Hopefully – Predict Volcano Activity," *Acta Polytechnica Hungarica*, Vol. 14, No. 3, 2017, pp. 209-221
- [7] D. Marček, M. Rojček, "The Category Proliferation Problem in ART Neural Networks," *Acta Polytechnica Hungarica*, Vol. 14, No. 5, 2017, pp. 49-63
- [8] N. Ádám, A. Baláz, E. Pietriková, E. Chovancová, P. Fecil'ak, "The Impact of Data Representation on Hardware Based MLP Network Implementation," *Acta Polytechnica Hungarica*, Vol. 15, No. 2, 2018, pp. 69-88
- [9] L. Nyulászi, R. Andoga, P. Butka, L. Fözö, R. Kovacs, T. Moravec, "Fault Detection and Isolation of an Aircraft Turbojet Engine Using a Multi-Sensor Network and Multiple Model Approach," *Acta Polytechnica Hungarica*, Vol. 15, No. 2, 2018, pp. 198-209
- [10] Y. Huhtala, J. Kärkkäinen, P. Porkka, and H. Toivonen, "TANE: An efficient algorithm for discovering functional and approximate dependencies," *The Comp. Journ.*, Vol. 42, No. 2, 1999, pp. 100-111
- [11] C. Wyss, C. Giannella, and E. Robertson, "FastFDs: A heuristic-driven, depth-first algorithm for mining functional dependencies from relation instances," In *Proc. of the Int. Conf. of Data Warehousing and Knowledge Discovery (DaWaK)*, 2001, pp. 101-110
- [12] T. Papenbrock *et al.*, "Functional Dependency Discovery: An Experimental Evaluation of Seven Algorithms," *Proceedings of the VLDB Endowment*, Vol. 8, No. 10, 2015, pp. 1082-1093
- [13] N. Asghar, A. Ghenai, "Automatic Discovery of Functional Dependencies and Conditional Functional Dependencies: A Comparative Study," 2015
- [14] A. R. Várkonyi-Kóczy, B. Tumor, and J. T. Tóth, "A Multi-Attribute Classification Method to Solve the Problem of Dimensionality," in *Proc. of the 15th Int. Conf. on Global Research and Education in Intelligent Systems (Interacademia'2016)*, Warsaw, Poland, Sept. 26-28, 2016, pp. PS39-1 – PS39-6
- [15] Maher, David. W. J. and John F. Makowski. "Literary Evidence for Roman Arithmetic with Fractions", *Classical Philology*, Vol. 96, No. 4, 2001, pp. 376-399

- [16] B. D. Zait, B. J. Super, F. K. H. Quek, "Comparison of five color models in skin pixel classification," in Proc. of the International Workshop on Recognition, Analysis, and Tracking of Faces and Gestures in Real-Time Systems, Corfu, Greece, Sep. 26-27, 1999, pp. 58-63
- [17] B. Tumor, A. R. Várkonyi-Kóczy, J. T. Tóth, "Active Problem Workspace Reduction with a Fast Fuzzy Classifier for Real-Time Applications," IEEE International Conference on Systems, Man, and Cybernetics, Budapest, Hungary, October 9-12, 2016, pp. 4423-4428, ISBN: 978-1-5090-1819-2
- [18] A. R. Várkonyi-Kóczy, B. Tumor, J. Tóth, "Robust Variable Length Data Classification with Extended Sequential Fuzzy Indexing Tables," 2017 IEEE Int. Instr. and Meas. Tech. Conf. (I2MTC) 22-25 May, 2017, Torino, Italy, pp. 1881-1886
- [19] B. Tumor, A. R. Várkonyi-Kóczy and J. T. Tóth, "A Fuzzy Data Structure for Variable Length Data and Missing Value Classification," 16th International Conference on Global Research and Education, 25-28 Sept. 2017, Iasi, Romania, pp. O.21-1 – O.21-6
- [20] B. Tumor, G. Simon-Nagy, A. R. Várkonyi-Kóczy and J. T. Tóth, "Personalized Dietary Assistant - An Intelligent Space Application," 21st IEEE Int. Conference on Intelligent Engineering Systems (INES 2017), Larnaca, Cyprus, 20-23 October, 2017, pp. 27-32
- [21] B. Tumor, A. R. Várkonyi-Kóczy, J. Bukor, "An ISpace-based Dietary Advisor," 2018 IEEE International Symposium on Medical Measurements and Applications (MeMeA) 11-14 June, 2018, Rome, Italy, pp.1-6
- [22] B. Kamiński, M. Jakubczyk, P. Szufel, "A framework for sensitivity analysis of decision trees". Central European Journal of Operations Research, Vol. 26, No. 1, 2017, pp. 135-159
- [23] D. Dua and C. Graff, UCI Machine Learning Repository [<http://archive.ics.uci.edu/ml>]. Irvine, CA: University of California, School of Information and Computer Science, 2019

Identification of a dynamic friction model and its application in a precise tracking control

Joanna Piasek, Radosław Patelski, Dariusz Pazderski, Krzysztof Kozłowski

Institute of Automation and Robotics, Poznan University of Technology,
ul. Piotrowo 3a, Poznań, Poland; joanna.z.piasek@doctorate.put.poznan.pl,
radoslaw.z.patelski@doctorate.put.poznan.pl, dariusz.pazderski@put.poznan.pl,
krzysztof.kozlowski@put.poznan.pl

Abstract: The goal of this paper is to examine the friction behaviour in a one-degree mechanical system designed for precise tracking. Friction as one of the main disturbances present in this system strongly influences its performance, which is most visible during the velocity reversals. Identification and compensation of the friction are crucial to achieve high tracking accuracy at very low velocities. In this paper the procedure for identification of static and dynamic frictional parameters of LuGre is presented. The experimental results show characteristic behaviours of friction present both in sliding and in presliding regime. Furthermore, it is experimentally proven in several control scenarios that dynamic friction model compensation causes significant decrease of trajectory tracking error.

Keywords: friction dynamic models; friction identification; precise tracking; the active disturbance rejection paradigm; control of astronomic mounts

1 Introduction

One of the main disturbances deteriorating the quality of control of mechanical systems is friction. Its characteristics can be divided into two stages: presliding (or micro-slip) regime and sliding regime. Classical methods of friction analysis are focused on the description of the sliding regime. Such models represent the static relationship between speed and friction force. The simplest of them consists of Coulomb and viscous friction superposition. Other models take into account also the Stribeck effect, which brings a better approximation of the phenomena at low speeds, [2]. Still, in each of these cases, the presliding behaviour is not considered. It is well known, however, that motion controllers taking advantage of only classical friction models may provide unsatisfactory results, especially at zero-crossing instants of the velocity due to the discontinuity in the velocity-friction characteristics. Therefore, it is important to study more complex models, including also dynamic phenomena, such as friction hysteresis and micro-slips in the presliding regime.

The problem of friction modelling becomes critical in applications where a precise control is required. Important examples of such applications can be found in astronomy. Nowadays, astronomical observations require often the use of mechanical and drive structures (so-called mounts, to which the telescope is attached) and control techniques known in robotics. One of the biggest challenges is to achieve precise trajectory tracking in the task space over a wide range of speed. Currently, at the Poznan University of Technology, an altitude-azimuth mounting structure for a 0.5 m diameter class telescope is being developed, [12]. It is expected that the device is able to track the objects at the sky at very low speeds in the order of several arcseconds per second (resulting from the daily rotation of the Earth on its axis) and larger ones reaching several degrees per second. Moreover, it is supposed to allow quick reconfiguration in order to shorten the time necessary to start the observation of the next object.

The paper covers two main topics. The first is focused on experimental identification of friction in a mechanical joint of the astronomic mount. The second deals with the application of friction models to design a tracking controller based on the active disturbance rejection (ADR) paradigm originally introduced by Han and Gao [7, 8]. The considered control strategy enables an adaptation to unknown dynamic terms of the process using a high-gain observer, [11]. Thus, it is possible to consider the ADR as a particular implementation of the concept of free-model control, [5, 6]. However, in many applications observer gains cannot be increased arbitrarily. This is due to the presence of measurement noises, additional actuators dynamics as well as the delays in control loop, [14]. Then in order to improve control quality an ADR controller can be supplemented with more complex models of the process. Taking advantage of this possibility we design a motion controller and investigate if the application of friction models brings a relevant improvement in the tracking precision for the astronomic mount. We compare experimentally an impact of various models on the controller performance.

Recently, preliminary results of the friction identification of the considered mount have been already reported in [15]. In this paper, however, they are revised and significantly extended. To the best authors' knowledge the implementation of dynamic friction models in the ADR control scheme is original and has not been reported in the literature.

The paper is organized as follows. In Section 2 basic friction models are recalled. Section 3 is focused on the design of tracking controller using the ADR approach supported by friction models. In Section 4 an extensive experimental research is discussed. The results of the friction identification and the tracking control using different models are shown. The last Section concludes the paper.

List of symbols

All symbols are given in the order of appearance.

J	moment of inertia	[kg · m ²]
q	axis angular position	[rad]
h	disturbances in the system	[Nm]

τ_f	friction torque	[Nm]
τ	control input, torque	[Nm]
σ_0	stiffness coefficient of the friction model	[Nm/rad]
σ_1	damping coefficient of the friction model	[Nm · s/rad]
σ_2	viscous coefficient of the friction model	[Nm · s/rad]
V_s	Stribeck velocity	[rad/s]
F_s	Stribeck friction	[Nm]
F_c	Coulomb friction	[Nm]
δ	empirical tuning coefficient of the friction model	
z	average displacement of bristles in the friction model	[rad]
\dot{q}, ω	axis angular velocity	[rad/s]
q_d	desired angular position	[rad]
\dot{q}_d	desired angular velocity	[rad/s]
\ddot{q}_d	desired angular acceleration	[rad/s ²]
e	tracking position error	[rad]
\dot{e}	tracking velocity error	[rad/s]
k_p	gain of proportional term of the tracking controller	[Nm/rad]
k_d	gain of derivative term of the tracking controller	[Nm · s/rad]
w	estimate of total disturbance $\tau_f + h$	[Nm]
d	lumped disturbance, $d = -w + h + \tau_f$	[Nm]
τ^*	estimate of input reduced by friction, $\tau^* = \tau - \hat{\tau}_f$	[Nm]
$\hat{\tau}_f$	estimate of friction force	[Nm]
ζ_1	estimate of q	[rad]
ζ_2	estimate of \dot{q}	[rad/s]
ζ_3	estimate of reduced lumped disturbance	[rad/s ²]
L	\mathbb{R}^3 vector of observer gains	

2 Friction models

Let us consider the following dynamics of one-degree of freedom mechanical system

$$J(q)\ddot{q} + h + \tau_f = \tau, \quad (1)$$

where q denotes a configuration, J is a moment of inertia, h describes a disturbance (including gravity, dynamic couplings between other links of a multi-body system, etc.), τ_f stands for friction and τ is a torque (force) input.

Further, we consider operation conditions in which inertial forces are negligible while friction τ_f constitutes a predominant term in dynamics (1). As a result, its proper modelling can be required for simulation analysis as well as control design. In the successive sections we briefly recall basic approaches to describe friction effects.

2.1 Static model

The static model is only dependent on the velocity $\omega = \dot{q}$. It describes the friction τ_f behaviour in the sliding state. The most common static model, taking into account

the Stribeck effect, was presented by Armstrong in the following form, [2]:

$$\tau_f = \sigma_2 \omega + \text{sign}(\omega) \left(F_c + (F_s - F_c) \exp \left(- \left| \frac{\omega}{V_s} \right|^\delta \right) \right). \quad (2)$$

The expression $\sigma_2 \omega$ represents viscous friction force, while the rest of the equation describes Stribeck effect. This model is characterized by 5 parameters: static friction F_s , Coloumb torque/force F_c , Stribeck velocity V_s , shape coefficient δ and viscous friction coefficient σ_2 .

The significant disadvantage of this model is the discontinuity by velocity reversals, what can cause errors and instability in the friction compensation procedure.

2.2 Dahl model

The Dahl model is one of the oldest friction models (1968), that describes behaviour of the friction in the presliding regime, that means in the stage when the input signal is not big enough to break the static friction force. In this regime, the rough structures building contact surfaces are getting deformed, resulting in micro-scale motion, [4]. These roughness form a system similar to a spring-system. When the external force is high enough, the spring breaks and the sliding movement begins. Dahl model takes into account the break-away moment of static friction F_s . It presents friction as a first order differential equation with respect to position q , [4]:

$$\frac{d\tau_f}{dq} = \sigma_0 \text{sign} \left(1 - \frac{\tau_f}{F_s} \right) \left| 1 - \frac{\tau_f}{F_s} \right|^n. \quad (3)$$

The model consists of three parameters: micro-stiffness coefficient σ_0 , static friction force F_s and shape factor n .

2.3 LuGre model

LuGre model was presented by Canudas de Wit [3], as an extension of Dahl model by function describing the Stribeck effect. Both regimes are described using the same group of equations without use of a switching function, what results in a smooth transition between sliding and presliding regimes.

This model is based on a system of bristles (bristle model), where the internal state variable z represents their average displacement. By usage of a first order differential equation authors described friction dynamic phenomena like frictional lag and presliding displacement. LuGre model consists of 7 parameters and is described below:

$$\dot{z} = \omega - \sigma_0 \frac{|\omega|}{s(\omega)} z \quad (4)$$

$$s(\omega) = F_c + (F_s - F_c) \exp \left(- \left| \frac{\omega}{V_s} \right|^\delta \right), \quad (5)$$

$$\tau_f = \sigma_0 z + \sigma_1 \dot{z} + \sigma_2 \omega, \quad (6)$$

For small deformations, the model behaves like a spring with stiffness σ_0 and damping coefficient σ_1 . In the steady state, this model is reduced to a static model. Setting the micro-stiffness coefficient to σ_0 and micro-damping friction coefficient σ_1 to 0 and equaling Coulomb F_c and Stribeck friction F_s reduces the LuGre model to the Dahl model with shape factor $n = 1$.

3 Tracking controller with friction compensation

3.1 The general form of the control law

Let q_d be a reference trajectory which is smooth enough (at least the second order time derivative is bounded). Next, we define tracking error, $e := q_d - q$, and consider a PD-like controller equipped with feed-forward and compensation terms, cf. [14],

$$\tau = J(q) (\ddot{q}_d + k_p e + k_d \dot{e}) + w, \quad (7)$$

where $k_p > 0$ and $k_d > 0$ are positive gains, and w is an estimate of $\tau_f + h$.

Substituting (7) to (1) one can obtain the following closed loop system

$$J(q)\ddot{e} = -J(q) (k_p e + k_d \dot{e}) + d, \quad (8)$$

where $d := -w + h + \tau_f$ denotes lumped disturbance which comes from a mismatch between the model and the real dynamics.

Now, assuming that the disturbance is at least locally bounded in a subset of the state-space where the system evolution takes place, one can expect that for any positive k_p and k_d tracking error converges to vicinity of zero, such that

$$\lim_{t \rightarrow \infty} |e(t)| \leq C \sup_t |d(t)|, \quad (9)$$

where C is a positive constant, which is dependent on the chosen gains. Hence, one can conclude that for fixed values of parameters k_p and k_d , the tracking accuracy can be improved by reducing the magnitude of disturbance d . Basically, such a reduction can be achieved in two ways: by using a more accurate model of the process or by application of adaptation techniques.

In this paper we combine two approaches. Specifically, in order to introduce an adaptation mechanism we take advantage of a high gain extended state observer (ESO) and assume that a friction model becomes a part of the controller, while estimate of h stays unknown. In such a case, the observer is designed based on the following dynamics

$$\ddot{q} = \frac{1}{J(q)} (-h + \tau^*), \quad (10)$$

where $\tau^* := \tau - \hat{\tau}_f$, while $\hat{\tau}_f$ stands for the assumed model of friction. Then the ESO observer can be designed as follows

$$\dot{\zeta} = \begin{bmatrix} 0 & 1 & 0 \\ 0 & 0 & 1 \\ 0 & 0 & 0 \end{bmatrix} \zeta + \begin{bmatrix} 0 \\ \frac{1}{J(q)} \tau^* \\ 0 \end{bmatrix} + L(q - \zeta_1), \quad (11)$$

where $\zeta = [\zeta_1 \ \zeta_2 \ \zeta_3]^\top$ denotes estimates and $L \in \mathbb{R}^3$ defines the observer gains which are chosen based on the Routh-Hurwitz stability criterion. It can be proved that for $\sup_t |\dot{h}| < M_1$ and $\sup_t |\dot{\tau}_f - \hat{\tau}_f| < M_2$, where M_1, M_2 are constants, estimate ζ satisfies the following

$$\lim_{t \rightarrow \infty} |\zeta_1 - q| \leq \varepsilon_1, \lim_{t \rightarrow \infty} |\zeta_2 - \dot{q}| \leq \varepsilon_2, \lim_{t \rightarrow \infty} \left| \zeta_3 - \frac{1}{J(q)} (\hat{\tau}_f - \tau_f - h) \right| \leq \varepsilon_3, \quad (12)$$

with $\varepsilon_1, \varepsilon_2$ and ε_3 being positive constants which can be made small enough by increasing the observer gains, for example see [18, 1].

Consequently, one can consider ζ_2 as an estimate of velocity \dot{q} , while $J(q)\zeta_3$ can be viewed as an approximation of the total disturbance. Following this observation, one can assume that w in (7) satisfies

$$w := \hat{\tau}_f - J(q)\zeta_3 \quad (13)$$

and can be considered as an approximation of $h + \tau_f$. Then recalling definition of d one can conclude that magnitude of this term can be attenuated. Alternatively, it can be stated that the disturbance is actively rejected in the control loop.

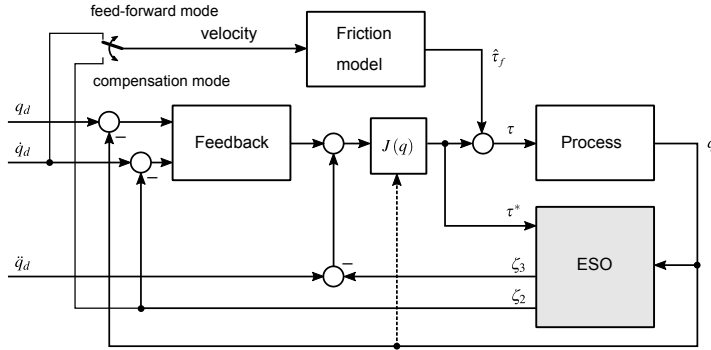


Figure 1

Diagram of the tracking controller with the friction model.

Remark. The stability of the closed loop system is considered under relatively strong assumptions. In particular, the requirements formulated with respect to time derivatives of h , τ_f and $\hat{\tau}_f$ could be seen as limiting factors. However, locally for the considered operation conditions, they can be justified. In particular, it is noteworthy that the application of dynamic friction models makes it possible to confirm that τ_f and $\hat{\tau}_f$ are bounded in a neighborhood of zero velocity.

3.2 Friction compensation

The outlined controller taking advantage of the ADR approach allows one to incorporate friction model $\hat{\tau}_f$ in different ways. Basically, a priori knowledge about the friction model may limit the process uncertainty that can lead to a better accuracy

of estimation of residual disturbances. Particularly, it is expected that term $|\hat{\tau}_f - \dot{\hat{\tau}}_f|$ can be reduced which leads to the improvement of tracking performance.

The main problem considered in this paper can be briefly stated as follows.

Problem. *We investigate the qualitative and quantitative aspects of using friction models in an ADR controller based on real experimental data.*

In particular, we consider control tracking performance in the case of a slow-time varying trajectory determined for a robotic revolute joint and take into account the following approaches to define friction model $\hat{\tau}_f$:

- C1 Nominal case: the friction model is not considered, $\hat{\tau}_f := 0$,
- C2 Compensation case: the friction model is computed based on the system state (i.e. velocity estimated by the observer), $\hat{\tau}_f := \hat{\tau}_f(\hat{q})$,
 - C2a Dynamic compensation case: full LuGre model is considered and dynamical effects are included based on the system state,
 - C2b Static compensation case: simplified static model is considered under assumption $\dot{z} \equiv 0$, based on the system state,
- C3 Feed-forward case: the friction model is computed based on the reference trajectory (i.e. reference velocity \dot{q}_d), $\hat{\tau}_f := \hat{\tau}_f(\dot{q}_d)$,
 - C3a Dynamic compensation case: full LuGre model is considered and dynamical effects are included based on the reference trajectory,
 - C3b Static compensation case: simplified static model is considered under assumption $\dot{z} \equiv 0$, based on the reference trajectory.

The controller diagram with the friction model employed in the compensation or feed-forward path is presented in Fig. 1.

4 Experimental work

The experiments have been conducted using telescope mount developed at Institute of Automatic Control and Robotic of Poznan University of Technology, [12]. The studied object consists of a two-axis altitude-azimuth gearless robotic platform with an astronomic telescope with a mirror of diameter 0.5 m. It is driven by permanent-magnet synchronous motors (PMSMs) which are capable of delivering torque of the order of 50Nm. The measurement of angular positions is performed by two sets of four absolute encoders with a resolution of 32 bits, [9], while speed is estimated by numerical differentiation of the position signal. Control algorithms have been implemented in C++ using Texas Instruments AM4379 Sitara processor with ARM Cortex-A9 core. The controller itself is implemented in a cascade form which consists of independent current and position loops. Both loops work simultaneously with frequency of 10 kHz.

The results reported in this paper have been obtained for the vertical axis of the mount which supported by a ball bearing. Since the identification procedure is

performed offline, in this report we have presented only the most representative results among a wide number of experimental trials. All the measurements used in the identification scheme have been collected under normal operating conditions (after the system has heated up, in constant temperature, and the fixed position of the horizontal axis). Value of the moment of inertia $J = 30 \text{ kg} \cdot \text{m}^2$ was estimated based on identification experiments and CAD model of the device.

The identification experiments of static friction as well as experiments investigating the controller performance have been conducted in the closed loop control regime with $k_p = 255$ and $k_d = 30$ what corresponds to bandwidth $\omega_c = 15$ and damping coefficient $\zeta = 1$ of PD regulator. The bandwidth of ESO observer was chosen as $\omega_o = 220$, cf. also [14]. Identification of dynamic parameters has been carried out in an open loop. Both identification experiments are outlined in Figs. 2 and 3.

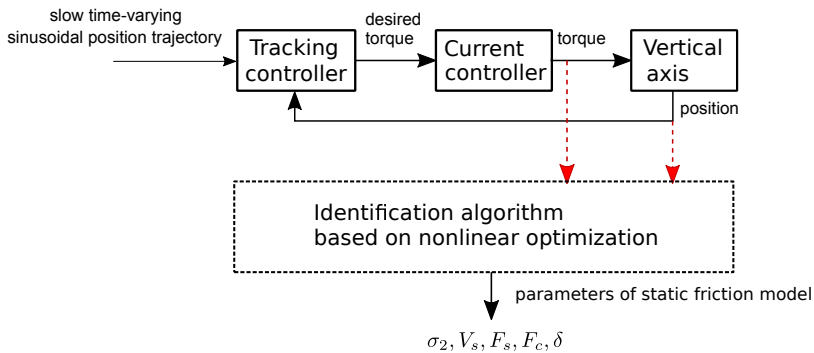


Figure 2

Diagram of the identification process of the static friction model in the closed loop regime (the case of a quasi-static excitation)

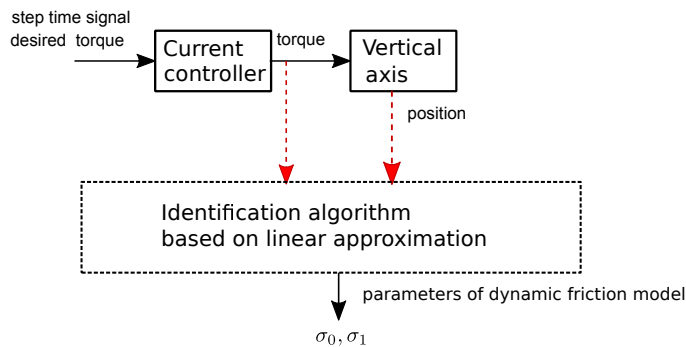


Figure 3

Diagram of the identification process of the dynamic friction model in the open loop regime (the case of a dynamic excitation)

4.1 Identification of friction model

4.1.1 Friction – velocity map

The most common way to find the friction-velocity map is by registration of the input torque at constant velocity in the full range of available velocities [13, 16, 3]. Due to limitations connected with the long-lasting recording process, it was very difficult to conduct the corresponding experiment. Furthermore, PMSM drives generate torque with unwanted ripples, resulting from the construction of the motor. This entails the need for a comprehensive analysis of movement – preferably averaging measurements of a few revolutions of a telescope. Taking into account the geometric constraints imposed on the considered system it was impossible to repeat the experiments reported for other mounts, [13].

Alternatively, in order to find a friction-velocity map one can measure the velocity of the mount as a response for triangular or sine input of very low frequency and amplitude bigger than break-away torque required to just initiate the motion. This solution was presented in [17] and [10].

Quasi-static excitation was achieved using reference trajectory q_d such that \dot{q}_d defines a sine wave of amplitude 0.056 rad/s and frequency 0.04Hz. The chosen stimulation minimizes the influence of mechanical dynamics, therefore the characteristics obtained in this way can be presented as quasi-static. To be more precise, recalling (1) in the considered conditions it is assumed that $|J(q)\ddot{q}| + |h| \ll |\tau_f|$. Hence, the following approximation can be justified: $\tau_f \approx \tau$.

Nonlinear optimization was performed in Matlab (Curve Fitting Tool) to find static parameters based on the torque-velocity data by minimizing cost function:

$$\min_{\sigma_2, V_s, F_s, F_c, \delta} \sum_{i=1}^n [\tau_{fi} - \hat{\tau}_{fi}]^2, \quad (14)$$

where $\hat{\tau}_f$ stands for the torque computed by the model.

Table 2
Estimated static parameters of LuGre model in the vertical axis

Parameter	$\omega > 0$	$\omega < 0$	nominal case	unit
σ_2	28.64	22.5	32.77	Nm s/rad
F_c	3.128	2.123	2.322	Nm
F_s	4.32	3.081	3.322	Nm
V_s	0.01129	0.02126	0.04129	rad/s
δ	1.2914	1.9	2	-

Estimated values are collected in Table 2. From the obtained results one can conclude that friction characteristics are not symmetrical for two directions of motion. Figures 4a and 4b show static friction parameters identification results for positive and negative velocities as well as for the nominal case, Fig. 4c, that collects results of all data independently of the velocity sign. The break-away torque takes smaller values when system velocity decreases than when it increases. The width of hysteresis loop grows with the acceleration increase. Stribeck effect in this system is

negligible, which can be partially explained by the application of rolling bearings (instead of plain bearings).

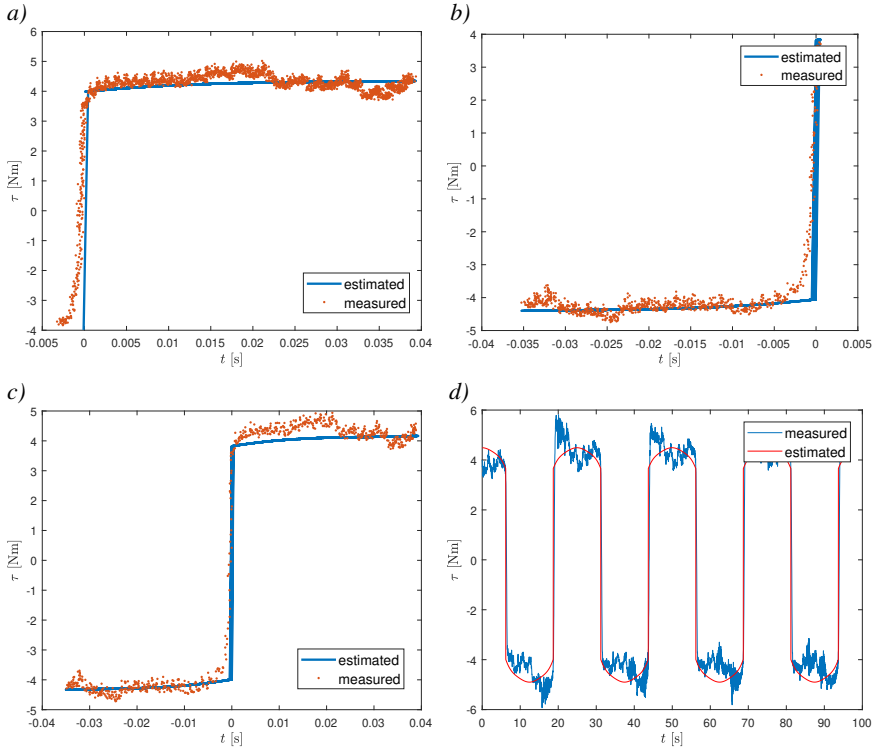


Figure 4

Static friction estimation when (a) $\omega > 0$ (b) $\omega < 0$ (c) nominal case (d) comparison of nominal static friction model with an input signal

From Fig. 5a one can conclude that the system behaviour in the open loop is not consistent, especially in the context of break-away friction torque, despite periodic input torque signal. Such properties of the object were not observed in any of the cited papers. This probably means that the assumed friction model does not reflect additional disturbances in the analyzed system. In Fig. 5b friction-velocity map for following periods are presented, the difference between curves reaches 2 Nm for the corresponding velocities, this property causes variability of static friction parameters and shows that system is non-stationary.

4.1.2 Dynamical parameters

Estimation of dynamic parameters values σ_0 and σ_1 is not possible by direct usage of linear estimation techniques because of the non-linear relationship between friction and these parameters and the impossibility of measuring the variable z , that represents bristle displacement due to junctional deformations at the surface interface. Instead, a simplified method based on the linear approximation of the system

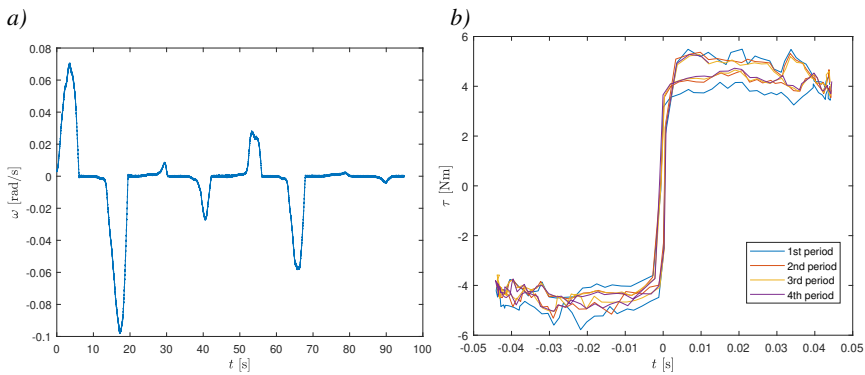


Figure 5

(a) system's response for the periodic input torque signal that results in varying break-away friction. (b) velocity-friction map in the closed loop system for several sine periods

in the presliding stage can be applied. Basically, when torque τ is less than the breaking torque, Eq. (4) reduces to $\dot{z} = \omega$ and the essential system dynamics can be described by:

$$J\ddot{q} + (\sigma_1 + \sigma_2)\dot{q} + \sigma_0 q = \tau. \quad (15)$$

The corresponding transfer function is as follows:

$$\frac{Q(p)}{U(p)} = \frac{\frac{1}{\sigma_0}}{\frac{J}{\sigma_0} p^2 + \frac{\sigma_1 + \sigma_2}{\sigma_0} p + 1}, \quad (16)$$

where p is a complex variable, $Q(p)$ and $U(p)$ stand for Laplace transforms of q and τ , respectively.

In the applied identification procedure, estimation of dynamic parameters σ_0 and σ_1 abridges to parameters estimation of the transfer function $\frac{Q(p)}{U(p)}$, for example by analyzing the system response for an input step of small amplitude (smaller than the break-away torque).

In the conducted experiments the desired torque defined by a step function of value of ± 1 Nm (the function jumps from 0 to ± 1 , respectively) was employed. Estimated parameters are presented in Table 3, measured and estimated step responses for velocities of different signs are presented in Fig. 6. The resulted characteristics are not symmetrical.

Table 3
Estimated dynamic parameters in the vertical axis

	$\omega > 0$	$\omega < 0$	unit
σ_0	$9.7869 \cdot 10^4$	$8.674 \cdot 10^4$	Nm/rad
σ_1	521.4151	473	Nm s/rad

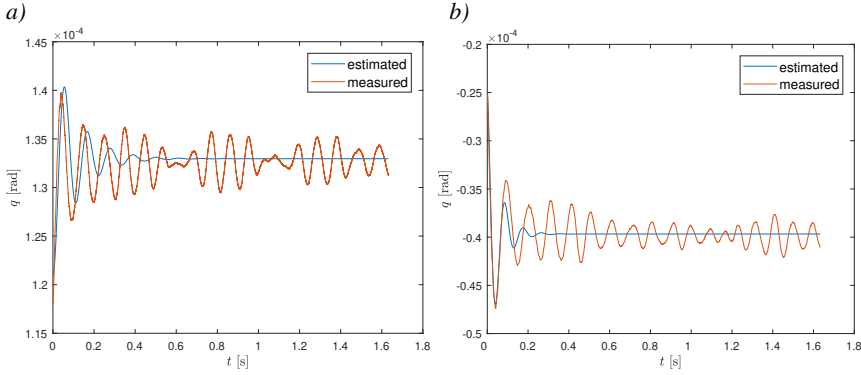


Figure 6

Dynamic friction estimation: (a) $\omega > 0$, (b) $\omega < 0$

4.2 Tracking control

4.2.1 Implementation of friction model

Typically, friction effects are described by fast dynamics. As a result, value of parameter σ_0 in (4) is large, which makes numerical integration of the friction model challenging. In such a case (4) can be considered as a stiff differential equation. In order to overcome this issue, we assume that velocity ω is a slow-time varying function. In particular, for $\dot{\omega} = 0$ one can find the following approximated analytic solution of (4)

$$z(t) = \left(1 - \exp\left(-\frac{|\omega| \sigma_0}{s(\omega)} t\right)\right) \frac{\text{sign}(\omega) s(\omega)}{\sigma_0} + \exp\left(-\frac{|\omega| \sigma_0}{s(\omega)} t\right) z(0), \quad (17)$$

where $z(0)$ stands for the initial condition. This result has been used to implement the friction model in the discrete time domain, namely a new value of z has been computed at each time interval for the given value of ω from t to $t + T_s$, where $T_s = 0.1$ ms is the sampling time.

4.2.2 Friction compensation

Having obtained both the identified parameters of the friction model and the numerical implementation of differential equations in the discrete time domain, series of experiments have been undertaken to investigate practical usability of LuGre model in a task of high-precision tracking control. Each of the cases defined in section 3.2 has been separately implemented and tested. During every experiment the desired trajectory was chosen as a sine wave with frequency of $f_d = \frac{1}{5}$ Hz and maximum velocity of $\omega_{dmax} = 5\omega_s$, where $\omega_s = 7.268 \cdot 10^{-5} \frac{\text{rad}}{\text{s}}$ stands for the velocity of stars observed on the night sky.

Tracking error $e(t)$, friction force $\hat{\tau}_f(t)$ computed from the implemented model, torque τ_d produced by the controller (for the real control system torque τ is achieved indirectly taking advantage of an auxiliary current controller – here for simplicity it is assumed that $\tau = \tau_d$, cf. [14]) and an estimate of the total disturbance represented

Table 4
Values of Integral Square Error criterion calculated for each experiment

	C1	C2a	C2b	C3a	C3b
ISE criterion [arcsec]	47.58	12.75	73.71	9.29	41.29

by $\zeta_3(t)J(q)$ and provided by the extended state observer have been recorded during each experiment. All measures were registered after a short initial stage when an auxiliary trajectory was generated in order to ensure a smooth transition from the motionless state. Thus, for $t \geq 0$ a discontinuity in the desired trajectory $t = 0$ is avoided. Obtained results are presented in Figs. 7-11. Integral square error criterion within time horizon $T_h = 15$ s has been calculated for each of the experiments and the corresponding values are presented in Tab. 4.

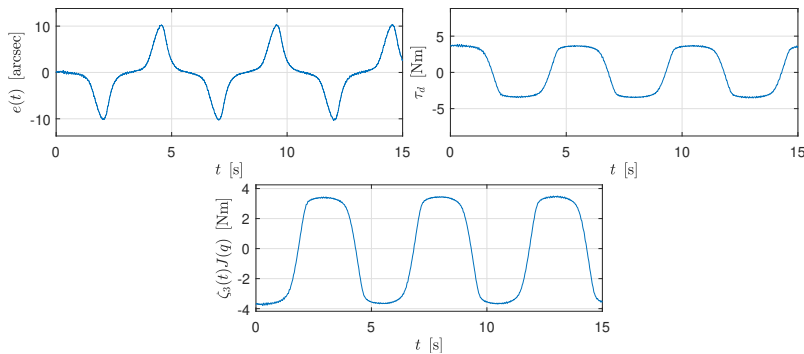


Figure 7
Tracking error, desired torque and estimated disturbance during C1 experiment

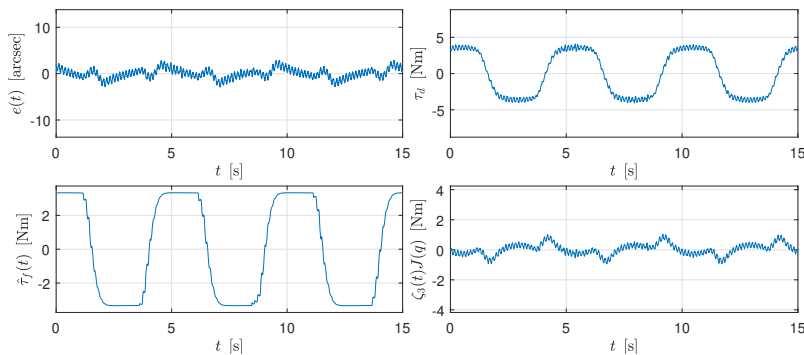


Figure 8
Tracking error, calculated friction force, desired torque and estimated disturbance during C2a experiment

Several conclusions can be drawn from the presented figures. The effectiveness of friction compensation using dynamic LuGre model is successfully confirmed by a significant decrease of the tracking error, especially in intervals where the sign of velocity changes. Over 80% decrease of ISE criterion was obtained by using the

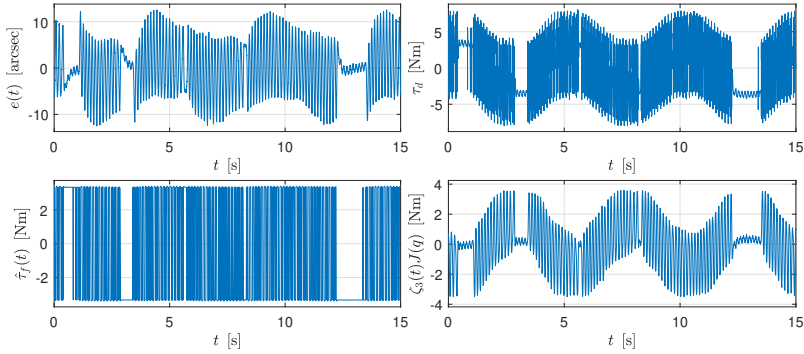


Figure 9
Tracking error, calculated friction force, desired torque and estimated disturbance during C2b experiment

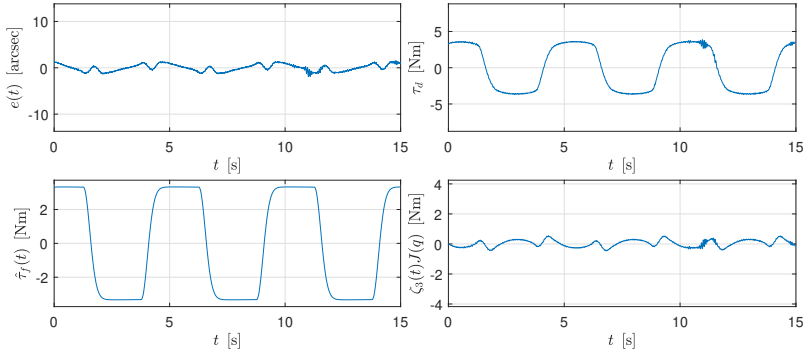


Figure 10

Tracking error, calculated friction force and estimated disturbance during C3a experiment

feed-forward compensation based on the desired velocity and almost 75% decrease by usage of the feedback variant based on the estimated velocity of the joint. Commonly used feed-forward compensation using static only friction model proved to be unable to significantly improve the tracking quality while feedback-based static model led to increase of tracking errors due to the noise present in the velocity estimate. Thus, it can be expected that the low-pass filtering properties of LuGre model dynamics are able to restore the usability of a disturbed velocity signal. Moreover, from a comparison of the disturbance torque in Fig. 7 and inverted (due to the definition of disturbance in (8)) friction torque obtained from the models in the other experiments, one can conclude about quality of chosen friction model, identified parameters and presence of other unmodelled dynamic effects in the system. The similarity of the compared signals suggests that friction is indeed the main disturbing torque in the considered telescopic mount and that model parameters have been, at least locally, identified correctly.

Conclusions

The aim of this study is to investigate the phenomenon of friction in a robotic system with application to precise motion control. Based on the experimental data dynamic

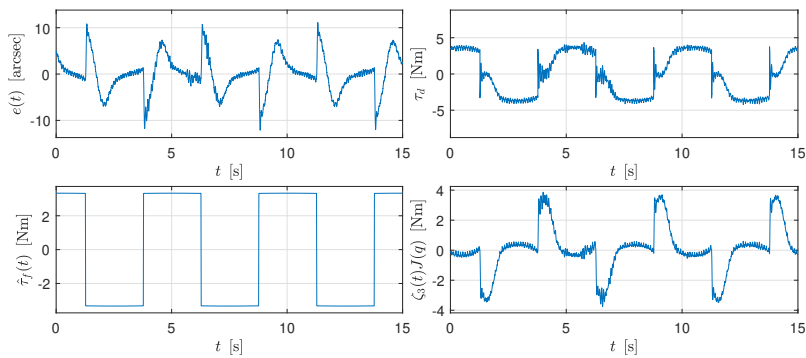


Figure 11
Tracking error, calculated friction force, desired torque and estimated disturbance during C3b experiment

friction model has been identified properly, however, the lack of symmetry with respect to the sign of the velocity has been noticed. Moreover, the studied object is strongly nonstationary.

In spite of these limitations, it was observed that a dynamic friction model makes it possible to improve the tracking precision when reversal motion in a revolute joint with a ball bearing is considered. Based on the experimental data, the best results for the proposed ADR-based controller are achieved when LuGre friction model is used in the feed-forward path. In contrast, static friction models seem to be inappropriate for the considered motion conditions. It is noteworthy to emphasize that model inaccuracies are effectively attenuated by the ESO observer at least for slow time-varying disturbances. However, in order to significantly improve the tracking performance, it is necessary to accurately model fast disturbances which cannot be precisely estimated by the observer due to limited bandwidth.

In future works, it may be interesting to enrich deterministic friction models with stochastic models. Additionally, the high variability of friction depending on parameters such as temperature shows on-line identification can be required to improve robustness of the controller. Alternatively, more complex dynamics of the friction can be implemented.

Acknowledgement

This work was supported by the National Science Centre (NCN) under the grant No. 2014/15/B/ST7/00429, contract No. UMO-2014/15/B/ST7/00429.

References

- [1] C. Aguilar-Ibanez, H. Sira-Ramirez, and J.A. Acosta. Stability of active disturbance rejection control for uncertain systems: A Lyapunov perspective. *International Journal of Robust and Nonlinear Control*, 27(18):4541–4553, 2017.
- [2] B. Armstrong-Hélouvy. *Control of machines with friction*. Norwell, MA: Kluwer Academic Publishers, 1991.

- [3] C. Canudas-de Wit, H. Olsson, K.J. Astrom, and P. Lischinsky. A new model for control of systems with friction. *IEEE Transactions on Automatic Control*, 40(3):419–425, 1995.
- [4] P. R Dahl. Measurement of solid friction parameters of ball bearings. Technical report, Aerospace Corp El Segundo Ca Engineering Science Operations, 1977.
- [5] M. Fliess and C. Join. Model-free control and intelligent PID controllers: Towards a possible trivialization of nonlinear control? *IFAC Proceedings Volumes*, 42(10):1531–1550, 2009. 15th IFAC Symposium on System Identification.
- [6] M. Fliess and C. Join. Model-free control. *International Journal of Control*, 86(12):2228–2252, December 2013.
- [7] Z. Gao. From linear to nonlinear control means: A practical progression. *ISA Transactions*, 41(2):177 – 189, 2002.
- [8] J. Han. From PID to Active Disturbance Rejection Control. *IEEE Transactions on Industrial Electronics*, 56(3):900–906, March 2009.
- [9] D. Janiszewski and M. Kielczewski. Kalman filter sensor fusion for multi-head position encoder. In *2017 19th European Conference on Power Electronics and Applications (EPE'17 ECCE Europe)*, pages P.1–P.7, Sep. 2017.
- [10] M.R. Kermani, Rajnikant V. Patel, and M. Moallem. Friction identification and compensation in robotic manipulators. *IEEE Transactions on Instrumentation and Measurement*, 56(6):2346–2353, 2007.
- [11] H.K. Khalil and L. Praly. High-gain observers in nonlinear feedback control. *International Journal of Robust and Nonlinear Control*, 24(6):993–1015, 2014.
- [12] K. Kozłowski, D. Pazderski, B. Krysiak, T. Jedwabny, J. Piasek, S. Kozłowski, S. Brock, D. Janiszewski, and K. Nowopolski. High precision automated astronomical mount. In R. Szewczyk, C. Zieliński, and M. Kaliczyńska, editors, *Automation 2019. Advances in Intelligent Systems and Computing*, volume 920. Springer, 2020.
- [13] T.S. Kumar and R.N. Banavar. Identification of friction in the 50/80 cm aries schmidt telescope using the LuGre model. *IFAC Proceedings Volumes*, 44(1):980–985, 2011.
- [14] R. Patelski and D. Pazderski. Tracking control for a cascade perturbed control system using the active disturbance rejection paradigm. *Archives of Control Sciences*, 29(2):387–408, 2019.
- [15] J. Piasek, K. Kozłowski, and D. Pazderski. Identification of friction in a robotic astronomical 0.5-m telescope mount. In *Proc. of IEEE International Conference on Intelligent Engineering Systems (INES) 2019 (To appear)*, 2019.

-
- [16] C.H. Rivetta and S. Hansen. Friction model of the 2.5-mts sdss telescope. In *Telescope Control Systems III*, volume 3351, pages 466–478. International Society for Optics and Photonics, 1998.
- [17] M. Ruderman, F. Hoffmann, J. Krettek, J. Braun, and T. Bertram. Robust identification of nonlinear frictional dynamics for advanced controller design. *IFAC Proceedings Volumes*, 42(10):474–479, 2009.
- [18] S. Shao and Z. Gao. On the conditions of exponential stability in active disturbance rejection control based on singular perturbation analysis. *International Journal of Control*, 90(10):2085–2097, 2017.

Virtual Design of Advanced Control Algorithms for Small Turbojet Engines

Ladislav Főző¹, Rudolf Andoga², Levente Kovács³, Michal Schreiner², Károly Beneda⁴, Ján Savka¹, Radovan Soušek⁵

¹Department of aviation engineering, Faculty of Aeronautics of Technical University of Košice, Rampová 7, 04001 Košice, Slovakia
ladislav.fozo@tuke.sk

²Department of avionics, Faculty of Aeronautics of Technical University of Košice, Rampová 7, 04001 Košice, Slovakia
rudolf.andoga@tuke.sk, michal.schreiner@tuke.sk

³John von Neumann Faculty of Informatics, Óbuda University
Bécsi út 96/b, H-1034 Budapest, Hungary
kovacs.levente@nik.uni-obuda.hu

⁴Department of Aeronautics, Naval Architecture and Railway Vehicles, Faculty of Transport Engineering, Budapest University of Technology and Economics, Műegyetem rkp. 3, H-1111 Budapest, Hungary
kbeneda@vrht.bme.hu

⁵Faculty of Transport Engineering, University of Pardubice
Studentská 95, 53210 Pardubice, Czech Republic
radovan.sousek@upce.cz

Abstract: Advanced control in the area of turbojet engines defines many different applied complex control strategies. Highly theoretical approaches and designs are often presented in this area. The article is aimed at practical aspects of adaptive controller design for a class of small turbojet engines in triple loop control architecture. The article presents a non-linear dynamic model of a small turbojet engine taking in account the environmental conditions, which it operates in. The designed triple loop control architecture shows increased precision of control keeping acceleration schedule of the simulated engine and is not susceptible to outer disturbances. The article shows pilot dynamic simulation tests, showing feasibility of the taken approach. It can also be used for other classes of turbojet engines as well other similar technical systems.

Keywords: turbojet engines; adaptive control; non-linear system; dynamic modelling

1 Introduction

Control systems of aircraft engines define their economic and operational efficiency as well as their safety. Digital control systems allow updating control algorithms as software packages, which can quickly and effortlessly improve fundamental operational characteristics of an engine. There are many approaches, which are today applied to fulfil this task [1, 2, 3, 4]. Apart from the classical PID control systems, which are quite effective [5, 6], more progressive approaches in control of turbojet engines can be taken [7, 8]. The ones, which expand on the classical control schemes are the adaptive control algorithms [8, 9, 10].

This means application and design of a controller, which is using some sort of adaptation not only to outer environmental conditions but also to state conditions of a turbojet engine, contrary to control systems using non-adaptive controllers with integrated limiters [5, 6]. Such approach can achieve a solid control quality and safety of operation in turbojet engines control and is today widely used and improved [11, 12, 13, 14].

Small turbojet engines usually use simple control algorithms. The aim of the paper is to show the advantage of combining an adaptive algorithm with a triple loop control architecture, which keeps acceleration/deceleration schedules of the engines steady throughout their whole operational life [7]. This is not typical for small turbojet engines, but it can be expected that combination of adaptability and multi-looped control system can be very efficient for this class of engines.

In order to show the advantages of adaptive and multi loop control in the area of small turbojet engines a non-linear simulation model has been developed taking in account altitude and velocity parameters and their influence on a small turbojet engine. The article covers a practical approach in adaptive controller design using a generalized non-linear engine model and shows advantages of such approach in control of small turbojet engines compared to traditional control approaches using fixed parameters PID controllers with limiters [7, 17, 18]. This practical approach is contrary to often presented results, which are only concepts or strictly simulation results [4, 5, 15, 17]. The resulting design should provide a controller design that is suitable for acceleration/deceleration control as well as steady state control in a wide area of changing aircraft velocities, altitudes and engine speeds with good efficiency [17].

2 Non-Linear Model of a Small Turbojet Engine

2.1 A Generalized Dynamic Engine Model

In order to design and test an adaptive control scheme for a turbojet engine, a generalized dynamic turbo-compressor model based on available data of the turbo-compressor TJ/TP 100 engine has been developed. The model also includes a dynamic actuator model and together with a non-linear approximation of speed/altitude characteristics [18, 19, 20].

The model can be expressed as the following transfer function after Laplace transformation:

$$\frac{n(s)}{FF(s)} = \frac{K_e}{T_e s + 1}, K_e = f(n, H, M), T_e = f(n, H, M) \quad (1)$$

Where:

- FF – fuel flow [l/min],
- n – rotational speed of the engine [RPM],
- K_e – static gain of the engine,
- T_e – time constant of the engine [sec],
- H – flight altitude [m],
- M – Mach number [-],
- f – a non-linear approximation function.

The first order transfer function is able to approximate the dynamics of the engine with sufficient precision [2, 18], its complexity is hidden mainly in the non-linear characteristics of its K_e and T_e variables. Both reflect the changes in outer environmental conditions and the engine's state conditions. These non-linear characteristics have been modelled according to data from TJ-100 engine. The graph in Figure 1 presents a non-linear approximation of the K_e parameter for the different engine's speeds, altitudes and velocities. The graph in Figure 2 shows approximation of the T_e parameter for the same input parameters. These approximations can be considered as valid for different engines. The equations used for these approximations are defined as follows (2) (3):

$$T_e = T_{p0} \frac{p_0}{p_H (1 + 0.2M^2)^{3.5}} \sqrt{\frac{T_H (1 + 0.2M^2)}{T_0}} \quad (2)$$

$$K_e = K_{p0} \frac{P_0}{p_H (1 + 0.2M^2)^{3.5}} \quad (3)$$

where T_{p0} and K_{p0} are obtained from equilibrium states of the engine at ground conditions at temperature and pressure for static ground conditions defined as $T_0=288^\circ\text{K}$ and $p_0=1.013e^5 \text{ N/m}^2$. The parameters T_H and p_H were defined using the international standard atmosphere (ISA) model [23]. The flight altitude is changing in the interval $H \in \langle 0, 4000 \rangle \text{ m}$ and Mach number in the interval $M \in \langle 0, 0.4 \rangle$.

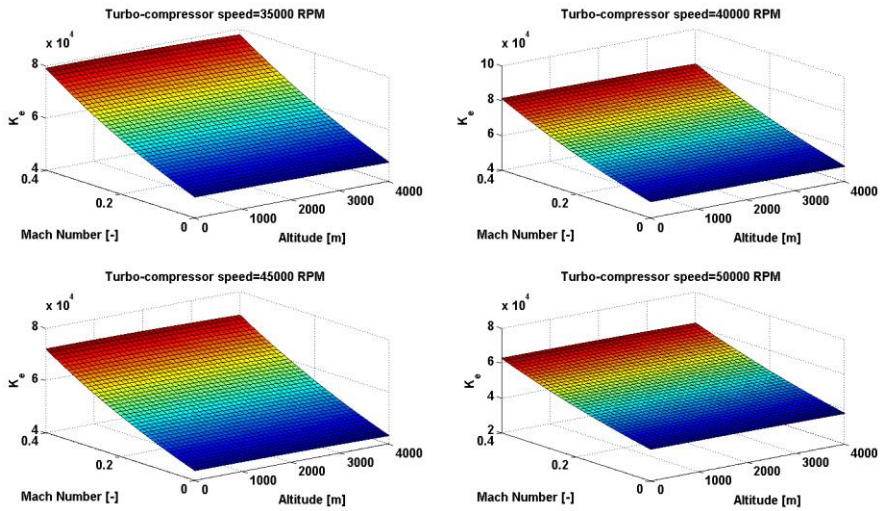


Figure 1
Approximation of the gain “ K_e ” parameter

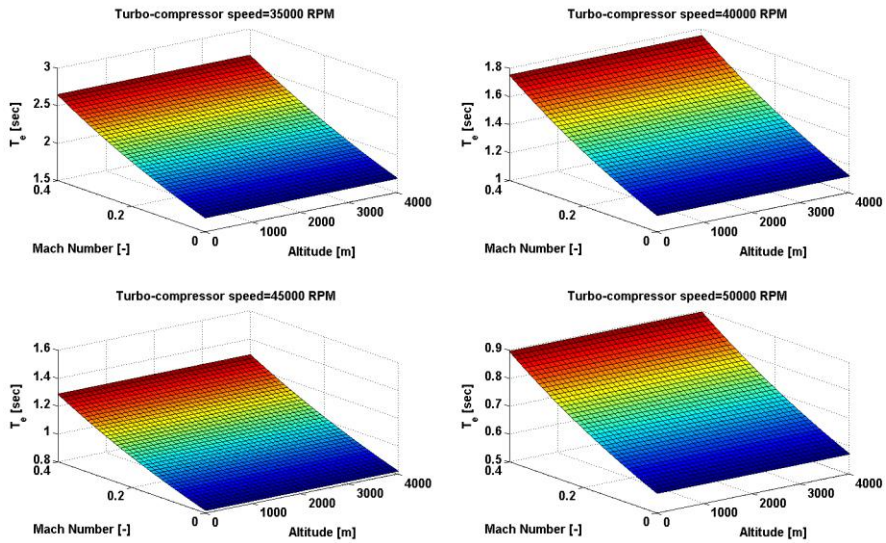


Figure 2

Approximation of the time constant " T_e " parameter

2.2 Architecture of the Model

The resulting model has a single input control parameter (fuel flow supply), two input outer/environmental parameters (Mach number and Altitude) and one state parameter, which is the rotational speed of the turbo-compressor. The state parameter represents a feedback in the model to approximate T_e and K_e parameters of the model.

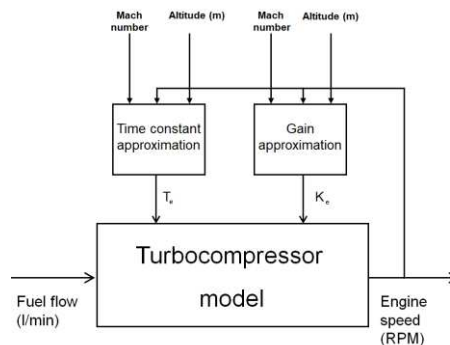


Figure 3

The architecture of the engine model

Dynamic response of the engine is also considerably influenced by dynamics of the fuel pump with a non-linear element by-pass valve [2, 9, 21]. Transfer function of the valve can be expressed by the transfer function $F_{bypass}(n)$, its operation being dependent on the engine's speed n . Fuel flow is partially transferred back into the engine up to a speed around 50 000 RPM. The resulting transfer function of the fuel pump with the non-linear function of the bypass valve is presented in the equation (4):

$$F_{FF}^{PWM} = \frac{FF(s)}{PWM(s)} F_{bypass}(n) \quad (4)$$

The control input of the fuel pump is a pulse width modulated signal PWM, output of the pump is given by its mass fuel flow. The dynamic simulation model of the engine and its fuel flow pump with the bypass valve is shown in Figure 4.

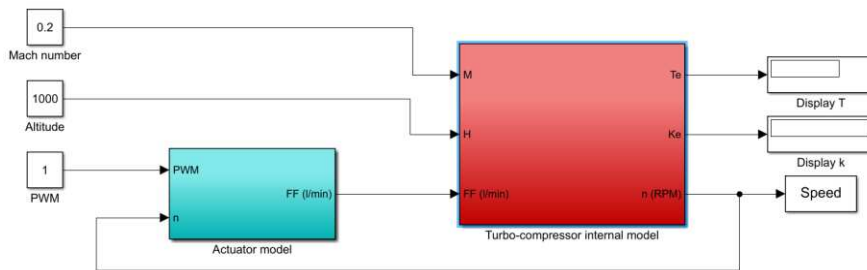


Figure 4

The model implemented in simulation environment

The simulation in Figure 5 presents a dynamic response of the engine's model to a step in the fuel flow supply at different altitudes running for 10 seconds. The model is able to capture dynamic characteristics of the real engine, it can be seen that with increased altitude its acceleration time is lower and achieved speed is higher with identical fuel flow.

The final model represents a non-linear dynamic system, which changes its characteristics according to different environmental and inner state conditions. The system is inherently stable as its base is defined by a first order transfer function and a traditional PI controller in a single loop is able to control it successfully. However, its efficiency decreases in off design conditions when altitude or velocity change. In order to secure qualitative control in all conditions with guaranteed acceleration times and constant control efficiency, different adaptive control methodologies will be investigated further.

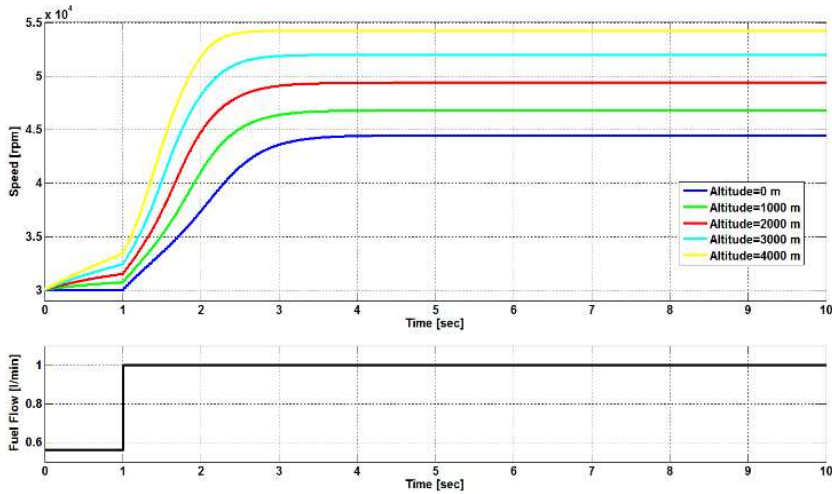


Figure 5

Dynamic step response of the constructed model

3 Controller Design

In order to meet the strict criteria in acceleration and deceleration times laid on modern turbojet engines, the methodology of n_dot control has been selected [7, 24]. This methodology is today widely used and is aimed at securing constant acceleration times by controlling the acceleration and set-point of the engine using a multiple loop control architecture [5, 6]. In order to decrease the complexity of the controllers a third inner-most loop is devised, which is aimed to precisely control and meter the fuel flow. The triple loop control system architecture is shown in Figure 6. Limiters and the engine protection logic is not considered, but can be added in any of the loops using the min-max methodology or others [25, 26, 27].

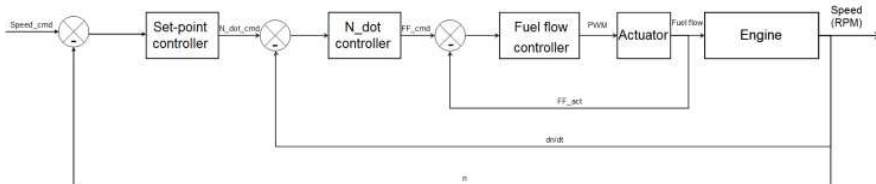


Figure 6

Triple loop controller design

The inner-most feedback loop controls the fuel flow supply into the engine by computing the pulse width modulated (PWM) signal controlling the fuel pump with control law defined as follows:

$$PWM(s) = (K + T_d s)(FF_{cmd}(s) - FF_{act}(s)) \quad (5)$$

The inner-most feedback loop controls the fuel flow supply into the engine by computing the pulse width modulated (PWM) signal controlling the fuel pump with control law defined as follows:

$$PWM(s) = (3.6625 + 0.001s)(FF_{cmd}(s) - FF_{act}(s)) \quad (6)$$

The next loop contains the n_{dot} controller, which is used to control the speed derivative of the engine keeping it at constant level until the desired engine speed is obtained. This loop computes the desired fuel flow into the engine to be stabilized by the lower level loop. This loop is crucial for the resulting control quality and is mainly influenced by state and environmental parameters. This means that adaptive control algorithm has to be applied at this level of control. The control law of this loop is defined as:

$$FF_{cmd}(s) = \frac{1}{s} \left(\frac{1}{T_i s} + K_{ndot} \right) (s \cdot ndot_{cmd}(s) - s \cdot n(s)) \quad (7)$$

The computed controller for the non-adaptive approach for the designed model is as follows:

$$FF_{cmd}(s) = \frac{1}{s} \left(\frac{1}{0.0001s} + 2.9881e - 05 \right) (s \cdot ndot_{cmd}(s) - s \cdot n(s)) \quad (8)$$

The outermost loop computes the derivative command for the engine in order to get to a selected set-point, the commanded rotational speed. The control law at this level is very simple and is defined as:

$$ndot_{cmd}(s) = K_{setp} (n_{cmd}(s) - n_{act}(s)) \quad (9)$$

the computed P controller at this level is as follows:

$$ndot_{cmd}(s) = 0.8(n_{cmd}(s) - n_{act}(s)) \quad (10)$$

3.1 Adaptive Triple Loop Control System

In order to change the dynamics of the system the K_{ndot} parameter of the control law was defined in (7). The dynamics of the control loop is mainly influenced by this parameter and it will be scheduled according the equation:

$$K_{ndot} = f(K_e, T_e) \quad (11)$$

The function f represents the function of the adaptor and K_e , T_e are the parameters of the internal model as defined in (1) and Figure 3. The resulting adaptive control system architecture therefore represents an adaptive control system with an internal model [28, 29, 30]. The designed control system architecture is shown in Figure 7.

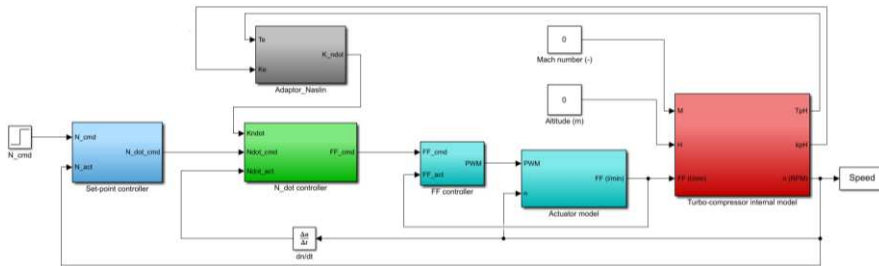


Figure 7

Adaptive triple loop controller design

Three different approaches when designing the adaptor have been tested. The first one is represented by the Naslin algorithm computation of the controller gain according the formula (12), which the coefficients of the characteristic equation have to satisfy [31, 32]:

$$(a_i)^2 \geq \alpha \cdot a_{i+1} a_{i-1} \quad (12)$$

The coefficient α represents allowed overshoot of the response characteristics of the system and a_i are coefficients of the characteristic equation of the linearized model of the engine.

The second taken approach in adaptation of the K_{ndot} parameter is the performance quadratic function of the deviation of acceleration from the commanded engine acceleration according to the following formula:

$$f : K_{ndot} = \alpha \cdot \frac{1}{2} (s \cdot (n_{cmd}(s) - n_{act}(s)))^2 \quad (13)$$

The third approach in adaptor design is application of a neural network. An offline trained neural network with time delayed inputs trained by the ‘‘Scaled Conjugate Algorithm’’ has been used. The neural network has the following structure:

- 2 neurons in input layer (T_e , K_e),
- 12 neurons in the first hidden layer, 7 neurons in the second hidden layer,
- 1 neuron (K_{ndot}) in the output layer.

All of the proposed approaches have been evaluated in the simulation environment in order to execute comparative test analysis with the non-adaptive triple loop control system [33].

4 Evaluation of the Control System

The aim of the evaluation is to test the multiple looped control system and see if it operates normally. The presented tests have to be taken as pilot experiments to show the abilities of the adaptive multi loop control system to operate in a range of simulated conditions. The evaluation will mainly be done in simulated environment with the following experimental set-up.

- Mach number $M=0, 0.3$,
- Maximal acceleration schedule = 3000 RPM/s,
- Engine set-point schedule represented by a step command from 40 000 RPM to 52 000 RPM, meaning that the engine should accelerate from idle to maximal speed at around 4 seconds,
- Altitude is set at the following values: 0, 1000 and 4000 meters.

The resulting dynamic responses of the engine in simulations are shown in the following figures. Figure 8 shows the engine's acceleration at ground at zero velocity. This also simulates laboratory conditions and can be used for comparison of the simulated and a real-world experiment using the engine iSTC-21v. It can be seen that all controllers operate with similar control quality at this level.

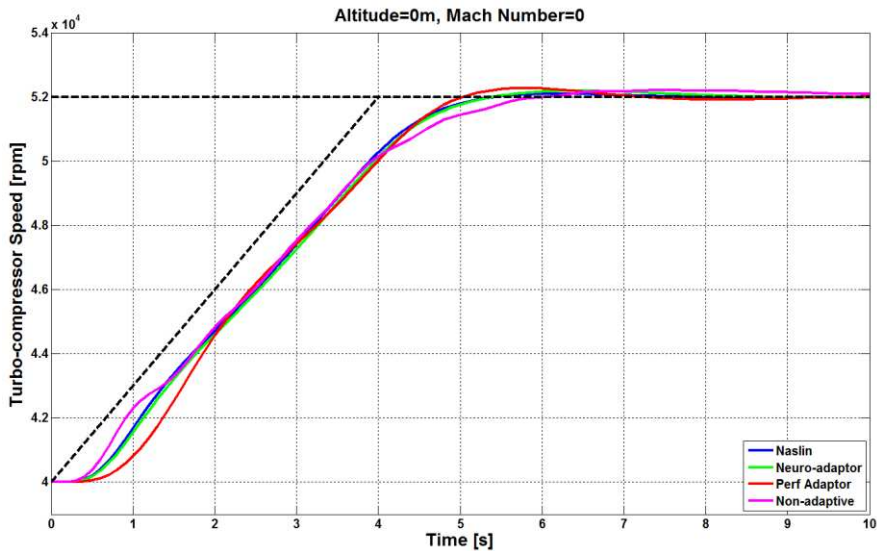


Figure 8
Ground simulation

The next simulation resembles a flight of an aircraft at an altitude of 1000 meters shown at a Mach number of 0.3. As shown in Figure 9, with higher altitude the

performance of the adaptive approaches has improved compared to the non-adaptive algorithm, acceleration time of which is slower. It is even more prevalent when the altitude is increased to 4000 meters in Figure 10, where the adaptive approaches show a considerable improvement. On the other hand, it can be stated that all controllers present good control quality keeping the desired acceleration schedule, this means that the turbojet engine is accelerating in approximately 6 seconds irrespective of flight conditions.

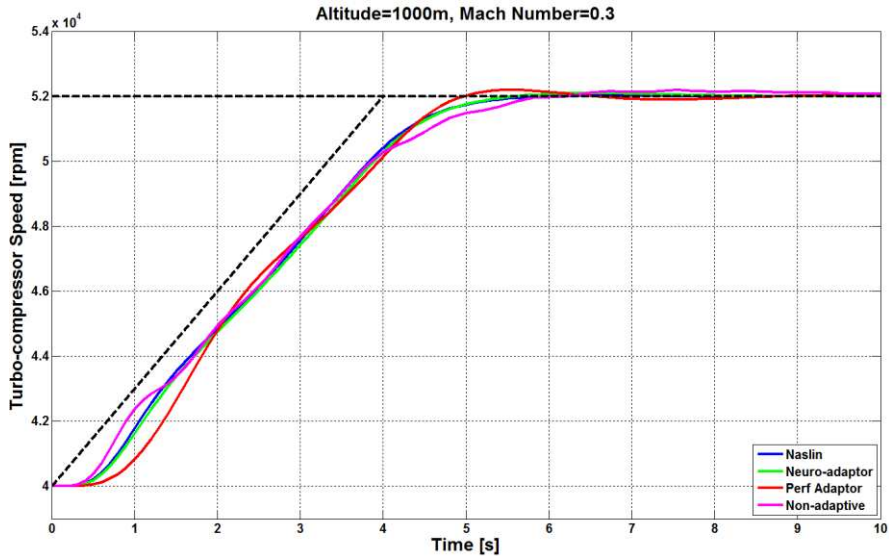


Figure 9
Flight at 1000 meters

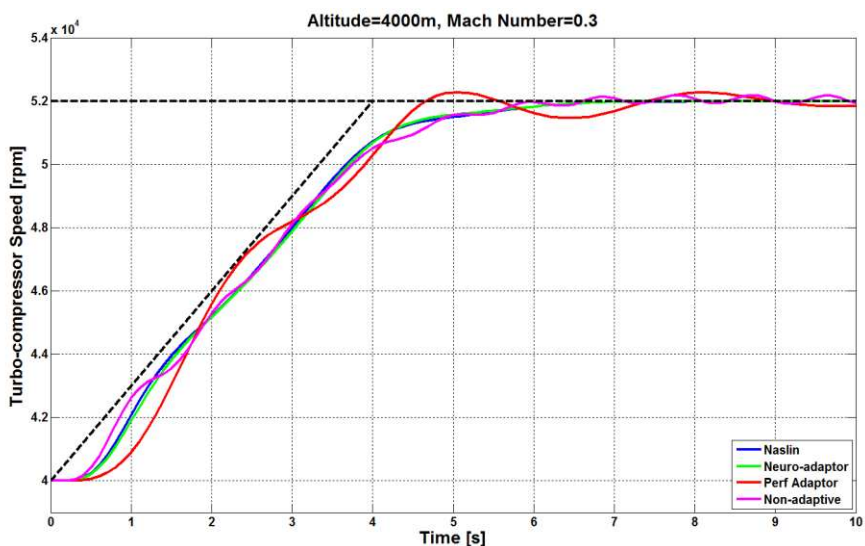


Figure 10
Flight at 4000 meters

Follow-up simulation tests with constant Mach number $M = 0.3$ and changing altitude have been done. The summarized performance of all controllers with changing altitude at the constant velocity is shown in Table 1. In order to compare the performance of individual controllers linear absolute control surface have been computed [22]. Lower control surface means that the controller is more efficient in acceleration of the engine. The table shows that the Naslin adaptive controller performs as the best followed by the neural network adaptive algorithm, non-adaptive and the last is the performance quadratic adaptive controller, although it has also achieved acceptable control quality.

Table 1
Comparison of performance between different adaptive controllers

Altitude \ Adaptor	0 [m]	1000 [m]	2000 [m]	3000 [m]	4000 [m]
Naslin	9295.6	8115.4	7498.8	6750.3	6261.8
Neuro-adaptor	9673.4	8475.3	7807.4	6994.9	6454.6
Perf adaptor	15005	13194	11819	10183	9187.9
Non adaptive	10571	9170.2	8054.1	6978.4	6383.7

To prove the validity of the concept, the triple loop control architecture was employed in laboratory conditions using the iSTC-21v engine [1, 35, 39]. The simulations are compared to the real data obtained in an experiment as shown in Figure 11, where the Naslin adaptor has been employed in the triple loop control system architecture. It can be seen that the experiment with the engine performs

with a lower quality compared to simulations, however it is keeping the schedule well and illustrates that the control concepts presented in simulations can be successfully applied in a digital control system of a real engine. Some further tuning of the designed controller would be needed in order to compensate for other non-linear properties of the engine iSTC-21v, which have not been included in the model. The experiment serves just as a proof of concept that the designed control system is stable and performs similarly to simulations. It needs also to be noted that the adaptive control with triple loop algorithm has been designed for the TJ-100 engine, however, is robust enough to control a different engine.

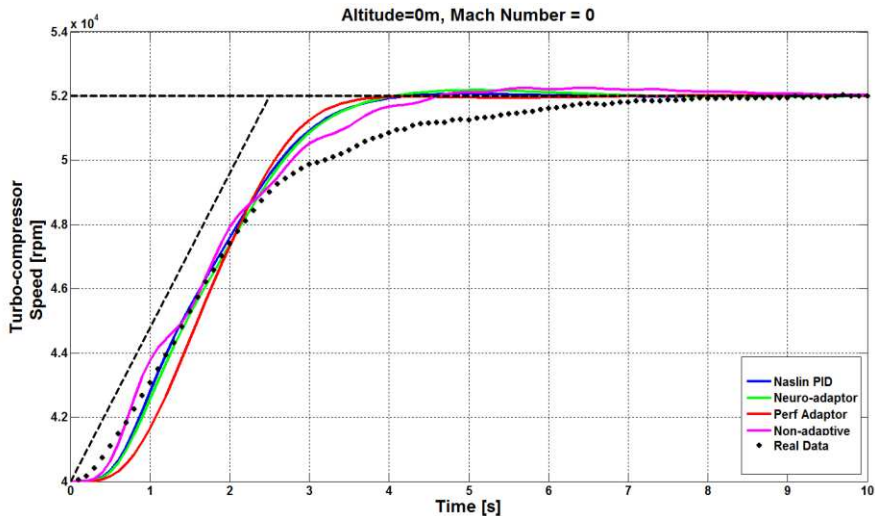


Figure 11

Comparison of simulation and experimental data using the iSTC-21v engine

Conclusion

A concept for efficient control of a small turbojet engine with fixed exhaust nozzle under different environmental conditions has been shown. Using a triple loop control scheme seems to be a promising concept decomposing the complex controller into several very simple controllers, which can achieve good performance even without adaptation. Adaptation of the middle loop according to a simple Naslin methodology can improve efficiency of the control system further. Further tuning of the adaptor could probably provide even better results. A practical test has confirmed that the control architecture works in a real experimental setup using the iSTC-21v engine and is robust enough to control different engine than it has been designed for. The practical test serves only as a proof of concept and a more complex set of tests can be done using the modified TJ-100 engine. The design can be implemented in an embedded microcontroller system as envisioned in [34]. More complex neural network with online training and with a broader data-set could improve efficiency of the adaptive control

system even further. A comprehensive set of tests will be prepared and presented as a follow-up study using the TJ-100 engine.

Acknowledgement

The work presented in this paper was also supported by KEGA under Grant No. 044TUKE-4/2019 – “A small unmanned airplane - the platform for education in the area of intelligent avionics.”. The work was supported by projects: ESPOSA – “Efficient Systems and Propulsion for Small Aircraft”, funded by funded by the European commission in the seventh frame work programme under grant agreement no ACP1-GA-2011-284859-ESPOSA and APVV – Slovak Research and Development Agency under grant agreement no. DO7RP-0023-11. The work was support of research and development potential in the area of transport means with ITMS project code: 313011T557.

References

- [1] R. Andoga, L. Főző, J. Judičák, et al., “Intelligent Situational Control of Small Turbojet Engines,” *International Journal of Aerospace Engineering*, Vol. 2018, Article ID 8328792, 16 pages, 2018
- [2] G. G. Kulikov, A. Thompson, “Dynamic Modelling of Gas Turbines Identification, Simulation, Condition Monitoring and Optimal Control,” Springer, p. 337, 2004
- [3] R. Hanz, “Advanced Control of Turbofan Engines,” Springer, p. 225, 2012
- [4] G. Sanjay, “Controls and Health Management Technologies for Intelligent Aerospace Propulsion Systems,” Glenn Research Center, AIAA–2004–0949, NASA/TM—2004-212915, 2004
- [5] P. P. Walsh, P. Fletcher, "Gas Turbine Performance", ASME press, Second edition, p. 631, 2004
- [6] J. Csank et al, "Control Design for a Generic Commercial Aircraft Engine," Glenn Research Center, AIAA–2010–6629, NASA/TM—2010-216811, 2010
- [7] L. C. Jaw, J. D. Mattingly, “Aircraft Engine Controls – Design, System Analysis, and Health Monitoring, American Institute of Aeronautics and Astronautics,” Inc. Reston. Virginia, ISBN 978-1-60086-705-7, p. 361, 2009
- [8] J. K. Tar, J. F. Bitó, I. J. Rudas, “Contradiction Resolution in the Adaptive Control of Underactuated Mechanical Systems Evading the Framework of Optimal Controllers,” *Acta Polytechnica Hungarica*, Vol. 13, No. 1, 2016
- [9] R. Andoga et al., “Basic approaches in adaptive control system design for small turbo-compressor engines,” in INES 2014 IEEE 18th International Conference on Intelligent Engineering Systems, Tihany, Hungary, pp. 95-99, 2014

- [10] V. Bobál, J. Böhm, J. Fessler, J. Macháček, "Digital self-tuning controllers," Springer, ISBN 978-1-84628-041-2, p. 318, 2005
- [11] Ch. Harris, X. Hong, Q. Gan, "Adaptive Modelling, Estimation and Fusion from Data," Springer, ISBN 3-540-42686-8, p. 323, 2006
- [12] R.-E. Precup, M.-L. Tomescu, and C.-A. Dragos, "Stabilization of Rössler chaotic dynamical system using fuzzy logic control algorithm," *International Journal of General Systems*, Vol. 43, No. 5, pp. 413-433, Jul. 2014, DOI: 10.1080/03081079.2014.893299
- [13] I. D. Landay, R. Lozano, M. M'Saad, A. Karimi, "Adaptive Control Algorithms, Analysis and Applications," Series: Communications and Control Engineering, 2nd edition, XXII, 590 p. ISBN 978-0-85729-664-1, 2011
- [14] N. Bungard, "Adaptive Computing Technologies Improve Propulsion Control and Efficiency," 41st AIAA/ASME/SAE/ASEE Joint Propulsion Conference & Exhibit, Joint Propulsion Conferences, 2005
- [15] W. A. Yonke, L. A. Terrell, & L. P. Meyers, "Integrated flight/propulsion control - Adaptive engine control system mode," 21st Joint Propulsion Conference, Joint Propulsion Conferences (1985)
- [16] B. Csanadi, P. Galambos, J. K. Tar, Gy. Gyorok, A. Serester, "Revisiting Lyapunov's Technique in the Fixed Point Transformation-Based Adaptive Control," 2018 IEEE 22nd International Conference on Intelligent Engineering Systems (INES) pp. 329-334, 2018
- [17] A. L. Diesinger, "Systems of Commercial Turbofan Engines," Springer-Verlag, p. 234, 2008
- [18] L. Föző, R. Andoga, K. Beneda, and J. Kolesár, "Effect of operating point selection on non-linear experimental identification of iSTC-21v and TKT-1 small turbojet engines," *Periodica Polytechnica Transportation Engineering*, Vol. 45, No. 3, pp. 141-147, 2017
- [19] ESPOSA Project website, <http://www.pbsvb.com/about-us/esposa-project> and PBS Velká Bíteš Aircraft Engines website, <http://www.pbsvb.com/customer-industries/aerospace/aircraft-engines>
- [20] L. Föző, R. Andoga, L. Madarász, J. Kolesár, and J. Judičák, "Description of an intelligent small turbo-compressor engine with variable exhaust nozzle," in 2015 IEEE 13th International Symposium on Applied Machine Intelligence and Informatics (SAMII), pp. 22-24, Herl'any, Slovakia, 2015
- [21] R. Andoga et al, "A Digital Diagnostic System for a Small Turbojet Engine," *Acta Polytechnica Hungarica*, Vol. 10, No. 4, pp. 14, 2013
- [22] N. S. Nise, "Control Systems Engineering," Kindle Edition, pp. 944, 2015

- [23] E. Torenbeek, "Advanced Aircraft Design: Conceptual Design, Analysis and Optimization of Subsonic Civil Airplanes," First Edition. Published 2013 by John Wiley & Sons, Ltd.
- [24] H. Richter, "Advanced Control of Turbofan Engines," Springer, ISBN 978-1-4614-1170-3, p. 259, 2012
- [25] X. Wang, J. Zhao, and X. Sun, "Overshoot-free acceleration of aero-engines: an energy-based switching control method," *Control Engineering Practice*, Vol. 47, pp. 28-36, 2016
- [26] S. Jafari, P. Khalaf, M. Montazeri-Gh, "Multi-Objective Meta Heuristic Optimization Algorithm with Multi Criteria Decision Making Strategy for Aero-Engine Controller Design," *International Journal of Aerospace Sciences*, 3(1): 6-17, DOI: 10.5923/j.aerospace.20140301.02, 2014
- [27] S. Jafari, T. Nikolaidis, "Turbojet Engine Industrial Min–Max Controller Performance Improvement Using Fuzzy Norms," *Electronics*, 7, 314, 2018
- [28] J., Q. Huang, J. G. Sun "Multi Variable Adaptive Control for Turbojet Engines," *The American Society of Mechanical Engineers*, 1993
- [29] Z. Knoll, G. Tao, "Multivariable adaptive LQ control of jet engines, Multivariable adaptive LQ control of jet engines," *American Control Conference (ACC)*, 2015, 978-1-4799-8685-9, pp. 1193-1198, DOI: 10.1109/ACC.2015.7170895, 2015
- [30] R.-E. Precup, M. L. Tomescu, S. Preitl, E. M. Petriu, J. Fodor, and C. Pozna, "Stability analysis and design of a class of MIMO fuzzy control systems," *Journal of Intelligent and Fuzzy Systems*, Vol. 25, No. 1, pp. 145-155, DOI: 10.3233/IFS-2012-0621, 2013
- [31] P. Naslin, *Essentials of Optimal Control*, Boston Technical Publishers, Boston, MA, USA, 1969
- [32] R. Breda, F. Adamcik, "Aircraft Automatic Control Systems and their Control Systems," *Nase More* Vol. 61, issue. 1-2, pp. S9-S12, 2014
- [33] B. Csanadi, P. Galambos, J. Tar, Gy. Györök, A. Serester, "A Novel, Abstract Rotation-Based Fixed Point Transformation in Adaptive Control," *2018 IEEE International Conference on Systems, Man, and Cybernetics (SMC)* pp. 2577-2582, 2018
- [34] Gy. Györök, "Continuous Operation Monitoring of Electronic Circuits with Embedded Microcontroller," *IEEE 18th International Symposium on Computational Intelligence and Informatics (CINTI)*, pp. 155-160, 2018
- [35] S. Fabry, M. Ceskovic, "Aircraft gas turbine engine vibration diagnostics," *Magazine of Aviation Development* 5(4):24-28, 2017

-
- [36] B. Bulko, I. Priesol, P. Demeter, et al., "Geometric Modification of the Tundish Impact Point," *Metals* Vol. 8, Issue 11, 2018
- [37] M. Hagara, F. Trebuna, R. Hunady, et al., "Experimental identification of modal parameters of thin metal sheets by using of DIC" 5th International Conference on Modelling of Mechanical and Mechatronics Systems (MMaMS) pp. 180-188, 2012
- [38] M. Stamborska, F. Simcak, M. Kalina, et al., "Identification of the Stress Fields from the Strain Fields in the Isotropic Materials," 5th International Conference on Modelling of Mechanical and Mechatronics Systems (MMaMS) pp. 665-672, 2012
- [39] L. Föző, R. Andoga, M. Schreiner et al., "Simulation aspects of adaptive control design for small turbojet engines," in IEEE 23rd International Conference on Intelligent Engineering Systems (INES), pp., Gödöllő, Hungary, 2019
- [40] R. Andoga, L. Föző, M. Schrötter, M. Českovič, S. Szabo, R. Bréda, M. Schreiner, Intelligent Thermal Imaging-Based Diagnostics of Turbojet Engines. *Appl. Sci.* 2019, 9, 2253

Episodes of Robotics and Manufacturing Automation Achievements from the Past Decades and Vision for the Next Decade

Geza Haidegger, Imre Paniti

Institute for Computer Science and Control (SZTAKI),
Kende u. 13-17, H-1111 Budapest, Hungary
geza.haidegger@sztaki.hu, imre.paniti@sztaki.hu

Abstract: The past 3 decades are characterized by the introduction of digital tools in the manufacturing sector, and by the advent of mechatronics being used for repetitive and fast material handling within logistics. Retrospectively this time is referred as the 3rd Industrial Revolution. Presently, the cyber-physical systems and cyber-physical production systems are being referenced as substituents of the 4th Industrial Revolution. The Authors have selected some outstanding episodes within this transition time to highlight the Hungarian successful achievements developed and implemented by talented researchers and innovative ideas by far-looking professors. The article also offers elements of visions for technology development, focusing on the new results of robotics and on biotransformation in manufacturing.

Keywords: Technology Platforms; Strategic Research Agenda; Robotics

1 Introduction

The authors decided to select special, outstanding topics from the relevant time frame, from the time when technology enabled the introduction of digital mechatronic devices, controllers in the manufacturing sector, i.e. in the industrial environment, where goods and wealth are being generated. With such controllers simple mechanical devices, with one or two joints based robotic arms, 2-degrees of freedom, e.g. latch machines and early robotic pick & place mechatronics were controlled and managed rather easily. By the application of digital MSI and LSI components based control-function with digital circuits; Hungarian scientists had achieved outstanding world-level success. By the special occasion of the present conference, celebrating the 70th birthday of professor Imre Rudas, we can heartily congratulate to the pioneers of that time, and praise the professors and scientists that had given internationally approved reputation to Hungarian scientific results, while also supporting the strong educational background and teaching the next

generation of scholars in robotics. There is only a small chance to mention all the outstanding events of those decades, so it is a personal selection of outstanding experiences of the authors that is to be mentioned below.

From our point of view, the final take-home message is not just a list of episodes of the past, but also to show the presently active open topics for scientists to solve. By the present process of re-electing the delegates to the European Parliament and the EU Commissions, the issues of how to manage the science and innovation at the EU-level is being debated. Presently, Europe, and in other continents of the world, the governments are pushing and forcing the digitalization of most sectors, like manufacturing, education, governance, etc. It is widely acknowledged that the fastest ROI (return-of-investment) will come from the manufacturing and logistics sector, and the social, educational changes probably need more time in this transition. The 4th Industrial Revolution, sometimes called as re-industrialization points out the high relevance of ROBOTICS, and the need for raising robotics to significantly be a dominant contributor of modern production technology. The paper runs along the transition or evolutionary path from the 3rd towards the 4th Industrial Revolution scenario, and dares to highlight some visionary views believed to become significant within the next couple of years.

2 High Achievements at Selected Episodes of Success

2.1 Industrial Controllers Built from SSI and MSI, later on by LSI Circuit Elements

Integrated semiconductor elements as coupling 10 to 50 transistors appeared on the shops that allowed logic gates and flip-flops to be implemented as low-level digital building blocks. Those small-scale integrated circuits were soon followed by higher-functional blocks, as registers, -for medium, and later on by 1000s of transistor-operated LSI-s, as arithmetic blocks, or microprocessor, memory arrays. In the middle of the 70thies, Small Scale-, Middle Scale- and Large Scale integrated semiconductor elements were widely used for a digital logic device as controllers. The special digital module from SSI and MSI building block elements to control 2 or more axes is named as hardware interpolator. NC machines had to be driven by such digital controllers. When LSI, i.e. microprocessors had entered the market, the NC machines got a controller with far more services and features, then managing, driving the axes. A real Hungarian success story is the development of the DIALOG CNC, several embedded microprocessor-based CNC (or RoC) capable of simultaneously driving 3 or even 5 axes featured mechatronics device. During the US Carter administration, this COCOM-breaker high-tech DIALOG CNC has outperformed Siemens and Fanuc controllers, and

the US Congress had to admit, that high-tech Hungarian products could outperform American machines, and are being sold in the States.

2.2 Bit-Slice-based Graphic Displays and Fast Control Systems with a Common Architectural Base

CAD workstations and vector-graphic based displays were designed and integrated for standalone applications. Using the bit-slice computer-building semiconductor elements, extremely fast interpolators were designed, developed and produced suitable both for driving CNCs and also for driving graphic workstations.

2.3 Developing Local Network-based Controllers

The national industrial electronic companies and factories working in cooperation with university teams had achieved to come up with high-tech control devices. When machinery became more sophisticated, more complex and distributed, data-networks were needed, and novel, Hungarian solutions were developed. Exceptional networked mechatronic devices were designed and implemented. One of the most outstanding results was the transporter of fuel-cells at the Hungarian Paks atomic power plant.

2.4 High-Tech Data Networks Being Implemented as International Standard

National experiences have shown the importance of being harmonized with international technical solutions. The research target was to get involved in international standardization. Due to the lack of key Hungarian individuals having personal contact at international standards fora, and experts, we should also get more and more involved in such technical groups. The development work on industrial networking had been with top-level COCOM regulations, but international standards' development has to be focused on at the ISO- and IEEE levels. General Motors automotive company's technical manager, Mike Kaminsky became the 'father' of the MAP standard, standing for Manufacturing Automation Protocol, the software element to connect factory shop-floor general equipment independently of vendor-specific interfaces. A philosophical dilemma ever since steers debates that deterministic networking protocol (token based or Master-Slave) is needed. or in contrast, stochastic protocol (e.g. TCP/IP) is adequate to operate data-networks on industrial shop-floors. Hungarian talented researcher, mathematician and philosopher, Ferenc Brody had given proof of a solution, by defining limitation for real-time and real-life applicability. Our Institute was the first partner from the Eastern Block to establish MAP Users Group to perform

experiments and implementation of the MAP Standard's OSI-layers matching the international standard-protocol stack being developed and promoted for ISO-approval.

2.5 Hungary as a New Member in the EUREKA Initiative's Family

EUREKA is a European initiative to integrate national research activities between two or among several countries' selected partners. The focus was to eliminate parallel efforts and to teach participants on working together from different cultures, backgrounds and ecosystems. Hungary should join this group as the first country from the East. The authors were appointed to manage several such development and research projects related to factory-automation and robotics topics.

2.6 Founding the ManuFuture Technology Platform

The international EUREKA 'umbrella' team had given high-priority warning to the (EC's) EU's decision-making politicians, to counteract for saving the European manufacturing activities (firms, companies and product-designs & productions) from leaving Europe for the Far-East.

In previous publications, [1] we have given details on manufacturing-related ETPs. Probably the largest ETP was given the name ManuFuture, pointing out the very high importance of maintaining and enhancing these manufacturing activities in Europe.

2.7 The Tasks and Responsibilities of the ETP-s

ETPs are industry-led technology-oriented fora as key participants (actors) in driving innovation, knowledge transfers for European successful competitiveness [2].

"ETPs develop vision paper(s), research and innovation agendas (SRAs) and roadmaps for actions at the EU and national level to be supported by both private and public funding. They mobilize stakeholders to deliver on agreed priorities and share information across the EU. ETPs are independent and self-financing entities. They conduct their activities in a transparent manner and are open to new members. The Tasks are:

Preparing and developing a VISION document, with a time-domain of 10 or 10+ years, so that the members of that Platform can share the same view for the future, explaining it in a harmonized, detailed view.

Preparing, developing a Strategic Research and Innovation (SRA) Agenda; listing what are the missing knowledge and practice solutions building blocks, that are not yet ready, but need to be applied rather soon in order to reach the future environment vision by the end of the next 10 years.

Preparing, developing a ROADMAP, that has scenarios for possible best or worst estimates or most probable scenarios, by allocating financial support, manpower and infrastructure parameters together with the time-duration estimates.

ETPs are also responsible for establishing a close, industry – academia- and educational partnership, to have a balanced view from many different domains.” [2].

2.8 ManuFuture ETP with National Support from Member States

The European ManuFuture Technology Platform [3] has been responsible for the preparation of the Vision 2020 document, followed by the SRA in 2006, and finally deployed the ManuFuture Roadmap in 2013.

This work has given a good base for the EC offices to generate the Work program(s) for the Horizon 2020 and the 7th Framework program.

Similarly, to other EU member-countries, National versions for Vision, for SRA and for Roadmap had been prepared, translated and distributed. In Hungary, the national TP on manufacturing was hosted by GTE, the Scientific Society for Mechanical Engineers [4]. All relevant documents and their translations on national reworked versions are available for download from www.gteportal.eu.

2.9 MTA SZTAKI as Centre of Excellence in the EU Framework Programs

From FP4 until FP8 Horizon2020, MTA SZTAKI has been a high winner of EU R&D&I projects. Key topics are ICT and Factory automation.

A special title, as “EU Centre of Excellence in Computer Science and Control” was donated by the EC. Industrial digitization projects and integration of related technologies has generated a trust with industrial end-users, e.g. with robotic laser-welding, implementing Digital Factory, Digital-TWIN solutions, Industry 4.0 Use-Cases, or Robotic sheet forming with cloud-application in digital factories [5].

3 The Present Work of ManuFuture ETP

The ManuFuture ETP has remained an active group of experts for the past 15 years. The first ROADMAP was deployed in 2008, after a consensus based Vision and SRA was harmonized and disseminated. In the organization chart you will see the following: the High Level Group, the Industrial Support Group, the Industrial Advisory Group, the Mirror Group for strengthening the ETP, and for establishing PPPs as EFFRA [6].

When the ManuFuture ETP was preparing its first Vision, SRA and Roadmap, -a full decade ago- the SRA has declared Competitiveness, Sustainability and High Added Value as Innovation and Research needs, with caring for environment and resource management. The Roadmap was explained based on Figure 1.



Figure 1

The structured ROADMAP of 2008 - ©ManuFuture

From 2016, a decision was accepted by the HLG group to go forward, and repeat the activities of the ManuFuture ETP starting with a vision paper for 2030. This harmonized version has been developed and is ready for distribution as a 'Consultation Version' *ManuFuture Vision2030*, while the SRIA for 2030 is also soon to be available.

Even when the documents are freely available, there is a need to support the dissemination, and HLG members are requested to actively help getting the documents to reach the targeted readers, i.e. the decision-makers, and technology-supporters.

3.1 Vision2030: The Structure with the Content

The first chapter of the Vision2030 [7] shows the Manufacturing Industry Today, while Chapter 2 details the megatrends and drivers for manufacturing. Chapter 3 gives vision for scenarios and models for the future manufacturing processes. Vision and strategy are detailed in Chapter 4, and the Vision Building Blocks are described in Chapter 5. A short terminating chapter deals with Manufacturing & Society relevancies in the vision. The document is a contribution to political, economic, ecologic, and social orientation from a European perspective.

3.2 European Manufacturing – to Cope with Local and Global Challenges

Manufacturing is the backbone of the European economy: with 2.1 million enterprises, employing 30 million workers. The decline in Europe of added value production is disturbing, thus priority must be given to manufacturing.

Competition and cooperation both increase at a global level, and thus the complete manufacturing innovation ecosystem needs to be involved for a change.

Today, society and world economies are undergoing major changes, driving a social transformation as important as the first industrial revolution. These changes are a global phenomenon, affecting the way we live, work and behave. An unprecedented increase in the speed of development in science and technology, fast diffusion of knowledge, the scarcity of resources and a new generation of consumers will pose challenges and opportunities for manufacturing. We are facing a shift in the paradigms for global productions and services.

Figures 2. Highlight the trends and drivers foreseen for the future of European Manufacturing:

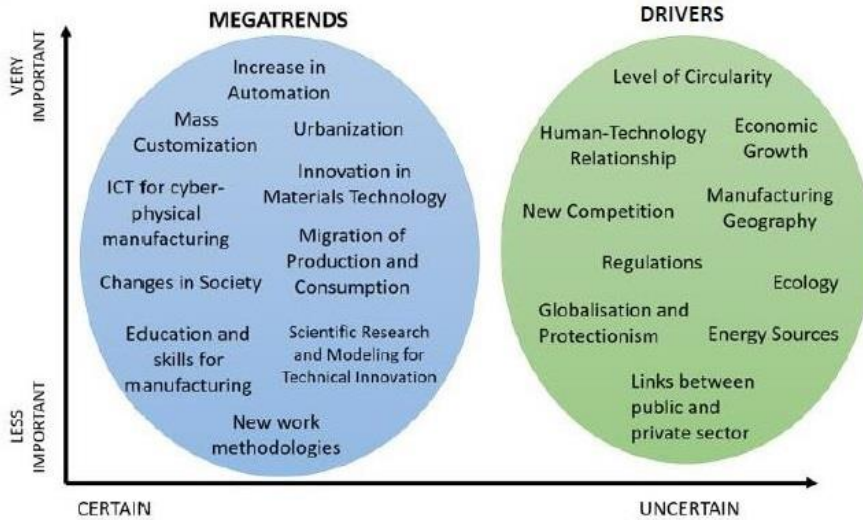


Figure 2

Megatrends and drivers by importance and certainty. ©ManuFuture

3.3 Models of Future Manufacturing Scenarios

European manufacturing will have to evolve to exceed the customer's expectations in design, quality, and service, and become even more flexible and adaptable. It must be user-centric; the customers will have a central role in value creation. **Bionic manufacturing** will enhance and augment relevant human capabilities. Nature-inspired manufacturing can lead to new frontiers. **Circular economy** is a large collaborative endeavor and manufacturing is at its core. **Education** and life-long learning will become a critical function, and the new concept of **learning factories** will offer new challenges.

MANUFUTURE ETP had a Vision with 4 scenario models for the development of value networks and manufacturing systems (see Fig. 3)

- *Globally Integrated Value Networks;
- *Regional Value Creation for Global Markets;
- *Regional Value Creation for Regional Markets;
- *Regionally Regulated Virtual Value Networks.

The entities in the Economy (factories, companies, SMEs, etc.) will probably integrate these to respond to requirements of the market, of the products, and of resource-availabilities.

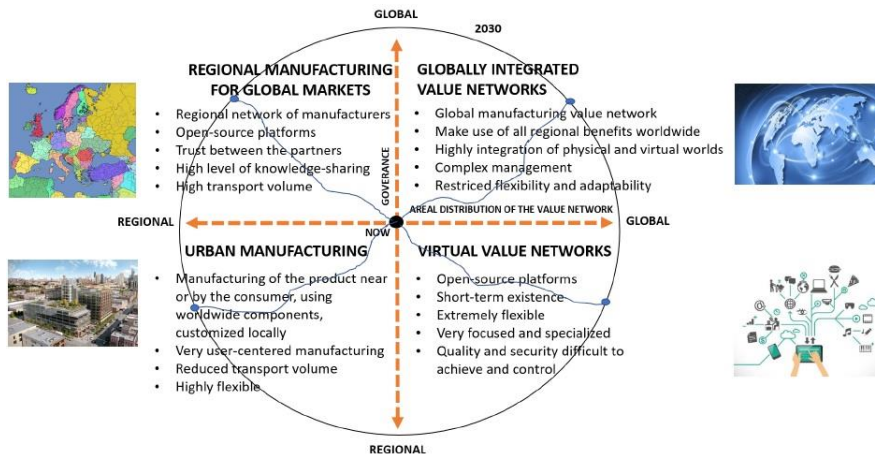


Figure 3

Scenarios for future manufacturing ©ManuFuture

4 Preparing the Strategic Research and Innovation Agenda (SRIA)

The HLG of ManuFuture is in the process of collecting the technologies in need to develop solutions for the realization of the vision mentioned in the VISION2030 documents. The working list is requested to be broadened and extended as further inputs are given and collected Europe-wide. The integration of suggested SRIA elements are being edited in the HLG by Luís Carneiro, from INESC TEC. [8]

Declared R&D&I priorities are:

- Manufacturing technology and processes;
- Digital transformation;
- Robotics and flexible automation;
- Nano-technology and new materials;
- Biological transformation of products, processes and value creation;
- Customer driven manufacturing;
- Human Centered Manufacturing;
- Agile manufacturing systems design and management;
- Circular economy, resource and energy efficiency;
- New business logics and models.

Other ETPs and also national TP-s are invited to share and harmonize these lists. We have information regarding the German National Platform, that their version has already reached a version classified as ARBRIDGED level for SRIA, by the consortium led by Stuttgart IPA. [9].

According to the Strategic Research Agenda (SRA) for Robotics in Europe two trends will demonstrate the impact of robotics technology and the importance of investments:

- 1) "Technologies traditionally associated with the service robotics sector will migrate into industrial automation yielding smarter robots and open up new markets."
- 2) "The maturing of navigation, localization, sensing and motion control technologies will enable economically viable service applications."

However, SRIA from both the ManuFuture and other ETPs, like BigData Value Association (GBVA), euRobotics, etc., jointly declare, that AI: Artificial Intelligence technology research will dominate future achievements globally.

The vision and plan is to generate, create a connected EU-wide Artificial Intelligence Ecosystem. The national governments are suggested to give high priority to support local and regional, furthermore EU-wide R&D&I actions to give a European boost for AI-based research results.

4.1 Robotics

The Hungarian Robotic MRTT Society was founded 40 years ago, and key individuals like Prof Imre Rudas set up robotic labs with special application areas, and initiated a robotics laboratory commemorating Prof. Antal Bejczy, a world-famous (CALTEC and NASA JPL) robotics expert with Hungarian origin and long-term supporter of the Hungarian education in robotics. [IROB]. Between 2012 -2017, this excellent robotic center had published 320+ scientific papers. Several scientists and lecturers had the chance to carry out experiments and gain degrees. An excellent example of interdisciplinary topics from intelligent robotics is on Teleoperation [10], and for AI, Deep Learning a Tutorial Survey should be high-lighted [11].

AUTOMATICA, the largest European Robotic event bi-yearly in Munich, had presented a survey by statistics to prove that where robots are installed in manufacturing, **more jobs are opened or created then lost**. We had also learnt there the "**Robotics LAW for 3D**". Wherever jobs are **DANGEROUS, DULL** or **DIFFICULT** for humans, it is a European ethic, to apply robots, and never humans.

Robotic & flexible automation research, innovation topics are envisaged on: Task-based Programming of Robots (including Cobots); Intrinsically Safe Robots;

Soft Robots; Cognitive and Smart Robots; Mobile Manipulators for Logistics; Robot Swarms; Drones for Manufacturing; Robot Machine Tools; Shared Autonomy in Manufacturing – Cobots – Cooperative Manipulation; Robot Skill Acquisition; Augmenting the Human; Reference Architectures, Digital Twins, Trust & Security, Navigation; Applications in Health Care, in Agriculture, in Construction. G. Z. Yang et al. [12] identified 10 grand challenges in Robotics that could have major impact in the next 5 to 10 years.

Those are: New Materials and Fabrication Schemes; Bioinspired and Bio-Hybrid Robots; Power and Energy; Robot Swarms; Navigation and Exploration; AI for Robotics; Brain-Computer Interfaces; Social Interaction; Robot Ethics and Security.

In the following section each topic is addressed in the light of Industrial Robotics.

4.1.1 New Materials and Fabrication Schemes

This area is touched by Soft Robotics and new fabrication methods including integrated sensors for adaptive control. Unfortunately, the mass production of the latter is still not solved.

4.1.2 Bioinspired and Bio-Hybrid Robots

As already mentioned Soft Robotics is one of the focus fields in robotics which includes designs from nature. Festo [13] is one of the pioneers in this topic who successfully developed Bioinspired Grippers and Manipulators for the industry. However, the spread of these products on the market is another question.

4.1.3 Power and Energy

While AGVs are becoming a part of everyday life in shop floors, Energy storage is meant to be a major bottleneck for mobile robotics. We are still looking forward to fundamental changes in the battery technology to reduce energy consumption to a sustainable level.

4.1.4 Robot Swarms

Flexible Robotics is an R&D topic for several years and the results are manifested in Lightweight Robot Control Enhancements. Mobile platforms with Lightweight Robot Arms are just now becoming a trend in the industry, but using them in small swarms is still a new research field.

4.1.5 Navigation and Exploration

Typical Use Cases for Robots is exploring places where human presence is dangerous like disaster zones, the deep sea or the space.

Industrial environments might change during production but those changes can be planned and digitally documented or traced by current sensors.

4.1.6 AI for Robotics

AI is indeed a revolutionary key to put Manufacturing Automation on a new path, including deep learning and model-based reasoning.

Current steps in the financing of AI & Robotics show that it is an important research field across the Globe. European investigations from two associations - Big Data Value Association (BDVA) and European Robotics Association (euRobotics) - are manifested in the Joint Vision Paper for an Artificial Intelligence Public Private Partnership [14]. "The Vision of the AI Public Private Partnership is to boost European industrial competitiveness and lead the world in developing and deploying value-driven trustworthy AI based on European fundamental rights, principles and values." [14]

4.1.7 Brain-Computer Interfaces (BCIs)

Developments to interact directly - through our brain - with the control of actuators seem to be essential in robotic prosthetics. Some people think that BCIs are needed to compete or at least have a chance against AI in the future. However, it might be a dangerous field to mix human brain activity with Artificial Intelligence.

4.1.8 Social Interaction

At first it may seem that Social Interaction is only a topic for Social Robotics, but it could be important also for Collaborative Robotics use cases. Some AGVs at shop floor level are already equipped with visual communication possibilities [15] to interact with humans (beam their trajectory on the floor).

4.1.9 Medical Robotics

To use Industrial Robots in the rehabilitation process and help stroke patients when restoring human activities of daily living is quite new. Some repetitive movements in the rehabilitation process can be tiring for the specialists, so there is a need for robotization. E.g. in a bilateral research project a robot therapeutic system has been clinically tested on 20 spastic hemiparetic post-stroke subjects [16]. Maybe some other medical fields can be covered with Cobots too, where special medical robots can be substituted.

4.1.10 Robot Ethics and Security

In the Manufacturing Industry the topic "Robotics and Ethics" is only engaged in when a robot-based vision system is integrated with an AI system. In terms of Security the challenges are more general and according to G. Z. Yang et al. [12] can be divided into two groups by looking at the IT infrastructure.

The first is "escalation" where Robotics and AI might refine strategies and launch more aggressive counter operations.

The second is "lack of control". "Pervasive distribution, multiple interactions, and fast-paced execution will make control of AI systems progressively less effective while increasing the risks for unforeseen consequences and errors." [12]

4.2 Biological Transformation of Products, Processes

The bio-transformation can be discussed in 3 layers:

- Bio-inspired manufacturing, "INSPIRATION";
- -Bio-integrated manufacturing "INTEGRATION"; and
- -Bio-intelligent manufacturing INTERACTION layer.

Biological transformation, [17], [18] and [9] shows that value in bio-intelligence will be either decentralized or personalized, or both. It will happen by seamless fusion among ICT, bio-, AI, robotics, etc. technologies or techniques. Selected research priorities are [19]: Bio-inspired structures, sensors, actuators, additive manufacture of bio-based materials, enzymatic processes, micro-bioreactors, smart bio-manufacturing devices, bio-packaging, ecology-based manufacturing, bio-refineries, as shown in Figure 4.

By the valuable "Industry 4.0" processes in getting the industry digitized, the acquisition and generating plus the storing of data and production-related information in huge data-centers and clouds can easily be obtained.

The studying of the living environment brings us closer to understand our environment and ecosystem. [20], [21], [22]. By understanding the processes, we might be able to influence and make production technology more efficient. The German Ministry had realized early the potentials of the biological transformation, and initiated a country-wide BIO-TRAIN [19] project to see a clear picture of challenges and opportunities, as Fig. 4 and Fig. 5 explain.

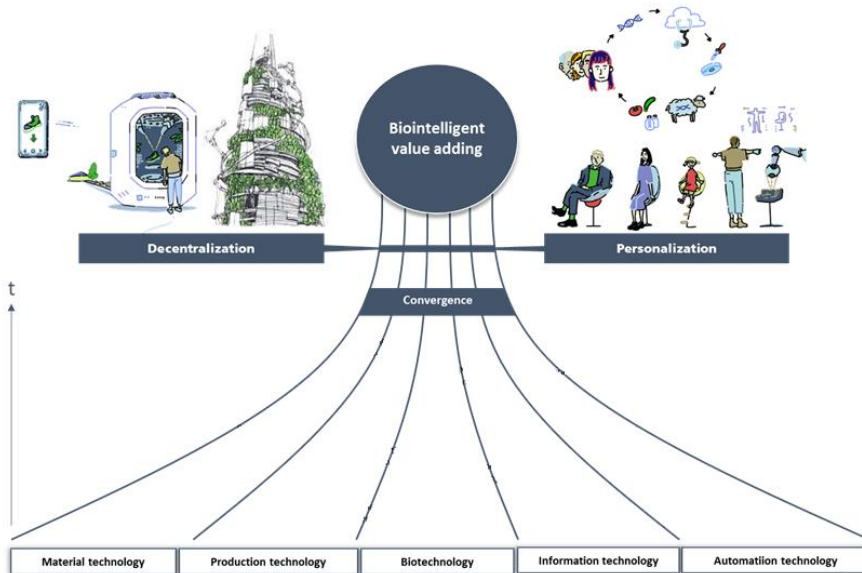


Figure 4

Integration process for Bio-transformation of products, processes ©IPA

Different aspects of the Biological Transformation

	Materials	Structures	Processes
Substitution	Fuels and chemicals from wood-waste and straw Isobutene production without fossil fuels 	Metallic foam Highly porous lightweight material modeled after bones 	Bio-based plastics plastics, additives and compounds with optimal recyclability 
Adaption	Biomanufacturing of silk proteins Industrial scale silk protein production the lab 	Bio-inspired machines Stress oriented structural design with carbon fibers inspired from trees 	Self healing materials Transfer of the self-healing properties of plants to technical materials 
Abstraction	Programmable materials Targeted adaptation of materials to environmental changes 	Artificial Neural Nets Neuro-inspired algorithms with learning capabilities 	Swarm logistics Transfer of swarm-intelligence to logistics systems 
Fusion	Living cells on microchips Toxicity-testing with living cells on physical transducers 	Theranostic implants Medical devices in symbiosis between technology and organism 	Brain Computer Interfacing Communication between biology and technology 

Figure 5

Biological transformations, BIO-TRAIN [19] project ©IPA

4.3 The Integration of Manufacturing and Food-Processing Technologies for Products and Processes

In several EU countries, the governments have declared the food-processing industry at a high-priority level. With the promises of the low-hanging fruits, fast ROI can be realized by applying robotics and ICT solutions which have been tested and verified in other industrial (automotive) sectors.

ManuFuture SRIA 2030 has selected the following actions and topics to address in the food industry [23]:

- Developing concepts and demonstration projects on the application of advanced manufacturing systems and industry 4.0 in the food factory, particularly in food processing.
- Establishing pilot plant/living lab facilities where food industry applications of advanced manufacturing solutions, systems, mechatronics, robotics, industry 4.0 solutions can be tested.
- To develop new business models to make the access of food businesses, particularly SMEs to new machinery, equipment, manufacturing systems easier, to reduce the limitations represented by the cost of investment.
- Establishing a systematic and regular dialogue between the manufacturing and food production, processing communities to enhance better mutual understanding and joint activities.
- Developing training and education programs to enable the adoption of Industry4.0 in the food industry.
- Exploring the opportunities for fostering innovations and entrepreneurship by transdisciplinary collaborations.
- Flexible, efficient, sustainable production of customised food products at costs approaching those of mass production, to meet the diverse and rapidly changing needs of customers and consumers.
- Reduction of unnecessary costs in food processing and supplying through efficient use of resources.
- Reduction of the environmental impact of food processing and packaging.
- More reliable food safety and hygiene and more uniform food quality through better process control and more efficient detection and removal of foreign bodies and other contaminations through smart sensor systems and robotics.
- Simulation, better design and optimisation of food manufacturing and supply processes and plants using concepts such as ‘digital twins’.

- Identification of the jobs, activities and their limitations and constraints which can be automated and robotised leading to the reduction of shortage of labour force, increasing the efficiency of controls, and improved analyses of data and trends.
- More efficient maintenance, prevention of breakdowns, reduction of the down time.

5 Summary

The authors' aim was to salute the pioneers of robotics and mechatronics in Hungary, in correlation to the 70th birthday of Prof. Imre Rudas, as he is one of the key fathers of Hungarian robotics. We highlighted selected episodes, where we are proud to have reached high results. Analyzing the present trends, we have referenced the VISION2030 scientific document, and have listed the presently available list of required research-innovation- topics, the SRIA. Special details were given for the future of robotics, and on the emerging prospect of digitizing the biological transformation of manufacturing. Learning from the living ecosystems of animals and plants, will mankind learn from them, how to eliminate wastes, live with reduced energy and material consumptions, care for the future for resources? It is a great task and challenge for the upcoming generation of researchers to pave the way for the manufacturing industries to serve the growing needs of humanity in healthy food and consumer product for higher living standards, while also caring for long-term ecological stability, sustainability, e.g. in a visional circular economy.

Acknowledgement

The authors declare that the VISION for European Manufacturing 2030 document is written and edited by the ManuFuture ETP HLG group members –, and this paper is just an appetizer to read the full documents. The SRIA working documents is also an open-access presentation within the ManuFuture HLG. The research in this paper was (partially) thankfully supported by the European Commission through the H2020 project EPIC (<https://www.centre-epic.eu/>) under grant No. 739592. This research has also been supported by the GINOP-2.3.2-15-2016-00002 grant on an "Industry 4.0 research and innovation centre of excellence". The research area for the futures, like the biological and robotic areas are acknowledged to be offered by IPA experts listed in the references, but additionally being supported by key scientists Prof. Dr. Ing. Thomas Bauernhansel, head of IPA, Dr. Marion Früchtel, Dr. Günther Hörcher, Dr. Ing. Robert Miede, members of the HLG of ManuFuture ETP.

References

- [1] G. Haidegger, Evolution of technology and users' requirements of factory communication systems from the 3rd to the 4th Industrial Revolution. In: IEEE 2nd International Conference on Telecommunication and Networks, TEL-NET 2017. Noida (Uttar Pradesh), India, 2017.08.10-11. IEEE, 2017, pp. 1-6
- [2] ETP; <https://ec.europa.eu/research/innovation-union/index.cfm?pg=etp>, last visited: 21.10.2019
- [3] ManuFuture ETP; <http://www.manufuture.org/>, last visited: 21.10.2019
- [4] GTE; <http://www.gteportal.eu>, last visited: 21.10.2019
- [5] Paniti I. Adaptation of Incremental Sheet Forming into cloud manufacturing. CIRP Journal of Manufacturing Science and Technology. 2014 Jan 1;7(3):185-90
- [6] EFFRA, European Factories of the Future Research Association; <https://www.effra.eu/>, last visited: 21.10.2019
- [7] HLG: MANUFUTURE –VISION 2030, consultation version, Competitive, sustainable and resilient European manufacturing, Digital ISBN:978-989-95853-7-9, December 2018
- [8] Luis Carneiro, INESC TEC, ManuFuture 2030, SRIA, presentation at the HLG Meeting 18-03-2019, www.manufuture.org, last visited: 21.10.2019
- [9] Günter Hörcher, Markus Bessner, Thomas Bauernhansl, IPA: SRIA, <http://www.ipa.fraunhofer.de/studien>, last visited: 21.10.2019
- [10] L. Marton, Z. Szanto, T. Haidegger, P. Galambos, and J. Kovacs, "Internet - based Bilateral Teleoperation Using a Revised Time-Domain Passivity Controller," Acta Polytechnica Hungarica, Vol. 14. No. 8. pp. 27-45, 2017
- [11] Károly, Artúr István, Róbert Fullér, and Péter Galambos. "Unsupervised Clustering for Deep Learning: A tutorial survey." Acta Polytechnica Hungarica, Vol. 15, No. 8 (2018): 29-53
- [12] Yang, G. Z., Bellingham, J., Dupont, P. E., Fischer, P., Floridi, L., Full, R., Jacobstein, N., Kumar, V., McNutt, M., Merrifield, R. and Nelson, B. J., 2018, The grand challenges of Science Robotics. Science Robotics, 3(14), p. 7650
- [13] <http://www.festo.com>, last visited: 21.10.2019
- [14] https://www.eu-robotics.net/cms/upload/downloads/VISION_AI-PPP_euRobotics-BDVA-Final.pdf, last visited: 21.10.2019

-
- [15] Chadalavada, R. T., Andreasson, H., Krug, R., & Lilienthal, A. (2016) Empirical evaluation of human trust in an expressive mobile robot. In RSS Workshop "Social Trust in Autonomous Robots 2016", June 19, 2016
- [16] <http://cosmosys.mm.bme.hu/sinhungindex.html>, last visited: 21.10.2019
- [17] Marion Früchtl, Biological Transformation in Manufacturing, ManuFuture HLG, Meeting Milano 08.11.2018.BIO
- [18] Robert Mieke, BIOINTELLIGENT VALUE ADDING; ManuFuture HLG Jubilee Conference, Milan 2018, November 8, www.Manufuture.org, last visited: 21.10.2019
- [19] Bauernhansl, T; Brecher, C; DROSSEL, W; Gumbsch, P; HOMPEL, M; Wolperdinger, M.: Biointelligence – A New Perspective for Sustainable Industrial Value Adding – Results of the Biological Transformation Preliminary Study on the Biological Transformation of Industrial Value Adding (BIOTRAIN) (Biointelligenz – Eine neue Perspektive für nachhaltige industrielle Wertschöpfung – Ergebnisse der Voruntersuchung zur Biologischen Transformation zur Biologischen Transformation der industriellen Wertschöpfung (BIOTRAIN)). Aachen, Dortmund, Dresden, Freiburg, Stuttgart, 2019, Fraunhofer-Verlag
- [20] Mieke R, Bauernhansl R, Schwarz O, Traube A, Lorenzoni A, Waltersmann L, Full J, Horbelt J, Sauer A. The biological transformation of the manufacturing industry - Envisioning biointelligent value adding. *Procedia CIRP*, 72, 2018, pp. 739-743
- [21] Mieke, R; Full, J; Sauer, A: Biointelligence in the product and in the production (Biointelligenz im Produkt und in der Produktion). In: Rieg F: *Handbook of Construction (Handbuch Konstruktion)* Munich: Hanser; 2018, pp. 621-634
- [22] Gerald Byrne, Dimitri Dimitrov, Laszló Monostori, et al.: Biologicalisation: Biological transformation in manufacturing, *CIRP Journal of Manufacturing Science and Technology*, 21 (2018), pp. 1-32
- [23] José Carlos Caldeira: MANUFUTURE Visison 2030 and Strategic Research and Innovation Agenda; Competitive Cooperation in Smart Specialization on the Modernization of the Food Industry Workshop, A platform for trans-sectorial collaboration 19.09.2019, Budapest University of Technology and Economics

Crime “Hot-Spots” Identification and Analysis in Hungary by Computational Intelligence

László T. Kóczy^{1,2}, Gábor Kovács³, Péter Földesi⁴, Szilvia Nagy⁵, Boldizsár Túú-Szabó², Gergő Fogarasi² [0000-0002-1854-2583]

¹ Budapest University of Technology and Economics, Department of Telecommunications and Media Informatics
Műegyetem rkp. 3, 1111 Budapest, Hungary
E-mail: koczy@tmit.bme.hu

² Széchenyi István University, Department of Information Technology
Egyetem tér 1, 9026 Győr, Hungary
E-mail: {koczy, tuu.szabo.boldizsar, fogarasi.gergo}@sze.hu

³ Széchenyi István University, Department of Criminal Sciences
Egyetem tér 1, 9026 Győr, Hungary
E-mail: gkovacs@sze.hu

⁴ Széchenyi István University, Department of Logistics and Forwarding
Egyetem tér 1, 9026 Győr, Hungary
E-mail: foldesi@sze.hu

⁵ Széchenyi István University, Department of Telecommunications
Egyetem tér 1, 9026 Győr, Hungary
E-mail: nagysz@rs1.sze.hu

Abstract: In the constantly growing and widening field of forensic science, crime maps are used in versatile ways. The representation of the data and analysis could offer some steps toward crime prevention and helps understand patterns, in terms of a timely distribution of crime types. Clustering is able to help identify criminal hot-spots and additional analysis may determine which areas require intervention. The aim of this study is to present an analysis of criminal information related to Hungary, in annual and monthly breakdown.

Keywords: clustering; Fuzzy C-Means; crime hot-spots; forensic science; crime prevention

1 Introduction

Computational intelligence (CI) methods are up-to-date IT approaches dealing with:

- Very complex problems
- Non-deterministic problems
- Uncertainty (not only Bayesian)

CI includes fuzzy systems [1] (applied in this study), evolutionary computation, and artificial neural networks.

The goal of this study is the identification and analysis of criminal hotspots (where far more crime cases happened than elsewhere, in a given area) in order to improve crime prevention, using CI methods.

To reach this goal the following steps will be carried out:

- Choose several types of crime, for detailed analysis
- Gather the related criminal data in a monthly breakdown
- Choose a (fuzzy) clustering method, for identification of geographic areas with similar patterns
- Generate (fuzzy) clusters
- Generate Dynamic maps, presenting their clusters
- Develop a Time series analysis and evolution

Considering certain types of crime in Hungary having a very low occurrence and so it is not possible to analyse them (for example car break-in). **Bodily harm** and **burglary** have been chosen for further investigation.

Pre-stat is a criminal database which was used to gather the required input data [2].

2 Preceding Research

As the initial step in the current study, in the earlier phase of this research, certain annual data for the years between 2010 and 2017 were used. The data have been graphically represented in 2D and 3D formats to show extreme areas, trends and predictable future tendencies. We attempted to interpret the charts and recorded the appropriate conclusions in a structured way. These new results were presented verbally at some conferences and published in a conference article [2].

The continuation of this research (published in the present paper), monthly breakdowns were used instead of the annual data, and a more sophisticated analysis has done, and so it would be possible to draw more in-depth conclusions and deepen the understanding of the phenomena.

3 The Public Administration Structure of Hungary

Hungary is divided into 7 regions, which include 19 Counties (in Hungarian: megye) and the capital (főváros), Budapest, as shown on Fig. 1, with the highlighted town of Győr, where this study was performed.

Counties are divided into 197 districts (járás):

- 174 within the Counties (járás)
- 23 in Budapest (kerület) – as shown on Fig. 2, with roman numbers
- Additionally, 23 individual towns are considered as districts

In this study, these 197 districts are considered single (homogenous) units.

Inside the districts, there are 322 towns, among them 23 cities with county rights. 126 "large municipalities" (város) among them and 2683 other municipalities (község) [2].



Figure 1

Public administration structure of Hungary

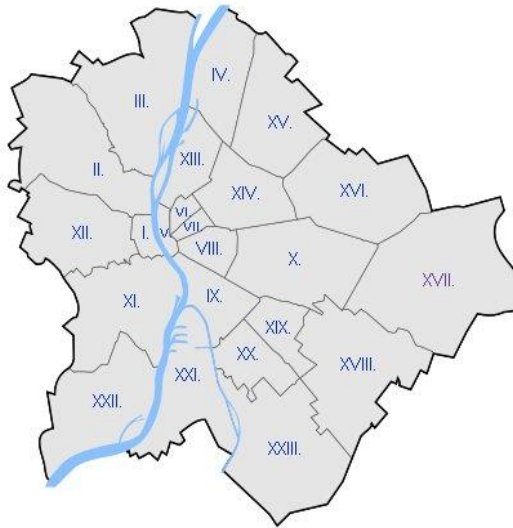


Figure 2

23 districts which are located in Budapest (in Hungarian: kerület)

4 Pre-Stat, the Structure of the Gathered Data

As mentioned above, Pre-Stat (available on <https://prestat.lechnerkozpont.hu/bunmegelozes/> for Hungarian citizens) is an interactive map of Hungarian crime data with database export features. Pre-Stat is not only for downloading databases, but it also provides generated maps as it can be seen on Fig. 3 as an example (for the given period and crime type, green means small number of cases, while red means high intensity of crime). It may be considered as a good example for an interactive up-to-date crime map system. The following data were downloaded from the Pre-Stat website for the two crime types mentioned (**bodily harm** and **burglary**, which were chosen for further investigation):

- Average criminal acts per 100,000 inhabitants, between 2010 and 2017 for 197 districts, in an annual breakdown
- Average criminal acts per 100,000 inhabitants, between 2013 and 2017 for 197 districts, in a monthly breakdown

Each district is represented with the coordinates of its seat on the related maps [2].

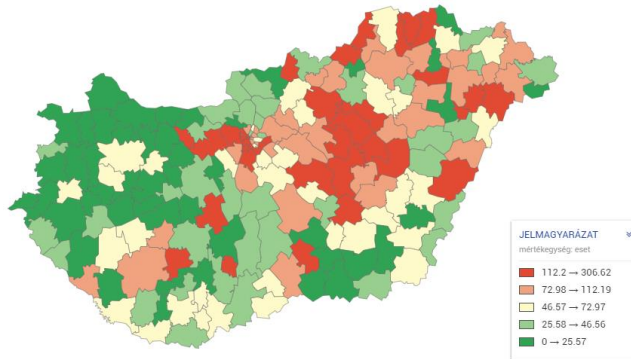


Figure 3
Sample image for Pre-Stat

5 Clustering Methods

5.1 The Aim of Using a Clustering Approach in this Study

The aim of this work is to determine the "crime hot-spots" consisting of several districts which are areas on the map with crime intensity of various levels. The crime hotspot detection and analysis can help with the decision making of the police to suggest where police actions need to be focused. Time series analysis can also help with the allocation strategy of a police force, by showing and predicting the tendencies of crime intensity [2].

5.2 Clustering in General

Clustering is an essential data mining tool that aims to discover inherent cluster structure in data [2] [3]. Its aim is to form clusters of objects (patterns), so that similar objects are grouped into the same clusters and different objects are grouped into different clusters [2] [4]. There are several methods known for clustering into vague clusters (with uncertain, maybe, overlapping borderlines), among various advantages and disadvantages [2].

5.3 Fuzzy C-Means Clustering (FCM)

The FCM algorithm is a clustering method which allows one instance of data to belong to two or more clusters with different degrees of membership. It is based on a clustering algorithm developed by Dunn [5] and later “fuzzified” and improved by Bezdek [6]. It can be used when the required number of clusters is known (is pre-determined). In each iteration of the FCM algorithm, the following objective function J is minimized: [2]

$$J = \sum_{i=1}^N \sum_{j=1}^C \mu_{ij} \|x_i - c_j\|^2 \quad (1)$$

For a given data point x_i , the degree of its membership to cluster j is calculated as follows:

$$\mu_{ij} = \frac{1}{\sum_{k=1}^C \left(\frac{\|x_i - c_j\|}{\|x_i - c_k\|} \right)^{\frac{2}{m-1}}} \quad (2)$$

where, m is the “fuzziness coefficient” and the center vector c_j is calculated as follows:

$$c_j = \frac{\sum_{i=1}^N \mu_{ij}^m \cdot x_i}{\sum_{i=1}^N \mu_{ij}^m} \quad (3)$$

5.4 Generating Clusters by the FCM Method

As mentioned in this work, the FCM algorithm was used for creating clusters. The coordinates of the seats of the districts and the corresponding crime intensities served as an input of the algorithm. The number of clusters was chosen to be 30, based on expert estimation. (Experiments with less and more clusters lead to less interpretable results while choosing 30 was lead to present the best results.)

Because of presence of fuzzy clusters, technically, every district is included in every cluster, but with various (seatings low) membership degrees. For assigning a given district to a primary cluster, the cluster with the highest membership value has chosen.

If two districts were geographically close to each other, and if the number of crime acts were similar, they were merged into the same cluster.

For generating clusters by the FCM algorithm the corresponding Matlab toolbar was used [2]. Using this technique, crime hot-spots will appear, their position are formed and determined.

6 Generating Crime Maps

2D and 3D crime-maps were generated visualizing the clusters and the crime intensities [2].

In the 2D maps the centres of the clusters are marked and the average crime act values within the clusters are indicated. Based on these maps, we propose, that in the districts belonging to clusters with high criminal act numbers, further police intervention is necessary, and that very unpredictable behavior of a cluster needs deeper investigation and possibly additional intervention [2].

The 3D crime maps show the problematic regions with high crime intensity [2] (see Figs. 8-13).

To summarize, the following crime maps were prepared (272 in total):

- Average criminal acts per 100,000 inhabitants, between 2010 and 2017 for 197 districts, in annual breakdown, **burglary**, 8 pieces of 2D maps
- Average criminal acts per 100,000 inhabitants, between 2010 and 2017 for 197 districts, in annual breakdown, **bodily harm**, 8 pieces of 2D maps
- Average criminal acts per 100,000 inhabitants, between 2010 and 2017 for 197 districts, in annual breakdown, **burglary**, 8 pieces of 3D maps
- Average criminal acts per 100,000 inhabitants, between 2010 and 2017 for 197 districts, in annual breakdown, **bodily harm**, 8 pieces of 3D maps
- Average criminal acts per 100,000 inhabitants, between 2013 and 2017 for 197 districts, in monthly breakdown, **burglary**, 60 pieces of 2D maps
- Average criminal acts per 100,000 inhabitants, between 2013 and 2017 for 197 districts, in monthly breakdown, **bodily harm**, 60 pieces of 2D maps
- Average criminal acts per 100,000 inhabitants, between 2013 and 2017 for 197 districts, in monthly breakdown, **burglary**, 60 pieces of 3D maps
- Average criminal acts per 100,000 inhabitants, between 2013 and 2017 for 197 districts, in monthly breakdown, **bodily harm**, 60 pieces of 3D maps

Figs. 4-13 are presenting visualized data for each counties. The counties are represented with dots, and the colours are showing which dots are in the same cluster (Figs. 4-7), or the crime intensity (Figs. 8-13). These dots together are forming the recognizable shape of Hungary, so the axes can be matched with geographical coordinates. However, the geographical location of the country is irrelevant, therefore, they are not better marked.

6.1 2D Maps

In total, 136 pieces of 2D maps were generated for each year between 2010 and 2017, for each month between 2013 and 2017, and for the previously mentioned two crime types. Then the crime intensities of the clusters were calculated. The clusters with high membership values indicate high risk areas. The centers of the clusters in the maps are marked with an "X" (see Figs. 4-7) [2].

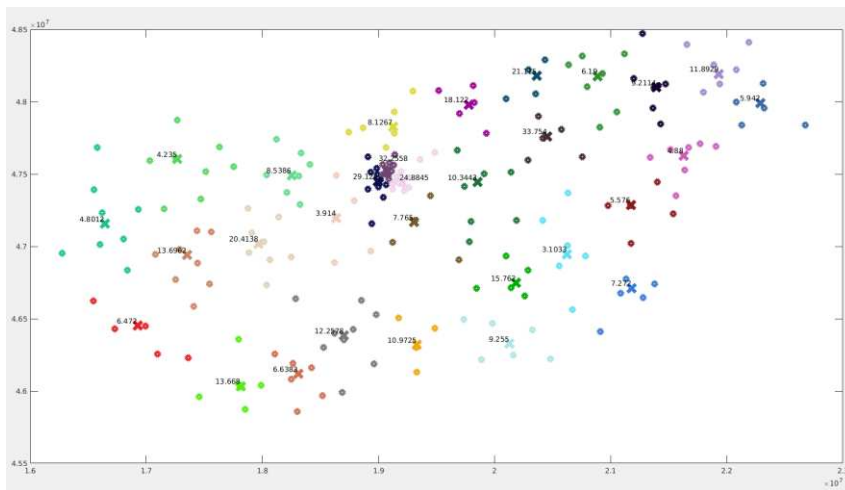


Figure 4
2D map of the burglary in January of 2013

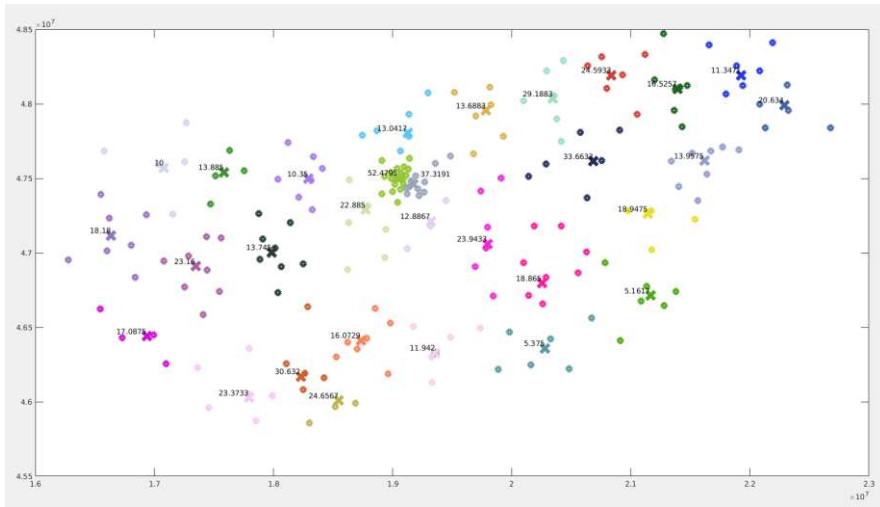


Figure 7
2D map of the burglary in March of 2013

6.2 3D Maps

Comparing the 3D maps of **bodily harm** in 2010 and 2017 (Figs. 8 and 9, show crime intensities) it can be concluded the crime prevention strategy in the North-Eastern region of Hungary is successful, however it still remained the most dangerous region in terms of **bodily harm** [2].

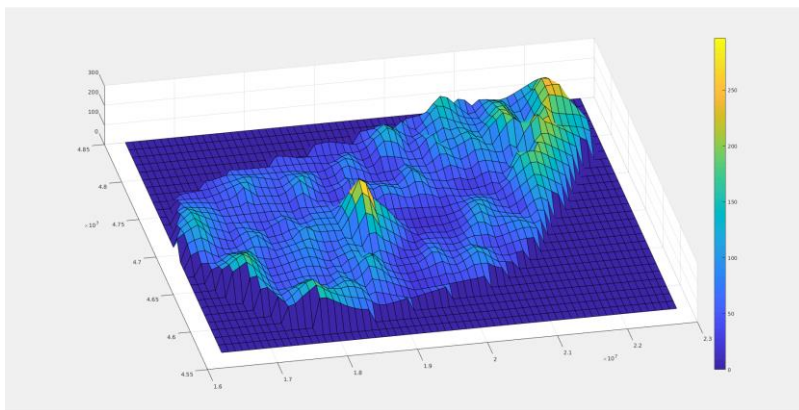


Figure 8
3D map of the bodily harm in 2010

In the early 2010 year, Budapest and its surroundings showed the highest **burglary** crime rate, but because of its decreasing tendency nowadays North-Eastern region of Hungary has the highest intensity (Figs. 8 and 9) [2].

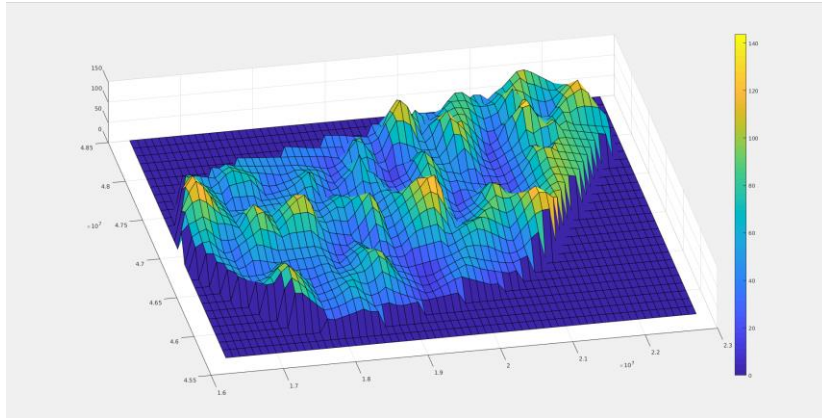


Figure 9
3D map of the bodily harm in 2017

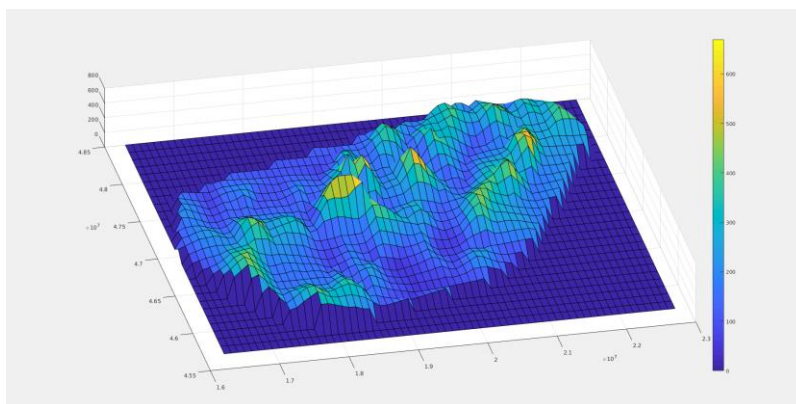


Figure 10
3D map of the burglary in 2011

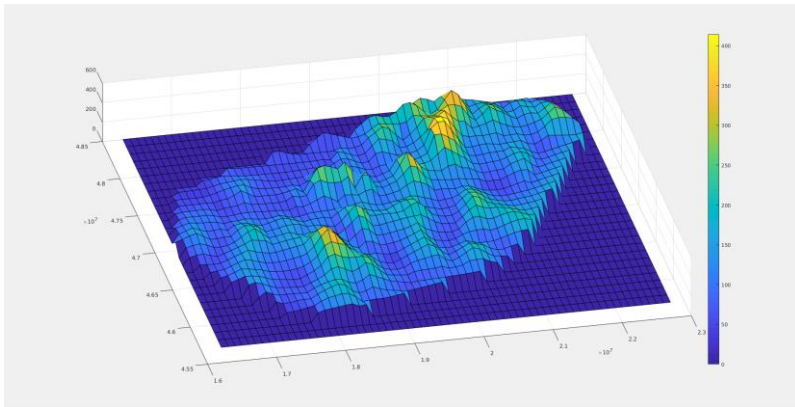


Figure 11
3D map of the burglary in 2017

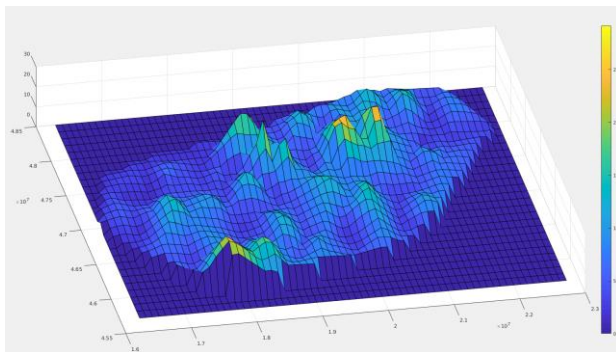


Figure 12
3D map of the burglary in November of 2014

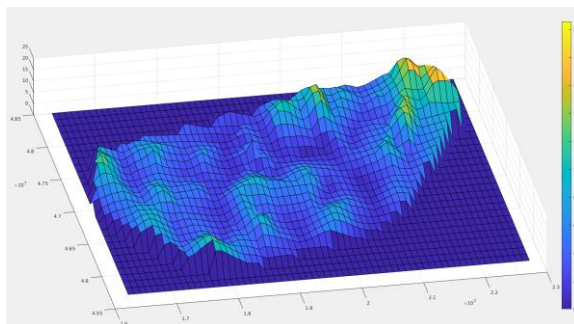


Figure 13
3D map of the bodily harm in February of 2014

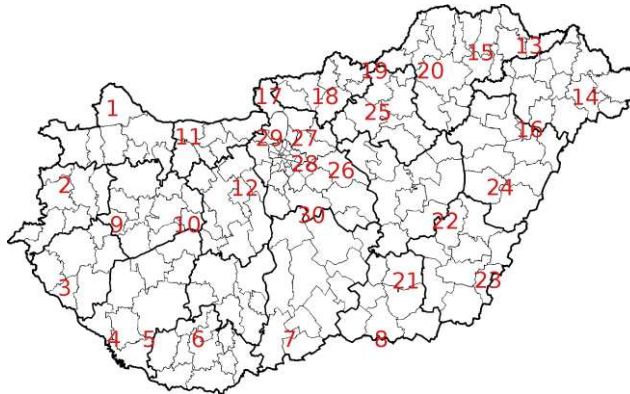


Figure 15

Bodily harm (time independent) clusters labeled by numbers

Figs. 14 and 15 show the labelled clusters for **burglary** and for **bodily harm**. The areas and the centres of these clusters are changing year to year, but not so extremely, so it is possible to identify more or less matching clusters in time. Using these numbered maps, it was possible to create a time series. It means, that the data for every available years was gathered into table form, using Figs. 14-15 helps to decide which actual annual cluster belongs to which general cluster, so where to put the data inside of the table. The result is presenting data rows for clusters on Figs. 14-15, for the entire time period which was examined. Using this, it is possible to draw as many charts as there are clusters on Figs. 14-15, for each crime types.

7.1 Burglary

Fig. 16 shows the changes of **burglary** crime intensity of the clusters in time. Most of the clusters indicate decreasing tendency or stagnation. However, cluster #19 presents randomly behavior with unexpected high values alternating with lower crime rates. Here, further detailed analysis is necessary [2].

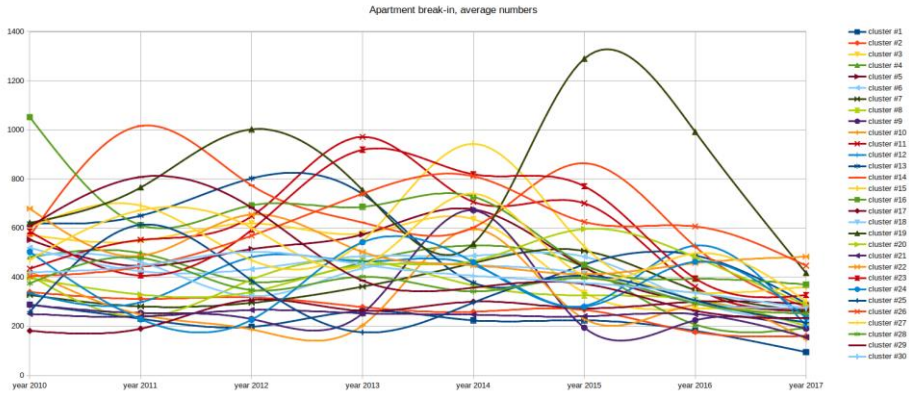


Figure 16
Time series of the burglary (2010-2017)

7.2 Bodily Harm

Similarly to **burglary** most of the clusters show decreasing tendency of **bodily harm**. There are also some clusters with random behavior (Fig. 17) [2].

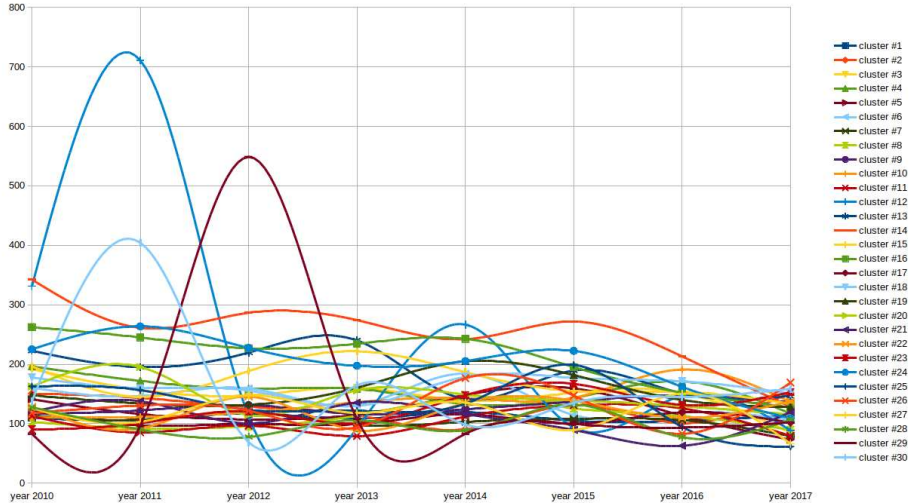


Figure 17
Time series of the bodily harm (2010-2017)

8 Further Technical Tools and Goals Suggested for the Future Research

In the preceeding work [2] of this research some initial steps were made in the field of crime map generation and its analization using the rough preprocessing of the collected data.

Then, the research was continued, using much more precise data, which made it possible to draw even further, more precise conclusions.

Fuzzy clusters help identify approximate areas of similar behavior, and thus suggest further police intervention (or lack of further investigation) areas/districts – independently, from the public administration borders. The time dependent behavior of these clusters reveal tendencies, and suggest further aspects of intervention. These tendencies and changes should be matched with historical data on past interventions and connections must be searched. Very irregular behavior may indicate unknown effects in the area and needs deeper analysis [2].

In the future research, instead of using districts in Hungary, towns, zip codes or even GPS coordinates could be used to reach more precise results.

A possible improvement could be to use the [7] DBMEA evolutionary-memetic algorithm or [8] the Gath-Geva method (instead of Fuzzy C-Means – FCM [12]) to produce more precise clusters.

Smoothing and filtering the data would be possible using [9] wavelet transform (which was first used and mentioned by A. Haar in his article about the Theory of Orthogonal Function Systems in 1910 [10] [11]).

The time series analysis part of the research could apply the traditional (statistical) Box-Jenkins method (named after G. Box and G. Jenkins) or other methodologies [2].

Considering more types of crime would make the study more comprehensive and useful, while proving cross-correlation between types of crime could help even more in crime prevention as well as crime forecast by various time series prediction approaches [2].

Conclusions

The preprocessing and the fuzzy clustering of the data clearly identified some areas of higher criminal activity (crime hot spots), and also the behavior of these areas, in real-time, was identified. The sub-normalization of the fuzzy clusters (assigning the heights of the clusters corresponding to the absolute crime intensities) point out problem areas, where the number of certain types of crimes is higher than the average. The tendencies of these crime hot spots in time (increasing, stagnating, decreasing, or random) may be the starting points for further police intervention. The first two tendencies, especially the increasing

tendency, mark the areas where immediate urgent intervention is necessary. It may mean the increase of the police force on spot, mounting more video cameras for observing public areas, or education, creating jobs, etc. A decreasing tendency is an indicator of proper police measures and regulations being carried out in any given area. Random behavior may be enigmatic, or the result of some sudden change in the general conditions, and these areas need further deeper investigation [2].

In future work, a full analysis of the time dependent behavioral patterns will be applied, and alternative clustering techniques may be compared, when they represent true images of statistical observations [2].

It is important to refine the investigations towards potentially periodical behavior within the year (connected to holiday seasons, mass events, etc.) and clusters depending on the part of the year (clusters of groups of weeks or days) should be identified. Having these results, police intervention measures may be recommended, in terms of exact places and times [2].

Acknowledgement

This research was sponsored by: „EFOP-3.6.1-16-2016-00017 Internationalization, initiatives to establish a new source of researchers and graduates, and development of knowledge and technological transfer as instruments of intelligent specializations at Szechenyi University.” and the number K124055 OTKA project.

References

- [1] I. Batyrshin, O. Kaynak and I. Rudas: Fuzzy modeling based on generalized conjunction operators. *Fuzzy Systems, IEEE Transactions on*. 10. 678 - 683. 10.1109/TFUZZ.2002.803500, 2002
- [2] L. T. Kóczy, G. Kovács, P. Földesi, Sz. Nagy, B. Túú-Szabó and G. Fogarasi: Identification and dynamic analysis of crime hotspots in Hungary by a complex Computer Intelligence approach. 23rd IEEE International Conference on Intelligence Engineering Systems, Gödöllő, Hungary, 2019
- [3] A. Adolfsson, M. Ackerman, N. Brownstein: To Cluster, or Not to Cluster: An Analysis of Clusterability Methods. *Pattern Recognition*. 88. 10.1016/j.patcog.2018.10.026, 2018
- [4] G. Desagulier: Clustering Methods. *Corpus Linguistics and Statistics with R*. DOI: 10.1007/978-3-319-64572-8_10, 2017
- [5] J. C. Dunn: A Fuzzy Relative of the ISODATA Process and Its Use in Detecting Compact Well-Separated Clusters. *Journal of Cybernetics* 3: 32-57, 1973
- [6] J. C. Bezdek: *Pattern Recognition with Fuzzy Objective Function Algorithms*. Plenum Press, New York, 1981

-
- [7] L. T. Kóczy, P. Földesi, B. Tüü-Szabó: A discrete bacterial memetic evolutionary algorithm for the traveling salesman problem. 3261-3267, 10.1109/CEC.2016.7744202, 2016
- [8] I. Gath and A. B. Geva: Unsupervised optimal fuzzy clustering. IEEE Transactions on Pattern Analysis and Machine Intelligence, Vol. 11(7), pp 773-781, 1989
- [9] A. Graps: An Introduction to Wavelets. IEEE Comput. Sci. Eng. 2, 2 (June 1995) 50-61, DOI: <https://doi.org/10.1109/99.388960> 1995
- [10] A. Haar: Zur Theorie der orthogonalen Funktionensysteme. Math. Ann. 69: 331, DOI: <https://doi.org/10.1007/BF01456326>, 1910
- [11] Sz. Nagy and J. Pipek: Wavelet Based Density Operators, Electron Density and Energy Functionals. 2005
- [12] J. Bezdek, R. Ehrlich, W. Full: FCM—the Fuzzy C-Means clustering-algorithm. Computers & Geosciences. 10, 191-203, 10.1016/0098-3004(84)90020-7, 1984
- [13] L. T. Kóczy, G. Kovács, P. Földesi, Sz. Nagy, B. Tüü-Szabó, G. Fogarasi and A. Czebe: Identification and dynamic analysis of crime hotspots in Hungary by a complex CI approach. FEE 2019 Conference, London, 2019, URL: https://www.researchgate.net/publication/331718127_Identification_and_dynamic_analysis_of_crime_hot-spots_in_Hungary_by_a_complex_CI_approach

Design of a Composite State Convergence Controller for a Nonlinear Telerobotic System

**Muhammad Usman Asad^{1,3}, Umar Farooq^{1,3}, Jason Gu¹,
Valentina E. Balas², Ghulam Abbas⁴, Marius M. Balas²**

¹Department of Electrical and Computer Engineering Dalhousie University, Halifax, N.S. B3H 4R2, Canada

²Department of Automatics and Applied Software, “Aurel Vlaicu” University of Arad, Romania

³Department of Electrical Engineering, University of The Punjab, Quaid-e-Azam Campus, Lahore, 54590 Pakistan

⁴Department of Electrical Engineering, The University of Lahore, Pakistan

mh549096@dal.ca, umar.farooq@dal.ca, jason.gu@dal.ca,
valentina.balas@uav.ro, ghulam.abbas@ee.uol.edu.pk, marius.balas@uav.ro

Abstract: This paper presents the design of a reduced complexity state convergence controller, termed as composite state convergence controller, for a single degree-of-freedom nonlinear telerobotic system. First, nonlinear master and slave models are feedback-linearized and composite states are formed by combining their respective position and velocity signals. These composite master and slave states along with the operator's force are then transmitted across the communication channel instead of full states. In this way, the complexity of communication structure is reduced. An augmented system composed of composite master and slave states is finally constructed and method of state convergence is applied to compute the control gains of the proposed scheme. It is shown that position and velocity states of the master and slave systems still converge in the absence and presence of time delays, even though the design is based on the reduced order composite system. The validity of the proposed scheme is confirmed through MATLAB simulations as well as semi-real time experiments.

Keywords: state convergence; nonlinear telerobotic system; feedback linearization; composite states

1 Introduction

A telerobotic system is used to perform a task in a remote location under the control of a human operator. In order to properly execute the task, feedback from the remote location is desired. The presence of feedback turns the unilateral telerobotic system into a bilateral one. This feedback can be audio, video or force signals. The force feedback can considerably improve the operator's perception of the remote environment. However, the control design of a telerobotic system involving force feedback becomes a challenging task, especially in the presence of time delays. Therefore, many research efforts have been directed to design such a robotic system [1]-[4]. The stability of a time-delayed robotic system was not guaranteed until the groundbreaking work of Anderson and Spong who employed the concepts of transmission line theory to stabilize the telerobotic system in the presence of time delays and force feedback [5]. Wave theory formalizes the transmission line concept and has become a popular framework for designing telerobotic systems [6]. The issue of wave reflection in wave-based telerobotic systems has also been addressed in the literature and improved wave-controllers have been proposed [7]. Further, more refined telerobotic systems have emerged which utilize wave variables in conjunction with neural networks [8]. The other control techniques such as H_∞ [9], sliding mode [10], adaptive control [11], fuzzy logic [12], disturbance-observer based control [13], etc. have also been utilized in designing telerobotic systems.

State convergence theory offers a simple and elegant way of designing the telecontrollers. This is a model-based linear control algorithm that allows the modeling of a telerobotic system on state space and requires the solution of $3n+1$ design conditions for establishing the motion synchronization of n^{th} order master and slave systems [14]. Various forms of these control algorithms are proposed in the literature. For instance, a state convergence controller with transparency condition is proposed in [15]. In another study, the state convergence controller is designed when an environment model is not available [16]. The design of nonlinear telerobotic systems based on state convergence theory has also been discussed. For instance, feedback linearization theory has been utilized to transform the nonlinear telerobotic system into a linear one and a state convergence algorithm is then employed to compute the control gains [17]. In another study, TS fuzzy model of the nonlinear telerobotic system is constructed and an appropriate parallel distributed compensation control law is designed whose gains are computed using the method of state convergence [18].

This paper is an extension of our earlier work on the channel simplification of the state convergence controller where we have only considered a linear telerobotic system [19]. The simplified architecture, termed as composite state convergence, allows transmitting fewer variables while the desired system behavior is also achieved at the same time. In this paper, we show that our reduced complexity algorithm can still be applied to a nonlinear telerobotic system. To this end, we

first utilize the feedback linearization theory to transform the nonlinear telerobotic system into a controllable linear system. In the second stage, composite states are constructed for the transformed master and slave systems. An augmented system is then formed from the composite slave and error systems. Finally, method of state convergence is employed to compute the control gains of the proposed composite state convergence controller. In order to validate the proposed scheme, simulations are performed in a MATLAB/Simulink environment where both the delay-free and delayed communication is considered. Semi-real time experiments using the haptic device are also conducted.

This paper is structured as: Problem formulation is given in Section 2. Controller design is described in Section 3 and Results are presented in Section 4.

2 Problem Definition

Consider a single degree-of-freedom nonlinear teleoperation system as:

$$\begin{cases} \text{Master: } J_m \ddot{\theta}_m + b_m \dot{\theta}_m + m_m g l_m \sin \theta_m = u'_m + F_m = u_m \\ \text{Slave: } J_s \ddot{\theta}_s + b_s \dot{\theta}_s + m_s g l_s \sin \theta_s = u'_s - F_e = u_s \end{cases} \quad (1)$$

Where $m_x, l_x, b_x, J_x, \theta_x, \dot{\theta}_x, \ddot{\theta}_x, g, u_x$ are the mass, length, friction coefficient, inertia, angular position, angular velocity, angular acceleration, acceleration due to gravity and torque inputs for the master ($x = m$)/slave ($x = s$) systems, respectively. Also, F_m and F_e are the operator's and environment forces, respectively. By defining angular position and angular velocity as state variables i.e. $x_{1x} = \theta_x, x_{2x} = \dot{\theta}_x, y_x = x_{1x}$, nonlinear dynamics of (1) can be written as:

$$\begin{cases} \dot{x}_{1m} = x_{2m} \\ \dot{x}_{2m} = -\frac{m_m g l_m}{J_m} \sin x_{1m} - \frac{b_m}{J_m} x_{2m} + \frac{1}{J_m} u_m \\ y_m = x_{1m} \end{cases} \quad (2)$$

$$\begin{cases} \dot{x}_{1s} = x_{2s} \\ \dot{x}_{2s} = -\frac{m_s g l_s}{J_s} \sin x_{1s} - \frac{b_s}{J_s} x_{2s} + \frac{1}{J_s} u_s \\ y_s = x_{1s} \end{cases}$$

The objective of the present study is to design control inputs for the master and slave system such that the slave is able to follow the master system and the

environment force is also reflected to the operator as the slave interacts with the environment. Mathematically,

$$\begin{aligned} \lim_{t \rightarrow \infty} x_{1m} - \alpha x_{1s} &= 0 \\ \lim_{t \rightarrow \infty} F_m + \beta F_e &= 0 \end{aligned} \quad (3)$$

Where α, β are scaling constants for the position and force responses, respectively. To achieve the objective in (3), we present a feedback-linearization supported composite state convergence controller in the next section.

3 Proposed Controller

The proposed tele-controllers for the position and force tracking task (3) are developed using the feedback linearization and composite state convergence theories. To start with, we recall the fundamentals of exact linearization.

Theorem 1: For a nonlinear system $\dot{x} = f(x) + g(x)u, y = h(x)$ having a relative degree n for all $x \in \mathbb{R}^n$, there exists a transformation $\phi(x)$ such that the resulting system $\dot{z} = Az + Bv$ is linear and controllable in new coordinates. The coordinate transform, nonlinear input and the resulting linear system are given as:

$$\begin{aligned} z = \phi(x) &= \begin{bmatrix} z_1 \\ z_2 \\ \vdots \\ z_n \end{bmatrix} = \begin{bmatrix} \phi_1(x) \\ \phi_2(x) \\ \vdots \\ \phi_n(x) \end{bmatrix} = \begin{bmatrix} h(x) \\ L_f h(x) \\ \vdots \\ L_f^{n-1} h(x) \end{bmatrix} \\ u &= \frac{1}{L_g L_f^{n-1} h(x)} \left(-L_f^n h(x) + v \right) \end{aligned} \quad (4)$$

$$\dot{z} = \begin{bmatrix} \dot{z}_1 \\ \dot{z}_2 \\ \vdots \\ \dot{z}_n \end{bmatrix} = \begin{bmatrix} 0 & 1 & 0 & \dots & 0 \\ 0 & 0 & 1 & \dots & 0 \\ & & \vdots & & \\ 0 & 0 & 0 & \dots & 1 \\ 0 & 0 & 0 & \dots & 0 \end{bmatrix} \begin{bmatrix} z_1 \\ z_2 \\ \vdots \\ z_n \end{bmatrix} + \begin{bmatrix} 0 \\ 0 \\ \vdots \\ 1 \end{bmatrix} v$$

Where $L_f h(x)$ is lie-derivative of $h(x)$ in the direction of $f(x)$ and is determined as $L_f h(x) = \sum_{i=1}^n \frac{\partial h}{\partial x_i} f_i(x)$.

The application of Theorem 1 on the nonlinear master and slave models in (2) yields the following linearized tele-robotic system:

$$\begin{aligned}
 \text{Master : } & \begin{cases} \phi_m = [x_{1m} \quad x_{2m}]^T \\ \dot{z}_{1m} = z_{2m} \\ \dot{z}_{2m} = v_m \\ u_m = b_m x_{2m} + m_m g l_m \sin x_{1m} + J_m v_m \\ y_m = x_{1m} = z_{1m} \end{cases} \\
 \text{Slave : } & \begin{cases} \phi_s = [x_{1s} \quad x_{2s}]^T \\ \dot{z}_{1s} = z_{2s} \\ \dot{z}_{2s} = v_s \\ u_s = b_s x_{2s} + m_s g l_s \sin x_{1s} + J_s v_s \\ y_s = x_{1s} = z_{1s} \end{cases}
 \end{aligned} \tag{5}$$

After the master and slave systems are exactly linearized through (5), communication between them is established using the composite state convergence methodology proposed by the authors. The overall control scheme is shown in Fig. 1. We now show the convergence of master and slave systems' states as well as force reflection ability of the proposed scheme.

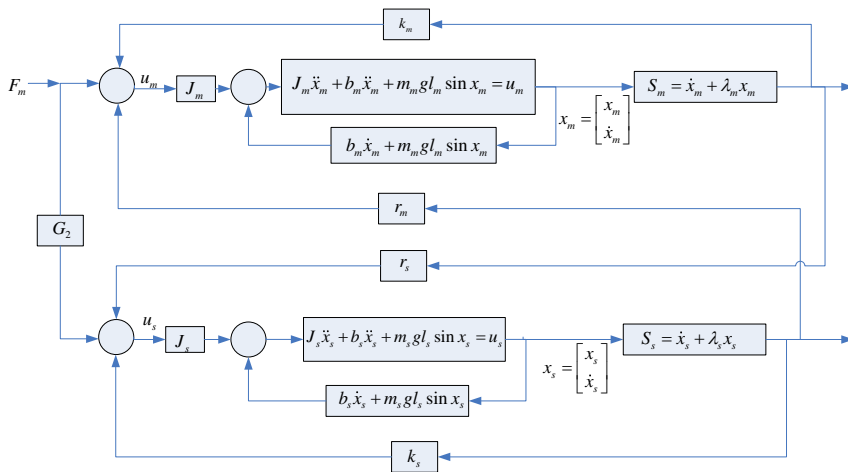


Figure 1
Proposed Scheme

Theorem 2: The slave system is able to follow the master system in the absence of communication time delay if gains of the composite state convergence controller are found as a solution of the following design conditions:

$$G_2 - 1 = 0 \quad (6)$$

$$k_s + r_s - k_m - r_m = 0 \quad (7)$$

$$k_s + r_s = -p \quad (8)$$

$$k_m - r_s = -q \quad (9)$$

Proof: Let us define the composite states for the master (s_m) and slave (s_s) systems as:

$$s_m = x_{2m} + \lambda_m x_{m1} \quad (10)$$

$$s_s = x_{2s} + \lambda_s x_{1s}$$

The time derivative of (10) along with (5) yields the composite dynamical system as:

$$\dot{s}_m = v_m + \lambda_m x_{m2} \quad (11)$$

$$\dot{s}_s = v_s + \lambda_s x_{s2}$$

Let us define the control inputs for the feedback-linearized tele-robotic system as:

$$v_m = -\lambda_m x_{m2} + k_m s_m + r_m s_s + F_m \quad (12)$$

$$v_s = -\lambda_s x_{s2} + k_s s_s + r_s s_m + G_2 F_m$$

By plugging (12) in (11), we get:

$$\dot{s}_m = k_m s_m + r_m s_s + F_m \quad (13)$$

$$\dot{s}_s = k_s s_s + r_s s_m + G_2 F_m$$

Let $s_e = s_s - s_m$ be the composite error. The composite error dynamics can be written using (13) as:

$$\dot{s}_e = (k_s + r_s - k_m - r_m) s_s + (k_m - r_s) s_e + (G_2 - 1) F_m \quad (14)$$

We now form an augmented system comprising of composite slave and error systems as:

$$\begin{bmatrix} \dot{s}_s \\ \dot{s}_e \end{bmatrix} = \begin{bmatrix} k_s + r_s & -r_s \\ k_s + r_s - k_m - r_m & k_m - r_s \end{bmatrix} \begin{bmatrix} s_s \\ s_e \end{bmatrix} + \begin{bmatrix} G_2 \\ G_2 - 1 \end{bmatrix} F_m \quad (15)$$

We now allow the composite error to evolve as an autonomous system, which yields the design conditions (6) and (7). The characteristic equation of the remaining augmented system is finally compared with the desired polynomial $(s + p)(s + q) = 0$ which yields the design condition (8) and (9). Now, it is left to show that states of the slave system converge to the states of the master system with the control gains in (6)-(9). These control gains yield the closed loop master

as well as slave system as $\ddot{x}_{1z} + (\lambda_z + p)\dot{x}_{1z} + \lambda_z p = F_m$ which implies that slave position can be made to track the master position with the scaling factor as $\alpha = \lambda_m / \lambda_s$ which also implies the zero convergence of the velocity states. This completes the proof.

Theorem 3: The motion of the slave system will be synchronized with the master system in the presence of communication time delay (T) if control gains of the composite nonlinear controller are found as a solution of the following design conditions:

$$G_2(1 + Tr_m) - Tr_s = 1 \quad (16)$$

$$k_s + (1 - Tk_m)r_s - k_m + (Tk_s - 1)r_m = 0 \quad (17)$$

$$k_s - Tr_s r_m + r_s - Tr_s k_m = -p \quad (18)$$

$$r_s - Tr_s k_m - r_m + Tr_m k_s = -q \quad (19)$$

Proof: Consider the tele-robotic system of Fig. 1 with time delay, T in the communication paths. Let the virtual inputs for the master and slave systems be introduced as:

$$v_m = -\lambda_m x_{m2} + k_m s_m + r_m s_s (t - T) + F_m \quad (20)$$

$$v_s = -\lambda_s x_{s2} + k_s s_s + r_s s_m (t - T) + G_2 F_m (t - T) \quad (21)$$

The delayed dynamical composite master and slave systems can be derived as:

$$\dot{s}_m = k_m s_m + r_m s_s (t - T) + F_m \quad (22)$$

$$\dot{s}_s = k_s s_s + r_s s_m (t - T) + G_2 F_m (t - T)$$

Let us now use the first order Taylor series expansion on the time delayed signals with the assumption of constant operator force, i.e.

$$s_x (t - T) \approx s_x - T \dot{s}_x, x = m, s \quad (23)$$

$$F_m (t - T) \approx F_m - T \dot{F}_m = F_m$$

Based on the above Taylor expansion and using the definition of composite error, the closed loop delayed composite master and slave systems can be written as:

$$\dot{s}_m = \frac{1}{(1 - T^2 r_s r_m)} \left((k_m - Tr_s r_m + r_m - Tr_m k_s) s_s - (r_m - Tr_m k_s) s_e + (1 - Tr_m G_2) F_m \right) \quad (24)$$

$$\dot{s}_s = \frac{1}{(1 - T^2 r_s r_m)} \left((k_s - Tr_s r_m + r_s - Tr_s k_m) s_s - (r_s - Tr_s k_m) s_e + (G_2 - Tr_s) F_m \right) \quad (25)$$

We now write the composite slave-error augmented system:

$$\begin{bmatrix} \dot{s}_s \\ \dot{s}_e \end{bmatrix} = \frac{1}{(1-T^2 r_s r_m)} \left(\begin{bmatrix} k_s - Tr_s r_m + r_s - Tr_s k_m & -r_s + Tr_s k_m \\ (k_s + r_s - Tr_s k_m - k_m -) & (r_s - Tr_s k_m -) \\ r_m + Tr_m k_s & r_m + Tr_m k_s \end{bmatrix} \begin{bmatrix} s_s \\ s_e \end{bmatrix} + \begin{bmatrix} G_2 - Tr_s \\ (G_2 - Tr_s - 1) \\ +Tr_m G_2 \end{bmatrix} F_m \right) \quad (26)$$

The composite error system is now allowed to evolve as an autonomous system which leads to the design conditions (16), (17). The rest of the augmented system is then assigned the desired dynamics formed from the poles $s = -p, s = -q$. This assignment leads to the design conditions (18), (19). An analysis similar to Theorem 2 reveals that the slave system indeed follows the master system. The proof is now completed.

4 Results & Discussion

The proposed composite nonlinear state convergence controller is simulated in MATLAB/Simulink environment to evaluate its effectiveness in motion synchronization of master and slave systems. For the purpose of simulations, parameters of the tele-robotic system are adopted from [17]:

$$\begin{aligned} \text{Master} : m_m &= 1, l_m = 0.2, b_m = 10, J_m = 0.33m_m l_m^2 \\ \text{Slave} : m_s &= 10, l_s = 1, b_s = 15, J_s = 0.33m_s l_s^2 \\ \text{Environment} : k_e &= 10, k_f = 1 \end{aligned} \quad (27)$$

We first perform simulations when no time delay exists in the communication channel. To this end, let the desired poles be placed at $s + p = s + 2, s + q = s + 20$ and let the motion scaling constants be selected as unity. The design conditions in Theorem 1 are then solved and following control gains are obtained:

$$\begin{aligned} G_2 &= 1 \\ k_m &= -12 \\ k_s &= -10 \\ r_s &= 8 \end{aligned} \quad (28)$$

By assuming zero initial conditions for both the master and slave systems, telerobotic system is simulated under a constant operator's force of 0.2 N and the control gains of (28). The result is depicted in Figs. 2-3. It can be seen that the composite states convergence and this leads to the convergence of master and slave systems' states. The motion scaling property of the proposed controller is

also evaluated in simulations. Let it be desired that slave's motion converges to 50% of the motion of the master system which leads to the selection of slave's scaling constant as $\lambda_s = 2$. The simulations are now run with the control gains of (28) and the result is shown in Fig. 4. It can be seen that the slave's position response is indeed 0.5 times the position profile of the master system.

We now test the proposed controller when time delay exists in the communication channel. Let the time delay be 0.2 s in each direction. With the parameters of the tele-robotic system in (27) and using the same desired dynamics as in the delay-free case, control gains are found based on the design conditions of Theorem 3 as:

$$\begin{aligned} G_2 &= 0.3521 \\ k_m &= -16 \\ k_s &= -2.3944 \\ r_s &= 0.2817 \end{aligned} \quad (29)$$

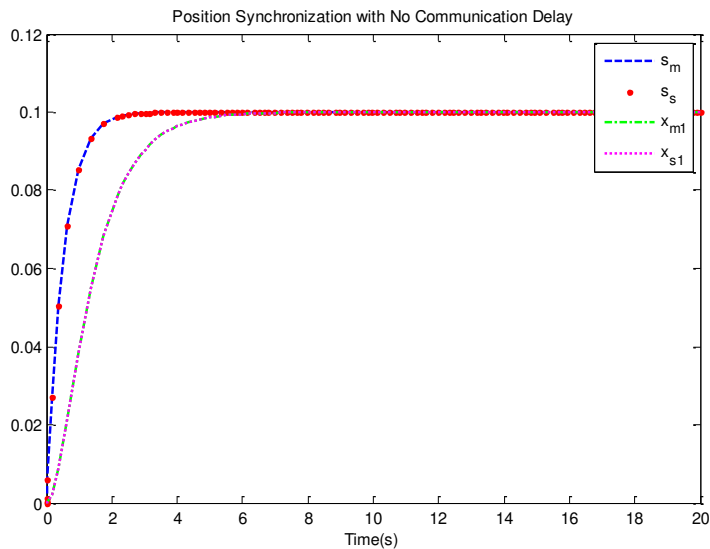


Figure 2

Position synchronization with no communication time delay

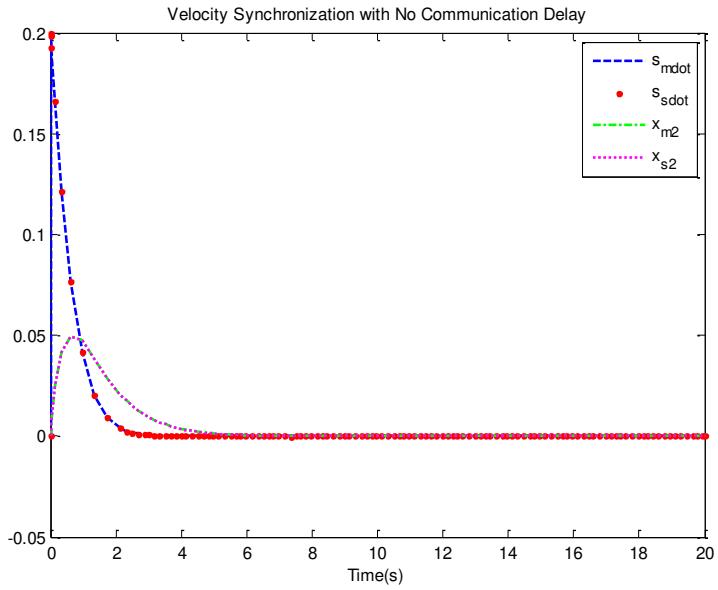


Figure 3

Velocity synchronization with no communication time delay

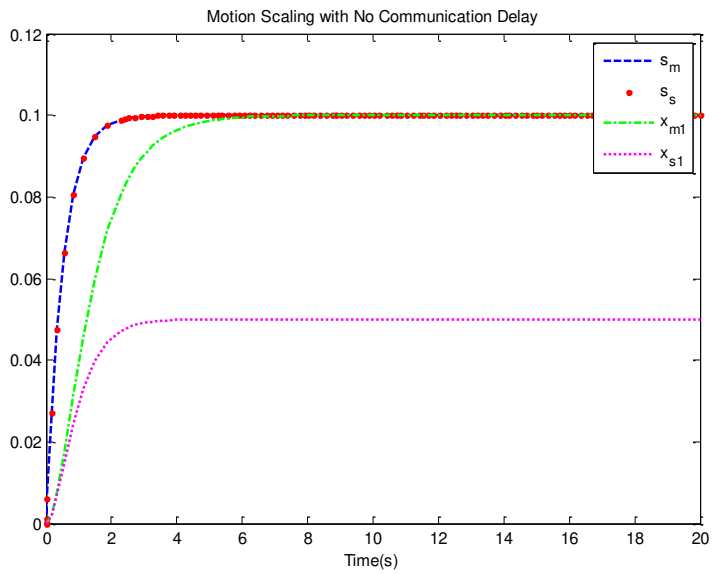


Figure 4

Motion scaling with no communication time delay

By selecting $x_m(0) = x_s(0) = 0$, $\lambda_m = \lambda_s = 1$ and with a constant operator's force of 0.2 N, we run the time-delayed tele-robotic system under the control gains of (29) and the results are shown in Figs. 5-6. The analysis reveals that the composite slave system follows the composite master system which leads to convergence of the position and velocity states of the master and slave systems. The motion scaling ability of the time-delayed tele-robotic system is also investigated. To this end, reference for the slave system is set as $0.25x_{m1}$ which implies $\lambda_s = 4$. The simulation result, as obtained under the control gains of (29), is shown in Fig. 7. It can be seen that the motion of the slave system has been achieved as desired.

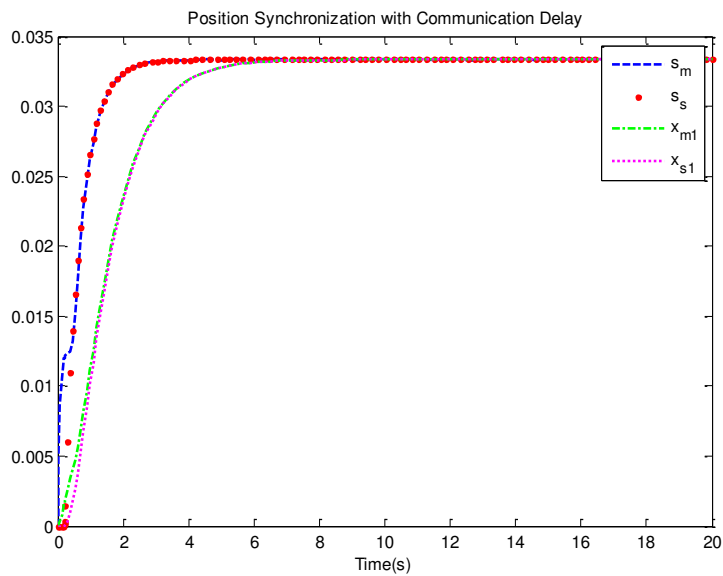


Figure 5

Position synchronization with communication time delay

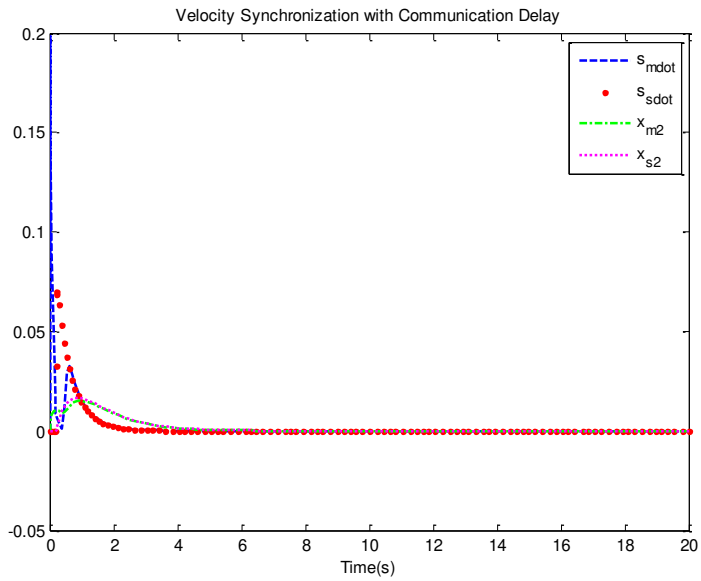


Figure 6

Velocity synchronization with communication time delay

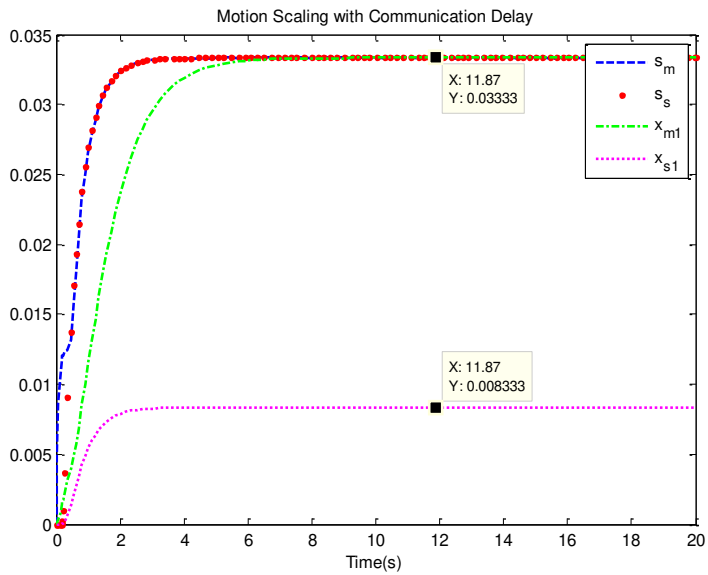


Figure 7

Motion scaling with communication time delay

We now include some semi-realtime results of the proposed nonlinear controller which are obtained using haptic device in QUARC/Simulink environment. A time-varying operator's force is generated by operating the haptic device along a single axis and trajectories of the resulting master and slave systems are recorded in a time-delayed environment under the control of (29). The results are shown in Figs. 8 and 9. It can be seen that the slave is following the master system and the states finally convergence when the operator's force becomes constant.

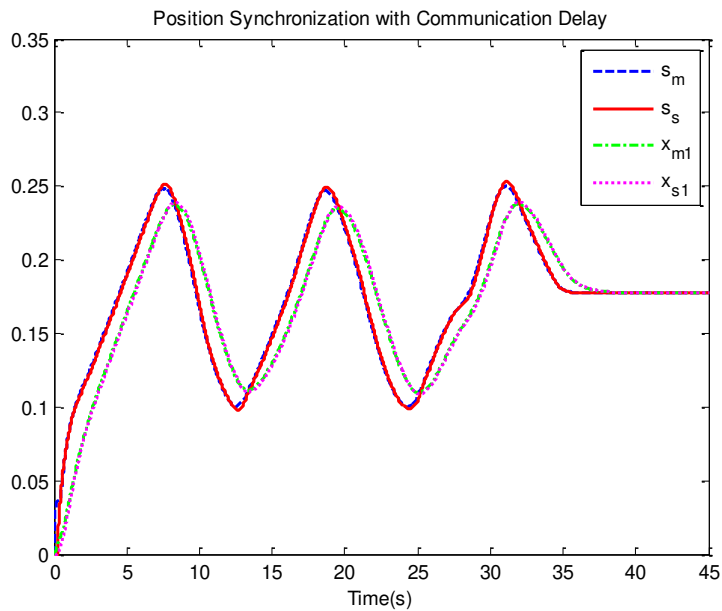


Figure 8

Position synchronization with communication time delay under time varying applied force

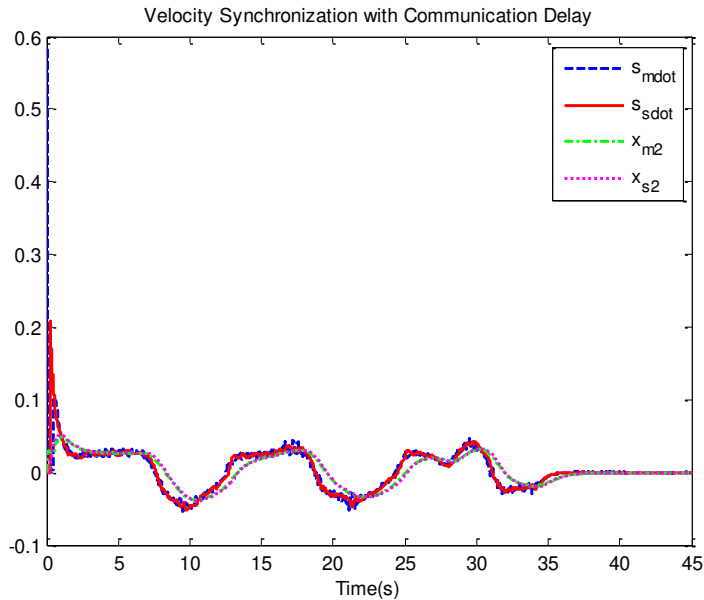


Figure 9

Velocity synchronization with communication time delay under time varying applied force

Conclusions

This paper has presented the design of a composite state convergence controller for a one degree-of-freedom nonlinear telerobotic system. To deal with the nonlinearity in the master and slave systems, a feedback linearization algorithm is used. The exactly linearized master and slave systems are then used to form the lower complexity composite systems. Through the use of a similarity transformation, a composite slave-error augmented system is constructed. After the composite error is made to evolve as an autonomous, desired behavior is assigned to the telerobotic system. This results in four design conditions which are solved to determine the four unknown control gains. Simulations, as well as semi-real time experiments, are finally performed in MATLAB/Simulink environment which shows good performance of the telerobotic system in the absence and presence of communication time delays.

Acknowledgement

This work was supported by NSERC.

References

- [1] M. Ferre, M. Buss, R. Aracil, C. Melchiorri, C. Balaguer: *Advances in Telerobotics*, Springer, 2007

-
- [2] P. F. Hokayem, M. W. Spong: Bilateral Teleoperation: an Historical Survey, *Automatica*, Vol. 42, 2006, pp. 2035-2057
- [3] R. Muradore, P. Fiorini: A Review of Bilateral Teleoperation Algorithms, *ACTA Polytechnica Hungarica*, Vol. 13, No. 1, 2016, pp. 191-208
- [4] J. Artigas, G. Hirzinger: A brief history of DLR's space telerobotics and force feedback teleoperation, *ACTA Polytechnica Hungarica*, Vol. 13, No. 1, 2016, pp. 239-249
- [5] R. Anderson, M. W. Spong: Bilateral Control of Teleoperators with Time Delay: *IEEE Transactions on Automatic Control*, Vol. 34, No. 5, 1989, pp. 494-501
- [6] G. Niemeyer, J. J. E. Slotine: Stable Adaptive Teleoperation, *IEEE Journal of Oceanic Engineering*, Vol. 16, No. 1, 1991, pp. 152-162
- [7] Da Sun, Fazel Naghdy, and Haiping Du: Stability Control of Force-Reflected Nonlinear Multilateral Teleoperation System under Time-Varying Delays, *Journal of Sensors*, vol. 2016, Article ID 4316024, 17 pages, 2016
- [8] C. Yang, X. Wang, Z. Li, Y. Li, C. Su: Teleoperation Control Based on Combination of Wave Variable and Neural Networks, *IEEE Transactions on Systems, Man, and Cybernetics: Systems*, Vol. 47, No. 8, pp. 2125-2136, Aug. 2017
- [9] M. Boukhnifer, A. Ferreira: H_{∞} Loop Shaping Bilateral Controller for a Two-fingered Tele-micromanipulation System, *IEEE Transactions on Control Systems Technology*, Vol. 15, No. 5, 2007, pp. 891-905
- [10] A. Hace, M. Franc: FPGA Implementation of Sliding Mode Control Algorithm for Scaled Bilateral Teleoperation, *IEEE Transactions on Industrial Electronics*, Vol. 9, No. 3, 2013, pp. 1291-1300
- [11] L. Chan, F. Naghdy, D. Stirling: Application of Adaptive Controllers in Teleoperation Systems, *IEEE Transactions on Human-Machine Systems*, Vol. 44, No. 3, 2014, pp. 337-352
- [12] Y. Yang, C. Hua and X. Guan: Adaptive Fuzzy Finite-Time Coordination Control for Networked Nonlinear Bilateral Teleoperation System, *IEEE Transactions on Fuzzy Systems*, Vol. 22, No. 3, pp. 631-641, June 2014
- [13] A. Suzuki, K. Ohnishi: Frequency Domain Damping Design For Time Delayed Bilateral Teleoperation System Based On Modal Space Analysis, *IEEE Transactions on Industrial Electronics*, Vol. 60, No. 1, 2013, pp. 177-190
- [14] J. M. Azorin, O. Reinoso, R. Aracil, M. Ferre: Generalized Control Method by State Convergence of Teleoperation Systems with Time Delay, *Automatica*, Vol. 40, No. 9, 2004, pp. 1575-1582

- [15] R. Aracil, J. M. Azorin, M. Ferre, C. Pena: Bilateral Control by State Convergence based on Transparency for Systems with Time Delay, *Robotics & Autonomous Systems*, Vol. 61, No. 2, 2013, pp. 86-94
- [16] J. M. Azorin, R. Aracil, C. Perez, N. M. Garcia, J. M. Sabater: Bilateral Control Architecture for Telerobotics Systems in Unknown Environments, *Proc. Euro Haptics*, 2008, pp. 13-22
- [17] J. M. Azorin, J. A. Berna, E. Ianez: Nonlinear Bilateral Control of Teleoperators by State Convergence, *Proc. European Control Conference (ECC)*, Budapest, 2009, pp. 2815-2820
- [18] U. Farooq, J. Gu, M. El-Hawary, M. U. Asad, G. Abbas: Fuzzy Model Based Bilateral Control Design of Nonlinear Tele-operation System Using Method of State Convergence, *IEEE Access*, Vol. 4, 2016, pp. 4119-4135
- [19] M. U. Asad, U. Farooq, J. Gu, G. Abbas, R. Liu, V. E. Balas: A Composite State Convergence Scheme for Bilateral Teleoperation Systems, *Accepted, IEEE/CAA Journal of Automatica/Sinica*, 2019

A Clustered Hybrid Honeypot Architecture

Eva Chovancová, Norbert Ádám

Department of Computers and Informatics, Faculty of Electrical Engineering and Informatics, Technical University of Košice
Letná 9, 042 00 Košice, Slovak Republic

eva.chovancova@tuke.sk, norbert.adam@tuke.sk

Abstract: Nowadays, when computers and computer systems are almost omnipresent and are part of most households and most people have access to them, they are more vulnerable than ever. Today, protection and security of computer networks and systems using passive protection does not suffice anymore. One has to anticipate attacks and be a step ahead of the attackers. To achieve this type of security, one has to employ active protection techniques, such as digital baits – honeypots. The primary goal of using honeypots is to divert the interest of potential attackers from other really important targets within a particular computer network. The secondary goal is to acquire information about the attackers' activities and methods. Subsequently, these data are thoroughly analysed. By analysing the attacks, security improvement measures aimed at the particular network and/or computer system may be proposed in order to prevent threats. The goal of this paper is to contribute to computer security by proposing a clustered, high-interaction-honeypot-based security system.

Keywords: security; honeypot; intrusion detection system; malware; clustered honeypot

1 Introduction

The world full of information and information resources means an ever growing amount of data stored in computer systems. The risk of threats is also increased by improving connectivity and access to data and computer system services from various locations within the computer network. Any system providing connectivity to a computer network may be at risk. Currently, security by authentication [1] [2] [3] and authorisation of production systems is considered to be insufficient since a potential attacker may steal identity data of another user or bypass authentication, violating system security [4] [5] [6]. With the development of information technology, our knowledge of computer systems advances, too – attackers can analyse weaknesses of the respective systems and use them during the attack itself. The task of any security technology operator is to detect and subsequently identify any attack; however, in heavily used systems, this may be

very hard, in some cases even impossible. After performing the attack, the attacker often infects the compromised system with malware [7] [8] [9] [10] [11]. The goal of this malware is to fulfil the attackers' goals; often, malware is capable to replicate and spread in the compromised computer network. This makes them very dangerous since all the attacker has to do is execute them, without the need of any later surveillance. As a result, malware may then spread within the network freely – if computers from other networks trust computers from such a compromised network, these computers are also at risk [12] [13].

An intrusion detection system (IDS) is a passive protection mechanism monitoring activity within the computer network/system [14] [15] [16] [17] [18] [19] [20]. It monitors and gathers data on the activities performed within the network/system, to detect intrusions. An intrusion detection system does not only detect intrusions, but it may also be used as a monitoring tool to identify suspicious activities aimed at compromising the particular network/system. The gathered data may then be used to increase the security of the network/system, following a thorough analysis. However, today, protection and security of computer networks and systems using passive protection does not suffice anymore. One has to anticipate attacks and be a step ahead of the attackers. Therefore, not only passive, but also active protection techniques – such as digital baits (honeypots) – have to be used.

This paper proposes a clustered intrusion detection system architecture, based on high-interaction hybrid honeypots [21], eliminating the disadvantages of intrusion detection systems using honeypot technology.

2 Honeypots

Digital baits – honeypots – represent flexible, constantly developing technology with numerous use cases [21] [22] [23] [24]. Honeypots may be used secure systems, but also to gather information for subsequent analysis. The analyses of the gathered data may result in the detection of suspicious activities, proposal and eventual implementation of countermeasures improving system security and preventing further similar attacks.

Essentially, honeypots are devices with purposely constructed security holes, while pretending a false identity. The goal of using honeypots is to divert the interest of the potential attackers from real devices. If an attacker focuses on the honeypot, one may register, identify and analyse his/her activities. To increase efficiency, intrusion detection tools may be added to the honeypot itself, to monitor the use of specific, monitoring and/or malicious applications.

Assuming that any interaction with the honeypot is a potential attack, the need to classify the gathered data falls to the minimum, increasing the speed of the analytic process and evaluation of the data gathered by the bait itself. To increase

computer system security and improve the efficiency of fending off the attack, it is wise to use honeypots with other standard security tools and methods.

One of the most important benefits of using honeypots is related to detection since it minimises the negative aspects of common intrusion detection systems. These include the following:

- evaluating an attack, which did not happen (false negative) or failure to detect an attack (false positive);
- elimination of errors in the configuration of intrusion detection systems.

Another advantage of this security solution is that they do not influence system operation during the interaction with the attacker.

2.1 Fundamental Functionality

Honeypots have numerous functions allowing multifaceted use. The basic functions are the following:

- to divert the interest of the potential attacker from production equipment.
- to identify security holes in the OS.
- to analyse the attackers' behaviour during the interaction with them.
- logging attacker behaviour.

2.2 Interaction Level

Honeypots may be classified also by the level of attacker interaction; in this case, "interaction" refers to the possibilities of the attackers' communication with the honeypot [25]. There are low-interaction and high-interaction honeypots. Low-interaction honeypots have no operating system; therefore, the attacker cannot initiate interaction with the OS. A disadvantage of these honeypots is that services and processes are emulated. The attacker may detect them easier and since it is impossible to gain full access to the honeypot, the amount of data that may be gathered about the attackers' activities, is also limited.

High-interaction honeypots are more sophisticated, having a more complex design since they use real operating systems. In this case, one may gather more information about the attackers. High-interaction honeypots record all attacker activities; the records may be then analysed to improve system security.

3 Clustered Hybrid Honeypots

Honey pots are frequently used means of system security [23] [24] [26] [27] [28]. When using honey pots, their level of security has to be taken into account. In case of weak honey pot security, the attacker may easily discover that the honey pot is not a production device. On the other hand, if the honey pot security level is too high, it may discourage the attacker.

Most existing honey pot systems focus on the configuration of the equipment running the honey pots. Configuring such equipment means mostly configuring these devices to allow them to find and allocate unused IP addresses automatically, after connecting them to the network and, eventually, to allow them to adapt to the changing environment of the computer network.

The architecture proposed herein is a clustered hybrid honey pot [22]. The proposed hybrid honey pot architecture combines two types of baits with different interaction levels, focusing on high-interaction honey pots since, in terms of security, to the attacker; it is an interesting target with an IP address. An ideal tool meeting the requirements of a low-interaction honey pot is Honeyd, an open-source program. With its help, the load of the high-interaction honey pot may be relieved, allowing focus mainly on the initial attack analysis. Attacks are detected by the architecture itself. The proposed solution differs from the security solution, in which any anomaly triggers diversion of the interaction to a "shadow honey pot" during the operation of the computer system. In this system [29], analysis of the incoming attack is performed by the shadow honey pot. However, such a solution increases the operating costs of the network/system.

3.1 Clustered Hybrid Honeypot Architecture

The proposed architecture consists of these 4 main parts:

- Internet access management
- clustered honey pots,
- auditing and data repository cluster, and
- correlation.

The architecture of the proposed clustered high-interaction honey pot is depicted in Fig. 1. The proposed architecture uses both low-interaction and high-interaction honey pots, increasing the efficiency of such a system in terms of attack discovery. The proposed architecture type requires fewer interventions into the configuration of the security computer system, related to the reinstallation of successfully compromised honey pots.

3.1.1 Access Management

This part of the proposed architecture consists of honeypots acting as computers connected directly to the Internet, having public IP addresses. A further part of the management is Honeywall – a tool limiting the speed of the Internet connection to 10 MB per hour, the number of TCP sessions to 100 sessions per hour and thus limiting bandwidth.

The network operation analyser and Honeywall are mutually separated. The reason for this separation is to minimise the threat to the protected computers if the network analyser is compromised. Should the network analyser get compromised and should it be used for an attack beyond the system, the chances of such an endeavour are minimal since Honeywall is configured to limit bandwidth.

3.1.2 Honeypot Cluster

The honeypot cluster consists of high-interaction honeypots, which are again clustered. In the proposed architecture (Fig. 1), there are three types of honeypots: a GNU/Linux OS with MAC access management, a GNU/Linux OS with DAC access management and representing MS-Windows operating systems. Every computer used as a honeypot has two network interfaces configured. One of these has a public IP address, while the other has a local one, such as 172.30.3.X.

By adding a private IP address to the second network interface, all honeypots are interconnected in a separate local network. By creating a local honeypot network, we limit the attackers' attempts only to local devices. This local network consists of 14 honeypots without any firewall installed.

Every honeypot using GNU/LINUX OS contains a modified OpenSSH service, which simplifies opening new relations for the attacker. As soon as the attacker tries to log in to one of the honeypots with the aforementioned configuration using an SSH connection and a brute force attack, the modified OpenSSH service shall generate a separate account for the attacker.

This part of the proposed architecture creates an account in the system for the attacker, along with a regular home directory. The created account is persistent, which allows authorisation of the attacker if he decides to return later, to continue the attack. To allow capturing all attacker activities, there are multiple IDS systems and security tools available for GNU/LINUX distributions, as well as Windows operating systems.

These intrusion detection systems monitor four types of information resources:

- system activities (system calls and processes);
- system file integrity;
- the kernel and the logging daemons;
- Bash relations.

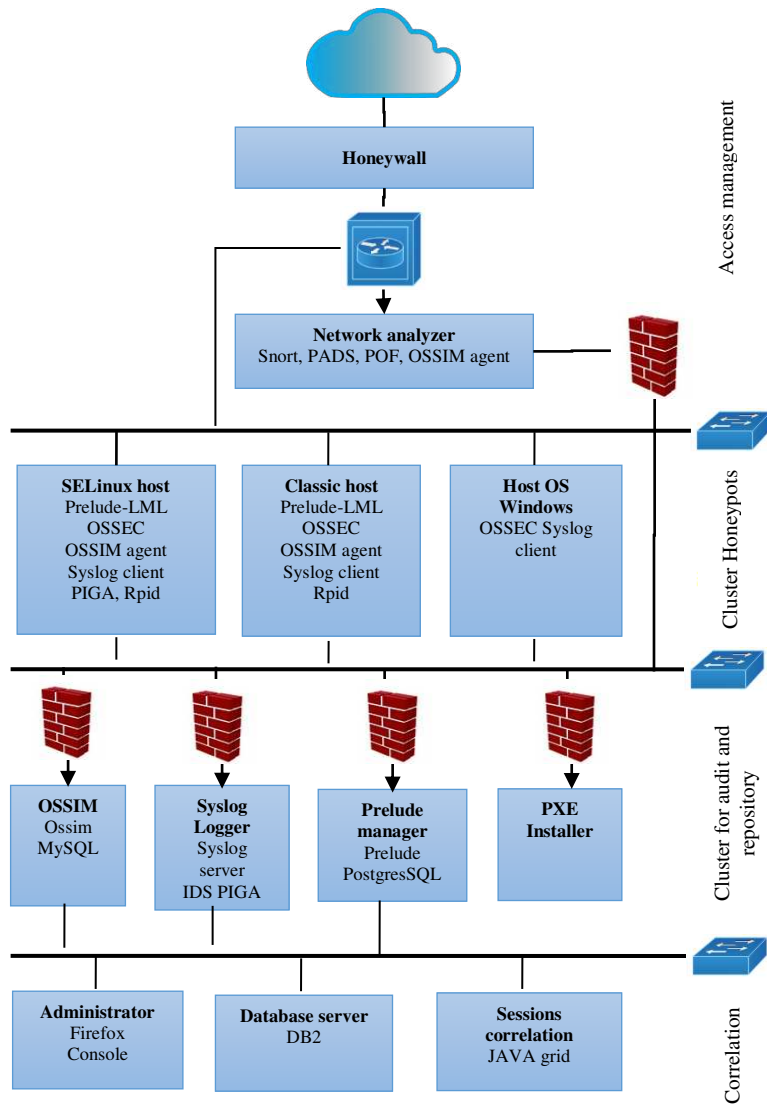


Figure 1: Clustered high-interaction honeypot architecture

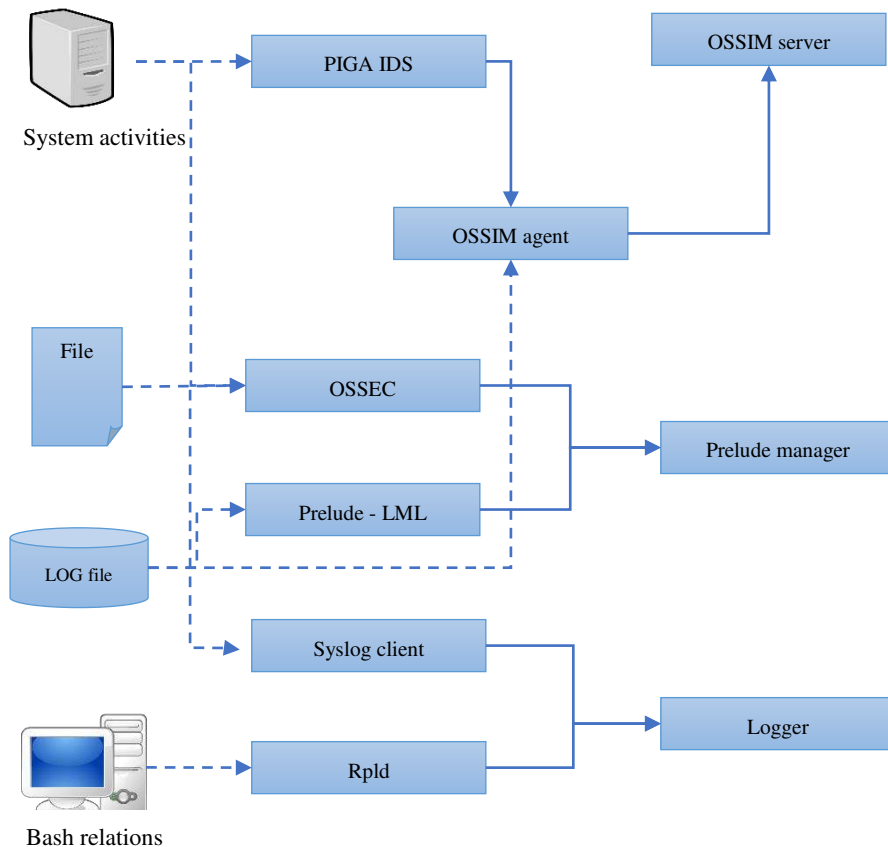


Figure 2

Tools and intrusion detection systems monitoring activity on the hosts

The gathered information shall then be used to discover the correlation between the host processes and network activity. Figure 2 is a summary of the data used by the respective security agents (using a dashed line). All registered alarms, logs, and relations are sent to another cluster of the proposed architecture – the cluster aimed at auditing and storage of the recorded data.

3.1.3 Auditing and Storage Cluster

The third part of the proposed architecture is dedicated to the storage and subsequent analysis of the registered alarms and logging records. Data storage equipment is connected to the network, e.g. using the 172.30.3.0 prefix. The whole auditing and storage cluster is protected by a firewall. This is configured to allow only incoming network traffic, the only allowed and opened ports are those used by the security tools OSSIM (gathers alarms generated by the Piga IDS and

analyses system log files), Prelude-LML (system log analyser reporting system activities) and the Syslog tool, dedicated to the servers (transfers kernel and system log files to the logger).

To gather all events and report alarms in a human-readable form, three analytic frameworks are used in the proposed solution:

- OSSIM – provides a security information management framework. The framework itself generates reports, aggregate alarms, and triggers incidents. It writes the gathered data into a MySQL database. If necessary, the framework may be configured to store data in a MySQL cluster server.
- Prelude manager – it aggregates the gathered data, it also provides means to visualise the data on websites. All registered events are stored using the Intrusion Detection Message Exchange (IDMEF) standard and a PostgreSQL server. If necessary, the framework may be configured to store data in a cluster.
- System logger – stores all syslog messages generated by any honeypot in a Lustre distributed file system.

All network and system alarms are stored by the system manager, which also allows their visualisation. Since these three frameworks do not use the same data recording standard, they have to be connected to the correlation part of the proposed clustered honeypot. One of the main advantages of using three different standards on the recording servers is that by this approach, it is harder to remove any attack analysis files generated by the honeypots. Such files include logging files, network communication fingerprints, and/or other activities.

3.1.4 Correlation

To visualise the recorded alarms, we shall use the last part of the proposed architecture, the correlation part. As a process, the task of correlation is to describe attacks by means of network and host IDS alarms. The algorithms used in the correlation part are open source, with minimum modifications performed to them. These algorithms use all three databases of the respective frameworks (OSSIM, Prelude manager and Syslog logger), using a private network, such as the one having the prefix 10.0.0.0. To optimise the execution times of the aforementioned algorithms, an available Java application was used.

3.2 Security Elements of the Proposed Architecture

A disadvantage of the proposed architecture is that they make real computer systems available for interaction with the attackers and thus the freight that the attacker manages to gain root privileges and conquer the honeypot is a real. Therefore, additional security elements have been implemented in the proposed

clustered hybrid honeypot, demonstrably increasing the security level of both the honeypot and the computer system, in which the clustered honeypot shall be operated.

3.2.1 Verification Module

During the interaction with the attacker, the verification module used in the clustered hybrid honeypot implementation manages all outgoing DNS requests to the Snort network intrusion detection tool, which stores them in log files for further analysis. Snort manages all outgoing traffic – it allows only using the attacker's IP address. Should Honeywall be compromised, any connection attempts will result in initiating the stability check process, or, eventually, restoring the original settings of the whole security system.

3.2.2 MAC Access Control

This access type makes sure root users cannot achieve super administrator privileges. The only way to gain super administrator privileges is to exploit a kernel bug or to successfully attack the MAC mechanism, i.e. to surpass SE Linux. If the attacker succeeds, the system shall be considered compromised and shall be reinstalled using the Pre eXecution Environment (PXE) server. The main advantage of using MAC access control is that honeypots using this access control type are persistent in time. If the same attacker performs a repeated attack, this access control type prevents the detection of system re-installation. In addition to this, all shell activities shall be recorded using an Rpld server.

3.2.3 DAC Access Control

This traditional access control system may be easily compromised by attackers. If the attacker manages to gain administrator privileges, the particular honeypot must be reinstalled using the PXE server. The main disadvantage of honeypots using this access control type is the associated higher administration costs. The registered alarms have to be inspected – it is up to the administrator to decide about the extent, to which the system is compromised and whether the honeypot has to be reinstalled or not.

To simplify the analysis in case of this honeypot type, a cron time-based job scheduler was implemented under Linux to monitor the changes to the file system of the Honeypot during its operation. If any file of the honeypot differs from the corresponding file stored at the PXE server, the system automatically generates and sends a warning to the administrator using the OSSEC integrity analyser, while simultaneously storing the specific difference at the PXE server for further analysis.

3.2.4 Automatic Installation of the Clustered High Interaction Honeypot

The PXE server shall use a TFTP server dedicated to the re-installation process if any of the high-interaction honeypots get compromised. Currently, the PXE server allows re-installation of the following honeypot types:

- SELinux with MAC based on Debian, Gentoo, Fedora, Ubuntu and RedHat GNU/Linux distributions.
- SELinux with DAC based on Debian, Gentoo and Ubuntu GNU/Linux distributions.
- MS Windows XP, Vista, 7 and 8.1 systems.

The PXE server is primarily used to re-install compromised honeypots using the PXE protocol in the private network, with a prefix of 172.30.3.0, for example.

4 Experimental Proof

To provide an experimental proof of the functionality of the proposed architecture, we selected a heterogenous computer network, following the concept model of the proposed clustered hybrid high-interaction honeypot security architecture (Fig. 1). The testing environment consisted of the following:

- The network of the student hostels of the Technical University in Košice, at Jedlíkova Street (the ŠD TUKE heterogeneous network with approximately 1,600 active users). In this environment, we verified the functionality of the clustered hybrid honeypot in terms of honeypot recovery.
- A closed network of the Institute of Computer Technology (ICT) at the Technical University of Košice (the ICT TUKE simulated and partly emulated heterogeneous network). We also verified the functionality of the clustered hybrid honeypot in terms of monitoring its behaviour during specific types of attacks, in a secure environment.

The verification processes were based on the execution of multiple experiments. The following chapters present the results of the experimental proof of functionality of the proposed clustered honeypot architecture and its respective parts.

4.1 Attacks Registered by the Honeypots

The first experiment was aimed at the influence of the applied access control policy – MAC and DAC, respectively – on the amount of alarms generated by the respective honeypots. Most generated alarms were issued by GNU/Linux

distributions with MAC access control policy (Fig. 3). Honeypots using DAC access control generated fewer alarms. The lower alarm count of honeypots using DAC access control can be explained in two ways. The DAC honeypots were assigned public IP addresses significantly later, while until then, the specific honeypots were subject to attacks only from the closed network. In this case, the Snort tool did not report any activity from the DAC honeypots. The second cause of the reported values was the impossibility of using the Piga IDS without using the MAC access policy, which also significantly impacted the number of generated alarms. Figure 3 shows an attack aimed at the logging server itself, in spite of the fact that no public IP address was allocated to it and it was protected by a firewall.

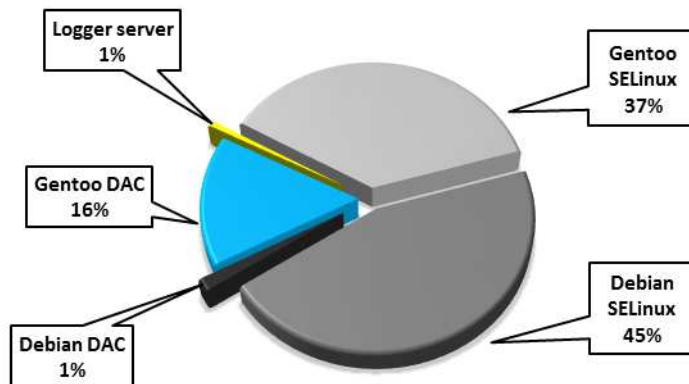


Figure 3

Generated alarms, by the respective hosts

During the experiment, we have not experienced any targeted attacks against specific Linux distributions.

4.2 Statistical Results of Intrusion Detection Tools

During the proof of functionality of the proposed architecture, a total of 2,469,840 events and 97,116 alarms were recorded in the respective server databases. That amounts to 1140 events and 45 alarms per hour. The events included also user login events. Alarms included also suspicious events, such as the discovery of bad packets, which also indicate attacks. During the experiment, we used also Snort. In the phase of detailed analysis, most alarms generated by Snort were evaluated subsequently as false alarms. Figure 4 shows the rate of alarms generated by the honeypots and the respective security tools.

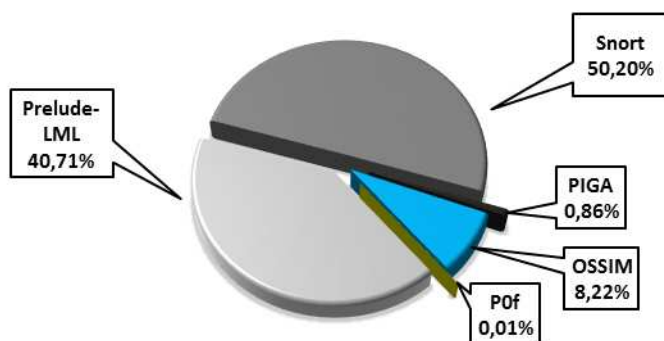


Figure 4

Generated alarms, by the respective IDS sensors

Snort generates a number of false alarms that are caused by the way, when detecting attacks. Snort detects attacks by using a database of signatures and attack patterns, which it compares to ongoing network traffic. The tool itself cannot correctly tell, whether the attack is real or successful. Due to this, in the proposed architecture, we included the Piga IDS to eliminate false alarms generated by the Snort NIDS. During the experiment, Piga recorded 13,965 open relations due to automated network environment scanning and only 779 relations performing any activity on the monitored honeypots.

Table 1

The main types of registered alarms

Detection sensor	Description	Count
Prelude-LML	SShd: Root login refused	124 617
Snort	Destination udp port not reachable	113 002
Prelude-LML	SShd: Bad password	27 305
OSSIM	SShd: Possible brute force tentative	13 361
Prelude-LML	SShd: Invalid user	10 827
PIGA	Integrity: system file modification	10 265
Prelude-LML	FTP bad login	5 341
Snort	Potential outbound SSH scan	4 995
PIGA	Confidentiality: information flow	4 047

The data in table 1 show the most frequent alarms registered by the intrusion detection system sensors. The most frequent were brute force attacks occurring with SSH connections, trying to break the password of the user and gain access to the system – in this case, a honeypot. The use of brute force resulted in the generation of vast numbers of alarms. Please note that the targets of brute force attacks were also FTP accounts.

As far as outgoing traffic is concerned, Snort found not less than 4995 SSH scanning procedures, trying to use user accounts to attack other equipment in the network. Since all honeypots were connected to a single local network, in the proposed architecture, this resulted only in further interaction with honeypots.

Piga registered some cases of modifying configuration files. In addition to the modification of files, it also registered information streaming mostly from these files to the system file folders of other users. On GNU/Linux distributions, these folders included `/etc/shadow`, `/etc/apache` and `/httpd.conf`, respectively.

The total share of alarms generated by Snort amounted to 50.20%. These alarms included UDP port scanning (160,502 activities), as well as a number of lower severity alarms, as far as the protected system was concerned. The analysis of the generated alarms in terms of the respective ports, as shown in Figure 5, corresponding to the data of table 1, clearly shows the dominance of activities aimed at SSH port 22/TCP. The next most popular was HTTP port 80/TCP, attacked in most cases from the outside, attempting the installation of phishing websites. Harmful ICMP packets amounted to a significant 10%. Other standard ports were used to exploit vulnerabilities of MS Windows, mainly by worms attempting to spread. The ports of the IRC protocol were mostly used by bots installed in the honeypots with the aim to create connections from the infected system to the Internet using different IRC channels. Using these newly created IRC channels the attacker may remotely control any of the installed bots.

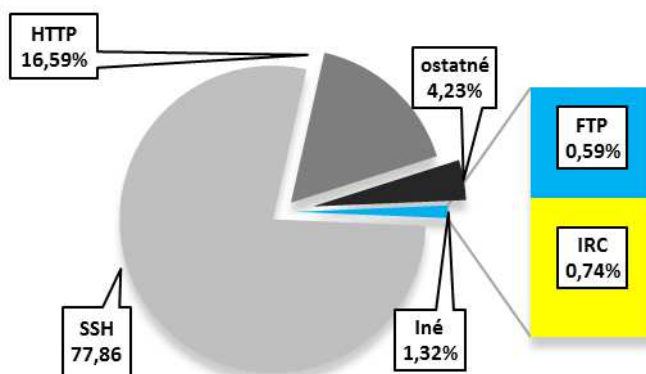


Figure 5

Generated alarms, by the respective ports

4.3 Malware Activity

A further experiment showed that the attackers used mostly i386 binary files to automate the attacks; these were most probably programs are written in C. Often, the attackers resorted to recompiling programs written in C directly on compromised honeypots. The experiment showed unusual attack types – programs

written in Pascal, C++ and/or shell scripts. The aim of these attacks was to perform automated operations to execute or compile malware source code. We also detected files containing malware documentation. The following table represents data related to the detected malware, installed by attackers into the corresponding testing environment.

Table 2
Main types of detected malware

Presence in the home folder	Presence in the /tmp folder	Malware type
46	48	Dynamically linked ELF 32-bit LSB executable (uses shared libs)
35	25	C source code (ASCII text file)
9	11	Shell script
4	3	Pascal source code (ASCII text file)
2	5	Statically linked ELF 32-bit LSB executable
1	0	Mach-O binaries / PPC binaries
1	3	C++ source code documentation

Conclusions

The proposed architecture allows detection of attacks and identification of tools and methods used by attackers and thus to improve the security of the computer network, in which the aforementioned security architecture is being used. An advantage of this solution is that if the specific honeypot is configured correctly, it can actively attract the attention of the attacker, immediately after being started and thus minimise the risk of compromising the protected system within the particular network.

The functionality of the proposed solution, i.e. the threat-detection capability of the presented architecture has been proven experimentally.

The results of the experiments showed that the proposed clustered high interaction hybrid honeypot security architecture can efficiently emulate typical services of low-interaction honeypots cooperating with high-interaction honeypots, without the necessity to create complicated low-interaction honeypot scripts manually. By using multiple IP addresses allocated to low-interaction honeypots and the Honeyd tool, the proposed clustered honeypot architecture is capable of filtering and analysing system operation, pursuant to the predefined requirements. One of the main advantages of Honeyd is the capability to simultaneously simulate virtual low-interaction honeypots. It has been experimentally proven that during the simulation of a LAN network, Honeyd could successfully simulate up to 65,536 heterogeneous devices of various kinds and functions. Honeyd requires an

appropriate configuration of the host hardware server/workstation configuration to correctly operate and run.

The analysis of the events registered by the intrusion detection systems showed that in almost every case, the host environment is being scanned before the attack to gather the most detailed information about the target computer. Following the acquisition of such information and their analysis, the attacker can identify the weaknesses of the protected system.

Acknowledgements

This work was supported by the Faculty of Electrical Engineering and Informatics, Technical University of Košice under the contract No. FEI-2018-59: Semantic Machine of Source-Oriented Transparent Intensional Logic and by KEGA Agency of the Ministry of Education, Science, Research and Sport of the Slovak Republic under Grant No. 003TUKE-4/2017 „Implementation of Modern Methods and Education Forms in the Area of Security of Information and Communication Technologies towards Requirements of Labour Market“.

References

- [1] S. Y. Lim, M. L. M. Kiah, and T. F. Ang, “Security Issues and Future Challenges of Cloud Service Authentication,” *Acta Polytechnica Hungarica*, Vol. 14, No. 2, pp. 69-89, 2017
- [2] L. Vokorokos, A. Pekár, N. Ádám, and P. Darányi, “Yet Another Attempt in User Authentication,” *Acta Polytechnica Hungarica*, Vol. 10, No. 3, pp. 37-50, 2013
- [3] M. Uchnár and J. Hurtuk, “Safe user authentication in a network environment,” in 2017 IEEE 15th International Symposium on Applied Machine Intelligence and Informatics (SAMII), 2017, pp. 000451–000454
- [4] Prajitha M V, Rekha P, and Amrutha George A, “A secured authentication protocol which resist password reuse attack,” in 2015 International Conference on Innovations in Information, Embedded and Communication Systems (ICIIECS), 2015, pp. 1-5
- [5] A. Balaz and R. Hlinka, “Forensic Analysis of Compromised Systems,” in 10th IEEE International Conference on Emerging Elearning Technologies and Applications (ICETA 2012), New York, USA, 2012, pp. 27-30
- [6] L. Vokorokos, A. Baláž, and N. Ádám, “Secure web server system resources utilization,” *Acta Polytechnica Hungarica*, Vol. 12, No. 2, pp. 5-19, 2015
- [7] M. K. A, *Learning Malware Analysis: Explore the concepts, tools, and techniques to analyze and investigate Windows malware*. Packt Publishing, 2018

-
- [8] W. A. Conklin, G. White, C. Cothren, R. L. Davis, and D. Williams, *Principles of Computer Security: CompTIA Security+ and Beyond*, Fifth Edition. McGraw-Hill Education, 2018
- [9] L. Vokorokos, J. Hurtuk, and B. Madoš, "Malware categorization and recognition problem," in *IEEE 18th International Conference on Intelligent Engineering Systems INES 2014*, 2014, pp. 105-108
- [10] J. Hurtuk, B. Madoš, Š. Halčín, "Sound-based communication in the process of malware distribution", in *Acta Electrotechnica et Informatica*, Vol. 15, No. 2, 2015, pp. 62-65
- [11] L. Vokorokos, B. Madoš, M. Čajkovský, J. Hurtuk, and K. Moravčík, "Analysis of the Software Behaviour Using Forensic Methods for Computer Security Purposes", in *Acta Electrotechnica et Informatica*, Vol. 14, No. 2, 2014, pp. 36-40
- [12] J. A. P. Marpaung, M. Sain, and Hoon-Jae Lee, "Survey on malware evasion techniques: State of the art and challenges," in *2012 14th International Conference on Advanced Communication Technology (ICACT)*, 2012, pp. 744-749
- [13] L. Vokorokos, A. Baláž, and B. Madoš, "Application Security through Sandbox Virtualization", *Acta Polytechnica Hungarica*, Vol. 12, No. 1, pp. 83-101, 2015
- [14] A. Borkar, A. Donode, and A. Kumari, "A survey on Intrusion Detection System (IDS) and Internal Intrusion Detection and protection system (IIDPS)," in *2017 International Conference on Inventive Computing and Informatics (ICICI)*, 2017, pp. 949-953
- [15] L. Vokorokos, A. Baláž, and M. Chovanec, "Intrusion detection system using self organizing map", in *Acta Electrotechnica et Informatica*, Vol. 6, No. 1, 2006, pp. 81-86
- [16] L. Dali et al., "A survey of intrusion detection system," in *2015 2nd World Symposium on Web Applications and Networking*, 2015, pp. 1-6
- [17] L. Vokorokos, M. Ennert, M. Čajkovský, and J. Radušovský, "A Survey of parallel intrusion detection on graphical processors," *Central European Journal of Computer Science*, Vol. 4, No. 4, pp. 222-230, Dec. 2014
- [18] L. Vokorokos, A. Baláž, and M. Chovanec, "Distributed Detection System of Security Intrusions Based on Partially Ordered Events and Patterns," in *Towards Intelligent Engineering and Information Technology*, Heidelberg: Springer Berlin Heidelberg, 2009, pp. 389-403
- [19] F. Sabahi, and A. Movaghar, "Intrusion Detection: A Survey," in *2008 Third International Conference on Systems and Networks Communications*, 2008, pp. 23-26

- [20] L. Vokorokos, A. Baláz, and B. Madoš, “Anomaly and Misuse Intrusions Variability Detection”, in *Acta Electrotechnica et Informatica*, Vol. 10, No. 4, 2010, pp. 5-9
- [21] E. Chovancová, and N. Ádám, “The Security of Heterogeneous Systems based on Cluster High-interaction Hybrid Honeypot,” in *2019 IEEE 23rd International Conference on Intelligent Engineering Systems (INES)*, 2019, pp. 81-85
- [22] J. Briffaut, J. Rouzaud-Cornabas, C. Toinard, and Y. Zemali, “A new approach to enforce the security properties of a clustered high-interaction honeypot,” in *2009 International Conference on High Performance Computing Simulation*, 2009, pp. 184-192
- [23] S. Morishita et al., “Detect Me If You... Oh Wait. An Internet-Wide View of Self-Revealing Honeybots,” in *2019 IFIP/IEEE Symposium on Integrated Network and Service Management (IM)*, 2019, pp. 134-143
- [24] D. Fraunholz, M. Zimmermann, and H. D. Schotten, “An adaptive honeypot configuration, deployment and maintenance strategy,” in *2017 19th International Conference on Advanced Communication Technology (ICACT)*, 2017, pp. 53-57
- [25] R. M. Campbell, K. Padayachee, and T. Masombuka, “A survey of honeypot research: Trends and opportunities,” in *2015 10th International Conference for Internet Technology and Secured Transactions (ICITST)*, 2015, pp. 208-212
- [26] P. Fanfara, M. Dufala, and J. Radušovský, “Autonomous Hybrid Honeypot as the Future of Distributed Computer Systems Security,” *Acta Polytechnica Hungarica*, Vol. 10, pp. 25-42, 2013
- [27] L. Vokorokos, P. Fanfara, J. Radušovský, and P. Poór, “Sophisticated Honeybot mechanism – the autonomous hybrid solution for enhancing computer system security,” in *2013 IEEE 11th International Symposium on Applied Machine Intelligence and Informatics (SAMII)*, 2013, pp. 41-46
- [28] E. Chovancova et al., “Securing Distributed Computer Systems Using an Advanced Sophisticated Hybrid Honeybot Technology,” *Computing and Informatics*, Vol. 36, No. 1, pp. 113-139, 2017
- [29] K. G. Anagnostakis, “Shadow Honeybots,” *International Journal of Computer and Network Security*, Vol. 2, No. 9, September 2010

Constructing Correlation Coefficients from Similarity and Dissimilarity Functions

Ildar Z. Batyrshin

Centro de Investigacion en Computacion, CIC-IPN, Av. Juan de Dios Bátiz S/N,
Nueva Industrial Vallejo, Gustavo A. Madero, 07738 Ciudad de México, CDMX,
e-mail: batyr1@cic.ipn.mx

Abstract. Correlation coefficients (association measures) were introduced more than one hundred years ago as measures of relationship between variables that usually belong to one of the following basic types: continuous, ordinal, or categorical. Nowadays, it appears the growing demand for the development of new correlation coefficients for measuring associations between variables or objects with more sophisticated structures. The paper presents a non-statistical, functional approach to the study of correlation coefficients. It discusses the methods of construction of correlation coefficients using similarity and dissimilarity measures. Generally, all these measures are considered as functions defined on the underlying (universal) domain and satisfying some sets of properties. The methods of construction of correlation functions on the universal domain can be easily applied for constructing correlation coefficients for specific types of data. The paper introduces a new class of correlation functions, satisfying a weaker set of properties than the previously considered correlation functions (association measures) defined on a set with involution (negation) operation called here strong correlation functions. The methods of constructing both types of correlation functions are discussed. The one-to-one correspondence between the strong correlation functions and the bipolar similarity and dissimilarity functions is established. The theoretical results illustrated by examples of construction of classical Pearson's product-moment correlation coefficient, Spearman's and Kendall's rank correlation coefficients, etc. from similarity and dissimilarity functions.

Keywords: similarity; dissimilarity; correlation; association; Spearman's and Kendall's rank correlations; Pearson's correlation; cosine similarity, and cosine correlation

1 Introduction

Similarity and association measures actively studied more than one hundred years as measures of relationship between data initially in pattern classification and statistics and later in data mining and machine learning [1, 9-11, 13, 14, 16-20]. Correlation coefficients (association measures) were introduced in statistics as measures of the relationship between variables of one of the following types: continuous, ordinal, or categorical. Nowadays, we see the growing demand for

measuring the relationship between data with diverse structures: sequences and time series, rating profiles, vectors with different attributes, fuzzy sets, matrices, images, texts with syntactic structures, etc. An application of classical correlation coefficients to new types of data often impossible or gives misleading results. For this reason, to have the correlation coefficients specific for the analyzed data type is of great interest.

The paper considers the methods of construction of correlation coefficients using similarity and dissimilarity measures defined on an underlying set referred to as a universal domain. One can easily apply these methods to a specific type of data. The similarity, dissimilarity, and correlation measures are considered as functions satisfying some sets of properties [3, 4, 8]. This paper introduces a new class of correlation functions, satisfying a weaker set of properties than the previously considered correlation functions (association measures) [4, 8] called here strong correlation functions and defined on a set with involution (negation) operation. We discuss the methods of constructing both types of correlation functions using (dis)similarity functions. We establish the one-to-one correspondence between the strong correlation functions and “bipolar” (dis)similarity functions. The examples of the construction of correlation coefficients for specific domains illustrate the theoretical results.

The paper has the following structure. Section 2 gives definitions of similarity and dissimilarity functions. Sections 3 and 4 consider the methods of construction of strong correlation functions (association measures) on the set with involution operation. In Section 5, we introduce generalized correlation functions that can be defined on a set without involution operation and study their relationships with (dis)similarity functions. In Section 6 we establish one-to-one correspondence between strong correlation functions and bipolar (dis)similarity functions. Section 7 discusses related works and includes the conclusion.

2 Similarity and Dissimilarity Functions

The paper considers similarity, dissimilarity, and correlation measures or coefficients as functions defined on some nonempty underlying set Ω [8]. As such set one can use, for example, any specific domain: the set of all real-valued n -tuples, the set of binary vectors, the set of membership values, the set of images, etc. To emphasize that the underlying set Ω is not a specific domain but any domain this set will be referred to as a universal domain.

Definition 1. A similarity function on a set Ω is a function $S: \Omega \times \Omega \rightarrow [0, 1]$ satisfying for all x, y in Ω the properties:

$$S(x, y) = S(y, x), \quad (\text{symmetry})$$

$$S(x, x) = 1. \quad (\text{reflexivity})$$

If for some x, y in Ω it is fulfilled:

$$S(x, y) = 0,$$

then S is called *(0)-normal* (in (x, y)).

Definition 2. A dissimilarity function on a set Ω is a function $D: \Omega \times \Omega \rightarrow [0, 1]$ satisfying for all x, y in Ω the properties:

$$D(x, y) = D(y, x), \quad (\text{symmetry})$$

$$D(x, x) = 0. \quad (\text{irreflexivity})$$

If for some x, y in Ω it is fulfilled:

$$D(x, y) = 1,$$

then D is called *1-normal* (in (x, y)).

Dissimilarity functions are *dual* to similarity functions.

Definition 3. Similarity S and dissimilarity D functions are called complementary if for all x, y in Ω it is fulfilled:

$$S(x, y) + D(x, y) = 1.$$

One can obtain one of these functions from the corresponding complementary function for all x, y in Ω as follows:

$$S(x, y) = 1 - D(x, y),$$

$$D(x, y) = 1 - S(x, y).$$

It is clear that a similarity function is 0-normal if and only if its complementary dissimilarity function is 1-normal.

Example 1. Let Ω be a set of nonnegative real-valued n -tuples $x = (x_1, \dots, x_n)$ such that $x \neq (0, \dots, 0)$. Then for any $x = (x_1, \dots, x_n)$ and $y = (y_1, \dots, y_n)$ in Ω the following function:

$$S(x, y) = \frac{\sum_{i=1}^n x_i y_i}{\sqrt{\sum_{i=1}^n x_i^2} \sqrt{\sum_{i=1}^n y_i^2}},$$

is the symmetric and reflexive similarity function called a *cosine similarity measure* and denoted as $\cos(x, y)$. It is 0-normal for orthogonal pairs of n -tuples x and y such that $x_i y_i = 0$ for all $i=1, \dots, n$.

The similarity function $\cos(x, y)$ has the following complementary dissimilarity function [8]:

$$D(x, y) = \frac{1}{2} \sum_{i=1}^n \left(\frac{x_i}{\sqrt{\sum_{i=1}^n x_i^2}} - \frac{y_i}{\sqrt{\sum_{i=1}^n y_i^2}} \right)^2.$$

Due to the duality of similarity and dissimilarity functions, one can consider only one of these functions, but they have different interpretations and methods of construction; hence, we consider them together. These functions studied in [8]. For short, we call them also (dis)similarity functions.

3 Strong Correlation Functions

The correlation functions (association measures) were introduced in [3, 4, 8] on a universal domain Ω with an involutive operation N as functions satisfying several properties of Pearson's product-moment correlation coefficient. Here these correlation functions called strong correlation functions. The methods of construction of correlation functions using similarity functions have been proposed, and it was shown how the Pearson's correlation and Yule's Q association coefficient could be constructed using suitable similarity functions [2, 5, 8]. In the following sections, we will consider correlation functions satisfying a weaker set of properties.

Definition 4. A function $N:\Omega\rightarrow\Omega$ satisfying for all x in Ω the property:

$$N(N(x))=x, \quad (\text{involutivity})$$

is called a *reflection* or a *negation* on Ω if it is not an identity function, i.e. if for some x in Ω it is fulfilled:

$$N(x) \neq x.$$

An element x in Ω such that $N(x) = x$ is called a *fixed point* and the set of all fixed points of the negation N in Ω is denoted as $FP(N, \Omega)$ or $FP(\Omega)$.

Below $\Omega \setminus FP(\Omega)$ denotes the set of all elements in Ω , which are not fixed points. The set $FP(\Omega)$ can be empty. It is easy to show that the set $\Omega \setminus FP(\Omega)$ is closed under reflection operation.

Proposition 1 [4]. Let $N:V\rightarrow V$ be a reflection on a set V , and $R:V\times V\rightarrow R$ be a symmetric real-valued function, i.e.:

$$R(x,y) = R(y,x),$$

for all x,y in V . The function R satisfies for all x,y in V the property:

$$R(N(x),N(y)) = R(x,y),$$

if and only if it is fulfilled:

$$R(x,N(y)) = R(N(x),y).$$

Symmetric function R satisfying these properties will be called a *co-symmetric* function [8]. Further, we will consider co-symmetric similarity, dissimilarity, and correlation functions.

A similarity function $S: V \times V \rightarrow [0, 1]$ satisfying for all x, y in V the property:

$$S(x, N(x)) = 0,$$

is called a *consistent* similarity function [8].

Dually, a dissimilarity function $D: V \times V \rightarrow [0, 1]$ will be called a *consistent* dissimilarity function if for all x, y in V it is fulfilled:

$$D(x, N(x)) = 1.$$

A similarity function S is consistent or co-symmetric if and only if its complementary dissimilarity function is consistent or co-symmetric, respectively.

Definition 5 [4]. Let N be a reflection on Ω and V be a subset of $\Omega \setminus FP(\Omega)$ closed under N . A *strong correlation function* (association measure) on V is a function $A: V \times V \rightarrow [-1, 1]$ satisfying for all x, y in V the properties:

$$A(x, y) = A(y, x), \quad (\text{symmetry})$$

$$A(x, x) = 1, \quad (\text{reflexivity})$$

$$A(x, N(y)) = -A(x, y). \quad (\text{inverse relationship}) \quad (1)$$

A strong correlation function will be also referred to as an *invertible correlation function*.

Proposition 2 [4]. A strong correlation function A on V satisfies for all x, y in V the following properties:

$$A(x, N(x)) = -1,$$

$$A(N(x), N(y)) = A(x, y). \quad (\text{co-symmetry})$$

Example 2. Let Ω be the set of all real-valued n -tuples $x = (x_1, \dots, x_n)$ with the reflection operation $N(x) = -x = (-x_1, \dots, -x_n)$. Let V be a set of all non-constant n -tuples from Ω such that $x \neq (q, \dots, q)$ for any real value q . It is clear that V is closed under N , and it has no fixed elements. It is easy to check that the Pearson's product-moment correlation coefficient:

$$A(x, y) = \frac{\sum_{i=1}^n (x_i - \bar{x})(y_i - \bar{y})}{\sqrt{\sum_{i=1}^n (x_i - \bar{x})^2} \sqrt{\sum_{i=1}^n (y_i - \bar{y})^2}}, \quad (2)$$

where $\bar{x} = \frac{1}{n} \sum_{i=1}^n x_i$, $\bar{y} = \frac{1}{n} \sum_{i=1}^n y_i$ is the strong correlation function on V .

Consider the methods of construction of strong correlation functions (association measures) [3, 4, 8].

Theorem 1. Let N be a reflection on Ω and V be a nonempty subset of $\Omega \setminus FP(\Omega)$ closed under N . Let $S: V \times V \rightarrow [0, 1]$ be a co-symmetric and consistent similarity function, then the function $A: V \times V \rightarrow [-1, 1]$ defined for all x, y in V by

$$A(x, y) = S(x, y) - S(x, N(y)), \quad (3)$$

is a strong correlation function on V .

The formula (3) has a simple interpretation: *the correlation between x and y is positive if x is more similar to y than to its negation, and the correlation is negative in the opposite case.*

Replacing in (3) the similarity function S by the complementary dissimilarity function: $D(x,y) = 1 - S(x,y)$ obtain the following formula for constructing a strong correlation function from a co-symmetric and consistent dissimilarity function:

$$A(x,y) = D(x,N(y)) - D(x,y). \quad (4)$$

This formula can be more convenient than (3) for constructing strong correlation functions when we use distance-based dissimilarity functions [8].

Example 3 [2, 5, 8]. Consider the dissimilarity function on the set V of non-constant n -tuples (see Example 2) that generates by (4) the Pearson's product-moment correlation coefficient (2):

$$D(x, y) = \frac{1}{4} \sum_{i=1}^n \left(\frac{x_i - \bar{x}}{\sqrt{\sum_{i=1}^n (x_i - \bar{x})^2}} - \frac{y_i - \bar{y}}{\sqrt{\sum_{i=1}^n (y_i - \bar{y})^2}} \right)^2.$$

One can check that it is co-symmetric and consistent.

Example 4. If the cosine function from Example 1 is defined on the set of all nonzero real-valued n -tuples with the negation operation $N(x) = -x = (-x_1, \dots, -x_n)$, then it will satisfy the properties of the strong correlation function and can be generated by (4) using the following dissimilarity function [8]:

$$D(x, y) = \frac{1}{4} \sum_{i=1}^n \left(\frac{x_i}{\sqrt{\sum_{i=1}^n x_i^2}} - \frac{y_i}{\sqrt{\sum_{i=1}^n y_i^2}} \right)^2.$$

This dissimilarity function is co-symmetric and consistent.

As it follows from Examples 1 and 4, the cosine function will be the similarity function if it is defined on the set of nonzero, nonnegative real-valued n -tuples, and it will be the strong correlation function if it is defined on the set of nonzero real-valued n -tuples [8]. The cosine is often used as a similarity measure between the texts represented by vectors of attributes where x_i equals to the frequency of appearing of the i th attribute in the text [18]. In this case, all vector components take nonnegative values. As a correlation function, the cosine used, for example, in measuring associations between time series presented by sequences of local trends that can have positive and negative values [2, 6]. Generally, the cosine correlation can be used instead of Pearson's correlation on the set of real-valued n -tuples when the calculation of means used in Pearson's correlation has not much sense, for example, when the signs of the elements of n -tuples are important, or these elements contain the values of attributes measured in different scales.

4 Pseudo-Differences in Constructing Strong Correlation Functions

Let $TC: [0,1] \times [0,1] \rightarrow [0,1]$ be a t -conorm [15], i.e. commutative, associative, monotonic function satisfying boundary condition: $TC(a,0) = 0$, for all a in $[0,1]$. Usually, t -conorm is denoted by the letter S , but in this paper, the symbol S is used for similarity functions and similarity measures, for this reason, we denote t -conorm as TC .

We will say that a t -conorm TC has no nilpotent elements if for all a, b in $[0,1]$ it is fulfilled: $TC(a,b) = 1$ if and only if $a = 1$ or $b = 1$.

Consider the examples of basic t -conorms defined for all a, b in $[0,1]$ as follows [15]:

$$TC_M(a,b) = \max(a,b), \quad (\text{maximum})$$

$$TC_P(a,b) = a+b-ab, \quad (\text{probabilistic sum})$$

$$TC_L(a,b) = \min(a+b, 1). \quad (\text{Lukasiewicz } t\text{-conorm})$$

t -conorms TC_M and TC_P have no nilpotent elements but TC_L has.

Definition 6 [12]. Let TC be a t -conorm. A pseudo-difference operation Θ_{TC} associated to TC is defined for all a, b in $[0,1]$ as follows:

$$a \Theta_{TC} b = \begin{cases} a^{TC}b & \text{if } a > b \\ -(b^{TC}a) & \text{if } a < b, \\ 0 & \text{if } a = b \end{cases}$$

where $a^{TC}b$ is the TC -difference defined by:

$$a^{TC}b = \inf\{c \in [0,1] | TC(b,c) \geq a\}.$$

Consider the pseudo-difference operations associated to basic t -conorms [12]:

$$a \Theta_M b = \begin{cases} a & \text{if } a > b \\ -b & \text{if } a < b, \\ 0 & \text{if } a = b \end{cases}$$

$$a \Theta_P b = \begin{cases} \frac{a-b}{1-\min(a,b)}, & \text{if } a \neq b \\ 0, & \text{if } a = b \end{cases}$$

$$a \Theta_L b = a - b.$$

Theorem 2 [3,4]. Let N be a reflection on Ω and V be a nonempty subset of $\Omega \setminus FP(\Omega)$ closed under N . Let $S: V \times V \rightarrow [0,1]$ be a co-symmetric and consistent similarity function then the function

$$A(x,y) = S(x,y) \Theta_{TC} S(x,N(y)).$$

is a strong correlation function on V .

Theorem 1 is a particular case of Theorem 2 when it is used the pseudo-difference operation $\Theta_{TC} = \Theta_L$ associated to Lukasiewicz t -conorm.

In some domains, it is difficult to construct consistent similarity functions. In such cases, the property of consistency S can be replaced by the property of *weak consistency (weak similarity of reflections)* of S defined for all x, y in V by:

$$S(x, N(x)) < 1.$$

Theorem 3 [3,4]. Let N be a reflection on Ω and V be a nonempty subset of $\Omega \setminus FP(\Omega)$ closed under N . Let $S: V \times V \rightarrow [0, 1]$ be a co-symmetric similarity function satisfying weak consistency, then the function

$$A(x, y) = S(x, y) \Theta_{TC} S(x, N(y)), \quad (5)$$

is a correlation function on V if t -conorm TC has no nilpotent elements.

From Theorem 3, it follows that if similarity function S is co-symmetric but only weakly consistent, then there is no reason to use in (5) pseudo-difference operation $a \Theta_{TC} b = a - b$ but one can use pseudo-difference operations associated to maximum TC_M and product TC_P t -norms. Some examples one can find in [3, 4].

5 Generalized Correlation Functions

Here we introduce the correlation functions that can be not strong. In the definition of such correlation functions, we do not require that the underlying set Ω equipped with some negation operation. We will consider the methods of construction of such correlation functions and, further, we will show when these methods will define strong correlation functions. Finally, we establish the one-to-one correspondence between “bipolar” similarity functions and strong correlation functions.

Definition 7. A function $A: \Omega \times \Omega \rightarrow [-1, 1]$ on a nonempty set Ω is a *correlation function* if it is symmetric, reflexive and has negative value for some x, y in Ω : $A(x, y) < 0$. A correlation function A is called *(-1)-normal (in (x, y))* if $A(x, y) = -1$ for some x, y in Ω .

A non-strong correlation function will be called a *weak or semi-correlation function*.

Proposition 3. Suppose S and D are similarity and dissimilarity functions on Ω such that for some x, y in Ω it is fulfilled: $S(x, y) < D(x, y)$, then the function defined for all x, y in Ω by:

$$A(x, y) = S(x, y) - D(x, y), \quad (6)$$

is a correlation function.

Proof. The similarity of A follows from the similarity S and D . The reflexivity of A follows from the reflexivity of S and irreflexivity of D . When for some x, y in Ω it is fulfilled $S(x,y) < D(x,y)$, the value of A in (6) is negative. ■

If S is 0-normal and D is 1-normal in the same pair of elements (x,y) then A is (-1)-normal. If similarity and dissimilarity functions in (6) are complementary, then the function (6) will be a correlation function if for some x, y in Ω it fulfills $S(x,y) < 0.5$.

The formula (6) has a reasonable interpretation: *the correlation between x and y is positive if the similarity between them is greater than the dissimilarity, and the correlation is negative in the opposite case.*

Definition 8. If the similarity S and dissimilarity D functions in (6) are complementary, then the correlation function A defined by (6) is called complementary to S and D , and (S,D,A) for such functions is called a *complementary (or correlation) triplet*.

From Definitions 3 and 8 and from Proposition 3 it follows that the similarity, dissimilarity and correlation functions from the complementary triplet (S,D,A) , can be obtained one from another for all x, y in Ω as follows:

$$S(x,y) = 1 - D(x,y), \quad D(x,y) = 1 - S(x,y), \quad (7)$$

$$A(x,y) = 2S(x,y) - 1, \quad S(x,y) = 0.5(A(x,y)+1), \quad (8)$$

$$A(x,y) = 1 - 2D(x,y), \quad D(x,y) = 0.5(1 - A(x,y)). \quad (9)$$

Example 5. The Spearman's rank correlation coefficient is equivalent to the Pearson's product-moment correlation coefficient applied to rankings of n objects [9, 14]. When each of rankings $x = (x_1, \dots, x_n)$ and $y = (y_1, \dots, y_n)$ contains n different integer ranks, $1 \leq x_i, y_i \leq n$, i.e. there are no ties, the Spearman's rank correlation coefficient is calculated as follows:

$$r_s = 1 - \frac{6 \sum_{i=1}^n d_i^2}{n(n^2-1)}, \quad (10)$$

where $d_i = x_i - y_i$. Consider the function:

$$D(x, y) = \frac{3 \sum_{i=1}^n (x_i - y_i)^2}{n(n^2-1)}.$$

It is irreflexive, symmetric and takes values in the interval $[0,1]$, hence it is the dissimilarity function and Spearman's rank correlation coefficient defined by $r_s(x,y) = 1 - 2D(x,y)$, is a correlation function, compare with (9).

Example 6. The Kendall rank correlation coefficient is defined for measurements without ties $x = (x_1, \dots, x_n)$ and $y = (y_1, \dots, y_n)$ of two variables for n objects as follows [11,14,17]:

$$\tau = \frac{\text{number of concordant pairs} - \text{number of discordant pairs}}{n(n-1)/2},$$

that can be represented as the difference between similarity S and dissimilarity D functions (6):

$$\tau(x, y) = S(x, y) - D(x, y),$$

defined as follows:

$$S(x, y) = \frac{\sum_{i=1}^{n-1} \sum_{j=i+1}^n s_{ij}}{n(n-1)/2}, \quad D(x, y) = \frac{\sum_{i=1}^{n-1} \sum_{j=i+1}^n d_{ij}}{n(n-1)/2},$$

where concordant and discordant pairs (i, j) , $i < j$, defined by:

$$s_{ij} = \begin{cases} 1, & \text{if } (x_i - x_j)(y_i - y_j) > 0 \\ 0, & \text{otherwise} \end{cases},$$

$$d_{ij} = \begin{cases} 1, & \text{if } (x_i - x_j)(y_i - y_j) < 0 \\ 0, & \text{otherwise} \end{cases}.$$

The Kendall rank correlation coefficient uses the signs of differences between measurement values: $(x_i - x_j)$ and $(y_i - y_j)$, hence takes into account only the ordering (or ranking) of these values. Note that S is reflexive, D is irreflexive, and both functions are symmetric, take values in $[0, 1]$; hence they are similarity and dissimilarity functions, respectively. Due to the measurements are without ties, i.e., all have different values, from $s_{ij} + d_{ij} = 1$ for all $1 \leq i < j \leq n$, it follows $S(x, y) + D(x, y) = 1$, i.e., S and D are complementary functions, and together with Kendall rank correlation coefficient τ compose complementary triplet (S, D, τ) , hence for S , D , and $A = \tau$ all relations (7)-(9) are fulfilled.

6 Relationship between Strong Correlation Functions and Similarity Functions

The following theorem answers the question: when the correlation function from a complementary triplet will be strong.

Theorem 4. Let N be a reflection on Ω and V be a nonempty subset of $\Omega \setminus FP(\Omega)$ closed under N . The formulas (8) establish the one-to-one correspondence between the strong correlation functions and the similarity functions satisfying for all x, y in V the following property:

$$S(x, y) + S(x, N(y)) = 1. \quad (11)$$

Proof. Suppose (1) is fulfilled, then

$$A(x, y) + A(x, N(y)) = 0, \quad (12)$$

applying (8) we obtain from (12): $2S(x, y) - 1 + 2S(x, N(y)) - 1 = 0$, and $2S(x, y) + 2S(x, N(y)) = 2$, i.e. (11) is fulfilled. Similarly, from (11), (8) we can obtain (1) ■

A similarity function satisfying (11) for all x, y in V will be referred to as a *bipolar similarity function*, see [7], because the right side of (11) one can consider as a sum: $1 = 0 + 1$, of “poles” 0 and 1 of the interval of similarity values $[0,1]$. Similarly, we can present the property (12) of the inverse relationship of correlation function (1) as *bipolarity condition*, where the right side equal to the sum: $0 = -1 + 1$, of the “poles” of the interval of correlation function values $[-1,1]$. For this reason, a strong correlation function one can consider also as a *bipolar correlation function*, and Theorem 4 one can interpret as follows: *there exists a one-to-one correspondence between bipolar correlation functions and bipolar similarity functions*.

From Theorem 4 it follows also that the formulas (9) establish a one-to-one correspondence between strong correlation functions and *bipolar dissimilarity functions* satisfying for all x, y in V the bipolarity condition:

$$D(x,y) + D(x,N(y)) = 1. \quad (13)$$

It is easy to see from (7) that for complementary similarity and dissimilarity functions the bipolarity relations (11) and (13) are equivalent to:

$$D(x,y) = S(x,N(y)), \quad S(x,y) = D(x,N(y)). \quad (14)$$

Proposition 4. Let N be a reflection on Ω and V be a nonempty subset of $\Omega \setminus FP(\Omega)$ closed under negation N . Let S be a bipolar similarity function on V then it is consistent and co-symmetric.

Proof. From (11) replacing y by x and from the reflexivity of S obtain the consistency of S : $S(x,N(x)) = 1 - S(x,x) = 1 - 1 = 0$.

Replacing in (11) x by $N(x)$ and y by $N(y)$ obtain: $S(N(x),N(y)) + S(N(x),N(N(y))) = 1$. Further, applying involutivity of N : $N(N(y)) = y$, and symmetry of S obtain: $S(N(x),N(y)) = 1 - S(N(x),N(N(y))) = 1 - S(N(x),y) = 1 - S(y,N(x))$. From (11) we have $S(y,x) + S(y,N(x)) = 1$, that together with symmetry of S gives: $1 - S(y,N(x)) = S(y,x) = S(x,y)$, and finally we obtain: $S(N(x),N(y)) = S(x,y)$, i.e. co-symmetry of S ■

From Proposition 4 and Theorem 1 it follows that the bipolar similarity function can be used for constructing a strong correlation function by (3): $A(x,y) = S(x,y) - S(x,N(y))$, and from (14) it follows that this strong correlation function is complementary to S , i.e. (6) is fulfilled: $A(x,y) = S(x,y) - D(x,y)$, hence the simplified formulas (8): $A(x,y) = 2S(x,y) - 1$, and (9): $A(x,y) = 1 - 2D(x,y)$, can be used. From (8) and (9) it follows that the strong correlation function is the rescaling of bipolar similarity and dissimilarity functions.

Example 7 (see Example 6). Let Ω be the set of real-valued n -tuples $x = (x_1, \dots, x_n)$. Define the reflection on Ω as follows: $N(x) = (M - x_1, \dots, M - x_n)$, where M is some constant, for example, $M = 0$ or $M = \max\{x_1, \dots, x_n\}$. For similarity function S from Example 6 denote s_{ij} the addends that will be used for calculating $S(x,N(y))$:

$$\begin{aligned}
s_{ij} &= \begin{cases} 1, & \text{if } (x_i - x_j) \left(N(y_i) - N(y_j) \right) > 0 \\ 0, & \text{otherwise} \end{cases} \\
&= \begin{cases} 1, & \text{if } (x_i - x_j) \left((M - y_i) - (M - y_j) \right) > 0 \\ 0, & \text{otherwise} \end{cases} \\
&= \begin{cases} 1, & \text{if } (x_i - x_j)(y_j - y_i) > 0 \\ 0, & \text{otherwise} \end{cases} \\
&= \begin{cases} 1, & \text{if } (x_i - x_j)(y_i - y_j) < 0 \\ 0, & \text{otherwise} \end{cases} \\
&= d_{ij}.
\end{aligned}$$

Hence, $D(x,y) = S(x,N(y))$, similarity function S is bipolar and the Kendall rank correlation coefficient is the strong correlation function.

Example 8. It can be shown also that the dissimilarity functions considered in Examples 3, 4 and 5 are bipolar and give by $A(x,y) = 1 - 2D(x,y)$, the following strong correlation functions, respectively: the Pearson's product-moment correlation coefficient, the cosine correlation coefficient, and the Spearman's rank correlation coefficient. In the last case, the reflection operation on the set of rankings reverses the rankings by $N(x_i)=n+1-x_i$.

7 Related Works and Conclusion

Some of the relationships between similarity, dissimilarity, and correlation coefficients considered in Sections 5 and 6 have been mentioned in several works. The formulas like (6), (9) appear in [14] in the calculation of Kendall rank correlation coefficient, where instead of similarity and dissimilarity functions, the positive and negative scores are used. The formula (10) of Spearman rank correlation also given in this book. Kendall [14] proposed the "general correlation coefficient" using the values a_{ij} and b_{ij} defined for Spearman, Kendall and Pearson correlation as functions of differences $x_i - x_j$ and $y_i - y_j$ for all $i, j = 1, \dots, n$. How to define a_{ij} and b_{ij} in general case, it is not clear. It is only required that $a_{ij} = -a_{ji}$ and $b_{ij} = -b_{ji}$. Also, the generalization of formulas like (6) and (9) on the universal domain not considered. The half of formulas from (7)-(9) used for constructing similarity and dissimilarity measures from correlation coefficients were considered in [1, 16]. The problem of the construction of correlation coefficients from similarity and dissimilarity measures not considered in these works. The properties like symmetry, inverse relationship and co-symmetry of a "good" relative measure of the association were also considered in [11] but the negation has been considered only for real numbers and the general methods of construction of such measures on the universal domain with involution were not

proposed. Some formulas like (6), and from (7)-(9) for the probabilities of concordance and discordance are considered in [11]. Theorems 1-3 are considered in [3, 4, 8].

The methods of construction of correlation functions on universal domain Ω as difference between similarity and dissimilarity functions proposed in this paper in Section 5 and one-to-one correspondence between strong correlation functions and bipolar similarity functions formulated in Section 6 together with the methods of construction of strong correlation functions (association measures) proposed in [2, 3, 4, 8] have more straightforward interpretation of the correlations in terms of similarities and dissimilarities. These methods give a general and regular methodology for constructing correlation functions on different domains where one can introduce a reflection (negation) operation.

The very surprising result has been obtained here in Theorem 4. It establishes deep relationships between correlation coefficients and similarity (dissimilarity) measures. The one-to-one correspondence between strong correlations and bipolar similarity functions together with (8) shows that there is no much difference between these two concepts. This result paves the way for the construction of new strong correlation functions on almost any domain where negation (reflection) operation and similarity or dissimilarity functions satisfying suitable properties can be defined. The methods of construction of similarity and dissimilarity functions suitable for the generation of correlation functions (association measures) can be based on the results obtained in [2, 8]. For example, one can construct dissimilarity functions using Minkowski distance and p -transformation of data, using the methods of co-symmetrization of similarity functions, etc.

Acknowledgment

This work was partially supported by project IPN SIP 20196374. The author also thanks Dr. Imre Rudas for his help in the publication of this work.

References

- [1] H. T. Clifford, W. Stephenson: An introduction to numerical classification, Academic Press, New York, 1975
- [2] I. Batyrshin: Constructing time series shape association measures: Minkowski distance and data standardization, BRICS CCI-2013, IEEE, 2013, pp. 204-212, <https://arxiv.org/ftp/arxiv/papers/1311/1311.1958.pdf>
- [3] I. Batyrshin: Association measures and aggregation functions, Advances in soft computing and its applications. Lecture Notes in Computer Science, Vol. 8266, Springer, 2013, pp. 194-203
- [4] I. Z. Batyrshin: On definition and construction of association measures, Journal of Intelligent & Fuzzy Systems, Vol. 29, 6, 2015, pp. 2319-2326
- [5] I. Batyrshin, V. Kreinovich: One more geometric interpretation of Pearson's correlation, Thailand Statistician, Vol. 13, 2015, pp.125-126

- [6] I. Batyrshin, V. Solovyev, V. Ivanov: Time series shape association measures and local trend association patterns, *Neurocomputing*, Vol. 175, 2016, pp. 924-934
- [7] I. Batyrshin, F. Monroy-Tenorio, A. Gelbukh, L.A. Villa-Vargas, V. Solovyev, N. Kubysheva: Bipolar rating scales: a survey and novel correlation measures based on nonlinear bipolar scoring functions, *Acta Polytechnica Hungarica*, Vol. 14, 3, 2017, pp. 33-57
- [8] I. Batyrshin: Towards a general theory of similarity and association measures: similarity, dissimilarity and correlation functions, *Journal of Intelligent and Fuzzy Systems*, Vol. 36, 4, 2019, pp. 2977-3004
- [9] P. Y. Chen, P. M. Popovich: *Correlation: Parametric and nonparametric measures*, Sage, Thousand Oaks, CA, 2002
- [10] J. D. Gibbons: *Nonparametric measures of association*, Sage Publications, Iowa, 1993
- [11] J. D. Gibbons, S. Chakraborti: *Nonparametric statistical inference*, Dekker, New York, 2003, 4th ed.
- [12] M. Grabisch, J. L. Marichal, R. Mesiar, E. Pap: *Aggregation Functions*, Cambridge Univ. Press, Cambridge, UK, 2009
- [13] P. Jaccard: Nouvelles recherches sur la distribution florale, *Bull. Soc. Vaud. Sci. Nat.*, Vol. 44, 1908, pp. 223-270
- [14] M. G. Kendall: *Rank correlation methods*, Griffin, London, 1970, 4th ed.
- [15] E. P. Klement, R. Mesiar, E. Pap: *Triangular norms*, Springer Science & Business Media, 2013
- [16] M-J. Lesot, M. Rifqi, H. Benhadda: Similarity measures for binary and numerical data: a survey, *Int. J. Knowledge Engineering and Soft Data Paradigms*, Vol. 1, 2009, pp. 63-84
- [17] A. M. Liebetrau: *Measures of Association*, Sage Publications, Iowa, 1983
- [18] G. Salton: *Automatic text processing: the transformation, analysis, and retrieval of information by computer*, Addison-Wesley, Boston, MA, 1989
- [19] P. N. Tan, V. Kumar, J. Srivastava: Selecting the right interestingness measure for association patterns, 8th Proc. Eighth ACM SIGKDD Int. Conf. Knowledge Discovery and Data Mining, 2002, pp. 32-41
- [20] G. U. Yule: On the association of attributes in statistics: with illustrations from the material of the childhood society, &c., *Phil. Trans. Royal Soc. of London. Series A*, Vol. 194, 1900, pp. 257-319

A coarse-grain model of growth and cell cycle in *Saccharomyces cerevisiae*: a mathematical analysis

**Pasquale Palumbo^{1,3*}, Federico Papa^{1,2*}, Marco Vanoni^{1,3},
Lilia Alberghina^{1,3}**

¹ SYSBIO/ISBE.IT, Centre of Systems Biology

² CNR-IASI via dei Taurini 19, Italian National Research Council (CNR), 00168 Rome, Italy

³ Department of Biotechnology and Biosciences, University of Milano-Bicocca, Piazza della Scienza, Milan, Italy

Corresponding author: pasquale.palumbo@unimib.it;

federico.papa@iasi.cnr.it, {marco.vanoni, lilia.alberghina}@unimib.it

*These authors contributed equally to this work.

*Abstract: In this paper a coarse-grain model is presented that describes the major features of cell growth and cell cycle in *Saccharomyces cerevisiae*. Central for the construction of the growth and cell cycle model has been the large amount of scientific papers covering the description of cellular growth in steady-state and perturbed growth conditions, describing ribosome and protein contents, and the description of cell cycle progression as percentage of budded cells (cells that have entered S-phase). The coarse model is composed by i) a growth module, i.e. a set of ODEs representing the dynamics of synthesis/degradation of ribosomes and proteins, and ii) a cell cycle module, i.e. a set of three consecutive timers (T_1 , T_2 and T_B) that temporally accounts for the yeast cell cycle, underlying the length of the G1 phase (timer T_1 plus T_2) and of the budded phase (timer T_B) entailing S, G2 and M phases. The growth module acts as a master, setting the length of the first of the three sequential timers. Main results coming from the mathematical analysis involve the qualitative behavior of the system, constraining ribosome synthesis and growth to the set of model parameters. Further results involve the generalization of a known constraint that involves the lengths of the cycles of parent and daughter cells, and accounts for the genealogical age heterogeneity, typical of budding yeast *Saccharomyces cerevisiae*.*

Keywords: Linear ODE models, Systems Biology.

1 Introduction

This work investigates the qualitative behavior of a coarse-grain mathematical model of the budding yeast *Saccharomyces cerevisiae*, a micro-organism known to be exploited as a model for eukaryotic cells. The model constitutes of two modules. The

former describes the cell growth by means of a pair of Ordinary Differential Equations (ODEs) dealing with ribosomes and protein content. The latter introduces a set of three timers that cover the whole cell cycle, namely T_1 , T_2 and T_B . Timer T_1 starts with the newborn cell and is formally over when the G1/S regulon is activated; then T_2 starts and is over with the end of the G1 phase. The notation used for the first two timers T_1 and T_2 is the same one that has been introduced in [1]. According to the mentioned paper, T_1 refers to the period a newborn cell takes to activate the G1/S regulon and is formally measured by the time the regulon inhibitor Whi5 takes to exit the nucleus; on the other hand, T_2 refers to the time cyclins Clb5/6 (responsible for the onset of the S phase) take to get rid of their inhibitor Sic1. The sum of T_1 and T_2 provides the length of the G1 phase.

At the end of the G1 phase, contemporary to the onset of the S phase, T_B starts and covers the rest of the cycle, i.e. S+G2+M phases. Such a period is called budded phase because the cell is characterized by a bud, and all protein and ribosome produced in T_B go straightforwardly to the bud (that will become the newborn cell at the end of the cycle).

Growth and cell cycle are linked together by timer T_1 , since its length depends on the cell size. More in details, the link is rendered by the fact that T_1 depends on the initial cell size, i.e. its length has an inverse dependence on the protein content at cell birth. This is a simplifying hypothesis with respect to the more accurate model developed in [2], where the link between growth and cell cycle is driven by a molecular sizer, that is able to account also for extra-small cell.

Figure 1 provides a graphical representation of the coarse-grain model, showing the details of each module and the connection point between them.

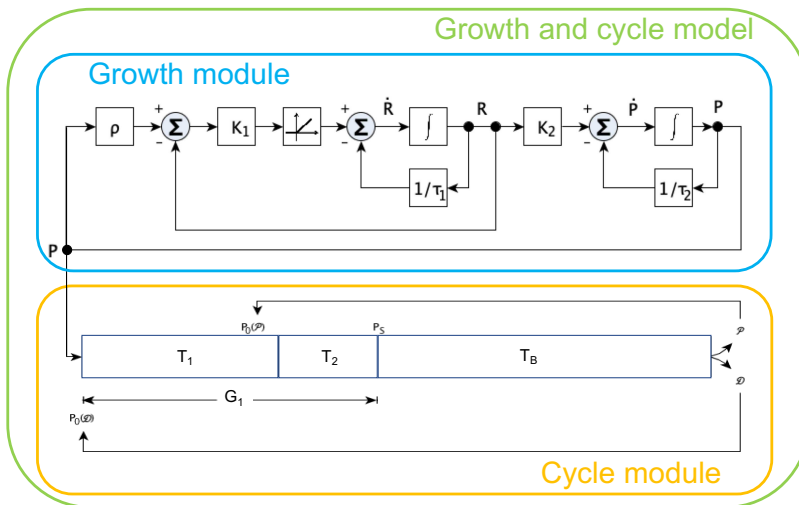


Figure 1
Block diagram of the growth and cell cycle model.

Part of the mathematical analysis dealing with the growth module has been developed in [3]. Here we extend those results and introduce a set of constraints straightforwardly related to the length of parent and daughter cycles.

2 The growth and cell cycle model

The growth and cell cycle model is composed of two modules (see Figure 1):

- the growth module based on a set of ordinary differential equations that describes the dynamics of synthesis and degradation of ribosomes and proteins;
- the cell cycle module consisting of a sequence of the three timers T_1 , T_2 and T_B that describes the cell cycle progression after cell birth.

2.1 The growth module

Cell proliferation is sustained by the increase of cell components. A large part of energy and building blocks utilized in cellular processes is exploited for the biosynthesis of ribosomes and proteins, whose increase results from the balance between the rate of protein/ribosome synthesis and degradation.

The growth module is taken from [4] and deals with the ribosome content R , expressed as number of ribosomes per cell, and the protein content P , expressed as number of polymerized amino acids per cell. The working hypothesis is that ribosome and protein contents are allowed to vary continuously, so that the dynamics of the two state variables is described by the following ODEs:

$$\begin{cases} \dot{R}(t) = K_1 [\rho P(t) - R(t)]^+ - \frac{R(t)}{\tau_1}, \\ \dot{P}(t) = K_2 R(t) - \frac{P(t)}{\tau_2}, \end{cases} \quad \begin{matrix} R(0) = R_0 \geq 0, \\ P(0) = P_0 \geq 0, \end{matrix} \quad (1)$$

where

$$[z]^+ = \begin{cases} z, & \text{for } z > 0, \\ 0, & \text{otherwise.} \end{cases}$$

Both ribosome and protein dynamics are described by the balance between production and degradation rates. A special role is played by the parameter ρ , that represents the ideal “ribosomes-over-proteins” ratio, for each steady-state growth condition. When the ratio $R(t)/P(t)$ is higher than ρ , then there is no ribosome production, so that the dynamics of R and P is described by the following linear working mode,

$$\mu_1 : \begin{cases} \dot{R}(t) = -\frac{R(t)}{\tau_1}, \\ \dot{P}(t) = K_2 R(t) - \frac{P(t)}{\tau_2}; \end{cases} \quad (2)$$

otherwise, the ribosome production rate is proportional to the (positive) difference $\rho P(t) - R(t)$ by means of parameter K_1 and the R - P dynamics is described by an-

other linear working mode as follows

$$\mu_2 : \begin{cases} \dot{R}(t) = -\left(K_1 + \frac{1}{\tau_1}\right)R(t) + K_1\rho P(t), \\ \dot{P}(t) = K_2R(t) - \frac{P(t)}{\tau_2}. \end{cases} \quad (3)$$

The switches between μ_1 and μ_2 depend on the position of the state variables of the system in the phase plane and, in particular, on the value of their ratio $R(t)/P(t)$ compared to the threshold ρ (see Figure 2 where an example of trajectory in the phase plane is reported).

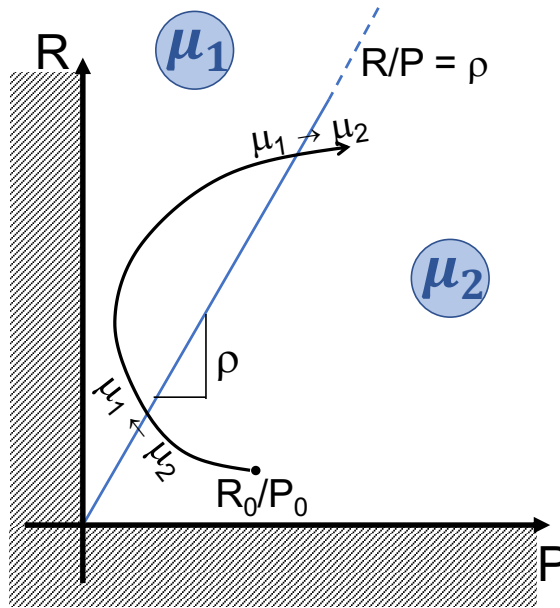


Figure 2

An explanatory trajectory in the phase-plane for a cell that is born according to ribosome synthesis conditions, then it first switches to absence of ribosome synthesis (from μ_2 to μ_1) and then it switches back to μ_2 again.

The properties of each working mode and the switching conditions from one mode to the other one are given in Section 3 and are partially demonstrated in [3]. Such properties are necessary to characterize the qualitative behaviour of $R(t)$ and $P(t)$, as well as to establish if the yeast cell is actually growing (i.e. if the linear model has at least one positive eigenvalue) or not.

Experimental evidences related to yeast populations in exponential growth show that each growth condition (i.e. each growth rate) is characterized by a specific ratio of “ribosomes-over-proteins”, although the molecular mechanism of the association is still unclear. The mechanism may involve TOR-dependent phosphorylation of Sfp1, a positive regulator of transcription of genes encoding ribosomal proteins [5].

Experimental evidences also support the choice of the non-linear ribosome production rate of model (1) as they show the existence of a negative feedback reducing the ribosome biosynthesis in presence of ribosomes not engaged in protein biosynthesis [6, 7]. In *Escherichia coli*, this mechanism runs via ppGpp and is relatively well understood; it appears to provide a robust and optimal partitioning of cellular resources over ribosomes and other proteins [8]. In eukaryotes it involves the TOR pathway [5, 9, 10]. Experimental values for the “ribosomes-over-proteins” ρ can be found in [11–14].

2.2 The cell cycle module

Saccharomyces cerevisiae cells divide asymmetrically [15], cell mass at division is unequally partitioned between a larger, old parent cell (\mathcal{P}) and a smaller, newly synthesized daughter cell (\mathcal{D}). The degree of asymmetry of cell division in *Saccharomyces cerevisiae* is modulated by nutrients: poor media – such as ethanol – yield a high level of asymmetry with large parent cells and very small daughter cells, whereas in rich media – such as glucose – parents and daughters at division are very close in size (reviewed in [16]). Since cells have to grow to a critical cell size before entering S phase and budding, small cells have longer cycle time than larger cells, most notably in poor media. As a matter of fact, this difference in cycle time is due to differences in the G1 phase, having the budded period T_B essentially the same length whatever the size of the cells [1].

The first timer T_1 starts with the birth of the new cell and is over when nuclear Whi5 exits the nucleus. Aiming not to detail the whole molecular machinery, Whi5 will not be explicitly involved in the model. The length of T_1 is strongly related to the initial size of the cell, according to a constraint that makes smaller the length of T_1 for larger cells and vice versa. So, the initial size of the cell plays a crucial role to assess the value of T_1 . More in details, T_1 is set according to the following equation

$$T_1 = \max\{T_{1P}, W_0 - W_1 \ln(P(0))\}, \quad (4)$$

with $P(0)$ denoting the size of the cell at birth. Notice that $P(0)$ plays an active role in the setting of T_1 only for cells small enough to ensure

$$W_0 - W_1 \ln(P(0)) > T_{1P} \implies P(0) < e^{\frac{W_0 - T_{1P}}{W_1}}. \quad (5)$$

Length of timer T_2 does not depend on protein content, and it is set to the same value for small and large cells. At the end of timer T_2 , the critical size expressed both as ribosome content and as protein content, R_s and P_s respectively, is estimated. Timer T_2 is related to the period inhibitor Sic1 takes to get out of the nucleus thus activating cyclins Clb5,6, responsible for the onset of the budded phase [1].

The third timer T_B refers to the budded period, which eventually leads to cellular division. Like timer T_2 , T_B length does not depend on the protein content, and it is set to the same value for small and large cells.

Notice that the setting of timer T_1 may allow small cells (i.e. the ones that comply with (5)) to reduce their critical cell size variability w.r.t. the initial variability.

Indeed, denote with \bar{P}_0 and Δ_0 the average value of the initial size and its corresponding variability in a population of cells in balanced exponential growth (growth rate λ), with the initial size complying with inequality (5). Define \bar{P}_s and Δ_s the average value of the critical size and its corresponding variability. Then, because of (5), we have:

$$P_s = P(0)e^{\lambda(T_1+T_2)} = P(0)e^{\lambda(W_0 - W_1 \ln P(0) + T_2)}, \quad (6)$$

By accounting for size fluctuations, we obtain after simple computations:

$$P_s = \bar{P}_s + \Delta_s = (\bar{P}_0 + \Delta_0)^{1-\lambda W_1} e^{\lambda(W_0+T_2)}. \quad (7)$$

Applying first-order approximation, we finally have

$$\Delta_s \simeq (1 - \lambda W_1) \bar{P}_0^{-\lambda W_1} e^{\lambda(W_0+T_2)} \Delta_0. \quad (8)$$

A biologically meaningful parameter setting provides $\Delta_s \leq \Delta_0$ (see for instance [2]), which is coherent with the idea that the G1/S transition is able to reduce size variability.

2.3 Genealogical age heterogeneity

When a yeast cell buds, a chitin ring, called bud scar, builds up at the bud isthmus and remains on the parent cell after the bud has separated (reviewed in [16]). Since each new bud starts at a new site, it is possible to determine the number of bud scars s present on the surface of a parent cell and consequently to establish the genealogical age k of the parent cell, meaning the age of the parent cell equal to the number of daughters it has generated (i.e., $k = s$). So, denoting by \mathcal{P}_k a parent cell of age k , a cell \mathcal{P}_1 has one bud scar since it has completed a cycle, a cell \mathcal{P}_2 has two bud scars since it has completed two cycles, and so on. On the other hand, a cell without bud scars ($s = 0$) is a daughter cell and it has not yet completed a cycle. The model of growth and cell cycle, however, distinguishes the genealogical age of the daughter cells: it can be 1 if the daughter is born from another daughter, while it is $k > 1$ if the daughter is born from a parent \mathcal{P}_{k-1} . We denote by \mathcal{D}_k a daughter of genealogical age k . It has to be stressed that such a notation refers to a cell in a specific cycle of its life. In other words, the same cell is labeled by a different name each time a new cycle starts. For instance, a newborn cell coming from any daughter cell is called \mathcal{D}_1 in its first cycle, will be called \mathcal{P}_1 in its second cycle, \mathcal{P}_2 in its third cycle, and so on.

Because at every generation each parent increases in size before starting to bud [17–19] and at division it receives the mass it had at budding (the mass synthesized during the budded phase going to the newborn daughter), it follows that in parents, the critical size increases with genealogical age. Experimental evidence shows that the higher is the genealogical age (i.e. the number of bud scars), the smaller is the increase in size at budding from one generation to the other [16, 20]. The reduction in cell size increase with genealogical age has been explained by the mechanical stress of the cell wall, which increases with cell size [21, 22].

In order to account for the aforementioned behavior, both K_2 and τ_2 in Eqs. (1) (rate of protein synthesis and time constant of protein degradation respectively) are decreased to lower and lower values during the pre-budded period (G1 phase, i.e. $T_1 + T_2$), according to the parent genealogical age. We define K_{2k} and τ_{2k} the K_2 and τ_2 parameters for a parent cell with genealogical age k . At the end of timer T_2 – coincident with the end of the G1 phase and with the onset of the budded phase – the values of K_{2k} and τ_{2k} return to the nominal values of K_2 and τ_2 , so that the parent cell \mathcal{P}_k grows again with the steady-state exponential rate (given by the positive eigenvalue, see next section). Daughter cells (of any genealogical age) are not affected by such a mechanical stress.

Table 1 collects all the model parameters introduced in this section, providing also the corresponding measurement units and definitions.

Parameter	Unit	Definition
ρ	rib/aa	Asymptotic ratio of ribosomes over proteins
K_1	min^{-1}	Ribosome production rate
τ_1	min	Ribosome degradation time constant
K_2	aa/(rib*min)	Protein production rate for any \mathcal{D}_k and for \mathcal{P}_k in budded phase
K_{2k} $k = 1, 2, \dots$	aa/(rib*min)	Protein production rate for \mathcal{P}_k in G1-phase
τ_2	min	Protein degradation time constant for any \mathcal{D}_k and for \mathcal{P}_k in budded phase
τ_{2k} $k = 1, 2, \dots$	min	Protein degradation time constant for \mathcal{P}_k in G1-phase
T_{1P}	min	Minimum value for T_1
W_0	min	T_1 length for unitary $P(0)$
W_1	min	Size-related coefficient to set T_1 length
T_2	min	Length of T_2
T_B	min	Length of the budded phase

Table 1
Measurement units and definitions of the model parameters.

3 Properties of the growth module

It is important to determine which are the conditions on the model parameters of system (1) required for cell growth, under each working mode μ_1 or μ_2 . So, let us introduce the notation g and \bar{g} to denote two opposite growing dynamics of the cell: the state g represents growth, i.e. ribosomes and proteins are actually increasing (after a transient period) because of the existence of a positive eigenvalue in system (1); conversely, the state \bar{g} represents a not growing cell in which ribosomes and proteins are non-increasing.

Let us now give some simple results on the growing dynamics related to system (1). Let us observe first that \bar{g} (no growth) is the only allowed dynamics for system (1)

when $R(t)/P(t) \geq \rho$, i.e. when the working mode is μ_1 (no ribosome synthesis). This trivially comes from the negative sign of the eigenvalues related to the linear system (2) ($\lambda_1 = -1/\tau_1$, $\lambda_2 = -1/\tau_2$).

The following theorem shows instead the growing dynamics of system (1) when $R(t)/P(t) < \rho$.

Theorem 1. *When the working mode of system (1) is μ_2 (presence of ribosome synthesis), both the growing dynamics are allowed. In particular it is:*

- g (growth) when $x > 0$,
- \bar{g} (no growth) when $-1 \leq x \leq 0$,

where x is the following function of the model parameters

$$x = 4 \frac{K_1 K_2 \rho - \left(K_1 + \frac{1}{\tau_1}\right) \frac{1}{\tau_2}}{\left(K_1 + \frac{1}{\tau_1} + \frac{1}{\tau_2}\right)^2}. \quad (9)$$

The condition $x < -1$ cannot occur for any non-negative setting of the model parameters.

Proof. The proof comes from the computation of the eigenvalues of the linear system (3) (working mode of system (1) when $R(t)/P(t) < \rho$), that is

$$\lambda_1 = y \left(-1 - \sqrt{1+x}\right), \quad \lambda_2 = y \left(-1 + \sqrt{1+x}\right), \quad (10)$$

where x is given by (9) and

$$y = \frac{1}{2} \left(K_1 + \frac{1}{\tau_1} + \frac{1}{\tau_2}\right). \quad (11)$$

Let us prove first that the condition $x < -1$ cannot be satisfied so that λ_1, λ_2 are always real (no oscillatory dynamics). In particular, it is shown by the following arguments that $x \geq -1$ for any non-negative setting of the model parameters.

Let us rewrite the quantity x as

$$x = t_1 + t_2, \quad (12)$$

where

$$t_1 = 4 \frac{K_1 K_2 \rho}{\left(K_1 + \frac{1}{\tau_1} + \frac{1}{\tau_2}\right)^2}, \quad t_2 = -4 \frac{\left(K_1 + \frac{1}{\tau_1}\right) \frac{1}{\tau_2}}{\left(K_1 + \frac{1}{\tau_1} + \frac{1}{\tau_2}\right)^2}. \quad (13)$$

The inequality $t_1 \geq 0$ straightforwardly comes from the non-negativity of the model parameters. In particular, $t_1 = 0$ if and only if $K_1 = 0$ or $K_2 = 0$ or $\rho = 0$ (as well

as it approaches zero if and only if K_1 tends to infinity or one parameter among τ_1, τ_2 approaches zero). On the other hand, the second term of x satisfies the inequality $-1 \leq t_2 \leq 0$. The non-positivity of t_2 trivially comes again from the non-negativity of the model parameters; conversely, the inequality $t_2 \geq -1$ holds if and only if $(K_1 + 1/\tau_1 - 1/\tau_2)^2 \geq 0$, which is trivially satisfied for any parameter setting. Moreover, the minimum value $t_2 = -1$ is obtained if and only if the condition $K_1 + 1/\tau_1 - 1/\tau_2 = 0$ holds. So, from the previous arguments we can conclude that

$$x = t_1 + t_2 \geq 0 - 1 = -1. \quad (14)$$

We also notice that

$$x = -1, \quad \iff \quad \begin{cases} K_1 = 0 \text{ or } K_2 = 0 \text{ or } \rho = 0, \\ \text{and} \\ K_1 + 1/\tau_1 - 1/\tau_2 = 0. \end{cases} \quad (15)$$

Finally, from property (14) and Eqs. (10), we easily get the following items:

- λ_1 is always real and negative (for any $x \geq -1$),
- λ_2 is always real; moreover, it is $\lambda_2 > 0$ for $x > 0$ and $\lambda_2 \leq 0$ for $-1 \leq x \leq 0$,

that complete the proof of the theorem. \square

The results on the growing dynamics of system (1) given above are summarized by the flow scheme of Figure 3, showing the possible combinations of working modes (μ_1, μ_2) and growing dynamics (g, \bar{g}) , on the basis of $R(t)/P(t)$ and x values. The figure shows that the population of ribosomes and proteins can actually grow only when $x > 0$, but it depends on the value of the ratio $R(t)/P(t)$: the growth dynamics g is actually obtained only under the working mode μ_2 , i.e. when $R/P < \rho$ (green block). Conversely, when $-1 \leq x \leq 0$ the growth is not allowed, independently of the values of the state variables (i.e. of the current working mode).

Let us now provide some properties on the switch between the two working modes μ_1 and μ_2 . In general, a piecewise affine system can show different behavior, spanning from stability to chaos [23]. The following results give conditions on the model parameters determining if each working mode remains stable or switches to the other one. Being in a given working mode at time t only depends on the ratio $R(t)/P(t)$ at the same time, but the value of the model parameters is the only knowledge that we need in order to determine if the working mode is stable, i.e. it is indefinitely maintained after t , or if it is unstable, i.e. a switch towards the opposite working mode soon or later will occur.

Let us study such properties for meaningful values of the model parameters, that is for positive values. Indeed, when some parameters vanish either the model is not defined or the switching mechanism has no meaning because no growth can be accomplished (the condition $x > 0$ is straightforwardly violated). In particular, the dynamical equations of (1) are not defined when $\tau_1 = 0$ or $\tau_2 = 0$. Conversely, according to definition (9), it is $x < 0$ when $K_1 = 0$ or $K_2 = 0$ or $\rho = 0$, meaning that ribosomes and proteins are not growing under such parameter conditions (see

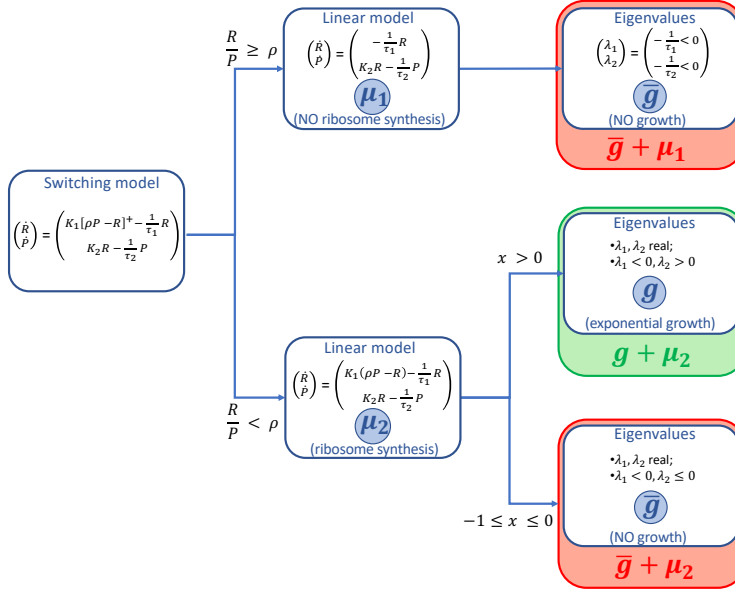


Figure 3
Possible combinations of working modes and growing dynamics.

Theorem 1). We finally notice that the condition $x > -1$ holds when only positive values of the model parameters are considered (indeed, according to relation (15), at least one of the parameters K_1, K_2, ρ must vanish in order to obtain $x = -1$).

Let us first give the result establishing whether the ratio $R(t + \delta)/P(t + \delta)$ remains larger than/equal to ρ (no synthesis, μ_1), or alternatively becomes lower than ρ (synthesis, μ_2), for $\delta \rightarrow \infty$.

Theorem 2. *Given the condition $R(t)/P(t) \geq \rho$ at a given time t , the ribosome synthesis of system (1) is not active and the working mode μ_1 is going to change or not in $t + \delta$, for $\delta \rightarrow \infty$, only depending on the model parameters. In particular,*

1. *the working mode μ_1 sooner or later will switch to μ_2 if*

$$\tau_1 \leq \tau_2, \tag{16}$$

or if

$$\tau_1 > \tau_2 \quad \text{and} \quad \rho K_2 > 1/\tau_2 - 1/\tau_1; \tag{17}$$

2. *otherwise the working mode μ_1 is indefinitely maintained.*

Proof. The proof of Theorem 2 is completely given in Section IV.A of [3]. □

From Theorem 2 the following corollary can be derived.

Corollary. *If the model parameters are such that $\rho K_2 > 1/\tau_2 - 1/\tau_1$, then the switch $\mu_1 \rightarrow \mu_2$ is unavoidable; otherwise it is forbidden.*

Proof. The proof of the corollary straightforwardly comes noticing that the condition $\tau_1 \leq \tau_2$ necessarily implies $\rho K_2 > 1/\tau_2 - 1/\tau_1$, as $1/\tau_2 - 1/\tau_1 \leq 0$ and $\rho, K_2 > 0$. So, the condition $\rho K_2 > 1/\tau_2 - 1/\tau_1$ is the largest condition on the parameter values implying that the switch $\mu_1 \rightarrow \mu_2$ sooner or later will happen, independently of the values of τ_1, τ_2 . \square

The next theorem deals with the behaviour of $R(t + \delta)/P(t + \delta)$ for $\delta \rightarrow \infty$, starting from $R(t)/P(t) < \rho$ (presence of synthesis, μ_2).

Theorem 3. *Given the condition $R(t)/P(t) < \rho$ at a given time t , the ribosome synthesis of system (1) is active and the working mode μ_2 is going to change or not in $t + \delta$, for $\delta \rightarrow \infty$, only depending on the model parameters. In particular,*

1. *the working mode μ_2 is indefinitely maintained if*

$$x > 0, \quad (\text{growth condition}) \quad (18)$$

or if

$$-1 < x \leq 0 \quad \text{and} \quad \rho K_2 \geq 1/\tau_2 - 1/\tau_1; \quad (19)$$

2. *otherwise the working mode μ_2 sooner or later will switch to μ_1 .*

Proof. The proof of the stability of μ_2 when the growth condition $x > 0$ holds is given in Section IV.B of [3]. Here we extend such results to include also the case $-1 < x \leq 0$.

In order to study the behaviour of the ratio $R(t + \delta)/P(t + \delta)$, $\delta \rightarrow \infty$, when $-1 < x \leq 0$ and $R(t)/P(t) < \rho$, we need to compute the explicit solutions of system (3). Such solutions in $t + \delta$ can be given as linear combinations of the natural modes $e^{\lambda_i \delta}$, $i = 1, 2$, where the eigenvalues λ_i are provided by Eqs. (10). In particular, we have:

$$\begin{bmatrix} R(t + \delta) \\ P(t + \delta) \end{bmatrix} = u_1 v_1^T \begin{bmatrix} R(t) \\ P(t) \end{bmatrix} e^{\lambda_1 \delta} + u_2 v_2^T \begin{bmatrix} R(t) \\ P(t) \end{bmatrix} e^{\lambda_2 \delta}, \quad (20)$$

where u_i and v_i are respectively the right and the left eigenvectors associated to the eigenvalues λ_i , $i = 1, 2$ (i.e. the solutions of the systems $(A - \lambda_i I)u_i = 0$, $v_i^T(A - \lambda_i I) = 0$, $i = 1, 2$). Recalling the expression of the eigenvectors reported in [3], we obtain:

$$\begin{aligned} R(t + \delta) = & \frac{\lambda_1 + \frac{1}{\tau_2}}{\lambda_2 - \lambda_1} \left(-R(t) + \frac{\lambda_2 + \frac{1}{\tau_2}}{K_2} P(t) \right) e^{\lambda_1 \delta} \\ & + \frac{\lambda_2 + \frac{1}{\tau_2}}{\lambda_2 - \lambda_1} \left(R(t) - \frac{\lambda_1 + \frac{1}{\tau_2}}{K_2} P(t) \right) e^{\lambda_2 \delta}, \end{aligned} \quad (21)$$

$$\begin{aligned}
P(t + \delta) = & \frac{K_2}{\lambda_2 - \lambda_1} \left(-R(t) + \frac{\lambda_2 + \frac{1}{\tau_2}}{K_2} P(t) \right) e^{\lambda_1 \delta} \\
& + \frac{K_2}{\lambda_2 - \lambda_1} \left(R(t) - \frac{\lambda_1 + \frac{1}{\tau_2}}{K_2} P(t) \right) e^{\lambda_2 \delta}.
\end{aligned} \tag{22}$$

According to the expression of eigenvalues (10) and to the condition $-1 < x \leq 0$, by also recalling the relations implied by the minimal condition $x = -1$ given by (15), it is easy to obtain the following inequalities:

$$\begin{aligned}
\lambda_1 < \lambda_2 \leq 0 & \implies e^{\lambda_1 \tau} < e^{\lambda_2 \tau} \leq 1, \quad \forall \tau > 0, \\
\lambda_2 - \lambda_1 = 2y\sqrt{1+x} & > 0, \\
\lambda_1 + \frac{1}{\tau_2} < 0, \quad \lambda_2 + \frac{1}{\tau_2} & > 0.
\end{aligned} \tag{23}$$

Inequalities (23) can be exploited to verify that the solutions of $R(t + \delta)$ and $P(t + \delta)$ given by Eqs. (21)-(22) are strictly positive for any pair $R(t), P(t) > 0$ and that their behaviours tend to be equal to the following ones for $\delta \rightarrow \infty$

$$\begin{aligned}
R(t + \delta) &= \frac{\lambda_2 + \frac{1}{\tau_2}}{\lambda_2 - \lambda_1} \left(R(t) - \frac{\lambda_1 + \frac{1}{\tau_2}}{K_2} P(t) \right) e^{\lambda_2 \delta} > 0, \\
P(t + \delta) &= \frac{K_2}{\lambda_2 - \lambda_1} \left(R(t) - \frac{\lambda_1 + \frac{1}{\tau_2}}{K_2} P(t) \right) e^{\lambda_2 \delta} > 0,
\end{aligned} \tag{24}$$

since the natural mode $e^{\lambda_1 \delta}$ tends to zero more rapidly than $e^{\lambda_2 \delta}$ (see inequalities (23)). This implies that the limit of the ratio $R(t + \delta)/P(t + \delta)$ is given by the following expression

$$\lim_{\delta \rightarrow \infty} \frac{R(t + \delta)}{P(t + \delta)} = \frac{\lambda_2 + \frac{1}{\tau_2}}{K_2} \triangleq \gamma_2 > 0. \tag{25}$$

Studying the sign of the time derivative of $R(t + \delta)/P(t + \delta)$, it is possible to prove its monotonic behaviour in approaching γ_2 . Indeed, by introducing the quantity $\gamma_1 \triangleq -(\lambda_1 + 1/\tau_2)/K_2$, from Eqs. (21)-(22) we have

$$\frac{R(t + \delta)}{P(t + \delta)} = \frac{\gamma_1 (R(t) - \gamma_2 P(t)) e^{\lambda_1 \delta} + \gamma_2 (R(t) + \gamma_1 P(t)) e^{\lambda_2 \delta}}{- (R(t) - \gamma_2 P(t)) e^{\lambda_1 \delta} + (R(t) + \gamma_1 P(t)) e^{\lambda_2 \delta}}. \tag{26}$$

By exploiting the time derivative:

$$\frac{d}{d\delta} \left[\frac{R(t + \delta)}{P(t + \delta)} \right] = \frac{\frac{P(t)^2}{K_2} \left(\gamma_2 - \frac{R(t)}{P(t)} \right) \left(\frac{R(t)}{P(t)} + \gamma_1 \right) (\lambda_2 - \lambda_1)^2}{\left(- (R(t) - \gamma_2 P(t)) e^{\lambda_1 \delta} + (R(t) + \gamma_1 P(t)) e^{\lambda_2 \delta} \right)^2} e^{(\lambda_1 + \lambda_2) \delta}. \tag{27}$$

Taking into account inequalities (23), it is easy to verify that the sign of (27) only depends on the value of $R(t)/P(t)$, i.e. on the sign of the factor $\gamma_2 - R(t)/P(t)$. Such

a sign cannot change with δ and the monotonic behaviour of $R(t + \delta)/P(t + \delta)$ is guaranteed for any value of the initial ratio $R(t)/P(t)$.

In order to complete the proof we need to find the parameter conditions under which the relation $\gamma_2 \leq \rho$, as well as the opposite one, is satisfied. Indeed, since $R(t)/P(t) < \rho$, requiring $\gamma_2 \leq \rho$ means that the ratio of ribosomes over proteins will remain lower than ρ for any finite time, being γ_2 the limit value of the ratio for infinite time. So, by imposing the relation

$$\gamma_2 = \frac{\lambda_2 + \frac{1}{\tau_2}}{K_2} \leq \rho, \quad (28)$$

we have

$$\lambda_2 \leq K_2\rho - \frac{1}{\tau_2}, \quad (29)$$

where $\lambda_2 \leq 0$ because of the condition $-1 < x \leq 0$. Now, substituting the expression of λ_2 given in (10) in the previous inequality and performing simple algebraic operations, it is possible to obtain the final relation

$$K_2\rho + \frac{1}{\tau_1} - \frac{1}{\tau_2} \geq 0, \quad (30)$$

meaning that

$$\gamma_2 \leq \rho \quad \Leftrightarrow \quad K_2\rho + \frac{1}{\tau_1} - \frac{1}{\tau_2} \geq 0. \quad (31)$$

Obviously, implications (31) can be also given exploiting the opposite inequalities, i.e.

$$\gamma_2 > \rho \quad \Leftrightarrow \quad K_2\rho + \frac{1}{\tau_1} - \frac{1}{\tau_2} < 0. \quad (32)$$

So, we can conclude that, when $-1 < x \leq 0$, the ratio $R(t + \delta)/P(t + \delta)$ remains under the threshold ρ for $\delta \rightarrow \infty$ if $K_2\rho \geq 1/\tau_2 - 1/\tau_1$ or it crosses the threshold otherwise. \square

From Theorem 3 the following corollary can be derived.

Corollary. *If the model parameters are such that $\rho K_2 < 1/\tau_2 - 1/\tau_1$, then the switch $\mu_2 \rightarrow \mu_1$ is unavoidable; otherwise it is forbidden.*

Proof. The proof comes from Theorem 3 noticing that the inequality $\rho K_2 \geq 1/\tau_2 - 1/\tau_1$ can be assumed as the only condition for the stability of μ_2 , independently of the value of x . Indeed, the growth condition $x > 0$ can be rewritten as

$$K_1 K_2 \rho > \left(K_1 + \frac{1}{\tau_1} \right) \frac{1}{\tau_2}, \quad (33)$$

or equivalently, for positive values of K_1 , as

$$K_2\rho > \frac{K_1 + \frac{1}{\tau_1}}{K_1} \frac{1}{\tau_2}. \quad (34)$$

From condition (34) and from the positivity of the model parameters we obtain the following chain of inequalities

$$K_2\rho > \frac{K_1 + \frac{1}{\tau_1}}{K_1} \frac{1}{\tau_2} > \frac{1}{\tau_2} > \frac{1}{\tau_2} - \frac{1}{\tau_1}, \quad (35)$$

showing that $x > 0$ implies $\rho K_2 > 1/\tau_2 - 1/\tau_1$. So, the condition $\rho K_2 \geq 1/\tau_2 - 1/\tau_1$ can be taken as the only constraint to be verified in order to establish the stability of μ_2 , independently of the value of x . \square

The results of the corollaries of Theorems 2 and 3 are depicted in Figure 4, where all the possible working modes and growing dynamics of system (1) are represented in the positive orthant of the parameter space, showing when the transitions are forbidden or unavoidable.

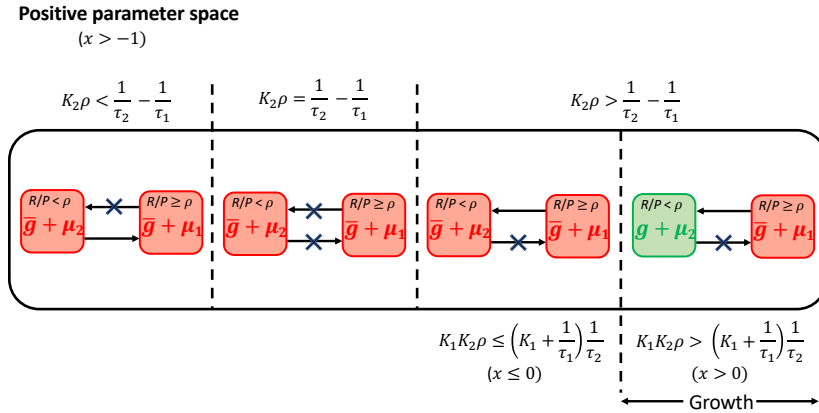


Figure 4
Switching of the working modes in the parameter space.

4 Properties of the cell cycle module

In 1977 Hartwell and Unger proposed in [15] a relationship that links the daughter and parent cycle period, T_D and T_P , to the growth rate of a budding yeast cell, namely the positive eigenvalue λ_2 in our growth model (1):

$$e^{-\lambda_2 T_D} + e^{-\lambda_2 T_P} = 1, \quad (36)$$

where $T_D = T_1(\mathcal{D}) + T_2 + T_B$ and $T_P = T_1(\mathcal{P}) + T_2 + T_B$.

The relationship can be derived from a minimal model of exponentially growing yeast populations that comprises only 2 cell types (parents and daughters of genealogical age 1) in either budded or unbudded state. The equation has been shown to be satisfied in exponentially growing cells [16,24]. Constraint (36) is graphically represented by the mesh in Figure 5, where the Mass Duplication Time (*MDT*) is exploited instead of λ_2 , on the basis of the relation $MDT = \ln(2)/\lambda_2$.

The remainder of this section is devoted to derive and extend analogous relationships among the cycle periods of the proposed growth and cycle cell model, that accounts for many kinds of daughter and parent cells, according to the rules that:

- a daughter cell of any genealogical age, \mathcal{D}_k , provides at cellular division a pair of newborn \mathcal{D}_1 and \mathcal{P}_1 cells;
- a parent cell of genealogical age k , \mathcal{P}_k , provides at cellular division a pair of newborn \mathcal{D}_{k+1} and \mathcal{P}_{k+1} cells.

Further rules involve the facts that:

- proteins and ribosomes produced during the budded phase go exclusively to the bud (the future daughter cell);
- T_2 and T_B are (in average) the same for daughter and parents of any genealogical age;
- cells are supposed to be in balanced exponential growth, with growth rate provided by λ_2 ;
- parent cells grow at a slower growth rate during their unbudded phase, due to the mechanical stress discussed in Section 3. The growth rate associated to \mathcal{P}_k cells in G1-phase will be denoted in the following as λ_{2k} and it can be computed from the model parameters exploiting the same function used for λ_2 , i.e. Eq. (10), but assuming that the mechanical stress influences the values of the parameters related to the protein dynamics. In other words, λ_{2k} will change for \mathcal{P}_k cells in G1-phase by changing the age k because of the relation $\lambda_{2k} = \lambda_{2k}(K_{2k}, \tau_{2k})$.

Denoting by T_{G1} the length of the G1 phase ($T_{G1} = T_1 + T_2$), the first relationship is derived taking into account the exponential growth of a \mathcal{D}_1 cell from birth to bud:

$$P_0(\mathcal{D}_1)e^{\lambda_2 T_{G1}(\mathcal{D}_1)} = P_s(\mathcal{D}_1), \quad (37)$$

and from bud to cellular division, assuming the newborn \mathcal{D}_1 cell to be identical to the original \mathcal{D}_1 :

$$P_s(\mathcal{D}_1)e^{\lambda_2 T_B} = P_{cd}(\mathcal{D}_1) = P_0(\mathcal{P}_1) + P_0(\mathcal{D}_1) = P_s(\mathcal{D}_1) + P_0(\mathcal{D}_1), \quad (38)$$

so that:

$$P_s(\mathcal{D}_1)e^{\lambda_2 T_B} = P_s(\mathcal{D}_1) + P_s(\mathcal{D}_1)e^{-\lambda_2 T_{G1}(\mathcal{D}_1)}, \quad (39)$$

and finally:

$$e^{-\lambda_2 T(\mathcal{D}_1)} + e^{-\lambda_2 T_B} = 1. \quad (40)$$

Notice that eq.(40) very well resembles eq. (36), and it can be represented again by the mesh of Figure 5. By explicitly accounting for $T(\mathcal{D}_1) = T_1(\mathcal{D}_1) + T_2 + T_B$, a mesh can be drawn constraining the three timers lengths ($T_1(\mathcal{D}_1)$, T_2 , T_B), for any given value of λ_2 :

$$T_1(\mathcal{D}_1) = \frac{1}{\lambda_2} \ln \left(\frac{1}{e^{\lambda_2 T_B} - 1} \right) - T_2. \quad (41)$$

In Figure 6 we report the case for $\lambda_2 = 0.0073 \text{ min}^{-1}$, corresponding to the experimental condition of $MDT = 97 \text{ min}$ in glucose 2%. It has to be stressed that, according to (41), not all the pairs (T_2, T_B) allow a feasible (i.e. positive) choice for timer $T_1(\mathcal{D}_1)$ length. In fact, for given values of T_2 , according to (41) it must be:

$$T_1(\mathcal{D}_1) > 0 \quad \rightarrow \quad T_B < \frac{1}{\lambda_2} \ln \left(1 + e^{-\lambda_2 T_2} \right). \quad (42)$$

Figure 7 shows the upper bound for T_B as coming from (42) according to different values of T_2 . The same reasoning can be generalized, this time taking into account the exponential growth of a cell \mathcal{D}_k from birth to bud, so that:

$$P_0(\mathcal{D}_k) e^{\lambda_2 T_{G1}(\mathcal{D}_k)} = P_s(\mathcal{D}_k), \quad (43)$$

and the exponential growth of a \mathcal{P}_{k-1} cell from bud to cellular division:

$$P_s(\mathcal{P}_{k-1}) e^{\lambda_2 T_B} = P_{cd}(\mathcal{P}_{k-1}) = P_0(\mathcal{P}_k) + P_0(\mathcal{D}_k) = P_s(\mathcal{P}_{k-1}) + P_0(\mathcal{D}_k), \quad (44)$$

so that:

$$P_s(\mathcal{P}_{k-1}) e^{\lambda_2 T_B} = P_s(\mathcal{P}_{k-1}) + P_s(\mathcal{D}_k) e^{-\lambda_2 T_{G1}(\mathcal{D}_k)}, \quad (45)$$

or equivalently:

$$P_s(\mathcal{P}_{k-1}) = P_s(\mathcal{P}_{k-1}) e^{-\lambda_2 T_B} + P_s(\mathcal{D}_k) e^{-\lambda_2 T(\mathcal{D}_k)}. \quad (46)$$

On the other hand, if we consider the exponential growth of a \mathcal{P}_k cell from birth to bud, we have:

$$P_0(\mathcal{P}_k) e^{\lambda_2 T_{G1}(\mathcal{P}_k)} = P_s(\mathcal{P}_k) = P_s(\mathcal{P}_{k-1}) e^{\lambda_2 T_{G1}(\mathcal{P}_k)}, \quad (47)$$

since $P_0(\mathcal{P}_k) = P_s(\mathcal{P}_{k-1})$. Notice that eq. (47) accounts for different growth rates for parent cells of different genealogical ages, due to the mechanical stress before the bud occurs. Differently from eqs. (40) and (36), constraints (45)-(47) involve size and cycle parameters together.

Conclusions

The coherence of a mathematical model (i.e. whether the associated solutions are meaningful for the largest range of the feasible model parameters) is an important feature a good model is required to attain, especially when aiming at describing a

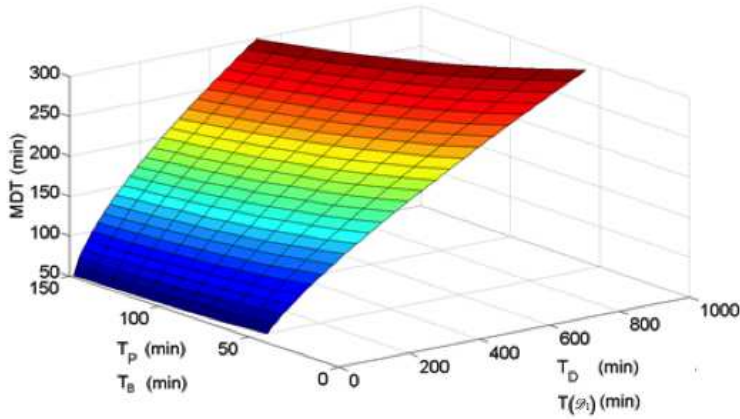


Figure 5

Constraint among MDT , parent and daughter cycle lengths (T_P and T_D , respectively). It is obtained from (36), exploiting also the relation $MDT = \ln(2)/\lambda_2$. The same mesh represents the relationship among MDT , budded phase and \mathcal{S}_1 cycle length (T_B and $T(\mathcal{S}_1)$, respectively) in our model, according to (40).

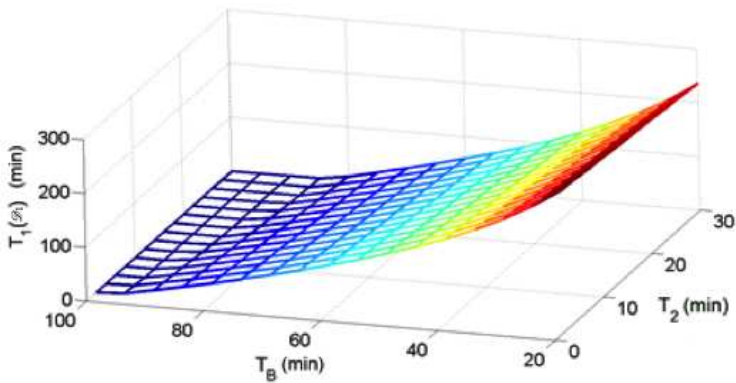


Figure 6

Constraint among $T_1(\mathcal{S}_1)$, T_B and T_2 for $MDT = 97$ min, as coming from (41).

wide range of possible working modes. In this work we have investigated the qualitative behavior of a coarse-grain model of cellular growth, recently exploited as a module of a larger interconnected model that integrates metabolism, growth and cell cycle in yeast. More in details, we found a specific sufficient condition ($x > 0$) for the growth of ribosome and protein populations. In particular, when starting the dynamic evolution with active ribosome synthesis such a condition guarantees to maintain synthesis and growth for any time. Conversely, when starting with the ribosome synthesis initially inactive, determining a temporary non-growing state, the system approaches a state condition that allows the switch for an active synthesis and, consequently, exponential growth. On the other hands, if such a condition is

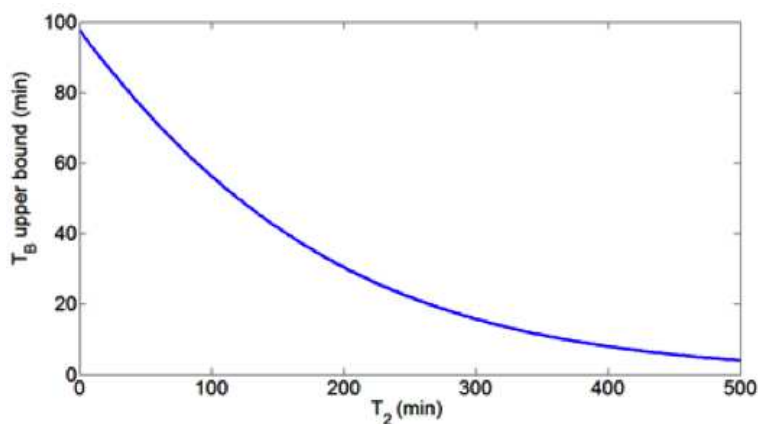


Figure 7

Upper bound for T_B as coming from (42) according to different values of T_2 .

violated ($x \leq 0$), no growth is possible, independently of the ribosome synthesis. Furthermore, by linking the growth module to a basic set of timers describing the cell cycle, we are able to derive constraints among timers and growth rate that somehow generalize, to the more complex case accounting for the variety of genealogical ages, analogous constraints achieved half a century ago and still exploited as a preliminary validity check for mathematical models of cell cycle in yeast.

Acronyms

For the convenience of the reader, the following table collects all the acronyms used in the text.

Acronym	Definition
Whi5	Transcriptional regulator in the budding yeast cell cycle, notably in the G1 phase.
Clb5/6	B-type S-phase cyclins in yeast that assist in cell cycle regulation.
Sic1	Stoichiometric inhibitor of Cdk1-Clb complexes (bindings of the Cyclin-dependent kinase 1 - a key player of the cell cycle regulation in yeast - and the B-type cyclins Clb).
TOR	Target Of Rapamycin, protein kinase
Sfp1	Transcription factor that regulates growth and cell division in yeast.
ppGpp	Guanosine tetraphosphate, an alarmone which is involved in the stringent response in bacteria, causing the inhibition of RNA synthesis when there is a shortage of amino acids present.

Table 2

List of the acronyms used in the text.

Acknowledgement

The institutional financial support of SYSBIO.ISBE.IT within the Italian Roadmap for ESFRI Research Infrastructures is gratefully acknowledged.

References

- [1] S. Di Talia, J. M. Skotheim, J. M. Bean, E. D. Siggia, and F. R. Cross. The effects of molecular noise and size control on variability in the budding yeast cell cycle. *Nature*, 448:947–951, 2007.
- [2] P. Palumbo, M. Vanoni, F. Papa, S. Busti, M. Wortel, B. Teusink, and L. Alberghina. An integrated model quantitatively describing metabolism, growth and cell cycle in budding yeast. In M. Pelillo et al., editors, *Artificial Life and Evolutionary Computation*, volume 830, pages 165–180. Springer, 2018. Communications in Computer and Information Science (CCIS book series).
- [3] P. Palumbo, F. Papa, M. Vanoni, and L. Alberghina. Qualitative behavior of a coarse-grain growth model. In *23rd IEEE International Conference on Intelligent Engineering Systems*, 2019.
- [4] L. Alberghina, L. Mariani, and E. Martegani. Cell cycle modelling. *Biosystems*, 19:23–44, 1986.
- [5] J. J. Turner, J. C. Ewald, and J. M. Skotheim. Cell size control in yeast. *Current Biology*, 22:R350–359, 2012.
- [6] E. Martegani, L. Popolo, L. Alberghina, and E. Sturani. Reduction of ribosome activity and synthesis of stable RNA in *Neurospora crassa*. *Biochimica et Biophysica Acta*, 610:318–330, 1980.
- [7] M. Nomura, R. Gourse, and G. Baughman. Regulation of the synthesis of ribosomes and ribosomal components. *Annual Review of Biochemistry*, 53:75–117, 1984.
- [8] E. Bosdriesz, D. Molenaar, B. Teusink, and F. J. Bruggeman. How fast-growing bacteria robustly tune their ribosome concentration to approximate growth-rate maximization. *The FEBS Journal*, 282:2029–2044, 2015.
- [9] V. Zinzalla, D. Stracka, W. Oppliger, and M. N. Hall. Activation of mTORC2 by association with the ribosome. *Cell*, 144:757–768, 2011.
- [10] M. Cook and M. Tyers. Size control goes global. *Current Opinion in Biotechnology*, 18:341–350, 2007.
- [11] K. W. Boehlke and J. D. Friesen. Cellular content of ribonucleic acid and protein in *Saccharomyces cerevisiae* as a function of exponential growth rate: calculation of the apparent peptide chain elongation rate. *Journal of Bacteriology*, 121:429–433, 1975.
- [12] C. Waldron and F. Lacroute. Effect of growth rate on the amounts of ribosomal and transfer ribonucleic acids in yeast. *Journal of Bacteriology*, 122:855–865, 1975.

- [13] C. Waldron, R. Jund, and F. Lacroute. Evidence for a high proportion of inactive ribosomes in slow-growing yeast cells. *Biochemical Journal*, 168:409–415, 1977.
- [14] L. Alberghina and E. Sturani. Control of growth and of the nuclear division cycle in *Neurospora crassa*. *Microbiological Reviews*, 45:99–122, 1981.
- [15] L. H. Hartwell and M. W. Unger. Unequal division in *Saccharomyces cerevisiae* and its implications for the control of cell division. *The Journal of Cell Biology*, 75:422–435, 1977.
- [16] D. Porro, M. Vai, M. Vanoni, L. Alberghina, and C. Hatzis. Analysis and modeling of growing budding yeast populations at the single cell level. *Cytometry A*, 75:114–120, 2009.
- [17] A. Lorincz and B. L. A. Carter. Control of cell size at bud initiation in *Saccharomyces cerevisiae*. *Journal of general microbiology*, 113:287–295, 1979.
- [18] B. L. Carter and M. N. Jagadish. The relationship between cell size and cell division in the yeast *Saccharomyces cerevisiae*. *Experimental Cell Research*, 1978:112, 112.
- [19] C. L. Woldringh, P. G. Huls, and N. O. Vischer. Volume growth of daughter and parent cells during the cell cycle of *Saccharomyces cerevisiae* α /alpha as determined by image cytometry. *Journal of Bacteriology*, 175:3174–3181, 1993.
- [20] G. C. Johnston, C. W. Ehrhardt, A. Lorincz, and B. L. Carter. Regulation of cell size in the yeast *Saccharomyces cerevisiae*. *Journal of Bacteriology*, 137:1–5, 1979.
- [21] L. Alberghina, Vai M., and M. Vanoni. Probing control mechanisms of cell cycle and ageing in budding yeast. *Current Genomics*, 5(8):615–627, 2004.
- [22] D. E. Levin. Regulation of cell wall biogenesis in *Saccharomyces cerevisiae*: the cell wall integrity signaling pathway. *Genetics*, 189:1145–1175, 2011.
- [23] R. Csikja, B. M. Garay, and J. Tóth. Chaos via two-valued interval maps in a piecewise affine model example for hysteresis. In *Proceedings of the 19th International Symposium on Mathematical Theory of Networks and Systems–MTNS*, pages 187–194, 2010.
- [24] M. Vanoni, M. Vai, L. Popolo, and L. Alberghina. Structural heterogeneity in populations of the budding yeast *Saccharomyces cerevisiae*. *Journal of Bacteriology*, 156:1282–1291, 1983.

2019 Reviewers

Ádám, Norbert	Dvorský, Marián
Ales, Prochazka	Eigner, György
Alontseva, Darya	Elek, Renata
Andoga, Rudolf	Fehér-Polgár, Pál
Ászity, Sándor	Ferenci, Tamas
Bakucz, Peter	Fiorini, Paolo
Balogh, Zoltán	Fischer, Gregory
Bán, Krisztián	Főző, Ladislav
Bánáti, Anna	Fullér, Róbert
Bányai, Tamás	Galambos, Péter
Baranyi, Péter	Gašpar, Vladimír
Bareith, Attila	Genci, Jan
Bednar, Peter	Hanakova, Lenka
Bobar, Zoran	Hermann, Gyula
Borri, Alessandro	Holicza, Péter
Bozóki, Sándor	Horvath, Ildiko
Bundzel, Marek	Horváth, László
Chinzei, Kiyoyuki	Horváth, Richárd
Chiu, Chris	Hošovský, Alexander
Chopra, Vikram	Ionescu, Clara Mihaela
Ciubotariu, Relu	Jaksa, Laszlo
Čonka, Zsolt	Juan Carlos Garcia Ojeda
Czakó, Bence Géza	Jurado, Francisco
Csanadi, Bertalan	Károly, Artúr István
Csapo, Adam	Kárpáti-Daróczi, Judit
Csato, Laszlo	Kasanicky, Tomas
Csiszár, Csaba	Kátai, László
Csiszárík-Kocsir, Ágnes	Katona, Ferenc
Csizmadia, Tamas	Katona, Jozsef
Dobrzanska, Magdalena	Kazanzides, Peter
Dombi, József	Kiss, Gábor
Domokos, Jozsef	Kluwak, Konrad
Dömötör, Ferenc	Kovacs, George
Dragan, Antic	Kovacs, Szilveszter
Draganova, Katarina	Kozma, Tímea
Duma, Florin	Kronreif, Gernot

Kuti, József	Piller, Imre
Kuzsela, László	Piricz, Noémi
Lang, Ján	Pokorádi, László Károly
Laššák, Miroslav	Precup, Radu-Emil
Lazanyi, Kornelia	Prochazka, Ales
Lewis, Andrew	Reicher, Regina Zsuzsánna
Li, Yangming	Ren, Jin
Lipovský, Pavol	Rétfalvi, Attila
Lukács, Pál	Rövid, András
Maček, Nemanja	Saracevic, Muzafer
Machova, Renata	Schrötter, Martin
Mariani, Andrea	Selvaggio, Mario
Markus, Zsolt Laszlo	Skapinyecz, Róbert
Marovac, Ulfeta	Skokan, Marek
Matiaszko, Karol	Stanescu, Daniela Natalia
Menyhart, Jozsef	Stević, Željko
Mester, Gyula	Strielkowski, Wadim
Mihajlovic, Ivan	Szabo, Ferenc János
Mikula, Martin	Szabolcsi, Robert
Milosavljevic, Cedimir	Szikora, Péter
Moccia, Rocco	Szilagyi, Laszlo
Molnar, Ildiko	Sztahó, Dávid
Molnar, Viktor	Takács, Árpád
Moreira, Pedro	Takacs, Istvan
Moya-Albor, Ernesto	Takacs, Marta
Nagy, Dénes Ákos	Taneski, Viktor
Nagy, István	Tar, József
Nagy, Tamas	Tick, Andrea
Nedelko, Zlatko	Tóth-Laufer, Edit
Nedeloni, Marian-Dumitru	Vámosy, Zoltán
Nemes, Csaba	Várlaki, Péter
Oancea, Gheorghe	Vascak, Jan
Odry, Peter	Velencei, Jolan
Oravec, Jakub	Veress, Árpád
Palumbo, Pasquale	Visioli, Antonio
Paniti, Imre	Vlahovic, Nikola
Pawliczek, Adam	Weber, Gyorgy
Pedro, Rodriguez	Zsoldos, Ibolya
Peter, Tamas	